The mitochondrial-cytosolic pathway of FeS cluster assembly in Arabidopsis thaliana

Inga Kruse

A thesis submitted to the University of East Anglia for the degree of Doctor of Philosophy

John Innes Centre
Norwich
September 2016

I hereby certify that the work contained within this thesis is my own original work, except where due reference is made to other contributing authors. This thesis is submitted for the degree of Doctor of Philosophy at the University of East Anglia and has not been submitted to this or any other university for any other qualification.

Abstract

The aim of this work was to unravel the molecular basis of the connection of mitochondrial and cytosolic FeS assembly. Following on from previous work showing that the mitochondrial ABC-transporter ATM3 is required for cytosolic FeS assembly (Bernard et al., 2009), one part of my project was to provide *in-vivo* evidence for the substrate of ATM3. I found that the mitochondrial glutathione pool in *atm3* seedlings is shifted towards oxidation, indicating accumulation of oxidised glutathione. Furthermore I showed that *ATM3* genetically interacts with two enzymes involved in persulfide metabolism (*ETHE1, NFS1*). This complemented i*n-vitro* studies by Dr. Schaedler (Schaedler et al., 2014) who showed that oxidised glutathione is a preferred substrate and glutathione carrying additional S^0 can be transported by yeast Atm1.

To gather further insight into biosynthesis of the ATM3 substrate I investigated the role of a cytosolic and a mitochondrial glutaredoxin (GRXS17, GRXS15). Mutants had minor but specific effects on FeS enzymes and I concluded that the glutaredoxins are not generally involved in *de-novo* cluster assembly.

Another approach was to identify unknown components of mitochondrial-cytosolic persulfide transport. I characterised two mutants with phenotypic resemblance to *atm3* mutants. For one, I located a point mutation in the sequence of *ATM3* leading to an amino acid exchange in the 6^{th} transmembrane domain and showed that the ATM3 protein was lacking. The second line was a mutant of *CNX2*, a mitochondrial enzyme necessary for generation of the first MoCo intermediate cPMP. I found ATM3 protein breakdown in *cnx2-2* and in a mutant of CNX5 which is involved in MoCo assembly and t-RNA thiomodification. ATM3 was previously suggested to export cPMP (Teschner et al., 2010). My findings give new evidence for a link between ATM3 and MoCo assembly.

Acknowledgements

First of all, I would like to express my special appreciation and gratitude to my advisor Dr. Janneke Balk for giving me the opportunity of conducting my PhD in her group. I also want to thank her for her guidance and advice, her invaluable help in developing my scientific skills throughout my PhD and for always having an open door.

I would also like to thank the other members of my supervisory committee, Dr. Stanislav Kopriva, Dr. Tony Miller and Dr. Gill Malin for their constructive advice and invaluable support.

Many thanks also to our collaborators, especially Prof. Dr. Andreas Meyer and Dr. Markus Schwarzländer for making the roGFP experiments possible and for their patience and advice during my time in their lab. I also would like to thank Dr. Martin Trick and Dr. Zamin Iqbal for the analysis of the whole genome sequencing data.
I want to thank Edgaras Laveckis for his support during the mapping procedure.

For funding I would like to thank the University of East Anglia and the John Innes Centre.

My special thanks go to the whole Balk group and lab 108, especially Emma Bastow, James Connorton, Kat Ignasiak, Andrew Maclean, Jorge Rodriguez-Celma and Jenny Walton; you have been great friends and created such a welcoming atmosphere. Thank you for all your support throughout my PhD. I especially want to thank Lesley Mitchenall and Sarah Tolland who always had an open ear and answers to my questions.

I also want to thank Tatjana Goss for the hours-long phone calls when I needed them.

Last but not least, I would like to thank, my mum, my sister, my grandma and Andrew for all the help love and support. You were always there for me in the good and the not so good times, you kept me sane and I could never have done it without you.

Table of Contents

List of Figures

List of Tables

Abbreviations

ABA	Abscisic acid
ABA3	Abscisic acid deficient 3
ABC	ATP-binding cassette
ADP	Adenosine diphosphate
AE7	Asymmetric leaves ½ enhancer 7
Aft	Activator of ferrous transport
AMP	Adenosine monophosphate
At	Arabidopsis thaliana
ATM	ABC-transporter of the mitochondria
ATP	Adenosine triphosphate
ATR	Aminotransferase
BIO	Biotin synthase
bp	Base pairs
BSO	Buthionine sulfoximine
cDNA	Complementary DNA
CaMV	Cauliflower mosaic virus
CER	Controlled environment room
CIA	Cytosolic iron-sulfur protein assembly machinery
CNX	Cofactor of Nitrate reductase and Xanthine dehydrogenase
CoA	Coenzyme A
Col-0	Columbia-0
cPMP	Cyclic pyranopterin monophosphate
dH_2O	distilled water
DI	Deionised
DNA	Deoxyribonucleic acid
DRE2	Derepressed for Ribosomal protein S14 Expression
DTT	Dithiothreitol
EDTA	Ethylenediaminetetraacetic acid
EMS	Ethyl methanesulfonate
ETHE	Ethylmalonic encephalopathy protein 1
F1	First filial generation

FAD	Flavin adenine dinucleotide
FDX	Ferredoxin
FeS	Iron-sulfur
gDNA	Genomic DNA
GFP/roGFP	Green fluorescent protein/ redox sensitive green fluorescent protein
GRX	glutaredoxin
GSH/GSSG	Reduced/oxidised glutathione
GSH1	Glutamate-cysteine ligase
GSH2	Glutathione synthetase
GTP	Guanosine triphosphate
HNA	2-hydroxy-1-naphthaldehyde
HNC	2-hydroxy-1-naphthoic acid
HEPES	4-(2-hydroxyethyl)-1-piperazineethanesulfonic acid
HSC	Heat shock cognate
IBA	Iron-sulfur cluster assembly factor for biotin synthase and aconitase-like mitochondrial proteins
ISC	Iron-sulfur cluster pathway
ISD11	Iron-sulfur protein biogenesis, desulfurase-interacting protein
ISU	IscU-like
Ler	Landsberg erecta
LIP	Lipoate synthase
mARC	Mitochondrial amidoxime reducing component
MES	2-(N-morpholino)ethanesulfonic acid
MET18	Methionine requiring 18
MoaD	Molybdopterin synthase, small subunit
MoCo	Molybdenum cofactor
MOCS	Molybdenum cofactor synthesis protein
MOPS	3-(N-morpholino)propanesulfonic acid
MPT	Molybdopterin
MS	Murashige and Skoog
NAD+	Nicotinamide adenine dinucleotide (oxidised)
NADH	Nicotinamide adenine dinucleotide (reduced)
NADP+	Nicotinamide adenine dinucleotide phosphate (oxidised)
NADPH	Nicotinamide adenine dinucleotide phosphate (reduced)

NFS1	Nitrogen Fixation S (NIFS)-like 1
NFU	Nitrogen fixation U (NIFU)-like
NF-YC11	Nuclear factor Y, subunit C11
NTP	Nucleotide triphosphate
OASTLC	O-acetylserine (thiol) lyase C
PAGE	Polyacrylamide gel electrophoresis
PCR	Polymerase chain reaction
PMS	Phenazine methosulfate
PMSF	Phenylmethylsulfonyl fluoride
Psa	Photosystem I subunit
RNA	Ribonucleic acid
S^0	zero valency sulfur/sulfane sulfur
SAM	S-adenosyl-L-methionine
SD	Standard deviation
SDS	Sodium dodecyl sulphate
SAT	Serine-acetyltransferse
SNP	Single nucleotide polymorphism
SOC	Super optimal broth
SSP	Sulfane sulfur probe
STR	Sulfurtransferase
SUF	Sulfur mobilization machinery
TAE	Tris base, acetic acid, EDTA buffer
TE	Tris-EDTA buffer
T-DNA	Transfer DNA
T_M	Melting temperature
Tris	Tris(hydroxymethyl)aminomethane
tRNA	Transfer RNA
v/v	Volume/volume
w/v	Weight/volume
WT	Wild-type
XD	Xinhua Dai

1. Introduction

Metal cofactors form the active site for numerous proteins in virtually all organisms. There is a vast diversity of metal cofactors which are of high importance. Several metals play important roles for enzymes such as zinc in alkaline phosphatases and alcohol dehydrogenases, manganese in photosystem II and isocitrate dehydrogenase, copper in cytochrome oxidase and superoxide dismutase, molybdenum in aldehyde oxidase or nitrate reductase just to name a few. However, the most prominent metal is probably iron. Iron cofactors are involved in processes like oxygen binding in the form of heme. Another well-known iron cofactor is the iron-sulfur (FeS) cluster which occurs in multiple forms. A defect in assembly or an excess of Fe or S can be fatal and thus a good understanding of the FeS cluster assembly pathways is important. The main focus of this work will be on FeS cofactors and their assembly in plant mitochondria and cytosol.

FeS cofactors are redox active and involved in processes like electron transport chains in the chloroplasts and mitochondria, in the assimilation of nitrogen and sulfur and also in DNA repair mechanisms and the maintenance of telomeres and genome stability (Balk and Schaedler, 2014; Lill, 2009). The most common types of FeS are the Fe_2S_2, the Fe_3S_4 and the Fe_4S_4 clusters, but other, more complex forms exist (Beinert et al., 1997; Drennan and Peters, 2003; Rees, 2002). Fe_2S_2 clusters are the most stable type of cluster; However, FeS clusters are easily oxidised when exposed to oxygen or reactive oxygen species (Balk and Schaedler, 2014; Imsande, 1999). In comparison to other Fe containing cofactors, FeS enzymes tend to have a more negative reduction potential (in the range between -590 and -20 mV with only a few exceptions) which makes them good electron donors but FeS clusters can also have catalytic or stabilising functions or serve as a sulfur donor making it a versatile cofactor. (Balk and Schaedler, 2014; Beinert, 2000a). It is the versatility of S as well as the redox activity of Fe which gives the clusters their unique properties. Sulfur in its lower oxidation states is chemically versatile with sulfenate (SO^-) being at the upper limit of oxidation (Beinert, 2000b). As summarised by Beinert in 2000 (Beinert, 2000a), S has several properties which contribute to the function and versatility of FeS clusters: (1) nuclear charge effects in S are not strong (2) S electrons can populate 3d orbitals (3) S has low tendency to form hydrogen bonds (4)

S can occur in formal valences 2- to 6+ (5) bonds with S are highly covalent (6) little energy is needed to change S from an electrophile to a nucleophile. Fe on the other hand is responsible for the redox reactivity of the cluster and in some cases acts catalytically. Cluster degradation releases Fe which can then catalyse the Fenton reaction which produces reactive oxygen species, increasing the damage to FeS clusters. Thus, the widespread usage of FeS clusters presents a risk for the organism but the benefits outweigh the dangers.

1.1. FeS enzymes in plants

FeS enzymes are involved in a vast variety of processes. In the following I will give an overview of many known processes in plants that involve FeS enzymes and will highlight a few examples.

FeS enzymes are involved in hormone biosynthesis, seedling establishment and vegetative growth. One of those enzymes is aldehyde oxidase ($2Fe_2S_2$, see also Section 1.4) which catalyses the last step of abscisic acid synthesis and is also thought to be involved in auxin biosynthesis, thus affecting various growth processes (Bittner, 2014; Dai et al., 2005; Seo et al., 2000). Another prominent example is the involvement of two FeS enzymes in the tricarboxylic acid cycle: (1) Aconitase (Fe_4S_4) (Arnaud et al., 2007; Bernard et al., 2009; Moeder et al., 2007) which mediates the conversion of cis-aconitate to isocitrate. (2) Succinate dehydrogenase (Fe_2S_2, Fe_4S_4, Fe_3S4) (Figueroa et al., 2001; Hagerhall, 1997; Leon et al., 2007; Millar et al., 2004; Sweetlove et al., 2010) which mediates the conversion of succinate to fumarate and the reduction of ubiquinone to ubiquinol. Succinate dehydrogenase is also part of the mitochondrial respiratory chain (Complex II). The respiratory complexes Complex I and III also require FeS clusters for their function (Beinert, 2000a; Hunte et al., 2010; Rieske, 1976).

The photosynthetic electron transport chain is also dependent on FeS as cofactors. Photosystem I subunits PsaA and PsaB (Amunts et al., 2007) are bridged by a Fe4S4 cluster and PsaC contains a further Fe_2S_2 cluster. Another important process is the electron transfer by ferredoxins (Fe_2S_2) (Hanke and Mulo, 2013; Takubo et al., 2003). Ferredoxins donate electrons to various processes including sulfur and nitrogen assimilation and amino acid synthesis. Sulfite and nitrite reductase require a

Fe_4S_4 cluster and siroheme which is synthesised in a pathway involving the FeS cluster enzyme sirohydrochlorin ferrochelatase (Fe_2S_2) (Guerrero et al., 1981; Raux-Deery et al., 2005; Saha et al., 2012; Saito, 2004). Nitrogen assimilation is vital for amino acid synthesis. There are several isoforms of glutamate synthase which contain FeS clusters (varying FeS clusters in the isozymes) (Vanoni and Curti, 2008) and also an enzyme involved in leucine biosynthesis (3-isopropylmalate isomerase, Fe_4S_4) (He et al., 2010; He et al., 2011; Knill et al., 2009; Sureshkumar et al., 2009) further linking FeS cluster enzymes to amino acid metabolism.

It has recently been discovered that FeS enzymes also play a pivotal role in DNA metabolism, repair and epigenetics (as reviewed for example by (Balk and Schaedler, 2014)). Amidophosphoribosyl transferase (Fe_4S_4) (Hung et al., 2004) and xanthine dehydrogenase (2 Fe_2S_2) (Bittner, 2014; Hesberg et al., 2004) for example are involved in purine metabolism. Various DNA glycosylases, helicases, primases and endonucleases are also dependent on FeS clusters for their function (Balk and Pilon, 2011; Balk and Schaedler, 2014).

FeS proteins are also important for cofactor biosynthesis. Various enzymes, electron donors and scaffolds are involved in FeS assembly itself and also in biotin synthesis (biotin synthase (BIO) 2, Fe_2S_2), lipoate synthesis (lipoate synthase (LIP) 1, 2 Fe_4S_4) as well as MoCo synthesis (Cofactor of Nitrate reductase and Xanthine dehydrogenase (CNX) 2), Fe_4S_4, see also Section 1.4) and NAD synthesis (Quinolinate synthase, Fe_4S_4) (Balk and Pilon, 2011; Balk and Schaedler, 2014).

1.2. FeS cluster assembly in plants

FeS cluster assembly pathways are based on a common principle. First, a S^0 is mobilised from cysteine by a cysteine desulfurase, producing alanine in the process. The S^0 stays protein-bound and is transferred to a scaffold protein. During cluster assembly with Fe the S^0 is reduced to S^{2-} requiring two electrons (Balk and Lobreaux, 2005; Paul and Lill, 2014). In a final step the cluster is then transferred to an apo-protein. The source of the iron in plants remains elusive. In yeast and mammals and plants frataxin has been suggested. It has to be taken into account that the role of frataxin is discussed controversially. Recent findings suggest that frataxin is involved in early sulfuration steps of the FeS assembly (as reviewed by Lill et al.,

2015). On one hand, there is *in-vitro* evidence suggesting that frataxin stimulates cysteine binding to Nfs1 by exposing substrate binding sites (Pandey et al., 2013; Bridwell-Rabb et al., 2014). On the other hand, Parent et al. (2015) showed kinetic stimulation of the subsequent trans-sulfuration. However, frataxin mutants of Arabidopsis showed only minor Fe-homeostasis defects in comparison to yeast mutants (Busi et al., 2006; Lill et al., 2012; Martin et al., 2009; Pastore and Puccio, 2013).

In plants three assembly machineries are known: the sulfur mobilization machinery in the plastids (SUF), the iron-sulfur cluster pathway in the mitochondria (ISC) and the cytosolic iron-sulfur protein assembly machinery in the cytosol (CIA) which also provides FeS clusters for nuclear proteins (see Figure 1.1). All three pathways depend on a cysteine desulfurase and several scaffolds and carriers (Balk and Pilon, 2011; Balk and Schaedler, 2014; Couturier et al., 2013). The mitochondrial and cytosolic machineries are thought to be linked in eukaryotes by the mitochondrial cysteine desulfurase and a mitochondrial ABC-transporter (Lill, 2009) (see Figure 1.1).

In plants, the link between mitochondrial and cytosolic FeS assembly is comprised of the mitochondrial cysteine desulfurase Nitrogen Fixation S (NIFS)-like 1 (NFS1) and the ABC transporter of the Mitochondria 3 (ATM3) which will be discussed further in Section 1.3 (see also Figure 1.1) (Bernard et al., 2009; Bernard et al., 2013).

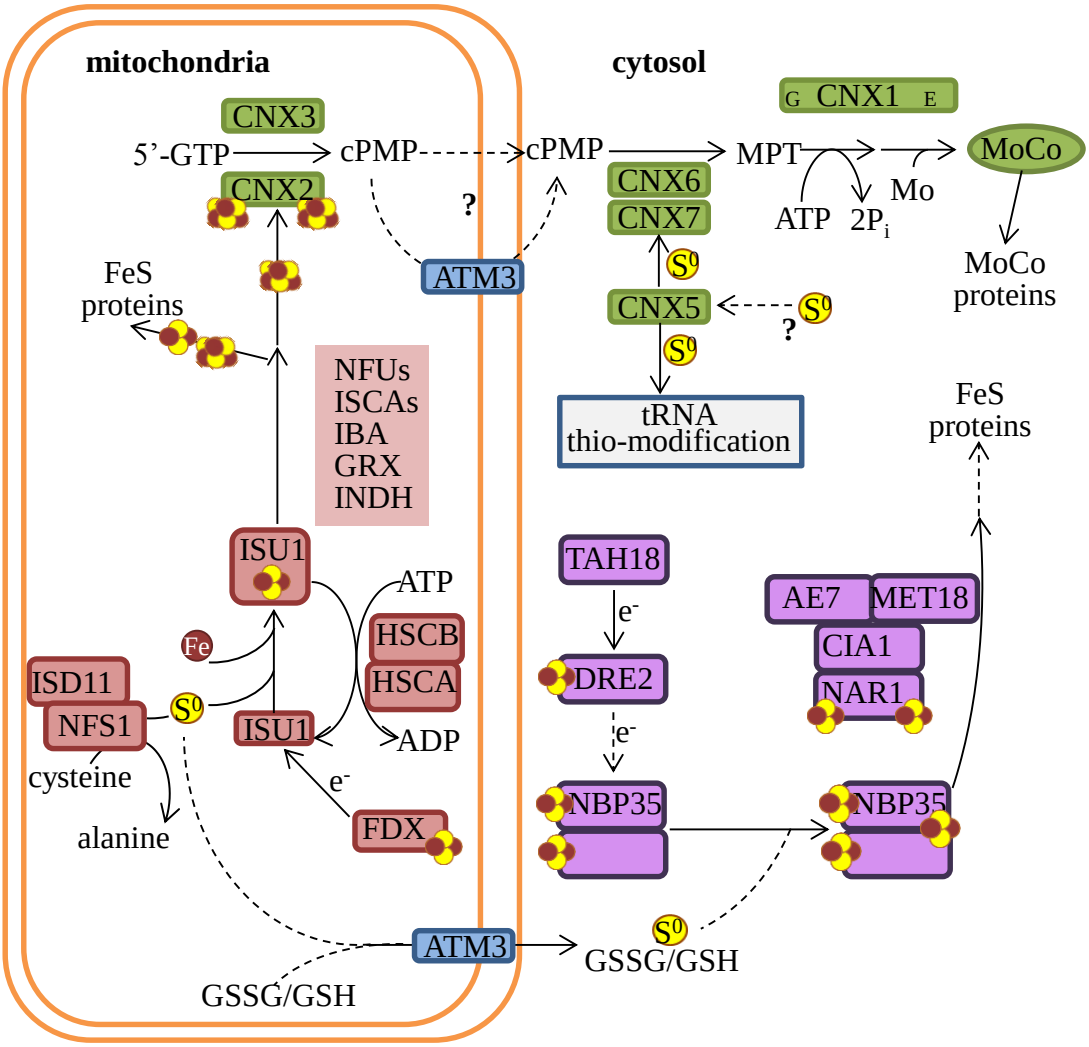

Figure 1.1 Scheme of the CIA, ISC and MoCo assembly in plants. Components of the ISC are indicated in red, components of the CIA in purple, components of the MoCo assembly in green. AE7 = Asymmetric leaves1/2 Enhancer 7; ATM3 = ABC Transporter of the Mitochondria 3; CIA1 = Cytosolic Iron-sulfur protein Assembly; CNX = Cofactor of Nitrate reductase and Xanthine dehydrogenase; cPMP = cyclic pyranopterin monophosphate ; DRE2 = Derepressed for Ribosomal protein S14 Expression; FDX = Ferredoxin; GRX = Glutaredoxin; GSH/GSSG = reduced/oxidised glutathione; GTP = guanosine triphosphate; HSC = Heat Shock Cognate, IBA = Iron-sulfur cluster assembly factor for Biotin synthase and Aconitase-like mitochondrial proteins; ISCA = IscA-like; ISD11 = Iron-Sulfur protein biogenesis, desulfurase-interacting protein; ISU1 = IscU-like, MET18 = Methionine requiring 18; MPT = Molybdopterin; NFS1 = Nitrogen fixation S (NIFS)-like 1, NFU = Nitrogen fixation U (NIFU)-like; S^0 = zero valency sulfur/sulfane sulfur. Dashed arrows indicate unknown/proposed steps.

1.3. ABC-transporters of the mitochondria

In the mitochondria of most eukaryotes, there are 2-4 ATP-binding cassette (ABC) transporters. ABC transporters have been linked to heavy metal transport, oxidative stress, and molybdenum and Fe cofactor synthesis. As mentioned above, the mitochondrial ABC transporter Atm1/ATM3/ABCB7 plays a pivotal role in cytosolic FeS assembly in yeast, plants and mammals (Schaedler et al., 2015).

In yeast, mutants of the ABC transporter of the mitochondria 1(Atm1) accumulated Fe in the mitochondria (Kispal et al., 1997) and in 1999 (Kispal et al.) found that the yeast cysteine desulfurase Nitrogen Fixation S-like 1 (Nfs1) as well as the ABC transporter of the mitochondria 1 (Atm1) are necessary for FeS assembly in the cytosol. Soon it was speculated whether FeS clusters could pass the mitochondrial membrane via Atm1 and what type of cluster could be transported (Beinert, 2000b). However, many years later it was found that the iron accumulation is due to a defect in iron sensing: A FeS cluster is needed to suppress the transcription factor activator of ferrous transport (Aft) 2 and its paralog Aft1 which, when active, upregulate Fe uptake genes (Poor et al., 2014; Ueta et al., 2012).

Similar observations were made in plants: In 2009, (Bernard et al.) found that mutants of the Arabidopsis Atm1 homolog ATM3 mutants did not accumulate Fe in the mitochondria thus providing further evidence that the transported compound does not contain Fe. In 2013 (Bernard et al.) showed that cytosolic FeS assembly depends on the mitochondrial cysteine desulfurase NFS1 but not on the plastid NFS2 or cytosolic abscisic acid deficient 3 (ABA3).

Taken together, this indicates that the compound exported from the mitochondria by ATM3 is a persulfide derivative. Evidence has been found that suggests glutathione as a carrier for the sulfur: In 2002 (Sipos et al.) found that maturation of cytosolic FeS proteins in yeast was dependent on glutamate-cysteine ligase 1 (Gsh1) which is involved in glutathione biosynthesis. Four years later, Kim et al. (2006) showed that *atm3* mutants had elevated levels of non-protein thiols and increased GSH1 levels. Furthermore, glutathione has been linked to ABC transporters and heavy metal transport on several occasions (see for example (Kang et al., 2011; Raichaudhuri, 2016)). Recently, crystallography studies by the R. Lill and D. Rees groups found reduced glutathione bound to yeast Atm1 (Srinivasan et al., 2014) and oxidised or reduced glutathione to bacterial Atm1 (Lee et al., 2014b) in crystal structures.

Furthermore, Schaedler et al. (2014) provided *in-vitro* evidence for the transport of oxidised glutathione by yeast Atm1 and Arabidopsis ATM3. They proposed oxidised glutathione containing a S^0 (glutathione trisulfide) as the substrate of Atm1 and ATM3 and verified *in-vitro* transport of oxidised glutathione carrying a S^0 (GSSSG) for Atm1 by mass spectrometry.

Interestingly, ATM3 has been linked to molybdenum cofactor (MoCo) biosynthesis before (see Figure 1.1). Teschner et al. (2010) found that *atm3* mutants had lower MoCo levels and activity of MoCo enzymes was decreased while mitochondria accumulated the MoCo precursor cyclic pyranopterin monophosphate (cPMP). This points to a dual role of ATM3 in FeS assembly and MoCo assembly, however this still needs to be proven.

1.4. MoCo assembly

MoCo biosynthesis is best studied in bacteria and *Neurospora* but the plant homologues have also been characterised (see Figure 1.1). The first step of MoCo biosynthesis is carried out in the mitochondria by Cofactor of Nitrate reductase and Xanthine dehydrogenase (CNX) 2 and 3. CNX2 is a radical SAM enzyme and binds and activates 5'-GTP which is then converted into cPMP by CNX3 (Hover et al., 2013; Hover et al., 2015; Mendel and Kruse, 2012; Mendel and Leimkuhler, 2015). Radical SAM enzymes catalyse the FeS dependent reduction of SAM, generating a 5'-deoxyadenosyl 5'-radical which is critical for the initiation of various reactions. cPMP then enters the cytosol, however, it has not been resolved if it passes the membrane or if it is transported via ATM3. In the cytosol the next step is carried out by the heterotetramer formed of the large subunit CNX6 and the small subunit CNX7 which mediates the conversion of cPMP to molybdopterin (MPT). cPMP is bound to CNX6 while CNX7 mediates the 2-step sulfur transfer which is coupled to the cleavage of the cyclic phosphate group and is vital for the binding and coordination of the molybdenum. After donating sulfur, the CNX7 subunit is replaced by a sulfurated subunit. Bacterial MoaD and human MOCS2A are the sulfurtransferases in the respective organism and CNX7 is annotated as the homologue in plants according to uniprot.org, arabidopsis.org (as in August 2016) and (Mendel and Kruse, 2012). The resulfuration of CNX7 is mediated by CNX5.

Interestingly, CNX5 also donates sulfur for cytosolic tRNA thiomodification (Nakai et al., 2012).

Molybdenum insertion into MPT is mediated by CNX1 in an ATP dependent manner. CNX1 has two distinct domains that are separate proteins in bacteria. The G-domain catalyses the formation of MPT-AMP which is necessary for the subsequent insertion of molybdenum by the E-domain. It has been proposed that all cytosolic components of the MoCo pathway form a complex that is anchored to actin filaments via CNX1 (Kaufholdt et al., 2016). The MoCo can be sulfurated which is necessary for xanthine dehydrogenase and aldehyde oxidase (see Figure 1.2). The sulfur for this modification is donated by the cytosolic cysteine desulfurase ABA3.

There are only 5 known MoCo enzymes in Arabidopsis (see Figure 1.2): There are two isoforms of xanthine dehydrogenase which is involved in purine metabolism (see above) and four isoforms of aldehyde oxidase which are involved in ABA and auxin metabolism (see above). Xanthine dehydrogenases and aldehyde oxidases are cytosolic and, in addition to MoCo, contain 2 Fe_2S_2 clusters and an FAD cofactor. In the peroxisome there is a sulfite oxidase which contains a MoCo as its only cofactor and is involved in sulfite detoxification (Eilers et al., 2001; Schrader et al., 2003). Nitrate reductase is located in the cytosol. It catalyses the first step of nitrate assimilation and contains MoCo, heme and FAD (Mendel and Kruse, 2012). Further MoCo enzymes are the mitochondrial amidoxime reducing component (mARC) 1 and 2 which are localised in the outer mitochondrial membrane and are involved in amidoxime metabolism in humans (Gruenewald et al., 2008; Havemeyer et al., 2006; Klein et al., 2012; Plitzko et al., 2013) and homologs are also found in the outer mitochondrial membrane and cytosol of Arabidopsis. However, the exact function in plants remains unclear. MoCo assembly and FeS assembly are not only linked by the FeS clusters in CNX2 and the function of ATM3 but also by the usage of both cofactors in aldehyde oxidase and xanthine dehydrogenase (Figure 1.2).

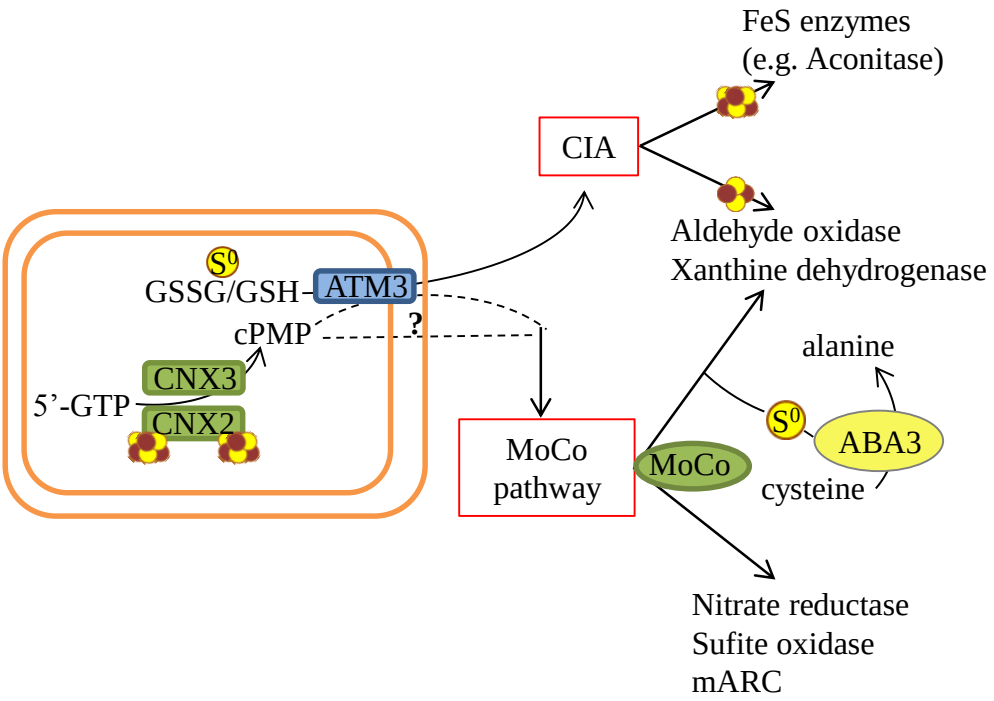

Figure 1.2 Links between FeS assembly and MoCo assembly in plants. ABA3 = ABA-deficient 3; ATM3 = ABC Transporter of the Mitochondria 3; CIA = Cytosolic Iron-sulfur protein Assembly; CNX = Cofactor of Nitrate reductase and Xanthine dehydrogenase; cPMP = cyclic pyranopterin monophosphate; GSH/GSSG = reduced/oxidised glutathione; GTP = guanosine triphosphate; mARC = mitochondrial amidoxime reducing component; MoCo = Molybdenum cofactor; MPT = Molybdopterin; Dashed arrows indicate unknown/proposed steps.

1.5. Sulfur metabolism in the mitochondria

Little is known about sulfur metabolism in plant mitochondria (see Figure 1.3). The protein bound zero-valent form of an additional sulfur is referred to as S^0 while an additional sulfur bound to a protein is referred to by adding the suffix -persulfide. This is only a formal denominator as S^0 is always protein bound and does not exist on its own (Beinert, 2000b). However, sulfur in this form is necessary for FeS assembly as it needs to be reduced to sulfide in the process of cluster formation. As described above the mobilisation of S^0 from cysteine is mediated by NFS1 which is used for FeS assembly in the mitochondria and possibly exported by ATM3. Thus, FeS assembly but also FeS turnover in the mitochondria contribute to sulfur metabolism. Cysteine can be transported from and to the cytosol (Lee et al., 2014a) and sulfide in the form of H_2S can freely pass the mitochondrial membrane (Jacques, 1936; Mathai et al., 2009) and thus can enter the mitochondria from the cytosol. Free

sulfide in the cell is in equilibrium between the forms $S^{2-} \leftrightarrow HS^{-} \leftrightarrow H_2S$. Strong basic conditions shift the equilibrium to S^{2-} which acts as a base but it is easily converted to gaseous H_2S under acidic conditions.

Sulfide has been found to inhibit Complex IV activity in mammals (Dorman et al., 2002; Leschelle et al., 2005; Li et al., 2011; Szabo, 2007) and plants (Allam and Hollis, 1972; Birke et al., 2012) and thus a tight regulation is vital. In bacteria, archaea and eukaryotes, but excluding plants, sulfide quinone reductase is also involved in sulfide detoxification mediating the generation of polysulfides from sulfide with the help of quinone (Griesbeck et al., 2002; Marcia et al., 2010). Inside the mitochondria sulfide is generated when sulfur-containing amino acids are broken down, in plants for example during senescence, extended darkness or short day conditions. The sulfur dioxygenase ETHylmalonic Encephalopathy protein 1 (ETHE1) is essential for detoxification of excess sulfide under these conditions (Tiranti et al., 2009) and uses glutathione as a cofactor. During cysteine catabolism, cysteine is converted to 3-mercaptopyruvate by a transaminase and the sulfhydryl group is transferred to reduced glutathione by sulfurtransferase 1 which releases glutathione-persulfide. The sulfhydrylgroup is then oxidised by ETHE1 which releases sulphite and reduced glutathione. Sulfite is converted into thiosulfate by sulfurtransferase 1 using an additional sulfur from glutathione-persulfide (Hofler et al., 2016; Holdorf et al., 2012; Krussel et al., 2014; Tiranti et al., 2009). Although the main substrate of ETHE1 is primarily formed in the process of amino acid degradation, free sulfide and glutathione in its oxidised form are also thought to form glutathione persulfide non-enzymatically or by means of an unknown enzyme (Birke et al., 2015; Krussel et al., 2014). Sulfide is also released during cyanide detoxification, where cyanide is incorporated into cysteine by beta-cyanoalanine synthase forming beta-cyanoalanine (Miller and Conn, 1980). Sulfide is incorporated into O-acetylserine to form cysteine which is mediated by O-acetylserine (thiol) lyase C (OASTLC) (Birke et al., 2012). The O-acetylserine is formed by serine-acetyltransferase from serine and acetyl-CoA (Wirtz and Hell, 2006).

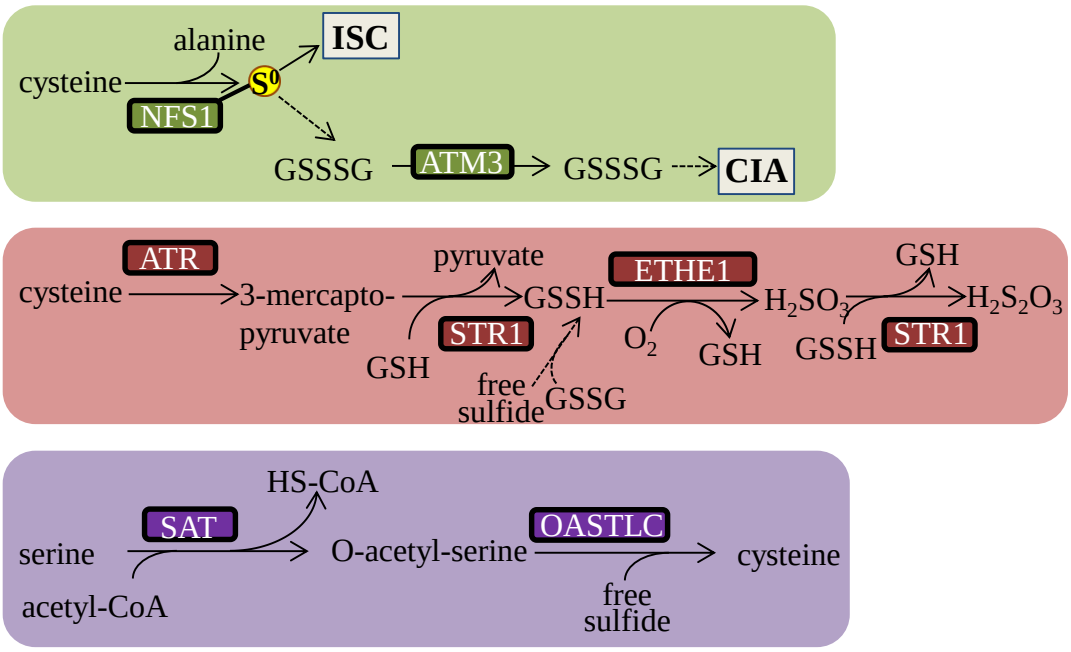

Figure 1.3 ATM3, NFS1, ETHE1, OASTLC and their role in mitochondrial cysteine metabolism. CoA = coenzyme A, SAT = serine-acetyltransferse, OASTLC = O-acetylserine(thiol)lyase C, NFS1 = nitrogen fixation S (NIFS)-like 1, ATM3 = ABC-transporter of the mitochondria 3, ATR= aminotransferase, STR = sulfurtransferase, ETHE1 = ethylmalonic encephalopathy protein 1, ISC = mitochondrial iron sulfur cluster pathway, CIA = cytosolic iron-sulfur protein assembly machinery.

1.6. Glutathione and glutaredoxins

Glutathione together with ascorbate is vital for the maintenance of the redox balance in the cell (Foyer and Noctor, 2011). Glutathione as well as glutaredoxins are also important in other processes like heavy metal detoxification, stress responses and protein regulation (Rouhier et al., 2008). Glutathione biosynthesis is carried out by the function of two enzymes: The first step is the generation of gamma-L-glutamyl-L-cysteine from glutamate and cysteine and is mediated by GSH1 in the plastids. The second step is mediated by glutathione synthetase (GSH2) which incorporates glycine into gamma-L-glutamyl-L-cysteine to form glutathione (Noctor et al., 1998) (see Figure 1.4). This step is thought to be mainly localised in the cytosol. Glutathione mainly acts as a reducing agent and is regenerated by the action of glutathione reductases.

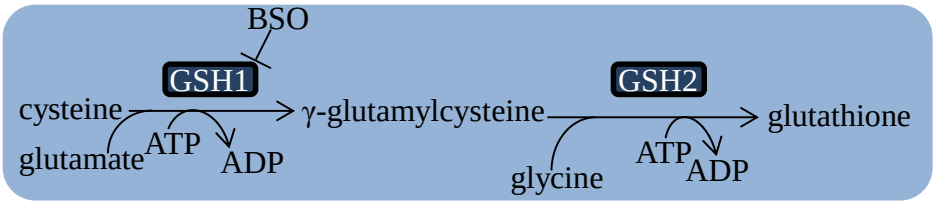

Figure 1.4 Glutathione biosynthesis in plants. BSO = buthionine sulfoximine, a competitive inhibitor of GSH1; GSH1 = glutamate-cysteine ligase 1; GSH2 = glutathione synthetase

It is important for the cell to maintain a high GSH:GSSG ratio which can also be accomplished by *de-novo* synthesis. Transport of oxidised glutathione from the cytosol to the vacuole has been suggested to contribute to the redox balance in the cytosol and several glutathione breakdown processes are also considered with specificity of the different enzymes to reduced or oxidised glutathione (Noctor et al., 2012).

As described above, glutathione is involved in sulfide detoxification and is also thought to be involved in the export of a sulfur component from the mitochondria into the cytosol for FeS assembly. Class II (monothiol) glutaredoxins are characterised by their active site motif (CGFS) and have been thought to be involved in FeS assembly for a long time (Couturier et al., 2013). The phenotype of Δ*grx5* mutants of the yeast *Saccharomyces cerevisiae* was found to be complemented by overexpression of genes involved in FeS assembly and Δ*grx5* mutants showed inactivation of FeS enzymes (Rodriguez-Manzaneque et al., 2002). Furthermore Grx5 was found to be required for cluster binding on the FeS scaffold Isu1 (Muhlenhoff et al., 2003). Grx5 of *Schizosaccharomyces pombe* was shown to interact with the putative FeS scaffold proteins Isa1 and Isa2 *in-vivo* and mutants had decreased cytosolic and mitochondrial FeS enzyme activity which could be partially rescued by overexpression of putative scaffold proteins of the FeS assembly (Kim et al., 2010). In *E.coli*, *grxD* mutants showed synthetic lethality when combined with mutants of the isc operon (Yeung et al., 2011). In plants there is mostly *in-vitro* evidence, like the ability to transfer a FeS cluster to apoproteins (see for example (Wang et al., 2012; Xia et al., 2015; Zhang et al., 2013)). Furthermore monothiol glutaredoxins, including Arabidopsis isoforms, have been shown to complement the Δ*grx5* phenotype of *S.cerevisiae*, however, it is not clear if plant glutaredoxins donate FeS clusters *in-vivo* as well (Couturier et al., 2015).

1.7. Objectives of this study

The aim of this study was to give further insight into the connection between the mitochondrial and cytosolic FeS assembly represented by NFS1 and ATM3. *In-vivo* experiments were conducted to provide evidence for oxidised glutathione carrying S^0 as a substrate of ATM3 to support the *in-vitro* evidence presented in Schaedler et al. (2014). In Chapter 3 I present roGFP measurements to investigate if oxidised glutathione specifically accumulates in *atm3* mutant mitochondria. In Chapter 4 I present the results of genetic interaction studies between *ATM3* and other components of mitochondrial sulfur metabolism. Many steps of the sulfur export from the mitochondria for the cytosolic FeS assembly remain unknown like the generation of the glutathione-sulfur compound and the delivery to and from ATM3. Thus I investigated the possible role of glutaredoxins in FeS assembly pathways (Chapter 5). In addition I also characterised mutants with a phenotype resembling *atm3* mutants in an attempt to identify new components of the cytosolic-mitochondrial FeS assembly (Chapter 6).

2. Materials and methods

2.1. Bioinformatics; databases, alignments, transmembrane helix prediction

2.1.1. Databases

Arabidopsis thaliana	http://www.arabidopsis.org/
Arabidopsis thaliana Ler-0 genome	http://mus.well.ox.ac.uk/19genomes/
Protein sequences	http://www.uniprot.org/
	http://www.ncbi.nlm.nih.gov/protein/

2.1.2. Alignments

Amino acid alignments were performed using the BLAST programme hosted at http://www.uniprot.org/ or http://www.ncbi.nlm.nih.gov/protein/.
Nucleic acid alignments were performed using ClustalOmega hosted at http://www.ebi.ac.uk/Tools/msa/clustalo/. Sequence similarities were highlighted using BoxShade hosted at http://www.ch.embnet.org/software/BOX_form.html (Kay Hofmann & Michael D. Baron).

2.1.3. Transmembrane helix predictions

Transmembrane helix predictions were performed using the following programmes:
TMPred hosted at http://www.ch.embnet.org/cgi-bin/TMPRED_form_parser
DAS hosted at http://www.sbc.su.se/~miklos/DAS/tmdas.cgi
TMHMM2 hosted at www.cbs.dtu.dk/services/TMHMM-2.0/
HMMTOP hosted at http://www.enzim.hu/hmmtop/server/hmmtop.cgi

2.2. Chemicals

All chemicals were obtained from Alfa Aesar (Heysham, UK), Amersham (Little Chalfont, UK), AMSBio (Abingdon, UK), Anachem (Luton, UK), Bio-Rad Laboratories Ltd (Hemel, Hempstead, UK), Biochem (Cosne-Cours-sur-Loire, France), DBC Foodservice (Petersfield, UK), Duchefa (Haarlem, Netherlands), Expedeon (Swavesey, UK), Formedium (Hunstanton, UK), Invitrogen ((Melford (Ipswich, UK)), Qiagen (Manchester, UK), Roche (Burgess Hill, UK), Sigma-Aldrich/Fluka (Dorset, UK), Starch Art Corporation (Smithville, US), Thermo Fisher Scientific/Acros (Loughborough, UK), VWR/BDH (Lutterworth, UK).

2.3. Bacterial Strains

Table 2.1 List of bacterial strains

Strain	Antibiotic resistance	Genotype	Source/Reference
E.coli			
BL21	n/a	B F^- *ompT gal dcm lon* $hsdS_B(r_B^- m_B^-)$ $[malB^+]_{K\text{-}12}(\lambda^S)$	Studier and Moffatt, 1986)
TOP10	Streptomycin	*F-mcrAΔ(mrr-hsdRMS-mcrBC)φ80lacZΔM15ΔlacX74nupGrecA1araD139Δ(ara-leu)7697galE15galK16rpsL(StrR) endA1 λ-*	Invitrogen (Thermo Fisher Scientific)
Stellar/ HST08	n/a	*F–, endA1, supE44, thi-1, recA1, relA1, gyrA96, phoA, Φ80d lacZΔ M15, Δ (lacZYA - argF) U169, Δ (mrr - hsdRMS - mcrBC), ΔmcrA, λ–*	Clonetech
A.tumefaciens			
LBA4404	Rifampicin	pAL 4404; disarmed version of Ach5, *RifR*	(Hoekema et al., 1983)

2.4. Arabidopsis lines and growth conditions

Table 2.2 List of Arabidopsis lines

Line	Ecotype	Reference
atm3-1	C24 backcrossed to Col-0	Kushnir et al., 2001 Bernard et al., 2009
atm3-3	Col-0	Bernard et al., 2009
atm3-4	Col-0	Bernard et al., 2009
ethe1-1	Col-0	Krussel et al., 2014
ethe1-3	Col-0	Krussel et al., 2014
grxS15-1	Col-0	Cheng et al., 2008 Stroher et al., 2015
grxs15-3 UBQ10:GRXS15 K83>A	Col-0	Moseler et al., 2015
grxS15 amiRNA	Col-0	Stroher et al., 2015
grxS17 knock-out	Col-0	Alonso et al., 2003 Cheng et al., 2011
grxS17 "C3" +GRXS17	Col-0	Knuesting et al., 2015
grxS17 "C17" +GRXS17	Col-0	Knuesting et al., 2015
nfs1-1	Col-0	Bernard et al., 2013
oastlC	Col-0	Heeg et al., 2006
xd22, xd31, xd32, xd54, xd105 xd442, xd460, xd576, xd724	Ler	Zhao et al., 2003 Dai et al., 2005 Kahlfeldt, 2006

Unless stated otherwise, the Arabidopsis lines were grown after 48 hours of vernalisation at 4°C under standard conditions, 16 hours light, 8 hours dark, 22°C at a light intensity of 180-200 µmol photons m^{-2} s^{-1} (growth on soil) or 120-160 µmol photons m^{-2} s^{-1} (growth on plate). Plants for mitochondria isolation were grown under short day conditions (8 hours light, 16 hours dark).

For growth on plates seeds were surface sterilised by incubation in a desiccator with chlorine gas released from a mixture of 100 ml Parazone thick bleach with 6 ml 5 M HCl. Seeds were sterilised for 3-4 hours and excess chlorine gas was allowed to volatise in a laminar flow hood under sterile conditions. Unless stated otherwise seeds were grown on 0.8% agar plates containing ½-strength Murashige and Skoog salts. Plants transformed with *A.tumefaciens* were isolated on plates containing 25 µM hygromycin.

Soil grown plants were grown on Levington's F2 (Levington Horticulture, Ipswich, UK).

Hydroponic cultures for mitochondria isolation were grown in 250 ml flasks containing 50 ml of ½ MS containing 0.5 g/l MES. 0.15% agar and 1% sucrose (w/v) at pH5.8. Seeds were surface sterilised and vernalised as described above. Samples were grown in a controlled environment chamber for 2 days without shaking and for further 7-11 days at 70 rpm.

2.5. Root callus cultures from Arabidopsis seedlings

Roots from 10-14-day-old plate-grown plants were placed on callus induction plates containing 0.8% agar. Roots were sliced with a sterile razor blade and incubated for 3-4 weeks under standard growth conditions. Formed callus tissue was then replaced on fresh callus induction plates without transferring original root material. Calli were subcultured every 3-4 weeks.

2.6. Media and antibiotics

Table 2.3 List of antibiotics

Antibiotic	Concentration (µg/ml)	Solvent	Target organism
Carbenicillin	100	H_2O	Gram negative bacteria
Gentamycin	50	H_2O	Gram negative bacteria
Kanamycin	50	H_2O	Bacteria, fungi, plants
Rifampicin	25	DMSO	Bacteria
Hygromycin	25	H_2O	Bacteria, fungi, plants

Table 2.4 List of media

Medium	**Components (per l of medium)**
Luria-Bertani Broth (LB) for bacterial cultures	10 g tryptone, 5 g yeast extract, 10 g NaCl, pH 7.0, 1.5% agar (w/v) for solid medium
Super Optimal broth with Catabolite repression (SOC) for bacterial cultures	20 g tryptone, 5 g yeast extract, 0.5 g NaCl, 0.186 g KCl, 20 mM glucose, 2 mM $MgCl_2$, pH 7.0
Yeast-peptone broth (YEP) for bacterial cultures	10 g yeast extract, 10 g peptone, 5g NaCl, pH 7
½ strength Murashige & Skoog medium from Duchefa) for plant growth (½ MS)	https://www.duchefa-biochemie.com/product/details/number/M0221
Callus induction medium	3.86 g Gamborg's B5 medium including vitamins, 20 g glucose, 0.5 g 4-morpholinoethanesulfonic acid (MES), 0.5 mg 2,4-dichlorophenoxyacetic acid, 0.05 mg kinetin, pH 5.7 Kinetin stock (1mg/ml) was prepared in 1M KOH 2,4-dichlorophenoxyacetic acid stock was prepared by dissolving 10 mg in 1 ml ethanol and 1 ml 0.1M KOH. After complete dissolution dH2O was added to a final concentration of 1 mg/ml in 0.01M KOH.

2.7. Antibodies

Table 2.5 List of antibodies

Antigen	Source	Dilution	Observed size	Source
Aconitase	Rabbit	1:5000	98 kDa	Agrisera
Actin	Mouse	1:1000	45 kDa	Affinity bio reagents
ATM3	Rabbit	1:1000	70 kDa	F. Bittner, University of Braunschweig
Biotin Strep-Tactin® HRP conjugate		1:100000	various	IBA-lifesciences
ETHE1	Rabbit	1:2000	28	J. Balk, John Innes Centre
GRXS15	Rabbit	1:1000	15	N. Rouhier, UMR, University of Lorraine
H-Protein	Rabbit	1:1000	various	Olivier Keech, University of Umeå
Lipoate	Rabbit	1:3000	various	Abcam
PsaA	Rabbit	1:1000	60 kDa	Agrisera
Secondary HRP-conjugated, anti-rabbit or anti-goat	Goat	1:5000	n/a	Biorad
TOM40	Rabbit	1:2000	36 kDa	J. Whelan, University of Western Australia

2.8. Oligonucleotides

Oligonucleotides were from Sigma-Aldrich Ltd (Haverhill, UK, http://www.sigmaaldrich.com/united-kingdom.html) or Eurofins (Ebersberg, Germany) and used at a concentration of 10 μM.

Table 2.6 Primers used for reverse transcriptase PCR

Oligonucleotide	**Gene**	**5'-3' sequence**
CNX2_RT_F1	*CNX2*	TAATTTCCCTTAGCGCCTCA
CNX2_RT_R1		CTTTACGATCGATGGGCATT
ATM3_RT_F1	*ATM3*	TTGAGTGGTGGAGAGAAACAAA
ATM3_RT_R1		TCCCGTTTTCCAGTACTACGAT
RTPCR-ACT2F2	*Actin*	CCCAAAGGCCAACAGAGAGA
RTPCR-ACT2R2		ACCATCACCAGAATCCAGCA

Table 2.7 List of primers for genotyping

mutant	**genotype**	**Oligonucleotide**	**5'-3' sequence**
ethe1-1/ ethe1-3	wild type	ETHE1_LP2	CTCTTGACCTAAACCGTGGAG
		ETHE1_RP	CAGTCTTGTCCACCGGATCAAT
	T-DNA	LBb1.3	ATTTTGCCGATTTCGGAAC
		ETHE1_RP	
atm3-1	wild type	ATM3_F3	GACATCACAAATACAAGTGACGC
		ATM3_R6	TTAGATGCTTAAACAGAAGAGG
	T-DNA	ATM3_F3	
		NPTII-R2	CATAGCCGAATAGCCTCTCC
cnx2-1	wild type	CNX2_RP	CTCAAGTTGGTTGCTTTTTCG
		CNX2_LP	TTTGAAGTTCCCATCTGCAAG
	T-DNA	CNX2_RP	
		LBb1.3	
cnx2-2: BsaWI digest: 3 bands for wild type, 2 bands for *cnx2-2*		gentCNX2endog F	CGATTTCATAACCCTATCATGCCCTT
		gentCNX2endog R	AGAAACTAGATTTGCATACCTGGT
CNX2 complementation construct		gentcnx2trans F	CGGTCTGGTGCTGATGATGA
		gentcnx2trans R	TAAAGTGCCCCTGATGATGAGATTTTCTTAAA

Table 2.8 List of primers used for mapping

Oligonucleotide	5'-3' sequence
AT1G07810 F	GTTCACGGACAAAGAGCCTGAAAT
AT1G07810 R	AAGCAGTCAATATTGCAGGAAGGG
AT1G49610 F	ACATTTTCTCAATCCTTACTC
AT1G49610 R	GAGAGCTTCTTTATTTGTGAT
AT1G72650 F	TGTTTTTTAGGACAAATGGCG
AT1G72650 R	CTCCAGTTGGAAGCTAAAGGG
AT1G09940 F	TCATGACGTGAAGAAGAAGAAAA
AT1G09940 R	CATATCGCTGCTACTAATTTTAAACAA
AT2G04066 F	GGGATAATGGATAGGACTCACG
AT2G04066 R	GCTGAGAAGGCAAGGAAGAG
AT2G14890 F	GAAACTCAATGAAATCCACTT
AT2G14890 R	TGAACTTGTTGTGAGCTTTGA
AT2G39010 F	TCGTCTACTGCACTGCCG
AT2G39010 R	GAGGACATGTATAGGAGCCTCG
AT3G11220 F	GGATTAGATGGGGATTTCTGG
AT3G11220 R	TTGCTCGTATCAACACACAGg
AT3G26605 F	CCCCGAGTTGAGGTATT
AT3G26605 R	GAAGAAATTCCTAAAGCATTC
AT3G50820 F	GTTCATTAAACTTGCGTGTGT
AT3G50820 R	TACGGTCAGATTGAGTGATTC
AT4G01710 F	AGATTTACGTGGAAGCAAT
AT4G01710 R	GGTTAAAAATTAGGGTTACGA
AT4G10360 F	GCCAAACCCAAAATTGTAAAAC
AT4G10360 R	TAGAGGGAACAATCGGATGC
AT4G29860 F	GCCCAGAGGAAGAAGAGCAAACTAGC
AT4G29860 R	TGGGAATTCATGAGAGAATATGTGGGAC
AT5G22545 F	TAGTGAAACCTTTCTCAGAT
AT5G22545 R	TTATGTTTTCTTCAATCAGTT
AT5G42600 F	CAGACGTATCAAATGACAAATG
AT5G42600 R	GACTACTGCTCAAACTATTCGG
AT5G63640 F	ATCACTGTTGTTTACCATTA
AT5G63640 R	GAGCATTTCACAGAGACG
AT2G21420 F	GATGCCTTTCTCCTGGTTG
AT2G21420 R	AATATAGCCGTCGTCTTCATCA
AT2G31070 F	AAAGAGATGAGAATTTGGAC
AT2G31070 R	CATATCAATATATTAAAGTAGC
AT2G44798 F	TGTTCTTCACTTTGCAAACCA
AT2G44798 R	GTGGCAAATGGGCTAAACTA
AT2G29995 F	CTGCATATTGTTAATGAGAAAAGAAT
AT2G29995 R	TCATGTCGAAAACATATAATTGAGC

Table 2.9 Primers used for sequencing

Oligonucleotide	5'-3' sequence
ATM3_IK1F	TTTGCTTCGAGGACCCATAC
ATM3_R4	GATGGTGAGTTATCTGAGAGG
GKPrimer	GCTCTTACTCTGTCGCGTTAATCT
ATM3_IK3R	TGAAAGTTGAAGAGAATGTATGAAGA
ATM3_IK2F	TCTTTGGATCGGCTTAAATCA
STA1_R1	GCGTCACTTGTATTTGTGATGTC
ATM3_F3	as above
ATM3_R5	CTTGGAAGCCTGATTGACTTAGC
ATM3_IK4F	AGGGGGCTCAAGGTCAGTAT
ATM3_R1	CACTATTCCAATTTGATAGCTGC
ATM3_F2	GCAGCTATCAAATTGGAATAGTG
ATM3_R3	CACCACTGAGTCCAGCTCTTCTACC
ATM3_IK2F	as above
ATM3_R6	as above
CNX2_R1	TTTCCTCTGTTTTTCGTTTCTG
CNX2_F2	GGAGCTTAGCCACCAATGTG
CNX2_R2	CCGGTTCATCGAGTTTATGC
CNX2_F3	GGGTGATCTTGCATTCGTTT
CNX2_R3	CCGTCTGAAGGTGTGGAACT
CNX2_F4	CCACCAGTCAACCGAATCTT
CNX2_R4	GGCTTTTAGCCAAACTCTCTC
CNX2 R5	TGTGAAGCTAGACAGATATGCAAAAAACCATTC
pUCAP F3	GAGTCAGTGAGCGAGGAAGC
pUCAP rev	GATTTGTAGAGAGAGACTGGTG

2.9. Molecular methods

2.9.1. Nuclei extraction from Arabidopsis leaves

Adapted from the user manual of the SIGMA nuclei purification kit. For extraction of nuclei from Arabidopsis leaves 2-3 g of leaf material from 80-100 plants was collected and immediately frozen in liquid nitrogen. The frozen material was ground at least three times in a mortar and pestle with liquid nitrogen, resting on dry ice. After evaporation of the liquid nitrogen leaf material was transferred into a 50 ml falkon tube with 50 ml of ice-cold NIBPlus and homogenised by inversion. The supernatant was filtered through a 100 µm filter into a precooled 500 ml conical

flask. 1.6 ml of 10% Triton X-100 (v/v) in NIB was added and the mixture was incubated on ice for 10 minutes and swirled every 2 minutes. The lysate was then spun down at 2753xg for 15 minutes at 4°C. The supernatant was discarded and the pellet was resuspended by swirling in 2 ml ice-cold NIB with freshly added dithiothreitol and protease inhibitor cocktail. The sample was then split equally over five 2-ml reaction tubes and spun down in a benchtop centrifuge at 2753xg for 5 minutes at 4°C. the supernatant was discarded and 600 µl of protein precipitation buffer (QIAGEN Puregen kit) was added to each pellet and homogenised by pipetting. Samples were incubated at 65°C for 60 minutes and cooled down to room temperature afterwards. 2 µl of RNAse One (10 mg/ml, DNAse free, Promega) were added to each tube and inverted 25 times. Samples were incubated at 37°C for 40-60 minutes and cooled down to room temperature afterwards. 200 µl of protein precipitation solution (QIAGEN Puregen kit) were added and samples were spun at 16100xg for 3 minutes at room temperature. Each supernatant was added to fresh tubes containing 750 µl isopropanol and inverted 50 times. The DNA was then centrifuged at 16100xg for 5 minutes at room temperature. The supernatant was discarded and the pellet washed with 70% ethanol (v/v) and spun as before. All ethanol was allowed to evaporate before reuspending the samples in 60 µl of TE buffer.

Table 2.10 Buffer for nuclei extraction

Buffer	**components**
Nuclei isolation buffer (NIB)	10 mM MES, 0.2 M sucrose, 0.01% Triton X-100 (v/v), freshly added: 1 mM dithiothreitol (DTT), protease inhibitor cocktail (Roche) pH 5.3
NIBPlus	NIB, 0.1 mM phenylmethylsulfonyl fluoride (PMSF)
Tris-EDTA buffer	10 mM tris(hydroxymethyl)aminomethane (Tris) (pH 8.0), 1mM ethylenediaminetetraacetic acid (EDTA)

2.9.2. DNA extraction from Arabidopsis leaves or callus material

Tissue was frozen in liquid nitrogen and ground with a mini pellet-pestle in 1.5 ml reaction tubes. 500 µl of extraction buffer (0.2 M Tris, 0.4 M LiCl, 25 mM EDTA, 1% sodium dodecyl sulfate (SDS), pH 8.0) was added and mixed by inversion. Samples were centrifuged for 10 minutes at 16100xg and room temperature. 400 µl of supernatant were transferred to fresh tubes containing 400 µl isopropanol and mixed by inversion. Samples were centrifuged as before and the supernatant was discarded. The pellet was washed with 70% ethanol (v/v) and spun as before and the supernatant was discarded. All ethanol was allowed to evaporate before dissolving the pellet in 100 µl TE buffer (see above).

2.9.3. DNA extraction from bacteria

Bacterial material was dissolved in 10 µl dH_2O and incubated at 95°C for 10 minutes. Debris was removed by centrifugation in a benchtop centrifuge at 16100xg and 2 µl of the supernatant was used for polymerase chain reaction.

2.9.4. RNA extraction from Arabidopsis seedlings

RNA from Arabidopsis seedlings was performed using the RNeasy Plant Mini Kit (Qiagen) kit according to the manufacturer's instructions.

2.9.5. cDNA synthesis and reverse transcriptase DNA

1-2.4 µg of RNA were used for cDNA synthesis with equal amounts for samples of the same set. Samples were mixed with 0.7 µl dT(20)VN primer (Eurofins) in a total volume of 12 µl and incubated for 5 minutes at 70°C. Samples were cooled and centrifuged briefly to collect condensation. 4 µl of 5xRT buffer (M-MLV Reverse Transcriptase kit, Invitrogen) 2 µl 10 mM dNTPs and 1 µl RNAse OUT (Invitrogen) were added and samples were incubated for 5 minutes at 37°C. 0.8 µl reverse transcriptase enzyme (M-MVL Reverse Transcriptase kit, Invitrogen) were added.

The sample was incubated for 60 minutes at 42°C followed by 10 minutes at 70°C. 1 µg RNA was used per 25 µl PCR reaction.

2.9.6. Polymerase chain reaction

Genotyping PCRs were performed using a *Thermus aquaticus* EcoTaq-polymerase. Expression in *E.coli* and purification was performed by Bahattin Tanyolac (Alison Smith's lab, University of Cambridge) and Janneke Balk (University of Cambridge; John Innes Centre, Norwich) using a pUC18 expression vector according to (Desai and Pfaffle, 1995).

Reactions were carried out intaq-buffer (16 mM ammonium sulfate, 67 mM Tris (pH 8.8), 0.01% Tween-20) containing 0.2 mM dNTPs, 5 pmol of each primer, 0.5-2 µl template (depending on DNA concentration and quality) and 0.2 µl Eco-taq. PCR reactions were performed based on the publication by (Sambrook et al., 1989). The standard protocol started with an initial denaturation step for 3 minutes at 95°C followed by 30 to 35 cycles of 95°C for 30 seconds, 40 seconds at the appropriate annealing temperature and elongation at 72°C for 60 seconds per 1 kbp of product. After the last cycle a final incubation at 72°C for 3 minutes followed. Unless otherwise stated, the annealing temperature was chosen as the melting temperature T_M minus 1 °C of the primer with the lower T_M.

The PCR reaction for the detection of the *atm3-1* T-DNA and wild-type product was an adapted protocol with the denaturing temperature changed to 94°C, 32 cycles and a elongation time of 1:10 minutes and a final incubation time of 7 minutes. The detection of the wild type DNA in the locus of the *atm3-1* T-DNA was similar to the T-DNA amplification protocol but with 1:20 of elongation time and 35 cycles.

Reverse transcriptase PCRs were performed using the phusion taq-polymerase as described in the manufacturer's instructions (New England Biolabs). For the amplification of the *CNX2* genomic sequence for subsequent ligation into the pUCAP plasmid, the HiFi taq-polymerase of the Clonetech infusion kit was used according to the manufacturer's instructions.

2.10. Map based cloning and whole genome sequencing

Coarse mapping was performed as described in Chapter 6.7. RNAse treated nuclear DNA of mutant plants from the mapping population was send to TGAC (Norwich Research Park) for Whole Genome Sequencing. This was performed on the Illumina GAIIx platform with 80 bp paired-end reads and expected ≥40x coverage.
The SNPs were filtered for EMS mutant exchanges (G>A, C>T) and a stringent level of homozygosity was applied (>90% of reads supporting the variant). This identified 2065 SNPs genome wide and 54 within the mapping interval (Chromosome 2, ~12799630-16291977).

2.11. Whole genome sequencing analysis

The initial alignment of the whole genome sequencing data against the Landsberg reference genome was performed by (1) Martin Trick (TGAC, Norwich) using the Integrative Genomics Viewer (Robinson et al., 2011; Thorvaldsdottir et al., 2013) hosted on http://software.broadinstitute.org/software/igv/ in combination with the Bowtie program (Langmead et al., 2009) hosted on http://bowtie-bio.sourceforge.net/index.shtml and (2) Zamin Iqbal (University of Oxford) using the Cortex software (Iqbal et al., 2012) hosted on http://cortexassembler.sourceforge.net/index.html. The Landsberg reference genome was obtained from http://mus.well.ox.ac.uk/19genomes/fasta/MASKED/ and *de-novo* annotation for the Integrative Genomics Viewer analysis was obtained from http://mus.well.ox.ac.uk/19genomes/annotations/denovo_annotation_9.4.2011/. The analysis of the whole genome sequencing data is described in Section 6.7.

2.11.1. Genotyping of plant mutants and transformed bacteria

For genotyping the oligonucleotides were used as listed under Section 1.11. T-DNA insertion mutants were analysed by PCR amplification of a region spanning one border of the insertion site and part of the genomic DNA and the T-DNA to test for the insert. To test for the absence of wild type DNA PCR amplification of a region spanning both borders of the insertion site resulting in a band for the wild type

genotype which was absent for the homozygous mutant. For the *cnx2-2* point mutation the PCR product spanned the site of the mutation. Digest with BsaWI resulted in 3 products for the wild type and two products for the mutant as the mutation destroys one of two restriction sites.
The presence of transformed plasmids containing the *CNX2* sequence in bacteria was determined by PCR amplification of a part of the *CNX2* gene. The presence of the reintroduced gene by agrobacterium transformation in plants was distinguished from the endogenous gene by amplification with one primer in the *CNX2* sequence and one in the flanking residual Ti sequence.

2.11.2. Restriction digest

Restriction digest for genotyping and cloning was performed according to the instructions given by the supplier (New England Biolabs).

2.11.3. Agarose gel electrophoresis

Agarose gel electrophoresis was performed in TAE (40 mM Tris , 20 mM Glacial Acetic Acid and 1 mM EDTA, Formedium) agarose-gels containing 0.04% ethidium bromide (w/v). For products between 300 and 2000 bp separation was performed in gels containing 1% agarose for 30-40 minutes at 100 V. For enhancing the resolution to distinguish between products smaller than 500 bp and/or a difference lower than 50 bp agarose content was 2-4% and the gels were ran at 80V until complete separation was achieved. The DNA bands were visualised by exposure to ultraviolet light using the Gel Doc 1000 system (Bio-Rad).

2.11.4. Cloning of PCR fragments into pUCAP and pBINH

For transformation of Arabidopsis *cnx2-2* plants the genomic *CNX2* sequence including UTRs and the promoter region was amplified with primers adding a 15 nucleotide overhang on both sides of the insert complementary of the sites flanking the insertion site in the pUCAP plasmid for E.coli transformation. The empty vectors

were amplified in *E.coli* TOP10 cells. The vector was linearised by restriction digest with HindIII and KpnI to remove the 35S promoter and translational enhancer sequence. Insertion of the sequence was performed using the Clonetech infusion kit according to the manufacturer's instructions but with the incubation time increased to 1 hour for ligation. The pUCAP plasmid containing the *CNX2* insert was transformed into E.coli Stellar cells for amplification. The amplified insert was then cut out by restriction digest with PacI and AscI. The pBINH plasmid was linearised by restriction digest with PacI and AscI. Ligation of the insert into the plasmid was performed using T4-ligase according to the manufacturer's instructions (Fermentas).

2.11.5. Plasmid extraction

Plasmid extraction of pUCAP plasmid (Mini) and the pBINH plasmid (Midi) were performed using the QIAGEN Plasmid Mini/Midi kits according to the manufacturer's instructions.

2.11.6. DNA sequencing

PCR products were excised from an agarose gel and purified using the QIAquick®Gel Extraction kit (Qiagen) according to the manufacturer's instructions. Sanger sequencing was performed by Eurofins (Ebersberg, Germany) (Sanger et al., 1977).

2.12. Transformation of organisms

2.12.1. *E. coli* transformation

For transformation of chemically competent *E.coli* 50 µl competent cells were mixed with ~5 ng of DNA and incubated on ice for 30 minutes. A heat shock was performed at 42°C for 60 seconds and samples were cooled on ice for 2 minutes afterwards. 450 µl of 37°C-warm SOC medium (see section 1.9) was added and incubated at 37°C and 200 rpm for 1.5 hours. Cells were pelleted, resuspended in

100 µl of supernatant and plated on appropriate antibiotic LB medium plates for incubation over night at 37°C.

2.12.2. *A. tumefaciens* transformation

50 µl of electro competent *A. tumefaciens* were thawed on ice and 10 µl of plasmid added. Electroporation was performed in a 2 mm electroporation cuvette with 25 µF capacitance, 2.4 KV voltage and 200 Ohm resistance for a pulse of 5 milliseconds. Cells were then resuspended in 1 ml LB medium and incubated in a 15 ml falcon tube for 2-4 hours at 28°C and 200 rpm. Cells were pelleted for 8 seconds at 16100xg and most of the supernatant was removed. The pellet was resuspended in remaining medium and plated onto LB agar containing rifampicin (bacterial selection), gentamycin (helper plasmid) and kanamycin (binary vector containing gene of interest). Colonies were picked for further growth and genotype analysis after 2 days of growth at 28°C.

2.12.3. Arabidopsis transformation

Electro competent A.tumefaciens were grown over night in 10 ml LB medium. The overnight culture was then diluted in 200 ml YEP containing rifampicin (bacterial selection), gentamycin (helper plasmid) and kanamycin (binary vector containing gene of interest) and grown for 24 hours at 28°C and 200 rpm. Cells were collected by centrifugation for 10 minutes at 4000xg and the pellet was dissolved in 200 ml 5% sucrose (w/v) and 0.05% silwet (v/v). Ripening siliques were removed from Arabidopsis plants and the remaining inflorescence was dipped in the bacteria solution for 20 seconds. Plants were contained in a plastic bag for increased humidity and incubated overnight in the dark. Plants were then transferred to a growth cabinet and the dip was repeated after 1 week. Seeds were collected after 3-4 weeks of the first dip. And after 3-4 weeks of the second dip.

2.13. Plasmids

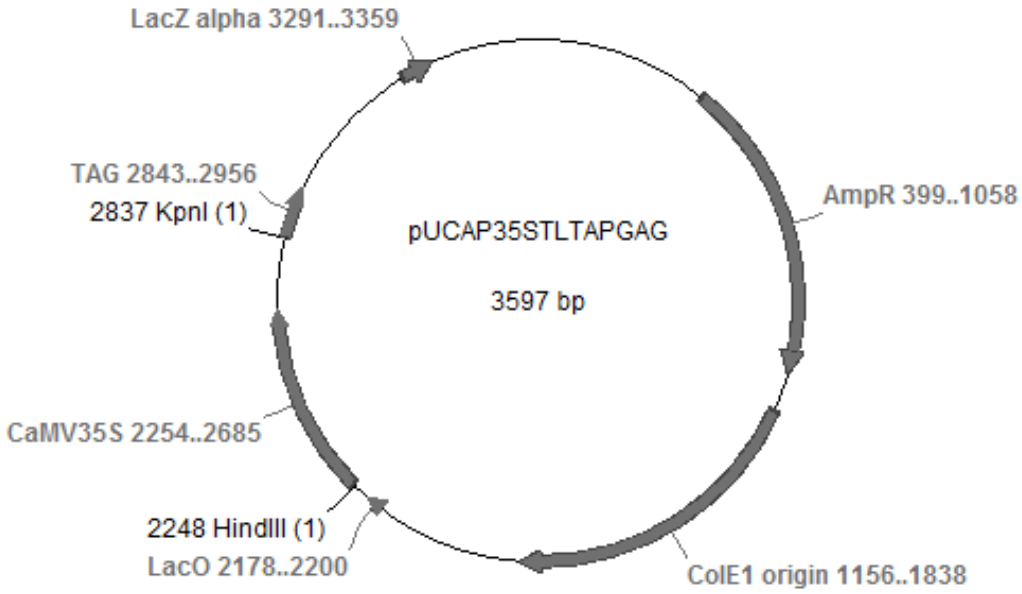

Figure 2.1 pUCAP plasmid map

Figure 2.2 pBinh plasmid map

2.14. Cross pollination of Arabidopsis plants

Flowers of the female parent were dissected before pollen was released, before opening of the flower. Flowers above and below the chosen female flower and the flower meristem were removed. Sepals, petals and anthers were removed using forceps and scissors that were cleaned of residual pollen with 100% EtOH. The pollination was performed using fully opened flowers visibly shedding pollen from the male parent. To access the pollen, the flower was opened by squeezing near the base. Siliques were contained in a paper bag and allowed to ripen fully before collecting the seeds.

2.15. Mitochondria extraction from leaves and hydroponic cultures

Mitochondria from soil grown Arabidopsis leaf material or hydroponic cultures were extracted essentially as described by (Sweetlove et al., 2007). Continuous Percoll density gradients were prepared on the same day in advance with 1 ml Percoll forming the bottom layer and 16 ml of heavy solution and 16 ml of light solution were mixed with a peristaltic pump. Plant material was harvested, washed and dried. All further steps were performed at 4°C. Homogenisation was performed in 4 volumes extraction buffer using a 2 cm polytron blender (2x3 seconds). The sample was filtered through 2 layers of muslin and 1 layer of miracloth and centrifuged for 5 minutes at 2000xg. The supernatant was transferred to a new tube and centrifuged for 20 minutes at 12500xg. The supernatant was discarded; the pellet resuspended in 1 ml 1xwashbuffer and the volume was made up to 15-20 ml per sample. Low and high-speed spins were repeated and the final pellet was resuspended in 1 ml 1xwash buffer and layered onto continuous Percoll density gradients. Gradients were centrifuged at 40000xg for 40 minutes with low break settings in a fixed angle rotor. Mitochondria were collected from the opaque white band in the lower third of the gradient. Mitochondria samples were washed twice with 1xwashbuffer by centrifugation for 20 minutes at 16000xg. Residual Percoll contaminations could be removed after transfer to a 1.5 ml reaction tube by washing with wash buffer at 16100xg for 2 minutes.

Table 2.11 Mitochondria extraction from leaves and hydroponic cultures

Buffer	Components
Extraction buffer	0.3 M sucrose, 25 mM $H_2Na_2P_2O_7$, 2 mM EDTA, 10 mM KH_2PO_4, 0.5 PVP-40 (w/v), 0.2% BSA, add fresh: 4 mM cysteine pH 7.5
2x wash buffer	0.6 M sucrose, 20 mM TES-KOH pH7.5
Light solution	50% volume 2x wash buffer, 0.2% BSA (w/v), 28% Percoll
Heavy solution	Heavy solution + 4.4% PVP40 (w/v)

2.16. Mitochondria extraction from callus cultures

Mitochondria were isolated essentially as described by (Leon et al., 2007). All steps were performed at 4°C. The callus material was homogenised with mortar and pestle in ~2 ml extraction buffer containing glass beads. Two layers of miracloth were used for filtration. Centrifugation as well as buffer composition was as described by (Leon et al., 2007).

2.17. Protoplast isolation

Protoplasts were prepared essentially as described by (Robertson et al., 1996).
Enzyme solution was prepared by shaking overnight in the dark and adjusting the pH to 5.6. Enzyme solution was then spun for 10 minutes at 3000xg and 4°C and the supernatant was filter sterilised.
Leaf material was cut into stripes, covered with enzyme solution and kept in the dark. Incubation was performed for 1 hour without movement followed by 1 hour at 40-70 rpm, followed by 1.5 hours without movement. Protoplast suspension was transferred into a new 50-ml Falcon tube without the leaf debris and mixed gently 1:1 with Mannitol/W5. Samples were centrifuged for 10 minutes at 30-50xg at room temperature with slow acceleration and deceleration. The supernatant was discarded and the protoplast pellet gently resuspended by rocking manually in a volume of Mannitol/Mg similar to Mannitol/W5. Protoplasts were washed twice with

Mannitol/Mg by centrifugation and resuspension as before and the final pellet was resuspended in a small volume of Mannitol/Mg depending on the yield.

Table 2.12 Buffers for protoplast isolation

buffer	**Components**
Enzyme solution	0.4 M mannitol, 3% sucrose (w/v), 8 mM $CaCl_2$, 1% cellulase (Gallard Schlesinger, "Onozouka" R10), 0.25% macerozyme (Serva, from *Rhizopus sp*. R10), pH 5.6
W5	5 mM glucose, 154 mM NaCl, 125 mM $CaCl_2$, 5 mM KCl, 1.5 mM MES, pH 5.7
W5/Mannitol	0.4 M mannitol, 0.2x W5, pH 5.7
Mannitol/Mg	0.4 M mannitol, 0.1% MES, 15 mM $MgCl_2$, pH 5.7

2.18. Protein determination

Protein measurements were performed using the Bio-Rad Protein Assay Dye Reagent Concentrate and the Pierce™ Bovine Serum Albumin (BSA) Standard Ampules (2mg/ml). 1-4 µl of sample were mixed with 100 µl of H_2O. 1 ml of 1x assay dye (1:5 dilution of concentrate) was added. Absorption at 595 nm was measured after incubation of ~5 minutes. Protein concentrations were determined using values of a BSA standard curve which was measured alongside for each sample set.

2.19. Native PAGE and enzyme activity staining of aldehyde oxidase and xanthine dehydrogenase

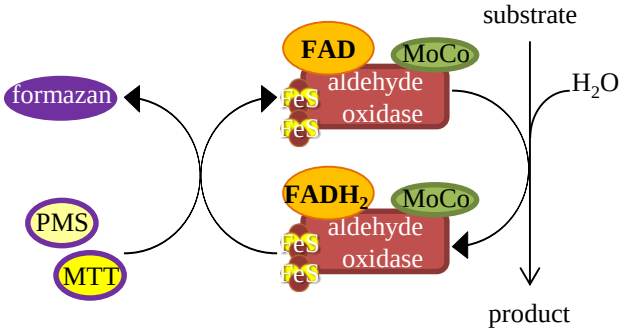

Figure 2.3 Reaction scheme of the aldehyde oxidase in-gel assay. MTT = thiazolyl blue tetrazolium bromide, PMS = phenazine methosulfate. The reaction is representative for the xanthine dehydrogenase assay as well as the reaction mechanism is identical.

Aldehyde oxidase activities were visualised in a native in-gel assay as described by (Koshiba et al., 1996) (see Figure 2.3). Four isoforms of aldehyde oxidase have been annotated for Arabidopsis which form homo- or heterodimers. (Akaba et al., 1999; Hoff et al., 1998; Sekimoto et al., 1998; Seo et al., 1998; Seo et al., 2000). These isozymes can be separated on a standard native gel. All steps were carried out at 4°C and using strictly detergent free components. Leaf material was homogenised in 1.5 volumes (w/v) extraction buffer (100 mM KP_i buffer, 5 mM DTT, 2 mM EDTA) using a mini pellet pestle. Samples were centrifuged for 10 minutes at 16100xg. The supernatant was transferred to a new tube, protein concentration was determined and samples were mixed with 1/10 volume of native gel loading buffer (2 M sucrose, 1% bromophenol blue (w/v)). For protein separation 35-100 µg of protein were loaded onto native gels (7.5% of 37.5:1 bisacrylamide in the separating gel). Gels and running buffer were prepared as for standard SDS-PAGE but omitting the SDS. Separation of protein was performed in a controlled environment room at 8°C and additional cooling of the running chamber with an ice pack. Proteins were separated at 150 V for 1.5 hours using a mini gel system (Hoeffer). After separation, gels were equilibrated in 100 mM KPi buffer pH7.4 (aldehyde oxidase) or 250 mM Tris buffer pH 8.5 (xanthine dehydrogenase) for 15 minutes. The buffer was replaced with 10 ml staining solution and staining was performed for 10-40 minutes. The reaction was stopped by washing the gel several times with H_2O.

Table 2.13 Staining solutions for aldehyde oxidase and xanthine dehydrogenase

Solution	Components
Aldehyde oxidase staining solution	in 10 ml 100 mM KPi buffer pH7.4: 4 mg 3-(4,5 dimethylthiazol-2-yl)-2,5-diphenyltetrazoliumbromide, 0.5 mg phenazine methosulfate, 3 mg 1-Naphthaldehyde, 3 mg Indole-3-(carb)oxaldehyde
Xanthine dehydrogenase staining solution	in 10 ml 250 mM Tris buffer pH 8.5: 4 mg 3-(4,5 dimethylthiazol-2-yl)-2,5-diphenyltetrazoliumbromide, 0.5 mg phenazine methosulfate, 5 mg hypoxanthine

2.20. Native starch PAGE and enzyme activity staining of aconitase

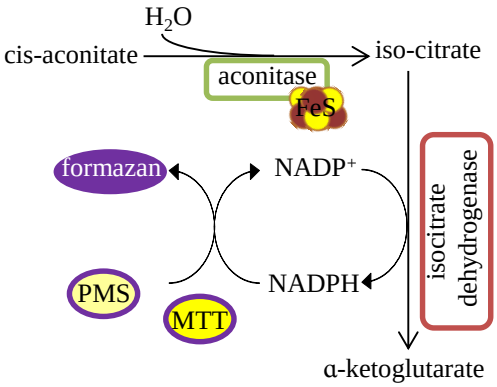

Figure 2.4 Reaction scheme of the aconitase in-gel assay. MTT = thiazolyl blue tetrazolium bromide, PMS = phenazine methosulfate.

In-gel activity assays for aconitase were performed essentially as described by (Bernard et al., 2009) (see Figure 2.4). Separation of protein was performed in a controlled environment room at 8°C and additional cooling of the running chamber with an ice pack. Proteins were separated at an initial 80 V for 20 minutes and when the sample entered the gel at 120 V for additional 3 hours and 20 minutes. Plant aconitase isoforms are very similar in molecular weight (98.15-108.48 kDa) and isoelectric point (6.36-7.17) (as annotated in the Arabidopsis.org database). Thus in this assay, the native proteins are separated on a starch gel which enables the separation of the three isoforms (Bernard et al., 2009). For activity staining, thiazolyl blue tetrazolium bromide and phenazine methosulfate are added which form a purple

precipitate upon reduction by NADPH. The colour formation is indicative of the enzyme activity and semi-quantitative.

2.21. Spectrophotometric measurement of aconitase activity

Aconitase activity in cell extracts and mitochondria was assayed in a spectrometric assay coupled to the activity of isocitrate dehydrogenase and the formation of NADPH as described by (Stehling et al., 2007). To obtain cytosolic fractions, leaf material was first homogenised on ice in 1.5x volumes of extraction buffer (0.6 M sorbitol, 50 mM Tris pH 8.0, 2 mM sodium citrate, 2 mM DTT, 1 mM EDTA) using a mini pellet pestle. The homogenate was then filtered through a cloth (Miracloth, 22-25 µm pore size) by centrifugation for 10 minutes at 4°C and 16100xg. The supernatant was retrieved and is enriched in cytosol. Absorption was measured at 340 nm.

2.22. Spectrophotometric measurement of nitrate reductase activity

Nitrate reductase activity was measured essentially as described in (Redinbaugh and Campbell, 1983). Leaf samples were frozen in liquid nitrogen and ground with a cold mini pellet pestle. 3 volumes of extraction buffer (50 mM KPi buffer pH 7.5, 1 mM EDTA, 10 mM beta-mercaptoethanol, 0.1 mM PMSF) were added and mixed until the sample was thawed completely. Samples were centrifuged for 5 minutes at 16100xg and 4°C and the supernatant was used for the assay. 20 µl extract were added to 480 µl assay buffer (50 mM KPi buffer pH 7.5, 10 mM KNO_3, 0.1 mM NADH and incubated for exactly 5 minutes at 28°C. The reaction was stopped by addition of 500 µl sulphanilamide (1% (w/v) in 3 M HCl) and vigorous mixing. 500 µl of N-naphthylethylenediamide (0.02% (w/v) in H_2O) was added and the sample was mixed. The formation of a pink azo-salt is dependent on NO_2 from KNO_3 by nitrate reductase. Samples were incubated for 15 minutes after which absorption at 540 nm was measured.

2.23. Spectrophotometric measurement of Complex II+III activity

Complex II+III activity was measured as the reduction of cytochrome *c* at 550 nm (see Section 4.4). Mitochondria were dissolved in 0.1 M Tris-SO4 pH 7.4 containing 1 mM KCN, 125 µg/ml oxidised cytochrome *c* and 12 mM succinate and absorption increase over time was measured at 550 nm. The baseline was established by addition of antimycin A to a concentration of 10 µg/ml which abolishes activity. Enzyme activities were calculated using the Lambert-Beer equation. The extinction coefficient of cytochrome *c* is $\varepsilon = 21.84\ mM^{-1}cm^{-1}$.

2.24. Spectrophotometric measurement of Complex IV activity

Complex IV activity was measured as the oxidation of cytochrome *c* at 550 nm (see Section 4.4). Mitochondria were dissolved in 0.1 M Tris-SO_4 pH 7.4 containing 100 µg/ml reduced cytochrome *c* and absorption decrease over time was measured at 550 nm. The baseline was established by addition of KCN to a concentration of 1 mM which abolishes activity. Enzyme activities were calculated using the Lambert-Beer equation. The extinction coefficient of cytochrome *c* is $\varepsilon = 21.84\ mM^{-1}cm^{-1}$.

2.25. SDS PAGE

SDS PAGE was performed according to (Laemmli, 1970) using a Biorad mini gel system with 0.75-1.5 mm spacers and 10-12.5% of 37.5:1 Bisacrylamide. Samples from native gel assays or spectrometric assays were prepared by addition of 4xLaemmli loading buffer for a final concentration of 1x buffer.

For preparation directly from leaf material samples were frozen in liquid nitrogen and immediately crushed with a mini pellet pestle in a 1.5 ml reaction tube. 2.5 volumes of lysis buffer (50 mM Tris pH 8, 5% glycerol (v/v), 1% SDS (w/v), 10 mM EDTA, 1 mM PMSF) were added and the cell debris was removed by centrifugation for 10 minutes at 16100xg and 4°C. The supernatant was transferred to a new reaction tube and mixed with 4x Laemmli loading buffer to a final concentration of 1x buffer.

2.26. Immunoblotting

Immunoblotting was performed according to (Towbin et al., 1979) in a biometra semi-dry blotting chamber (Analytic Jena) at 170 mA (1 gel per chamber) or 200 mA (2 gels per chamber) for 30 minutes to a nitrocellulose membrane (Whatman Protran 0.2 µm). Total protein was visualised using Ponceau solution (0.1% Ponceau Red (w/v), 5% acetic acid (v/v)). Primary antibodies were prepared in Tris-buffered saline (50 mM Tris-Cl, pH 7.5. 150 mM NaCl) containing 5% milk powder (w/v) and 0.1% Tween-20 (v/v) (TBS+TM). Membranes were blocked in TBS+TM overnight. Primary antibody was incubated for 2-3 hours and washed off thoroughly. Secondary antibody horseradish peroxidase conjugate was used for enhanced luminescence (ECL) staining of the primary antibody. Membranes were incubated with secondary antibody in TBS+TM for 45-60 minutes. ECL staining was performed by mixing solution1 1:1 with solution 2 and incubating the membrane for 1 minute. Luminescence was detected in a ImageQuant LAS 500 (GE Healthcare).

Table 2.14 Solutions for immunoblotting

Solution	Components
Luminol stock	4.4 % 3-aminophthalhydrazine (w/v) in DMSO (Fluka)
Coumaric acid stock	1.5% p-coumaric acid (w/v) in DMSO
Solution 1	0.1 M Tris (pH 8), 10 µl/ml luminol stock, 4.4 µl/ml coumaric acid stock
Solution 2	0.1 M Tris (pH 8), 0.018% H_2O_2

2.27. Detection of biotin by Immunoblotting

After the transfer of proteins to the nitrocellulose membrane membranes are incubated in PBS buffer (4 mM KH_2PO_4, 16 mM Na_2HPO_4, 115 mM NaCl) containing 3% BSA (w/v) and 0.5% Tween-20 (v/v). for 1 hour at room temperature or at 4°C overnight. The membrane was washed 3 times for 5 minutes at room temperature with PBS + 0.1% Tween-20 (v/v). Strep-Tactin® HRP conjugate was pre-diluted 1:100 in enzyme dilution buffer (PBS + 0.2% BSA (w/v) and 0.1% Tween-20 (v/v)). The enzyme was diluted to a final dilution of 1:100000 in

PBS+0.1% Tween-20 (v/v). Membranes were incubated with the antibody dilution for 60 minutes at room temperature. Wash steps were performed 2 times with PBS+0.1% Tween-20 (v/v) and 2 times with PBS only for 1 minute each and ECL was detected as described in Section 1.26.

2.28. Light microscopy

A Leica FluoIII Stereo-Fluorescence or a Leica M205FA Fluorescent Stereo microscope was used for screening for seedlings expressing roGFP and for seed counts, embryo dissection and dissection of floral organs. Images were taken using the Leica M205FA Fluorescent Stereo Microscope.

For higher magnification the Leica DM 6000 was used for embryo development analysis and pollen/anther morphology. Seed clearing was performed using Hoyer's solution (prepared as described in a Cold Spring Harbor Protocol (2011)).

Visualisation of sulfane sulfur was performed using SSP4 (see Section 4.3 and (Chen et al., 2013)). Plant material was incubated with 50 µM SSP4 in 0.1 M KP_i buffer (pH 7.4) for 30 minutes. 10x concentrated stock solutions of SSP4 were prepared in 100% acetonitrile (v/v).

2.29. Confocal laser scanning microscopy and ratiometric calculations of roGFP fluorescence

CLSM microscopy and ratiometric analysis of the roGFP fluorescence were performed essentially as described in (Lehmann et al., 2009; Schwarzlander et al., 2008), see also Sections 3.3 and 3.5.

2.30. Statistical analysis of significance

Statistical tests (Student's t-test, χ^2 goodness of fit) were performed as indicated in the figure legends using Genstat (version 18).

3. In vivo evidence for the substrate of ATM3

As described in Section 1.3 the activity of cytosolic FeS enzymes depends on the mitochondrial ABC-transporter ATM3 as well as the mitochondrial cysteine desulfurase NFS1. Based on this it has been suggested that ATM3 transports a substrate containing a S^0 mobilised by NFS1(Bernard et al., 2009; Bernard et al., 2013). S^0 is highly reactive and has to be transported in a stable form. Gluathione is a likely carrier for this S^0: In 2002, (Sipos et al.) showed that maturation of cytosolic but not mitochondrial FeS proteins was decreased in a Δ*gsh1* yeast strain lacking gamma-glutamyl-cysteine synthase and that genetic depletion of both Gsh1 and Atm1 was lethal. A study by (Kim et al., 2006) showed a link between Arabidopsis ATM3 and glutathione synthesis. They showed that *atm3* mutants contained more non-protein thiols and had higher expression of glutathione synthase *GSH1*. They also found that genetic (*GSH1* antisense plants) or chemical (buthionine sulfoximine) inhibition of glutathione biosynthesis led to an increase of ATM3 expression levels. Furthermore, in-vitro assays carried out by (Schaedler et al.) in 2014 showed the specific ATPase stimulation of ATM3 and yeast Atm1 by oxidised glutathione and oxidised glutathione carrying an additional S^0 (glutathione-persulfide). The transport of glutathione-persulfide by Atm1 was confirmed by transport assays and mass spectrometry.

To provide *in-vivo* evidence supporting the *in-vitro* experiments presented in (Schaedler et al., 2014) I analysed the redox status of the glutathione pool in *atm3* mutants and studied the effect of chemical glutathione depletion in *atm3* mutants and the wild type.

3.1. *atm3* mutants are hypersensitive to glutathione depletion

Buthionine sulfoximine (BSO) was used to test the effect of glutathione depletion on the growth phenotype of the *atm3-3* and *atm3-4* alleles. *atm3-3* is a point mutant with no visible growth phenotype and decreased cytosolic FeS enzyme activities, *atm3-4* has a promoter deletion, is chlorotic and has strongly decreased cytosolic FeS enzyme activities (as described in (Bernard et al., 2009)). BSO is a specific inhibitor for glutathione biosynthesis acting as a competitive inhibitor for

gamma-glutamylcysteine synthetase (Griffith and Meister, 1979). Chemical depletion was chosen over the generation of double mutants of glutathione biosynthesis and *atm3* as the generation of double mutants is time consuming and potentially leads to nonviable plants. Concentrations of 200 µM of DL-BSO (racemic DL-buthionine-(SR)-sulfoximine) were chosen as the wild type was not visibly affected in growth under this treatment. As a control plants were also grown on plates containing 200 µM DL-BSO plus 200 µM GSH. Roots of both *atm3* plants are ~50% shorter than wild type under standard growth conditions ((Bernard et al., 2009) and Figure 3.1) and growth is further decreased under DL-BSO treatment to about 19% of untreated wild type which was restored upon addition of GSH (Figure 3.1). When comparing plants treated with BSO to the respective untreated control wild-type plants show a decrease in root length to about 80% while *atm3-3* plants show a decrease to 39% and *atm3-4* a decrease to 36%. To conclude, *atm3* mutants were found to be hypersensitive to chemical glutathione depletion which was also found by Theresia Schaedler (see (Schaedler et al., 2014)).

A

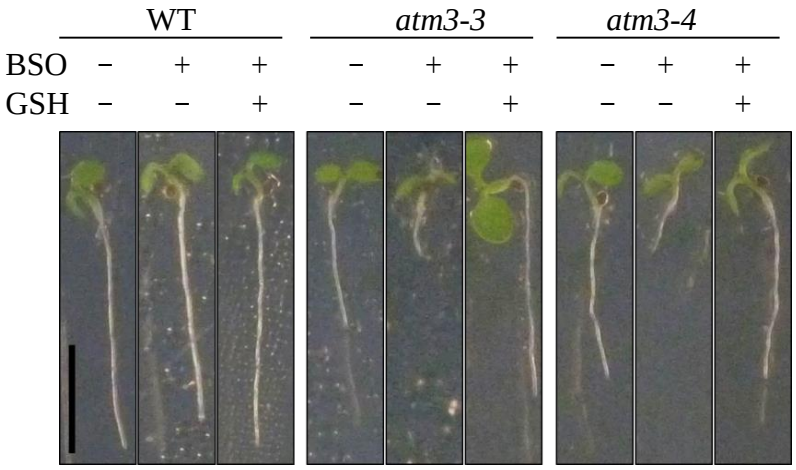

B

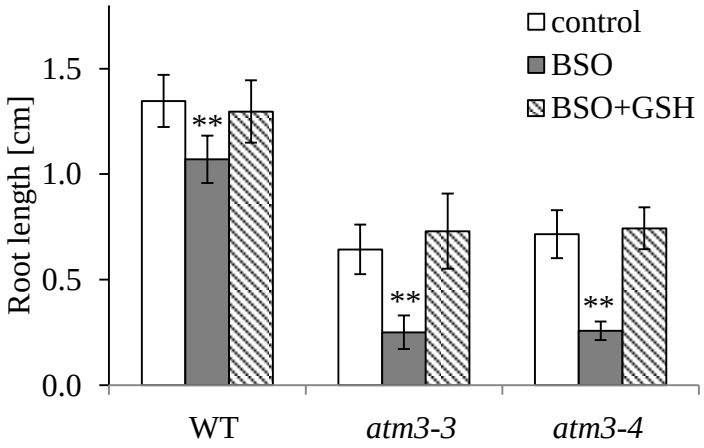

Figure 3.1 Root lengths of *atm3* mutants under glutathione depletion. GSH was chemically depleted in 7-8 days old wild type (WT) and *atm3* seedlings by BSO (buthionine sulfoximine). Plants were grown on ½ MS-agar containing either 400 µM of DL-BSO (racemic mixture of the D and L form) or 400 µM DL- BSO and 200 µM GSH. **A.** Growth phenotype of seedlings after 8 days of growth on ½ MS-Agar. Scale bar is 0.5 cm**. B.** Root lengths of plants from A, quantified using ImageJ. Values are mean root lengths in cm ± SD; n≥12, ** $p<0.01$ (Student's t-test against the respective untreated control).

3.2. Glutathione depletion affects FeS enzyme activity

To determine the effect of glutathione depletion on FeS enzymes, activities of the cytosolic FeS enzyme aldehyde oxidase and the mitochondrial and cytosolic isoforms of aconitase were measured using an in-gel assay coupled to the production of the purple precipitate formazan. Aconitase activity was strongly affected in the wild type when grown on 400 µM of BSO while aconitase protein levels were unaffected. Aldehyde oxidase activity was mildly decreased (Figure 3.2). It was not possible to gain significant and reproducible results for the *atm3* mutants under the BSO treatment despite multiple attempts and conditions.

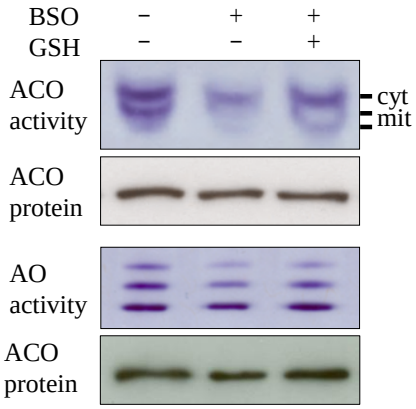

Figure 3.2 FeS cluster enzyme activities upon glutathione depletion. Glutathione was chemically depleted in wild type seedlings using 400 µM of BSO (racemic DL-buthionine-(SR)-sulfoximine). Another sample was treated with 400 µM BSO and 200 µM GSH; untreated plants served as a control. Plants were grown for 7-8 days on ½ MS-agar plates containing the respective chemicals. Enzyme activities of aconitase and aldehyde oxidase were visualised in-gel enzyme assays. Aconitase protein was visualised using specific antibodies after denaturing-PAGE of an identical gel.

3.3. roGFP as a sensor for the redox state of the glutathione pool

The redox sensitive sensor roGFP was used to determine whether oxidised glutathione accumulates in mitochondria of *atm3* mutants. If ATM3 does transport oxidised glutathione carrying an additional sulfur, then the redox state of the mitochondrial glutathione pool should be shifted towards oxidation in *atm3* mutants. Ratiometric measurements using the redox sensitive reporter roGFP were chosen over measuring glutathione levels in isolated mitochondria because 1) the process of mitochondria isolation changes the redox balance in mitochondria as it exposes the

extract to oxygen 2) Measuring and distinguishing between oxidised and reduced glutathione involved a lengthy protocol which could further alter the redox balance. 3) *In-vivo* data from intact plants is more desirable than data from isolated mitochondria.

The used variant of a green fluorescent protein, roGFP2, has two amino acid exchanges to cysteine which changes the fluorescent properties in comparison to conventional GFP and depending on disulfide formation (Dooley et al., 2004; Hanson et al., 2004; Meyer et al., 2007; Schwarzlander et al., 2008) (Figure 3.3A). roGFP2 has two excitation maxima, one at 405 nm and one at 488 nm (Figure 3.3B). These maxima change in intensity depending on the redox state and by means of this reflect the redox state of the surrounding medium. The glutaredoxin GRX1 fusion to the reporter increased specificity for the glutathione pool as glutaredoxin specifically binds to glutathione as a substrate thus transmitting the redox state of the glutathione pool to the transporter.

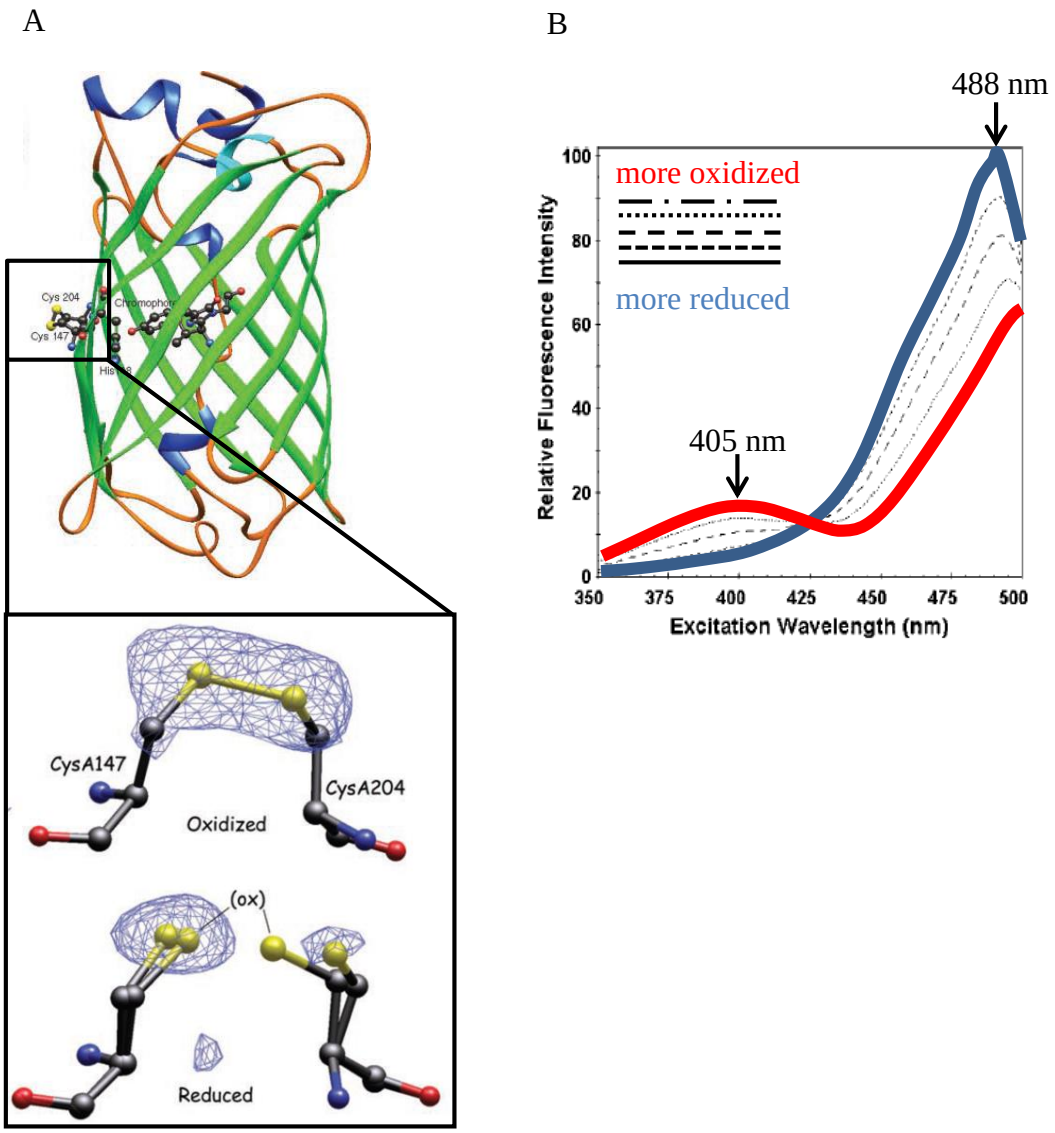

Figure 3.3 roGFP2 as a redox sensor. roGFP2 has two amino acid exchanges to cysteines which make it sensitive for redox changes. **A**. Structure of the roGFP sensor. The two amino acid exchanges to cysteine are at position 147 and 204 (S147C, Q204C) and lead to formation of a disulfide bond under oxidising conditions. **B.** Emission spectrum of the roGFP sensor. roGFP emits at 510 nm and has two excitation maxima, one at 405 and one at 488 nm. The ratio between the emission intensity upon excitation at 488 and 405 nm depends on the redox state of the reporter, where high values represent more oxidised conditions and low values more reducing conditions. Images are modified from (Hanson et al., 2004).

3.4. Isolating *atm3* mutants expressing mitochondrial and cytosolic roGFP

Three *atm3* mutant alleles were transformed with a cytosolic expressed GRX1-roGFP2 (Marty et al., 2009) or a mitochondrial expressed roGFP2-GRX1 (Albrecht et al., 2014) construct under the control of the CaMV-35S promoter kindly donated by Andreas Meyer and Markus Schwarzländer (INRES, Bonn) (Figure 3.4A). The transformation was done by Theresia Schaedler and Jonathan Foster (Group of Janneke Balk, Department of Plant Sciences, University of Cambridge; John Innes Centre, Norwich). The strong allele *atm3-1* was chosen in addition to the weak *atm3-3* and the intermediate *atm3-4* allele as it was not clear how strongly *atm3* mutations affect the redox state of the glutathione pool. Lines with a clear mitochondrial or cytosolic signal were isolated by screening for a strong signal in the progeny, in the expected cell compartment (Figure 3.4B).

The *atm3-1* line has a T-DNA insertion resulting in an ATM3 fusion protein lacking the nucleotide binding domain. Plants are delayed in growth and chlorotic and have only 40% or less activity of FeS enzymes as shown in (Bernard et al., 2009). Not a single plant of the *atm3-1* allele expressing the mitochondrial construct was found. Thus seeds from transformed *atm3-1/ATM3* plants were screened for *atm3-1* homozygotes expressing the mitochondrial roGFP construct. Additionally, crosses were generated between a homozygous *atm3-1* line and a wild type expressing the mitochondrial construct. Seeds from 4 crosses and 10 transformations were used (Figure 3.5A). However, no homozygous plants were recovered expressing the mitochondrial construct. Over 1000 seedlings from the progeny were screened for roGFP expression and a putative *atm3-1* phenotype. Mature plants were re-screened for roGFP signal and positive plants were tested for their genotype. Of the 15 remaining plants none had the *atm3-1* T-DNA insertion and thus this line had to be excluded from further experiments (Figure 3.5B).

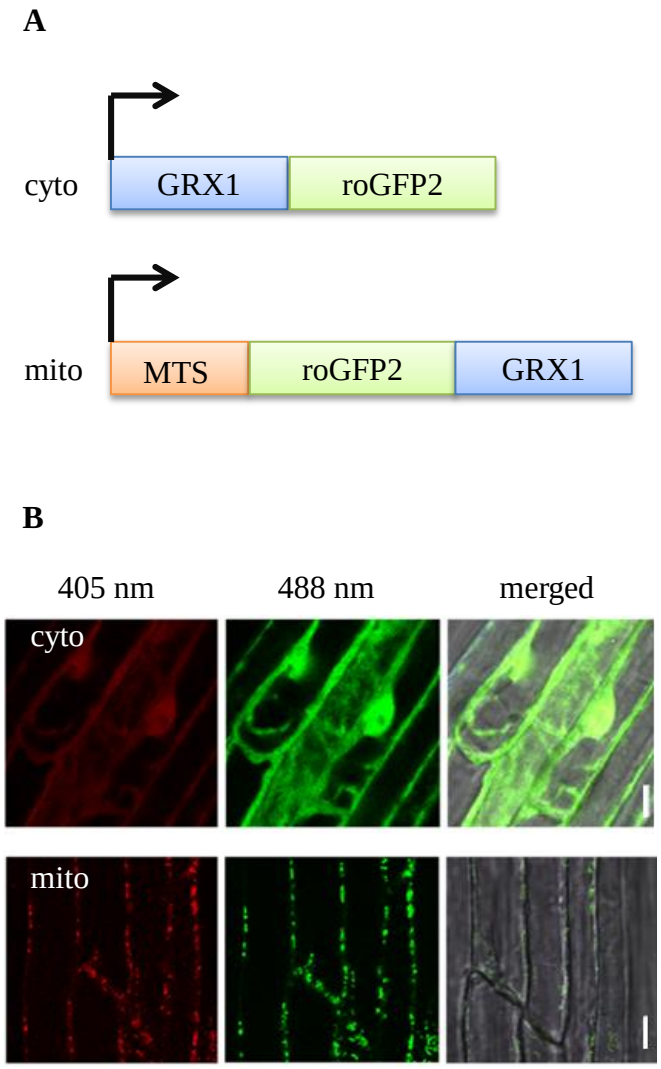

Figure 3.4 Subcellular localisation of the roGFP reporter. *atm3* mutant alleles and wild-type plants were transformed with the roGFP2 construct either targeted to the cytosol or mitochondria. Constructs were kindly provided by A.J. Meyer (INRES, Bonn). **A.** Scheme of the cytosolic and mitochondrial expressed construct under the control of a CaMV-35S promoter. **B.** Subcellular localisation of the cytosolic and mitochondrial targeted construct. Scale bar is 20 µm.

A

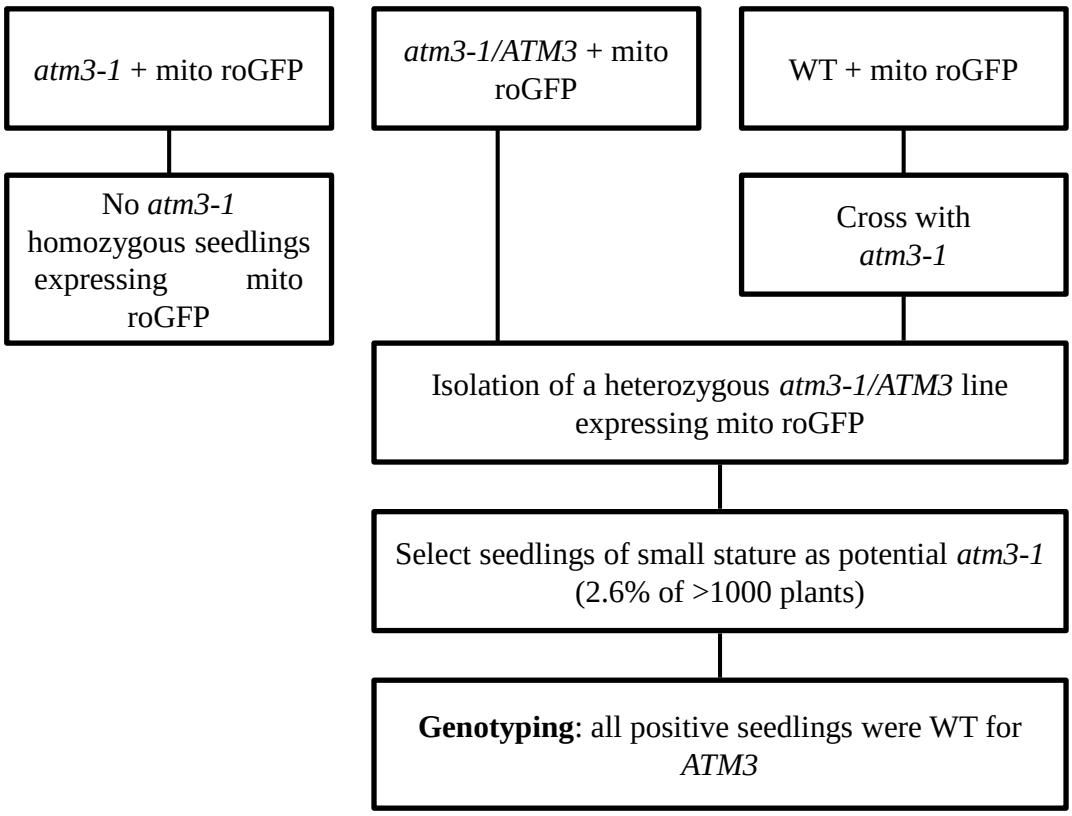

B

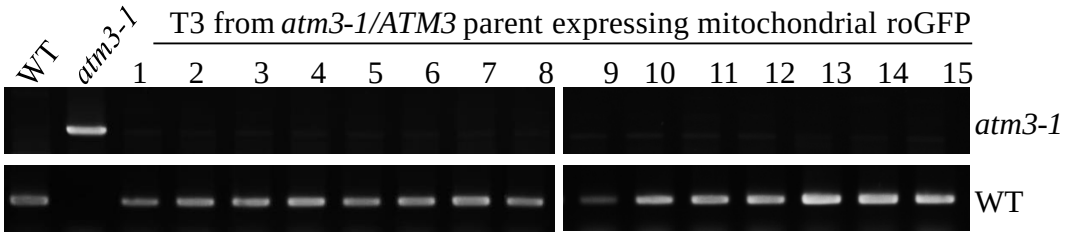

Figure 3.5 Selection of *atm3-1* mutants expressing mitochondrial roGFP. A. Selection scheme **B.** Genotyping for the *atm3-1* allele in plants expressing roGFP2-GRX1 as indicated in A.

3.5. ATM3 is involved in the transport of oxidised glutathione

As described above, ratiometric analysis of the roGFP signal at 488 and 405 nm excitation is representative for the redox state of the glutathione pool in the cytosol or the mitochondria of transformed plants. High values of the 405/488 ratio indicate a shift to oxidation, low values indicate a more reduced redox state. The ratios were calculated using a program developed by Mark D. Fricker (Department of Plant Sciences, University of Oxford), essentially as described in (Lehmann et al., 2009;

Schwarzlander et al., 2008). I carried out the experiments in collaboration with and in the laboratory of Andreas Meyer and Markus Schwarzländer (INRES, Bonn). Measurements were performed on root tips as these have a high mitochondrial density and showed the best roGFP signal. The false colour visualisation shown in Figure 3.6A is representative for the readout of the sensor and shows that the signal is very similar between cytosolic but not mitochondrial samples. The areas with a very high 405/488 ratio (red) at the root tip were dead cells of the root cap and were excluded from measurements. Root cell auto fluorescence was measured at 435-485 nm upon excitation at 405 nm and bleed-through into the roGFP channel was accounted for in the calculations (as described in (Lehmann et al., 2009)). Cells with high auto fluorescence (not shown) were excluded. Cells which passed a visual quality check were marked and used for calculation of ratiometric values on a pixel-by-pixel basis. The mitochondrial lines had some leakage to the cytosol as some of the construct can lose the mitochondrial targeting sequence. This was accounted for by background corrections of the values (not shown). Quantification of 10-15 samples showed that the redox state of the mitochondrial glutathione pool of *atm3* mutants was significantly more oxidised than in the wild type (Student's t-test), despite a high variation between plants which is represented by the high standard deviation (see Figure 3.6B). The redox state of the cytosolic glutathione pool was similar in all samples.

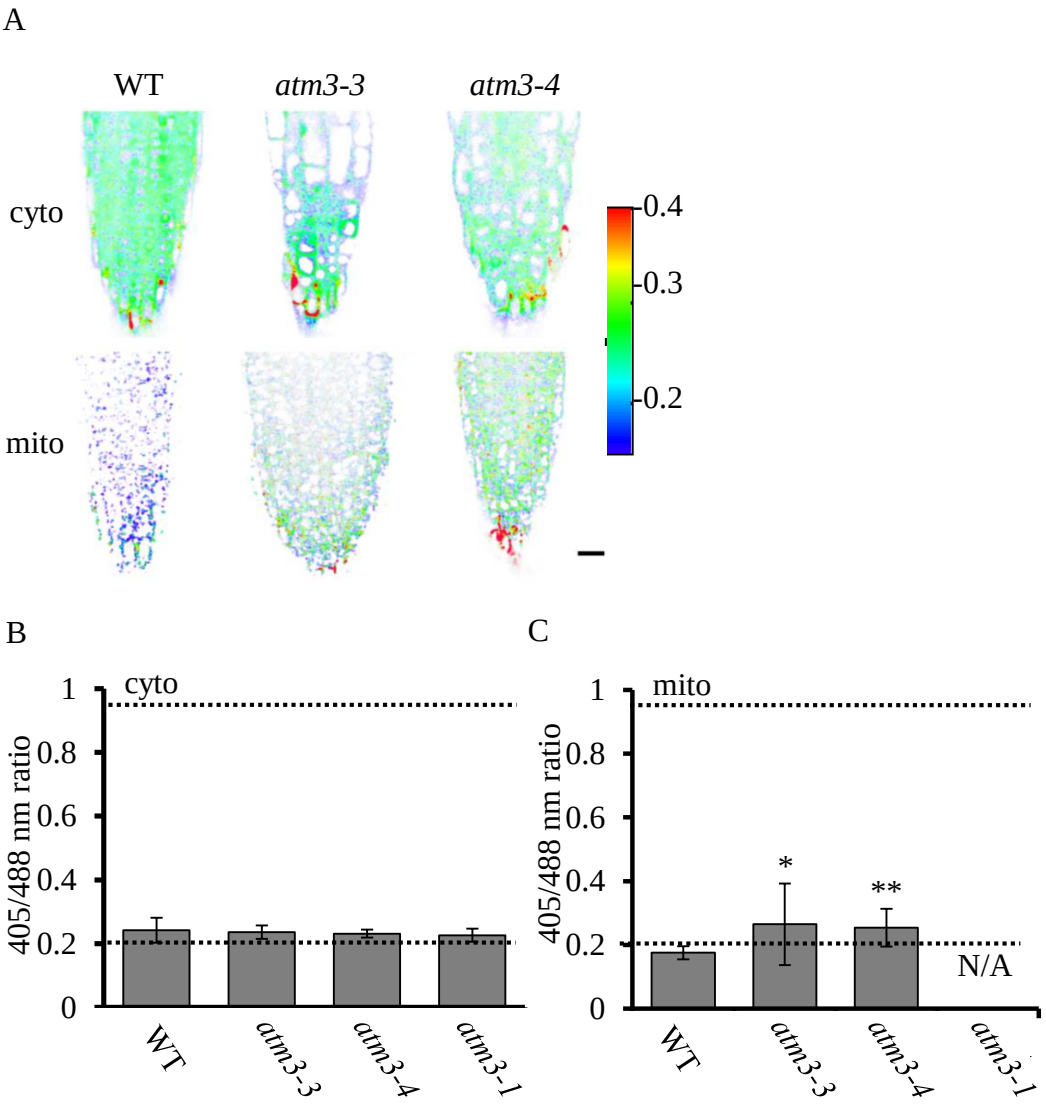

Figure 3.6 The redox state of the glutathione pool in *atm3* mutant mitochondria is shifted towards oxidation. The roGFP2 sensor fused to GRX1 was targeted to the cytosol (cyto) or mitochondria (mito) and the 405/488 nm ratio values were determined using image analysis of confocal microscopy data. The ratio is a measure for the redox state of the local glutathione pool. Measurements were performed on indicated *atm3* alleles and the wild type (WT) after 7-8 days of growth on ½ MS-agar. **A.** False colour ratiometric images of root tips. Red areas indicate dead cells of the root cap. Scale bar is 20 µm **B.** and **C.** Quantified ratiometric measurements of root tip cells from A. The lower dotted line indicates the ratio of the fully reduced sensor, the upper dotted line indicates the ratio of the fully oxidised sensor.. The values are the mean ± SD of 10 – 15 images. * $p<0.05$, ** $p<0.01$ (Student's t-test against WT control). N/A, not available.

3.6. The redox state of the glutathione pool in *atm3* mutants is more susceptible to glutathione depletion than in the wild type

To investigate if the chemical depletion of glutathione further increased the reduction potential of the glutathione pool in the *atm3* mutants than in the wild type I conducted roGFP measurements of plants treated with BSO (see Figure 3.7). The untreated control values from Section 3.5 were added for comparison. Depletion of the glutathione pool in the mitochondria caused a shift towards oxidation in the wild type and the *atm3* alleles which was rescued by addition of GSH in the wild type and the weak *atm3-3* mutant but not in the intermediate *atm3-4* mutant. In wild type seedlings, mitochondrial roGFP showed a more pronounced shift towards oxidation (3.2x) than cytosolic roGFP with the same treatment (1.2x). For *atm3* mutants the opposite was observed. Interestingly, the mild *atm3-3* mutant showed stronger shifts towards oxidation than the *atm3-4* mutant despite having no growth phenotype (5x vs 2.1x for the cytosolic reporter and 2.9x vs 1.6 fold for the mitochondrial reporter). Addition of GSH to the BSO treatment returned the values of the mitochondrial reporter to control levels in the wild type and *atm3-3*. For the cytosolic reporter addition of GSH to the BSO treatment shifted the redox state towards the reduced form in *atm3-3* plants only. The wild type did not show a significant difference and for *atm3-4* and *atm3-1* the additional treatment of GSH appeared to shift the values even more towards oxidation; however, this was difficult to assess due to the high variability of values due to an uneven effect of the treatment on different cells of the same sample.

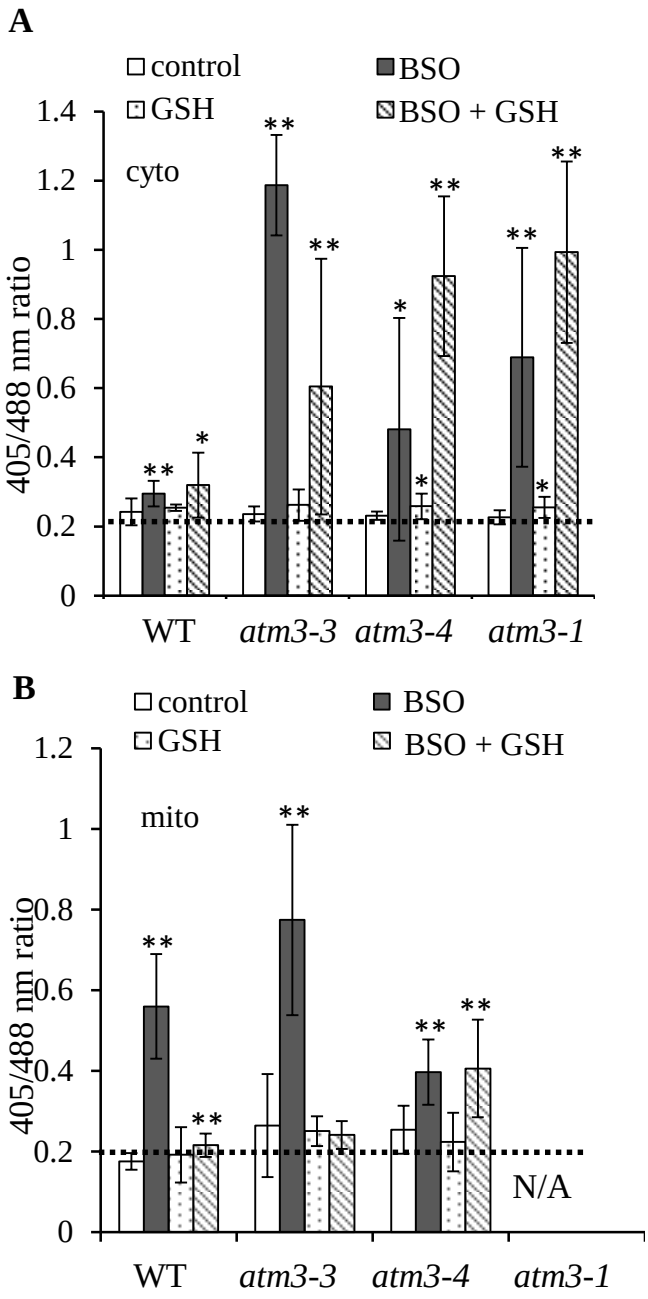

Figure 3.7 Redox state of the glutathione pool in glutathione-depleted *atm3* and wild type. 7 to 8-days-old wild-type (WT) and *atm3* seedlings were treated with either 200 µM of DL-BSO (racemic DL-buthionine-(SR)-sulfoximine), 200 µM DL-BSO plus 200 µM GSH or 200 µM GSH only. The roGFP2 sensor fused to GRX1 was targeted to the cytosol (**A**) or mitochondria (**B**) and the 405/488 nm ratio values were determined using image analysis of confocal microscopy data. The ratio is a measure for the redox state of the local GSH pool. The dotted lines indicate the ratio of the fully reduced sensor. The values are the mean ± SD of 5 – 15 images of root tip cells. * $p<0.05$, ** $p<0.01$ (Student's t test against untreated control). N/A, not available.

3.7. Mitochondrial morphology is altered in *atm3-4* plants with or without glutathione depletion

The roGFP reporter was mainly used to assess the redox state of the glutathione pool in atm3 plants; however the experiments also showed changes in the mitochondrial morphology of *atm3-4* plants. *atm3-4* samples treated with BSO showed mitochondrial aggregation in 7 out of 10 examined roots (Figure 3.8D, H, L). This effect was partially rescued by addition of GSH (data not shown). Untreated *atm3-4* samples (figure 3.8B, F, J) also showed aggregation but to a far lesser extent. The weaker *atm3-3* allele showed mitochondrial aggregation in 2 out of 14 roots under BSO treatment (data not shown) of about the same frequency as the untreated intermediate allele *atm3-4*. These mitochondrial aggregates were not observed in wild-type seedlings, whether treated with BSO or not (Figure 3.8A, E, I and C, G, K).

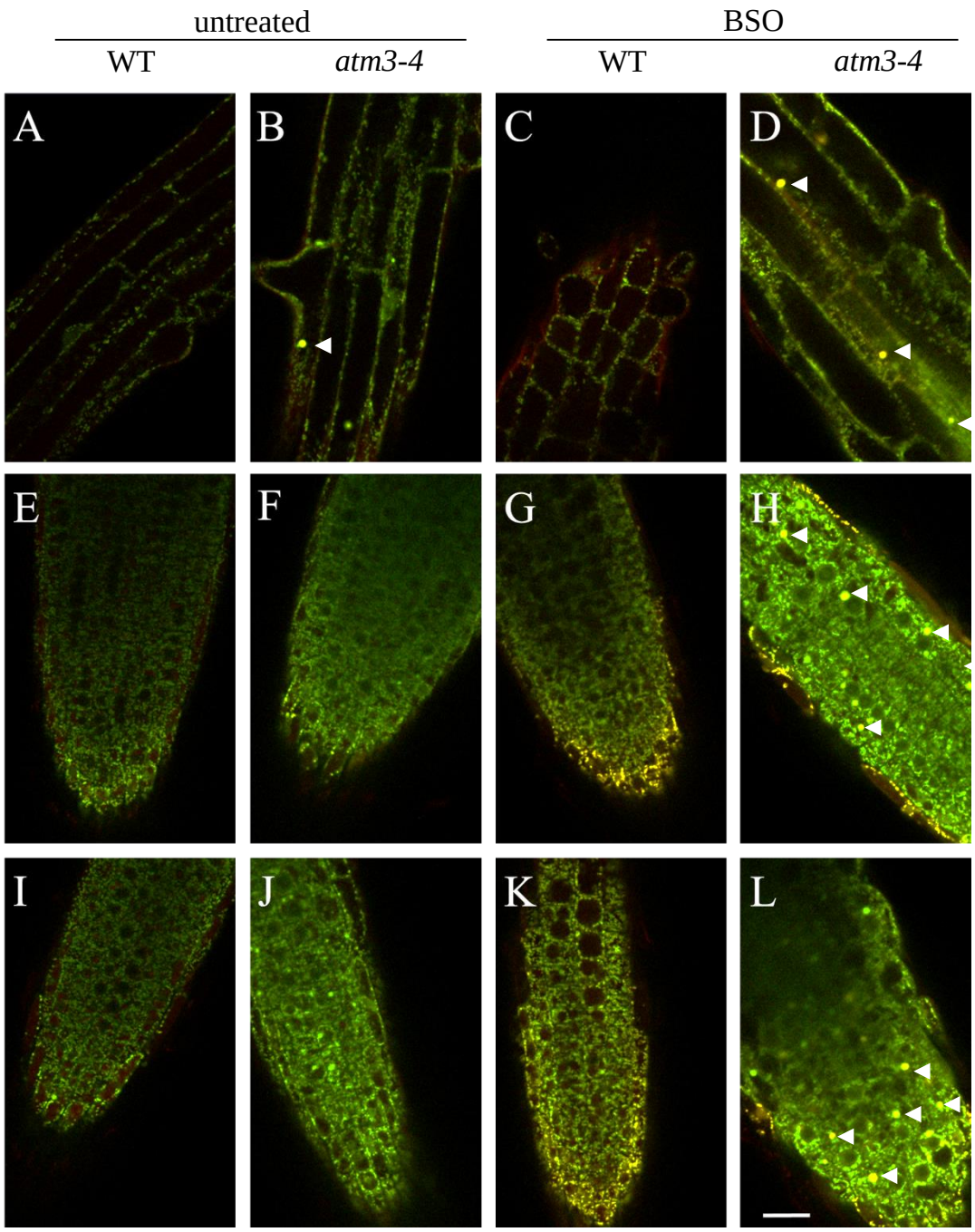

Figure 3.8 Mitochondrial aggregation in *atm3-4* mutants. 7-8 days old wild-type (WT) and *atm3-4* seedlings were treated with 200 µM of DL-BSO. The roGFP2 sensor fused to GRX1 was targeted to mitochondria. Shown is the overlay of the signal at 405 nm (red channel) and at 488 nm (green channel). The 405/488 ratio indicates the redox state of the glutathione pool. A relative increase of fluorescence upon excitation at 405 nm indicates a more oxidised glutathione pool. Images were taken of root tip or epidermis cells of the root elongation zone. White arrows indicate mitochondrial aggregation. Representative images are shown of 5-15 roots. Scale bar is 20 µm.

3.8. Discussion

In this Chapter I presented *in-vivo* evidence for the transport of GSSG by ATM3. Root growth in *atm3* mutants was found to be more sensitive to glutathione depletion by treatment with BSO than in the wild type. Furthermore, the glutathione pool of *atm3* mutants showed a mild but significant shift towards oxidation in comparison to the wild type. Treatment with BSO caused a further shift towards oxidation in all *atm3* samples in the cytosol and mitochondria (between 1.6x and 5x). A shift towards oxidation can be caused by either a decrease in the overall glutathione level in the mitochondria or by an increase in the GSSG:GSH ratio (Meyer et al., 2007). However, (Kim et al., 2006) showed that *atm3-1* mutants had a 2-fold increase of non-protein thiols (like glutathione) and (Schaedler et al., 2014) confirmed that *atm3-1* and *atm3-4* mutants did not have a decrease of non-protein thiols. Thus it is reasonable to assume that the shift towards oxidation of the glutathione pool in *atm3* mitochondria is due to an increase in the GSSG:GSH ratio rather than due to lower glutathione levels. The observed shift of the redox state of the mitochondrial glutathione pool towards oxidation in *atm3* mutants (405/488 = 0.25-0.27) in comparison to the wild type (0.18) was mild compared to previously observed changes and the capacity of the mitochondrial sensor which can show 4.5-5.3-fold changes (Schwarzlander et al., 2008). However, this may be due to the tight regulation of the redox balance of the glutathione pool (Noctor et al., 2012).

To assess if an accumulation of the hypothetical ATM3-substrate GSSSG in *atm3* mutants could be detected by roGFP2, I analysed the theoretical shift in the roGFP2 reduction state if GSSSG would accumulate 10-fold. For this purpose I will assume that the total concentration of glutathione is 10 mM and that [GSSSG] equals [GSSG]. The reduction potential can be calculated according to the Nernst Equation (Eq. 1).

$$E' = E'_0 - \frac{2.303\,R \cdot T}{z \cdot F} log_{10} \frac{[GSH]^2}{[GSSSG]} \qquad \textbf{Eq. 1}$$

E'_0 is the standard mid-point potential for glutathione which is -0.240 V (Schafer and Buettner, 2001)
R is the universal gas constant
F is the Faraday constant
T is the standard temperature
z is the number of transferred electrons (2 in this case)
[GSH] and [GSSSG] are the concentrations of reduced and oxidised glutathione, respectively

The $E_0^{'}$ has to be adapted to the pH of 7.8 in the mitochondrial matrix according to Eq.2 (Nobel, 1991; Schwarzlander et al, 2008):

$$\boldsymbol{E_0^{'pH} = E_0^{'} - \frac{2.303 \cdot R \cdot T}{z \cdot F}(pH - 7)} \qquad \textbf{Eq.2}$$

$$E_{0\,glutathione}^{'pH} = -0.240\,V - \frac{2.303 \cdot 8.31\,\mathrm{J}\,K^{-1}\,mol^{-1} \cdot 298.15\,K}{2 \cdot 96485.34\,C\,mol^{-1}}(7.8 - 7)$$

$$E_{0\,glutathione}^{'pH} = -0.240\,V - \frac{2.303 \cdot 8.31\,\mathrm{C\,V}\,K^{-1}\,mol^{-1} \cdot 298.15\,K}{2 \cdot 96485.34\,C\,mol^{-1}}(7.8 - 7)$$

$$E_{0\,glutathione}^{'pH} = -0.240\,V - \frac{2.303 \cdot 8.31\ \mathrm{V} \cdot 298.15}{2 \cdot 96485.34}(0.8)$$

$$E_{0\,glutathione}^{'pH} = -0.240\,V - \frac{2.303 \cdot 8.31\ \mathrm{V} \cdot 298.15}{2 \cdot 96485.34}(0.8)$$

$$E_{0\,glutathione}^{'pH} = -0.240\,V - 0.0237\,V$$

$$\boldsymbol{E_{0\,glutathione}^{'pH} = -0.264\,V}$$

Glutathione is the most abundant redox buffer and thus determines the intracellular reduction potential. The intracellular resting reduction potential of wild-type mitochondria has been measured to be -0.356 V before (Schwarzlander et al., 2008). Thus if we assume that the total glutathione concentration is 10 mM, then [GSSSG] has to be about 0.08 µM in wild-type plants to reach -0.356 V.

$$\boldsymbol{E' = E_{glutathione}^{'pH} - \frac{2.303\,R \cdot T}{z \cdot F} log_{10} \frac{[GSH]^2}{[GSSSG]}}$$

$$E'_{glutathione} = -0.264\,V - \frac{2.303 \cdot 8.31\,\mathrm{J}\,K^{-1}\,mol^{-1} \cdot 298.15\,K}{2 \cdot 96485.34\,C\,mol^{-1}} log_{10} \frac{[GSH]^2}{[GSSSG]}$$

$$E'_{glutathione} = -0.264\,V - \frac{2.303 \cdot 8.31\,\mathrm{C\,V}\ K^{-1}\,mol^{-1} \cdot 298.15\,K}{2 \cdot 96485.34\,C\,mol^{-1}} log_{10} \frac{[GSH]^2}{[GSSSG]}$$

$$E'_{glutathione} = -0.264\,V - \frac{2.303 \cdot 8.31\ \mathrm{V}\ \cdot 298.15}{2 \cdot 96485.34} log_{10} \frac{[GSH]^2}{[GSSSG]}$$

$$E'_{glutathione} = -0.264\,V - 0.0296\,V\ log_{10} \frac{[GSH]^2}{[GSSSG]}$$

$$E'_{glutathione} = -0.264\,V - 0.0296\,V\ log_{10} \frac{(1 \cdot 10^{-2})^2}{8 \cdot 10^{-8}}$$

$$\boldsymbol{E'_{glutathione} = -0.264\,V - 0.0296\,V \cdot log_{10}(1250) = -0.356\,V}$$

If the *atm3* mutation leads to a 10-fold accumulation of GSSSG, then the reduction potential would change to -0.326 V with concentrations of [GSH] ≈ 10 mM and [GSSSG] ≈ 0.8 µM

$$E'_{glutathione} = -0.264\,V - 0.0296\,V\ log_{10}\frac{(1\cdot 10^{-2})^2}{8\cdot 10^{-7}}$$

$$\boldsymbol{E'_{glutathione} = -0.264\,V - 0.0296\,V\cdot log_{10}(10) = -0.326\,V}$$

As mentioned above, glutathione is the most abundant redox buffer in the cell and thus the roGFP2 reduction potential will be directly dependent on the reduction potential of the glutathione couple. To assess if a 10-fold accumulation of GSSSG will be detectable by roGFP2, I will calculate the change in the ratio of oxidised to reduced roGFP2 at the above calculated reduction potentials according to equation 3.

$$\boldsymbol{E' = E'^{0}_{roGFP2} - 0.0296\,V\ log_{10}\frac{[red]}{[ox]}} \qquad \textbf{Eq. 3}$$

As before, the standard potential for roGFP2, which is -0.272 V (according to Hanson et al. (2004)), has to be adjusted for the alkaline pH of the mitochondrial matrix:

$$\boldsymbol{E'^{pH}_{0(roGFP2)} = E'_{0(roGFP2)} - \frac{2.303\cdot R\cdot T}{z\cdot F}(pH-7)}$$

$$E'^{pH}_{0(roGFP2)} = -0.272\,V - \frac{2.303\cdot 8.31\ \mathrm{J}\,K^{-1}\,mol^{-1}\cdot 298.15\,K}{2\cdot 96485.34\,C\,mol^{-1}}(7.8-7)$$

$$E'^{pH}_{0(roGFP2)} = -0.272\,V - \frac{2.303\cdot 8.31\ \mathrm{C\,V}\,K^{-1}\,mol^{-1}\cdot 298.15\,K}{2\cdot 96485.34\,C\,mol^{-1}}(7.8-7)$$

$$E'^{pH}_{0(roGFP2)} = -0.272\,V - \frac{2.303\cdot 8.31\ \mathrm{V}\cdot 298.15}{2\cdot 96485.34}(0.8)$$

$$E'^{pH}_{0(roGFP2)} = -0.272\,V - \frac{2.303\cdot 8.31\ \mathrm{V}\cdot 298.15}{2\cdot 96485.34}(0.8)$$

$$E'^{pH}_{0(roGFP2)} = -0.272\,V - 0.0237\,V$$

$$\boldsymbol{E'^{pH}_{0(roGFP2)} = -0.296\,V}$$

For the calculated reduction potential of glutathione in a wild-type plant of -0.356 V the roGFP2 would be highly reduced (see also Schwarzlander et al. (2008)):

$$\boldsymbol{E' = E^{'pH}_{0\,(roGFP2)} - 0.0296\,V\ log_{10}\frac{[red]}{[ox]}}$$

$$-0.356\,V = -0.296\,V - 0.0296\,V\ log_{10}\frac{[red]}{[ox]}$$

$$\frac{-0.356\,V + 0.296\,V}{-0.0296\,V} = log_{10}\frac{[red]}{[ox]}$$

$$2.03 = log_{10}\frac{[red]}{[ox]}$$

$$\boldsymbol{104.7 = \frac{[red]}{[ox]}}$$

This means that in the wild-type mitochondria the roGFP2 could be estimated to be 99.05% reduced:

$$\boldsymbol{ox + red = 100\%}$$

$$\frac{red}{ox} = 104.7$$

$$\frac{red}{100\% - red} = 104.7$$

$$red = 10470\% - 104.7red$$

$$105.7\,red = 10470\%$$

$$\boldsymbol{red = 99.05\%}$$

Upon a 10-fold accumulation the reduction potential is calculated to be -0.326 V and the ratio changes as follows:

$$-0.326\,V = -0.296\,V - 0.0296\,V\ log_{10}\frac{[red]}{[ox]}$$

$$\frac{-0.326\,V + 0.296\,V}{-0.0296\,V} = log_{10}\frac{[red]}{[ox]}$$

$$1.01 = log_{10}\frac{[red]}{[ox]}$$

$$\boldsymbol{10.23 = \frac{[red]}{[ox]}}$$

A 10-fold accumulation thus could be estimated to change the redox state of roGFP2 to 91.1% reduction.

$$\frac{red}{100\% - red} = 10.23$$

$$red = 1023\% - 10.23red$$

$$11.23\, red = 1023\%$$

$$\boldsymbol{red = 91.1\%}$$

To summarise, at wild-type glutathione balance I predict roGFP2 to be 99.05% reduced and upon a 10-fold accumulation of GSSSG roGFP2 to be 91.1% reduced. This means that already a 10-fold change of the low total concentrations of GSSSG (0.08 µM to 0.8 µM in 10 mM total glutathione) theoretically causes a big change in the redox state of the reporter thus making it an effective probe for the assessment of GSSSG accumulation in *atm3* mutants.

To estimate if the calculated shift in the redox state of roGFP2 would be detectable I estimated how the 405/488 ratio would change according to above calculations. The fully reduced sensor had a ratio of 0.2, the fully oxidised a ratio of 0.95. Thus a ratio change of 0.75 corresponds to a change from fully reduced to fully oxidised. According to my calculations, a 10-fold accumulation of GSSSG would result in an 8% more oxidised roGFP2. The equivalent 405/488 ratio would be 0.26 which, interestingly, is close to the measured ratio in *atm3-4* mutant mitochondria of 0.256±0.053. Thus, I conclude that (1) roGFP2 is an appropriate probe to measure even changes in the redox balance of the glutathione pool even with very low starting concentrations of oxidised glutathione and (2) the observed small shift towards oxidation in *atm3-4* mitochondria could indicate a considerable accumulation of oxidised glutathione.

Taken together, the described experiments gave supporting *in-vivo* data for the *in-vitro* data presented by (Schaedler et al., 2014) thus providing evidence that oxidised glutathione is the substrate of ATM3.

4. Genetic interactions of ATM3 with genes involved in sulfur metabolism

One aim of my PhD was to provide *in-vivo* evidence for the substrate of ATM3. In eukaryotes, S^0 is mobilised by the cysteine desulfurase in the mitochondria Nfs1 is thought to be exported to the cytosol via Atm1 (ATM3 in plants) (Lill, 2009). (Schaedler et al., 2014) showed that *Lactococcus* inside-out vesicles containing yeast Atm1 accumulated GSSSG, providing evidence for transport of additional S^0 *in-vitro*. However, data gathered *in-vitro* are not always representative for processes *in-vivo* and need to be confirmed. As a direct approach of measuring if S^0 accumulates in *atm3* mutant mitochondria I tested the newly developed Sulfane Sufur Probe 4. In addition, a more indirect approach was to measure the damaging effect of sulfide accumulation on Complex IV activity. However, these quantitative methods did not yield any conclusive data and will be discussed at the end of the chapter.

First I will describe genetic interaction studies of ATM3 with components of the mitochondrial sulfur metabolism ETHE1, OASTLC and NFS1. As described in Chapter 1.5, ETHE1 is a mitochondrial sulfur dioxygenase involved in S^0 detoxification after cysteine degradation and it uses glutathione as a cofactor; OASTLC incorporates sulfide into O-acetylserine to form cysteine. NFS1 uses cysteine as a substrate to transfer a S^0 for FeS assembly.

Genetic interaction studies can reveal if two proteins act in the same pathway or compete for the same substrate and can be investigated by analysing the phenotype of double mutants of the genes of interest in comparison to the parental single mutants. Five different effects can be observed when studying genetic interactions: **(1) Epistatic mutations**: The term epistasis is used under different definitions, however for reasons of simplicity, for this study the following definition will be used: a gene A is epistatic for another gene B if a knock-out of A masks the phenotype of B, whether B is mutated or not. **(2) Additive mutations** due to mutations in genes of different pathways: Combination of mutants A and B with different phenotypes results in a double mutant that combines phenotypes of both parents without aggravation of the phenotypes. Additive mutations can appear similar to **(3) Allelic mutations**: Two allelic mutations affect the same gene and thus a combination results in an intermediate phenotype (see also Chapter 6.4). For

recessive mutants it can be distinguished between additive mutations and allelic mutations: In heterozygous mutants, the phenotype of additive mutations is restored but if the mutations are allelic the phenotype is not restored. **(4) Suppressor mutations**: A mutation in A suppresses a mutation in B if the phenotype of mutant B is complemented by an additional mutation in A. **(5) Synergistic interactions**: Combination of mutants of A and B which are part of the same pathway result in a double mutant which has a phenotype that is stronger than the sum of the parental phenotypes. Epistatic effects can only be clearly observed in knock-out mutants. Knock-out mutants for *ATM3* are sterile and lethal for *ETHE1* and *NFS1* and thus epistasis could not be investigated. Combinations of knock-down alleles for *ATM3*, *ETHE1* and *NFS1* as well as a knock-out of *OASTLC* were analysed to determine if *ATM3* is involved in sulfur metabolism. Details of all mutants are given in Table 4.1.

4.1. *ATM3* shows a synergistic genetic interaction with *ETHE1*

The interactions between *ETHE1* and *ATM3* and *OASTLC* and *ATM3* were included in the publication of Schaedler et al (2014) and will be presented first.

Plants homozygous for *atm3-1* and heterozygous for *ethe1-1* were selected by Dr. Schaedler who did not find homozygous double mutants. To investigate if there is a defect in seed formation or germination I analysed seed development in *ethe1-1atm3-1/ATM3* plants compared to the wild type and both parents (Figure 4.1).

Table 4.1 Mutant lines in mitochondrial sulfur metabolism.

line	mutation	expression and enzyme activity	phenotype	publication
ethe1-3	T-DNA insertion in 5'-UTR (-64) *SALK_127065*	transcript ~60-70 enzyme activity ~36%	No growth difference to wild type	Krussel et al., 2014
ethe1-1	T-DNA insertion in 5'-UTR (-327) *SALK_021573*	transcript ~25% enzyme activity 1%	delayed embryo and seedling development, early senescence (short day/ extended darkness)	Krussel et al., 2014
atm3-4 /M2934	39 nucleotide deletion in promoter	transcript ~8%	growth delay, chlorophyll 90%, Seedling root length ~40%	Bernard et al., 2009
atm3-1 /starik1	T-DNA insertion at the position +1458	fusion protein of the membrane domain and neomycin phosphotransferase i.e. ATPase domain is lacking but protein is expressed	dwarfed, chlorophyll 50%, Seedling root length ~30%	Kushnir et al., 2001 Bernard et al., 2009
oastlc	T-DNA insertion in intron 1 *SALK_000860*	No OASTLC detected by immunolabelling	freshweight 75% Shorter root hairs, Growth phenotype under short day conditions	Heeg et al., 2006
nfs1-1	T-DNA insertion in 5'-UTR *SALK_083681*	transcript ~50%		Bernard et al., 2013

A

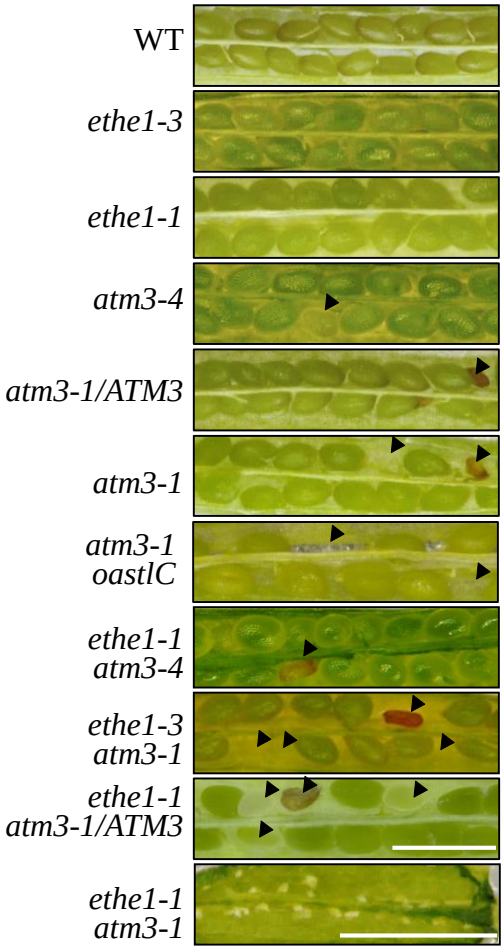

	healthy [%]	aborted [%]	not fertilised [%]	n
WT	97.2	1.4	1.4	847
ethe1-3	98.5	0.8	0.7	608
ethe1-1	97.7	1.90	0.4	1266
atm3-4	94.7	1.7	3.6	526
atm3-1/ATM3	94.6	4.7	0.7	1209
atm3-1	83.4	5.6	11	619
atm3-1 oastlC	80.9	1.9	17.2	577
ethe1-1 atm3-4	94.5	2.9	2.6	453
ethe1-3 atm3-1	73.2	8.7	18.1	358
ethe1-1 atm3-1/ATM3	74.1	25.2	0.7	1212
ethe1-1 atm3-1	0	0	100	--

B

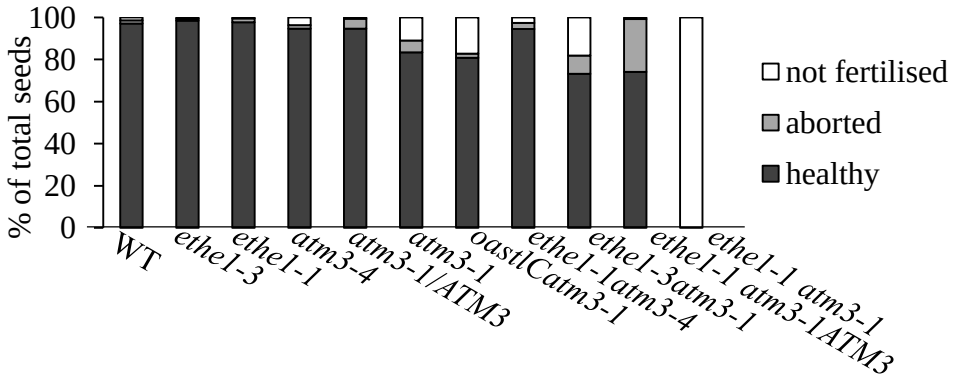

Figure 4.1 Seed development in single and double mutants of *ethe1* and *atm3* alleles. A. Percentages of normal and aborted seeds in siliques of indicated double mutants and parental lines. Scale bar is 1 mm. **B.** Bar graph of data in A.

Siliques from the hemizygous parent had 25.2% aborted and 0.7% unfertilised seeds which are most likely the *ethe1-1atm3-1* double mutant. *ethe1-1* as well as *oastlC* (characterised before, as described above) siliques showed maximally 2% in aborted or unfertilised seeds similar to the wild type, and *atm3-1* siliques had 5.6% aborted and 11% unfertilised seeds.

For further characterisation of the defect in the *ethe1-1atm3-1* double mutant, I investigated at what stage the embryo development is arrested (Figure 4.2). A third of the embryos were arrested in early development (globular to heart stage) while two thirds were arrested in the torpedo stage.

n	WT	aborted		
185	146	39		
		early abortion - globular	heart	torpedo - late torpedo
		5	8	26

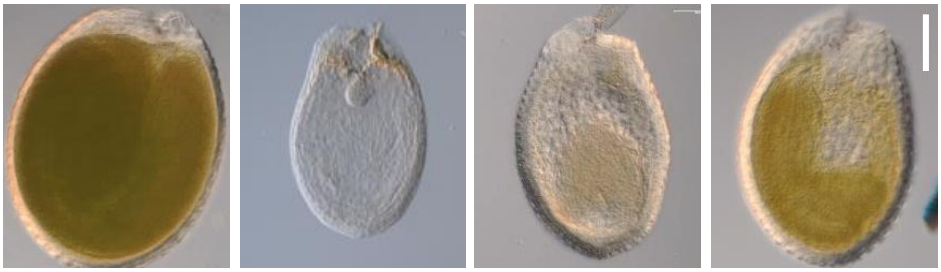

Figure 4.2 Embryo development in seeds from a *ethe1-1atm3-1/ATM3* parent. Seeds were scored when the majority of seeds were fully developed and healthy and aborted embryos were counted in 5 siliques from 2 independent plants. Pictures are representative for each category, scale bar is 100 μm.

Further analysis of over 2400 plants revealed that *ethe1-1atm3-1* double mutants segregate in a low percentage (1.9%) from the *ethe1-1atm3-1/ATM3* parent (data not shown). I analysed the growth phenotype of double mutants in young seedlings and mature plants (see Figure 4.3).

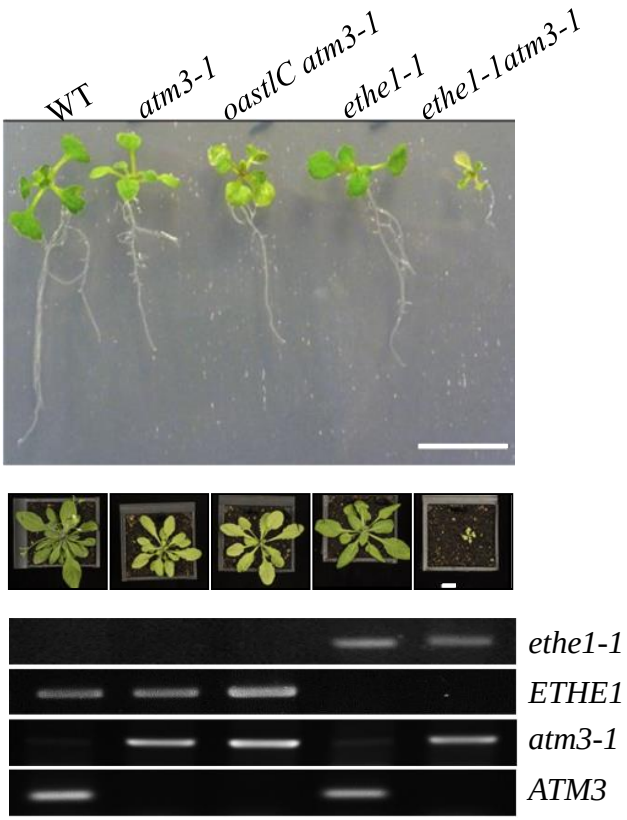

Figure 4.3 Growth phenotype of *ethe1-1atm3-1* double mutants. The *atm3-1 oastlC* double mutant served as a control. Seedlings were grown on ½ MS-agar for 16 days (upper panel), transferred to soil and grown for further two weeks (middle panel). Double mutants had to be isolated from a segregating *ethe1-1atm3-1/ATM3* parent and the genotype was confirmed (lower panel). Scale bar is 1 cm.

atm3-1ethe1-1 double mutants are smaller than both parents and show a severe delay in growth (Figure 4.3). Mature plants were found to be sterile and siliques were shortened and showed asymmetric valve growth (Figure 4.4). In contrast, seedlings as well as adult plants of *oastlCatm3-1* double mutants had an *atm3-1*-like growth phenotype with no enhanced phenotype. *oastlCatm3-1* double mutants were viable and fertile with 1.9% aborted and 17.2% unfertilised seeds. This indicates that there is no synergistic interaction between *ATM3* and *OASTLC*.

Figure 4.4 Silique phenotype of *ethe1-1atm3-1* plants in comparison to WT. Scale bar is 1 mm.

Because the *ethe1-1atm3-1* double mutant is infertile and difficult to obtain (~1 in 1000) I repeated the genetic analysis with weaker alleles of *ethe1* and *atm3* (Table 1.1) in the following combinations: *ethe1-1atm3-4* and *ethe1-3atm3-1*. As shown in Figure 4.5, the *atm3-4 ethe1-1* and the *atm3-1 ethe1-3* double mutant had a growth phenotype similar to the respective *atm3* parent.

Figure 4.5 Phenotypes of *ethe1atm3* double mutants. The *atm3-4* allele was crossed with the *ethe1-1* allele, the *atm3-1* allele was crossed with the *ethe1-3* allele. Seedlings were grown for 16 days on ½ MS-agar (upper panel), transferred to soil and grown for further two weeks (lower panel). Scale bar is 1 cm.

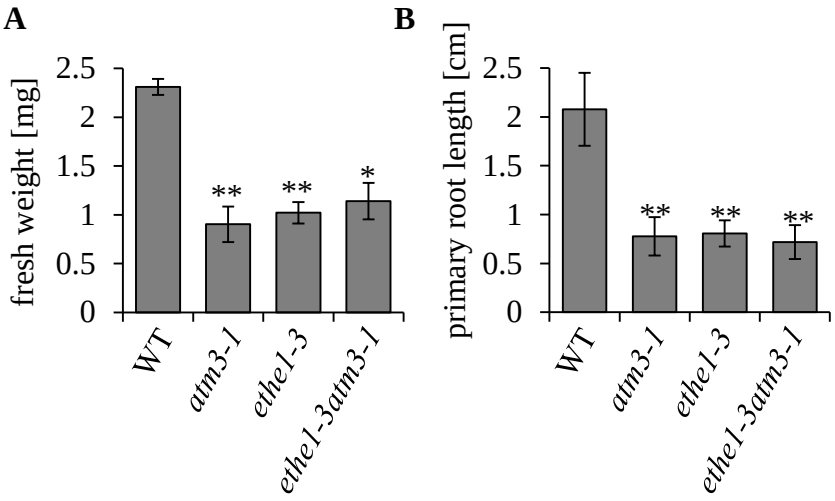

Figure 4.6 Phenotype characterisation of *ethe1-3atm3-1* seedlings in comparison to parental lines and the wild type. **A**. Fresh weight of 10-day-old individual seedlings grown on ½-MS agar. Values were calculated from measurements of 3-7 samples with 5 seedlings each. **B**. Primary root lengths of seedlings from A. Values are ± SD; * = p≤0.05, ** = p≤0.001 (Student's t-test).

When analysing the growth phenotype of the *ethe1-3atm3-1* mutants more closely, no growth differences to the more severe *atm3-1* parent were found in fresh-weight and root lengths in 10 day old seedlings grown on ½ MS-agar. *atm3-1* plants are known to have delayed growth and shorter roots (Bernard et al., 2009). The double mutant differed from the *atm3-1* parent only in the number of healthy versus non-viable seeds (aborted and unfertilised together). Healthy seeds were 83.4% in *atm3-1* siliques and 73.2% in the *ethe1-3atm3-1* mutant (see Figure 4.1) which was found to be significantly different (Student's t-test, $p<0.003$).

Taken together, *ETHE1* and *ATM3* show a synergistic genetic interaction. This is genetic evidence that *ATM3* and *ETHE1* function in the same pathway, thus supporting the hypothesis that ATM3 transports a persulfide compound from the mitochondria into the cytosol. However, *ATM3* did not show a synergistic genetic interaction with *OASTLC*.

4.2. ATM3 interacts genetically with *NFS1*

NFS1 mobilises S^0 in the mitochondria (which is then transferred to specific targets, generating persulfides) while ETHE1 oxidises the sulfhydryl group of glutathione-persulfide (see Chapter 1.5). Thus combining the *ethe1-1atm3-1* mutant with a *nfs1-1* allele could alleviate the phenotype by decreasing S^0 accumulation or it could worsen the phenotype by a further decrease of FeS assembly in the cytosol. This could be distinguished if a suppressor-phenotype or an additive phenotype is observed in the triple mutant, however, it is possible that a combination of both effects occurs. The *atm3-1* allele was chosen for this study because, as described in the previous section this showed most clearly a genetic interaction with *ethe1-1*. The *ethe1-1atm3-1/ATM3* plants were crossed with *nfs1-1* plants. In a first selection step, three lines were isolated from the segregating F2 generation: (1) *ethe1-1nfs1-1*/*NFS1atm3-1*/ATM3, (2) *nfs1-1atm3-1/ATM3* which lost the *ethe1-1* mutant allele and (3) *ethe1-1nfs1-1/NFS1* which lost the *atm3-1* mutant allele. The genotype analysis to identify these three lines was performed by Isobel Blower, an undergraduate doing work experience in the summer.

I isolated a line with the genotype *nfs1-1ethe1-1atm3-1/ATM3* from (1) but segregation was very low (1 in 24 plants). I will first describe phenotypes of the lines (2) and (3) and the isolation of a line with the genotype *nfs1-1ethe1-1*. I will then compare the results to the phenotype and segregation of *nfs1-1ethe1-1atm3-1/ATM3*. No double homozygous *nfs1-1atm3-1* segregated from line 2 (see Figure 4.7). The expected segregation rate for *nfs1-1atm3-1, nfs1-1atm3-1/ATM3* and *nfs1-1ATM3* was 1:2:1, however, all 16 analysed plants were of the *nfs1-1ATM3* genotype. This could indicate that the homozygous *nfs1-1* mutation in combination with the homozygous *atm3-1* mutation is lethal but only 16 plants were tested further analysis would be necessary to confirm this. In contrast, double homozygous plants for *nfs1-1ethe1-1* were isolated from line number 1 and 3 without difficulty (data not shown). These plants did not show any major growth differences in comparison to wild type (Figure 4.7B).

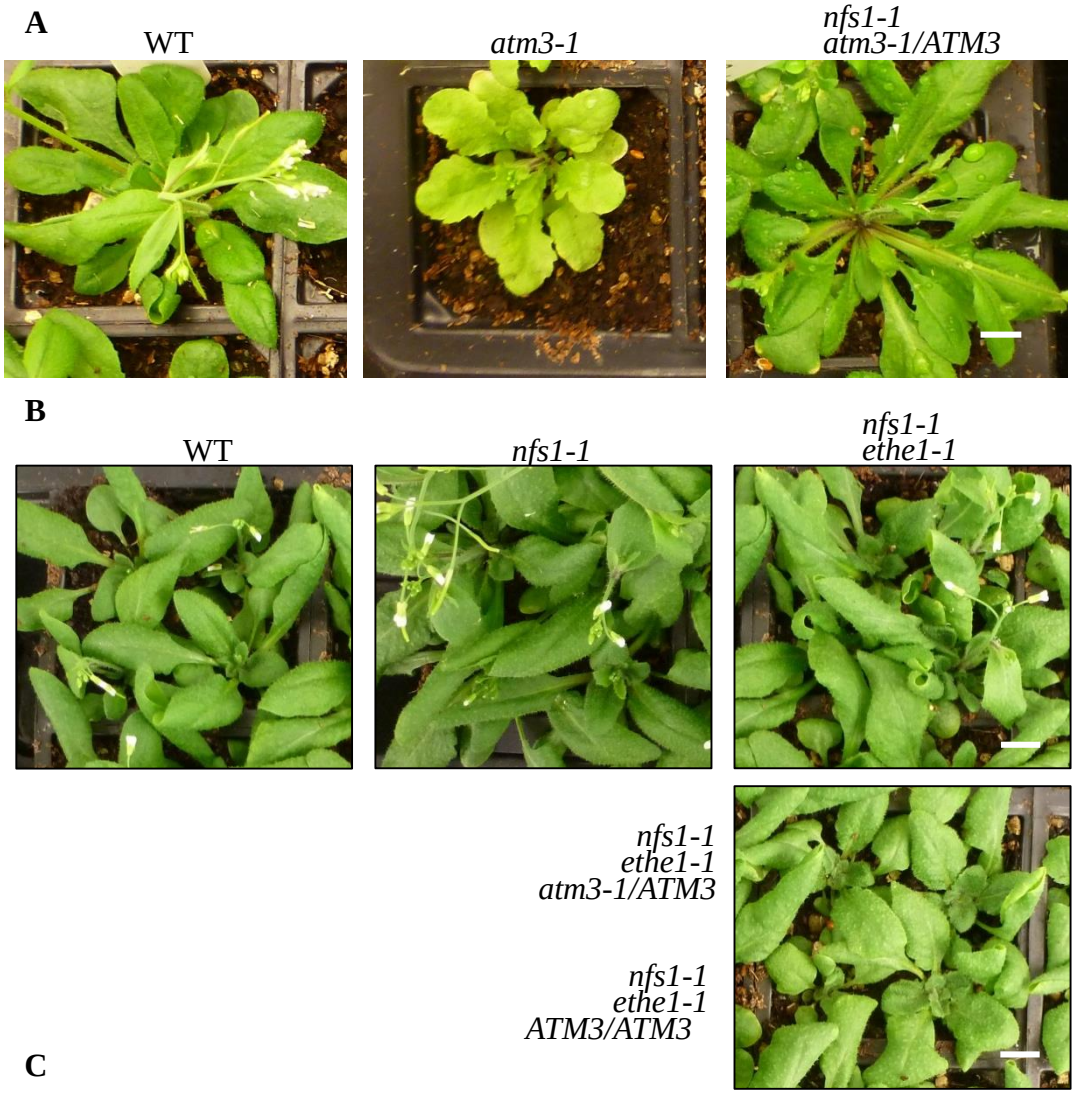

C

offspring atm3 genotype / parent	n	*ATM3/ATM3* [%]	*atm3-1/ATM3* [%]	*atm3-1/atm3-1* [%]
nfs1-1 ethe1-1 atm3-1/ATM3	24	46	54	0
nfs1-1 atm3-1/ATM3	16	100	0	0
ethe1-1 atm3-1/ATM3	82	28	67	5

Figure 4.7 Mutant phenotype of *nfs1-1ethe1-1* mutants in combination with *atm3-1*. A. Phenotype of mature *nfs1-1ethe1-1atm3-1/ATM3* plants recovered from the F1 generation of a *nfs1-1* plant cross fertilised with *ethe1-1atm3-1/ATM3*. Wild type (WT) and *atm3-1* as comparison. Scale bar is 1 cm. **B.** Phenotype of mature *nfs1-1ethe1-1ATM3/ATM3* and *nfs1-1ethe1-1atm3-1/ATM3* plants recovered from the offspring from A. WT, *nfs1-1* and *nfs1-1ethe1-1* as comparison. Scale bar is 1 cm. **C.** segregation of the *atm3-1* allele in the offspring from indicated lines, including *ethe1-1atm3-1/ATM3* (latter performed by Luke Browning).

Half of the analysed offspring from an *ethe1-1nfs1-1/atm3-1/ATM3* were heterozygous for the *atm3-1* allele (χ^2 goodness of fit p = 0.423) but it was not possible to isolate a triple mutant (Figure 4.7C). The parental line did not show any obvious growth difference to the *ethe1-1nfs1-1* double mutant (Figure 4.7B). As there are no visible growth defects in mature plants, it is likely that the lack of the *atm3-1* allele is due to defect in seed formation or fertilisation.

Luke Browning analysed the segregation from *ethe1-1atm3-1ATM3* plants. Here the *atm3-1/ATM3* genotype in comparison to the ATM3 genotype was found in a ratio close to 2:1 and a few plants were found to be homozygous for *atm3-1* which indicates that the *atm3-1* genotype is lethal.

To investigate if no triple mutant was recovered due to fertilisation or embryo development defects I analysed the seed segregation in siliques of *ethe1-1/ethe1-1nfs1-1/nfs1-1atm3-1/ATM3* plants in comparison to those of the *nfs1-1ethe1-1* mutant (see Figure 4.8).

A

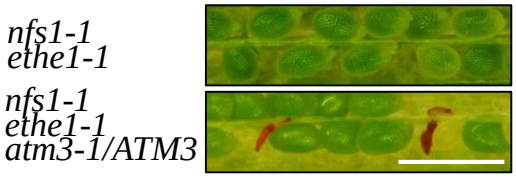

B

line	n	healthy	aborted	not fertilised
nfs1-1ethe1-1	589	95.9	1.2	2.9
nfs1-1ethe1-1atm3-1/ATM3	883	65.8	29.6	4.6

Figure 4.8 Segregation analysis of the *atm3* allele in *nfs1-1ethe1-1atm3-1/ATM3* and *nfs1-1ethe1-1* plants. **A.** Silique phenotype. Scale bar siliques 1 mm. B. Seed phenotype of mature siliques. **B.** Quantification of seed segregation in mature siliques from 2-4 plants.

Siliques from *nfs1-1ethe1-1* plants were wild-type like with 95.9% healthy seeds compared to 97.2% (Figure 4.1 and 4.8). In contrast, siliques from *ethe1-1nfs1-1atm3-1/ATM3* plants only had 65.8% healthy seeds.

To conclude, the *atm3-1/ATM3* genotype was only found in combination with the homozygous *nfs1-1* genotype when segregating from a *nfs1-1/NFS1atm3-1/ATM3*

background but not in the absence *NFS1*. However, from an *nfs1-1* homozygous genotype combination with an *ethe1-1* homozygous genotype, the *atm3-1* allele segregated 1:1 ATM3 to *atm3-1*/*ATM3*. The 1:1 genotype segregation indicates female sterility when the *atm3-1* allele is present as defect pollen could be replaced by *ATM3* pollen to fertilise healthy ovules in case of male sterility of the *atm3-1* genotype. The segregation ratio of the *atm3-1*/ATM3 genotype was found to be higher in the *ethe1-1* background than in the *nfs1-1* background. All in all this shows that the combination of a *nfs1-1* mutant allele and a *atm3-1* mutant allele is more harmful than combining either, *nfs1-1* or atm3-1 with an *ethe1-1* allele.

4.3. Quantitative analysis of persulfide accumulation using a sulfane sulfur probe

As stated above, ATM3 could transport an oxidises glutathione carrying S^0. A direct approach to test for persulfide accumulation was by using a S^0 specific probe. Chemical compounds that can be used *in-vivo* to detect S^0 have recently been developed (Chen et al., 2013). The Sulfane Sulfur Probe 4 (SSP4) is an improved version of the SSP2 which was described in (Chen et al., 2013) and kindly donated for testing *in-planta*. (Chen et al.) successfully tested SSP2 in mammalian cells; however, it was not clear if SSP4 would also be suitable for plant cells. The probe consists of an inactive fluorophore linked to a nucleophilic compound. Sulfane sulfur can react with the nucleophilic component to form an intermediate containing a SH group. The fluorophore serves as an electrophile causing the SH group to undergo a spontaneous cyclisation thus releasing an activated fluorophore (see Figure 4.9, taken from (Chen et al., 2013)).

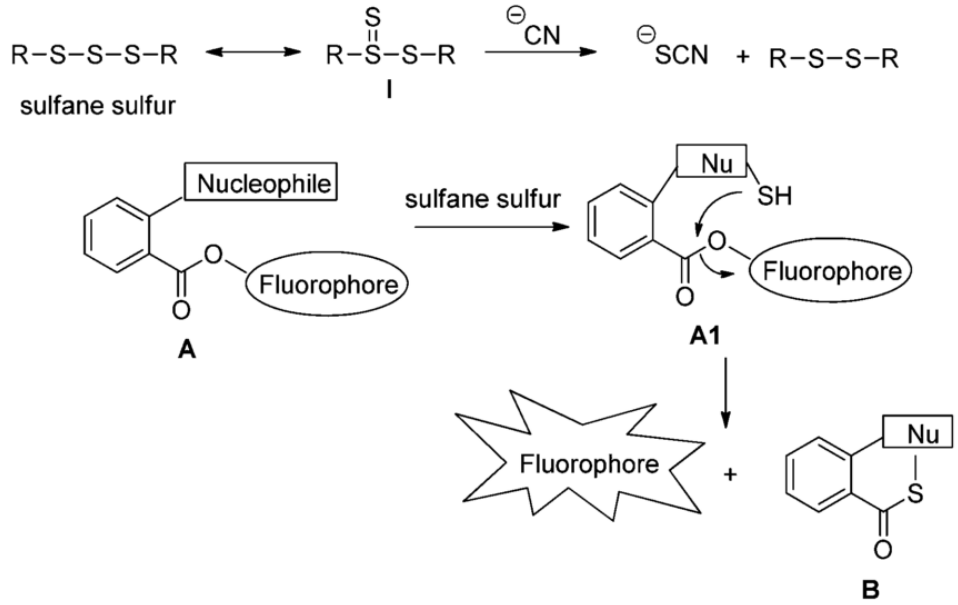

Figure 4.9 Idea of the reaction-based fluorescent probes for sulfane sulfur detection. figure from (Chen et al., 2013)**.**

I tested SSP4 *in-vivo* on whole leaves, dissected embryos, root tissue and protoplasts of *ethe1-3atm3-1* mutants. The expectation was that S^0 staining would be most intense in *ethe1-3atm3-1* double mutants and localised in the mitochondria. However, it was difficult to find samples emitting a visible signal at all and results were not consistent with or between experiments. The comparison between the double mutant and the wild type showed hints of stronger staining in some experiments but this was not reproducible and not true for all experiments. To illustrate the localisation of the SSP4 probe, selected root samples and protoplast samples of the double mutant are shown in Figure 4.10. The probe will be discussed further in Section 4.5. The SSP4 probe has potential to be a very accurate tool to monitor persulfide accumulation *in-vivo*, however, infiltration of plant material needs to be optimised and it is still unclear why the localisation of the probe is inconsistent.

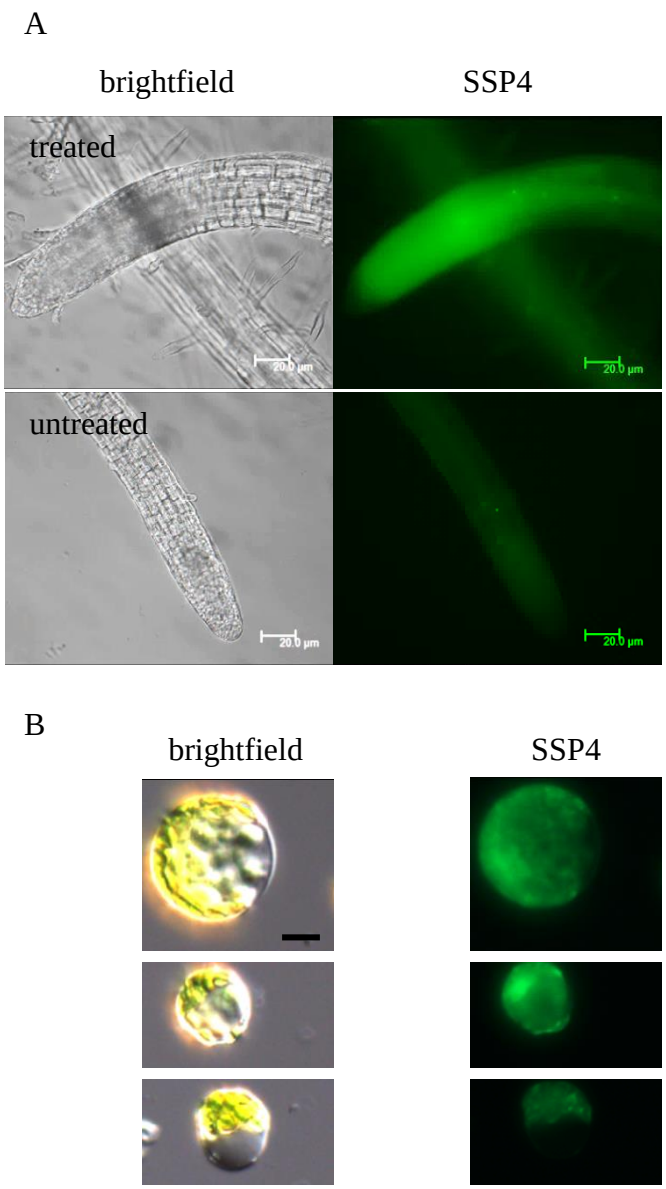

Figure 4.10 Visualisation of sulfane sulfur in *ethe1-3atm3-1* double mutants. Sulfane sulfur was detected using the specific sulfane sulfur probe 4 (SSP4) with maxima of excitation at 485 nm and emission at 515nm. Excitation range was 460-500 nm, emission range 512-543 nm **A.** SSP4 fluorescence in roots. Samples without SSP4 treatment served as a control. Scale bar is 20 µm. **B.** SSP4 fluorescence in leaf protoplasts. Scale bar is 10 µm.

4.4. Analysis of persulfide accumulation by measuring Complex IV activity

As described in Section 1.5 Sulfur components and especially non-physiological levels of the signalling molecule H_2S strongly inhibit cytochrome *c* oxidase activity (Complex IV) in mammals and plants and thus a decrease of Complex IV activity could indicate sulfide accumulation as shown in (Birke et al., 2012). This could possibly be used to indirectly detect persulfide accumulation in the mitochondria.

Cytochrome *c* oxidase activity can be quantified in isolated mitochondria by measuring the oxidation of cytochrome *c* photospectrometrically (see Figure 4.11). Activity of Complex II/III was used as a reference. Isolation of mitochondria requires a large amount of plant tissue and as the *ethe1-1atm3-1* double mutant is infertile and only few plants are found from a segregating parent. Thus I generated root callus cultures for mitochondria isolation. Measurements were carried out from 4-5 preparations and assays were repeated 4-5 times. However, it was not possible to yield conclusive data from the measurements, as the values for cytochrome *c* oxidase activity were very variable and thus no conclusions could be drawn (see Figure 4.12).

To conclude, indirect assessment of persulfide accumulation by measuring Complex IV activities in mitochondria from callus cultures were found to be not suitable and a viable double mutant with a strong phenotype would be needed for further experiments.

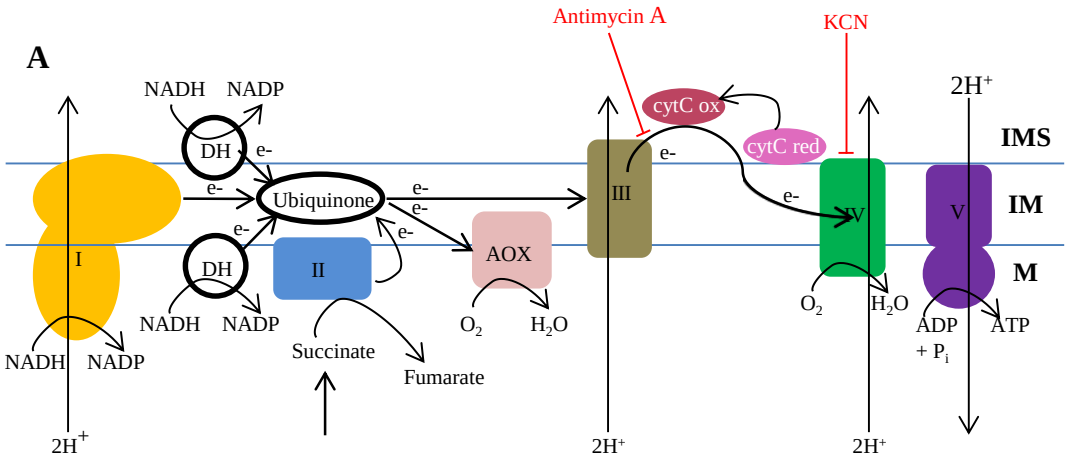

Figure 4.11 Schematic diagram of the respiratory chain. The mitochondrial respiratory chain is shown schematically. Combined Complex II+III activity was measured by addition of succinate for electron donation and oxidised cytochrome *c* as an electron acceptor. Enzyme activity was monitored as the reduction of cytochrome *c* (increasing absorption at 550 nm). Non-specific cytochrome *c* reduction was measured after inhibition with Antimycin A.
Complex IV activity was measured as the oxidation of cytochrome *c* which was measured spectrophotometrically at 550 nm. Non-specific cytochrome *c* oxidation was measured after inhibition of Complex IV with potassium cyanide (KCN).
I = NADH:Ubiquinone-Oxidoreductase,
II = Succinate:Ubiquinone-Oxidoreductase,
III = Ubiquinone:Cytochrome-*c*-Oxidoreductase,
IV = Cytochrome-*c*-oxidase, V = ATP-synthase, DH = dehydrogenases, AOX = alternative oxidase, cytC = cytochrome *c*, ox = oxidised, red = reduced

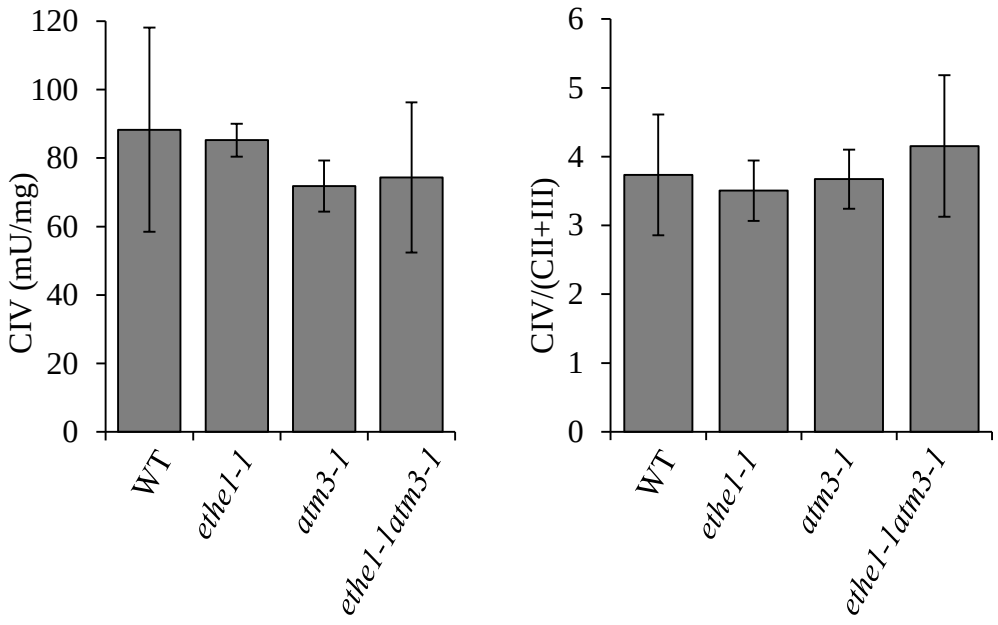

Figure 4.12 Complex IV activity in callus mitochondria of *ethe1-1atm3-1, atm3-1, ethe1-1* and wild type. Complex IV activity was measured as the oxidation of cytochrome *c* at 550 nm. Complex II+III activity was measured as the reduction of cytochrome *c* at 550 nm. Values are the mean of 3-5 measurements ±SD. **A.** Complex IV activities in mU/mg. **B.** Normalised complex IV activity displayed as the ratio of complex IV to complex II+III activity.

4.5. Discussion

As discussed above, the substrate of ATM3 was proposed to be an oxidised glutathione-persulfide. Evidence for the persulfide being transported is difficult to obtain *in-vitro* and more so *in-vivo*. As an indirect approach to gain *in-vivo* data, I conducted genetic interaction studies with *ATM3* and three other components of the mitochondrial sulfur metabolism: *NFS1* which mobilises S^0 from from cysteine, *ETHE1* which is involved in sulfide detoxification during amino acid break down and *OASTLC* which contributes to cysteine homeostasis by generating cysteine from sulfide and O-acetylserine. The genetic interaction studies showed that *ATM3* synergistically interacts with *ETHE1* as well as *NFS1* but not with *OASTLC*.

The interaction of *ATM3* with *NFS1* is a good indicator that ATM3 transports a substrate containing a S^0 as NFS1 is the only cysteine desulfurase in the mitochondria. The interaction between *ATM3* and *ETHE1* provides further evidence as ETHE1 was found to be highly specific for glutathione-persulfide (Krussel et al., 2014). Thus, if ATM3 does transport an oxidised glutathione-persulfide it would be possible that excess glutathione-persulfide in *atm3* mutants is detoxified by ETHE1.

The SSP4 probe was tested successfully in human cell cultures before (Chen et al., 2013). When testing the probe in plant cells I observed inconsistency of the SSP4 fluorescence and it seemed that the localisation varied as well. Especially in protoplasts it was evident that the probe located to the chloroplasts, cytosol and mitochondria to varying extends between preparations of the mutant line *ethe1-3atm3-1*. Of all tested tissues (dissected embryos, leaves, roots, protoplasts) only root tips and protoplasts showed a signal that was significantly different from the untreated control. It is possible that the plant cell wall inhibits SSP4 uptake. The cell wall is removed during protoplast preparation which probably leads to the uptake in protoplast samples. Roots are prone to take up the probe during natural liquid uptake. Root hairs should be more susceptible for uptake of SSP4 as the cell wall here is thinner, however, no increase in SSP4 signal was found in this tissue compared to other root cells. The strong signal in root tips specifically could be due to the high cell and mitochondria density in this tissue. However, it was difficult to locate mitochondrial patterns. It remained unclear if the signal was specifically higher in mitochondria. Unfortunately, neither the signal in root tips nor in protoplasts was stably reproducible. It remains unclear if this was due to inconsistent penetration of

the probe or if sulfur accumulation of the same plant line varied. For future research it will be necessary to test the uptake into plant cells also using methods to increase permeability of whole plant cells and to investigate the variation in localisation.

As a different approach of measuring persulfide accumulation I tested an assay to measure the decrease of Complex IV activity in isolated mitochondria as an indicator for sulfur toxicity. The results from this assay were variable. This could be due to suppressor mutations occurring in the cell cultures. The initial root tissue cultures of double mutants grew very slowly in comparison to parental and wild-type lines. Callus cultures need to be maintained over several months to harvest enough material and cultures of double mutants showed enhanced growth over time (data not shown). Suppressor mutations can occur in a high frequency in callus tissue and could overcome the effect of the original mutations, however, more research would be needed to fully understand the reason for improved growth. Another factor that has to be considered is the isolation procedure of mitochondria which could stress cells to varying extends, depending on the quality of the preparation leading to altered metabolism.

It is, however, also possible that the accumulation of persulfide due to the lack of export by ATM3 and the lack of detoxification by ETHE1 in the *ethe1-1atm3-1* double mutant never reaches a level that would cause notable damage to complex IV activity. In this case even the optimisation of sample production would not show a decrease of complex IV activity in the double mutant.

Taken together, further optimisation is needed for successful *in-vivo* visualisation of persulfide accumulation in Arabidopsis in a quantitative way. ATM3 shows synergistic genetic interactions with NFS1 which mobilises a S^0 which is then thought to be incorporated into oxidised glutathione and with ETHE1 which uses a glutathione-persulfide as a substrate but not with OASTLC which uses sulfide exclusively. This provides *in-vivo* evidence that ATM3 does transport a glutathione with an additional S^0 as it is needed for FeS assembly.

5. The role of glutaredoxins in mitochondrial and cytosolic FeS assembly

The mitochondrial and cytosolic FeS assembly pathways in plants are linked by the mitochondrial components NFS1 and ATM3 (Bernard et al., 2009; Bernard et al., 2013). As discussed before, there is *in-vitro* evidence that ATM3 exports a glutathione compound with an additional S^0 into the cytosol (Schaedler et al., 2014). In Chapter 3 I provided supporting *in-vivo* evidence for the transport of oxidised glutathione. It is possible that glutaredoxins are involved in the assembly or transfer of the glutathione compound transported by ATM3. Class II monothiol glutaredoxins have been linked to FeS assembly in yeast and animals (see Chapter 1.6). The mitochondrial monothiol glutathione Grx5 in yeast is vital for the activity of FeS cluster enzymes (Rodriguez-Manzaneque et al., 2002). In plants all four identified monothiol glutaredoxins GRXS14-17 were shown to complement the yeast *grx5*Δ mutant. GRXS14 and GRXS16 are located in the plastids, GRXS17 in the cytosol and GRXS15 in the mitochondria (Bandyopadhyay et al., 2008; Cheng, 2008; Knuesting et al., 2015; Moseler et al., 2015). However, it remains unclear if and how plant glutaredoxins are involved in FeS assembly as *in-planta* data is scarce. In Arabidopsis, the nucleo-cytosolic GRXS17 and the mitochondrial GRXS15 glutaredoxin are the only confirmed class II glutaredoxin in the respective compartment. Arabidopsis mutants of GRXS17 and GRXS15 have become available recently which provided a good opportunity to study the effect of glutaredoxin depletion on FeS assembly *in-vivo*. The results for GRXS17 were included in the publication by (Knuesting et al., 2015) and will be presented first.

5.1. The growth phenotype of *grxS17* mutant plants differs from that of *atm3* mutants

To investigate the effect of GRXS17 depletion on cytosolic FeS enzymes three *grxS17* lines (kindly donated by the group of Pascal Rey, Biosciences and Biotechnologies Institute of Aix-Marseille) were analysed: a T-DNA insertion line with no detectable GRXS17 protein (*grxS17*), a partially complemented *grxS17* line (C3) and a fully complemented *grxS17* line (C17); the complemented plants were

transformed with the *GRXS17* cDNA under the control of the CaMV-35S promoter (see Knuesting et al., 2015). *grxs17* mutants were compared to the intermediate *atm3-4* and the severe *atm3-1* mutants, which served as a reference for the phenotype of mutants involved in cytosolic FeS assembly. *grxS17* plants show elongation of petioles under standard conditions which is increased under heat stress conditions at 28°C (Cheng et al., 2011) and thus experiments were conducted on plants grown under both conditions (see Figure 5.1).

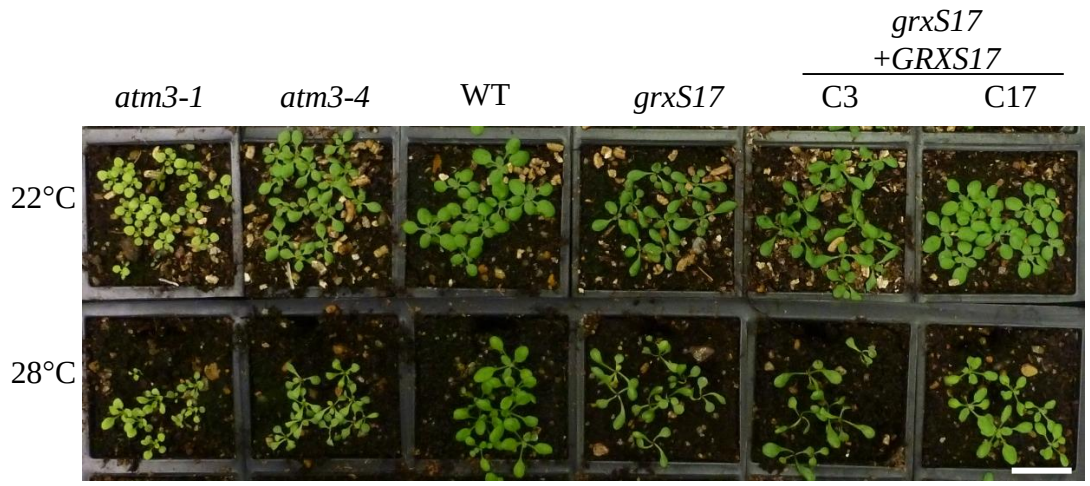

Figure 5.1 Growth of *grxS17* mutants at 22°C and 28°C. *grxS17* knock-out mutants, two complemented lines (C3, C17), two *atm3* alleles and the wild type (WT) were grown for 14 days under standard conditions (22°C) or transferred after 7 days to 28°C.

Under standard growth conditions, the *grxS17* knock-out had elongated petioles and narrow, elongated leaves. In contrast, *atm3* mutant lines were chlorotic and delayed in growth. The *grxS17* phenotype was partially rescued in the complemented C3 line. The complemented line C17 had a fully restored growth phenotype. Under high temperatures (28°C), the *grxS17* mutants showed a further increase in petiole length and the meristem is arrested (not shown, see (Knuesting et al., 2015)). The C17 line was not fully rescued under these conditions in comparison to the wild type. At 28°C the *atm3* mutants had elongated petioles but did not show any other visible phenotype alterations. It has to be noted that the *grxS17* mutant presented here is a full knock-out and shows considerable differences to *atm3-1* which has part-functional ATM3 protein. A full knock-out of ATM3, the *atm3-2* T-DNA insertion mutant, was described to be male sterile with dwarfed, chlorotic plants

(Bernard et al., 2009). This indicates that GRXS17 has a non-essential function under standard growth conditions.

5.2. *grxS17* mutant plants have a minor decrease in FeS enzyme activities

In order to determine whether FeS enzyme activities in the cytosol or mitochondria are altered in *grxS17* mutants I investigated protein stabilities and activities of the cytosolic and mitochondrial isoforms of aconitase and isoforms of the cytosolic aldehyde oxidase (see Figure 5.2).

Aconitase protein levels were analysed by immunoblotting. The *grxS17* and C3 plants were found to have a decrease in aconitase activity, similar to *atm3* mutants under both temperature conditions while the aconitase activity in C17 line was similar to the wild type. However, there was an inverse correlation between enzyme activity and mutant phenotype at 22°C and 28°C. Aconitase activities were measured in an in-gel assay which separated mitochondrial and cytosolic isoforms. *grxS17* and C3 plants had decreased cytosolic aconitase activity and increased mitochondrial activity in comparison to the wild type, however, the change was not as severe as in *atm3* mutants. Activities were partially complemented in the C17 mutant. Densitometric analysis of 3 repeats showed that the relative change in mitochondrial and cytosolic aconitase activities was similar under standard and elevated temperatures. All three *grxS17* mutants showed a mild decrease in aldehyde oxidase activity under standard temperature conditions but not at 28°C. *atm3* mutants had undetectable aldehyde oxidase activities under both conditions. PsaA levels served as a protein loading control and were unaltered in all samples. This also indicates that FeS assembly in the plastids is not affected in mutants of *GRXS17*.

The data presented here show that FeS activity is only mildly affected in *grxS17* knock-out plants, however, knock-out of components of FeS assembly (like NFS1 and the cytosolic assembly proteins AE7, NAR1, DRE2, NBP35) are lethal (Bernard et al., 2009; Bernard et al., 2013). This indicates that GRXS17 does not have a function in *de-novo* FeS assembly. The results are included in the publication by (Knuesting et al., 2015) in which evidence is presented that GRXS17 interacts with the nuclear factor Y subunit C11 (NF-YC11) in the maintenance of the shoot apical meristem under long-day conditions.

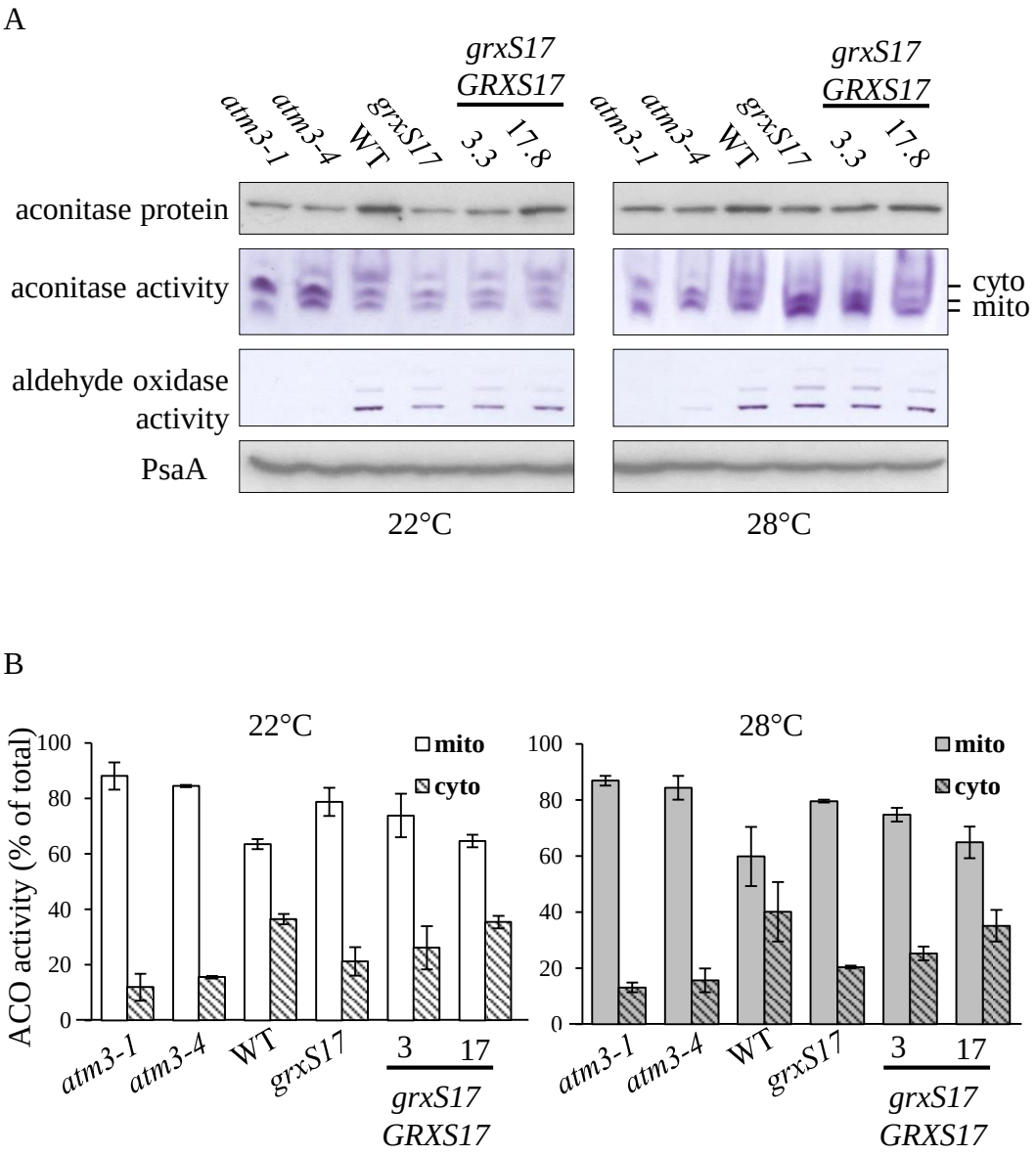

Figure 5.2 FeS enzyme activities in *grxS17* lines under standard and elevated temperature conditions. *grxS17* knock-out mutants, two complemented lines (C3, C17), two *atm3* alleles and the wild type (WT) were grown for 14 days under standard conditions (22°C) or transferred after 7 days to 28°C. **A.** The activities of aconitase and aldehyde oxidase isozymes were visualized as a formazan precipitate in a native gel assay using synthetic substrates. The cytosolic (cyto) and mitochondrial (mito) isoforms of aconitase are indicated. Protein levels of aconitase and PsaA (Photosystem I) were visualised by immunoblotting under denaturing conditions and labelling with specific antibodies **B.** Densitometric analysis of cytosolic and mitochondrial aconitase activity as quantified using ImageJ software. Values are percentages of the sum of all band intensities per lane (mean ± SD; n = 3).

5.3. Growth phenotype of *grxS15* mutants in comparison to *atm3*

For investigation of the role of GRXS15 in FeS cluster assembly two mutant lines of GRXS15 were used: A *grxS15* knock-out complemented with a copy containing a codon change to substitute K83 to A, which was generated by Anna Moseler (*grxs15-3* UBQ10:GRXS15 K83>A). K83 is a conserved residue predicted to be involved in glutathione binding (Moseler et al., 2015). This line will be referred to as *K83A*. The second line was an amiRNA suppressor line generated by Elke Stroher and will be referred to as *amiR* (Stroher et al., 2016). The phenotypes of grxS15 mutants are shown in Figure 5.3. The phenotype of the *amiR* line was heterogeneous but all plants were smaller than the wild type. Individuals of the *amiR* line with a severe phenotype and all plants of the K83A line had dwarfed stature and altered root growth in common. When comparing these plants to *atm3-1*, the *grxS15* mutants were smaller and only showed patches of chlorosis along the mid rib.

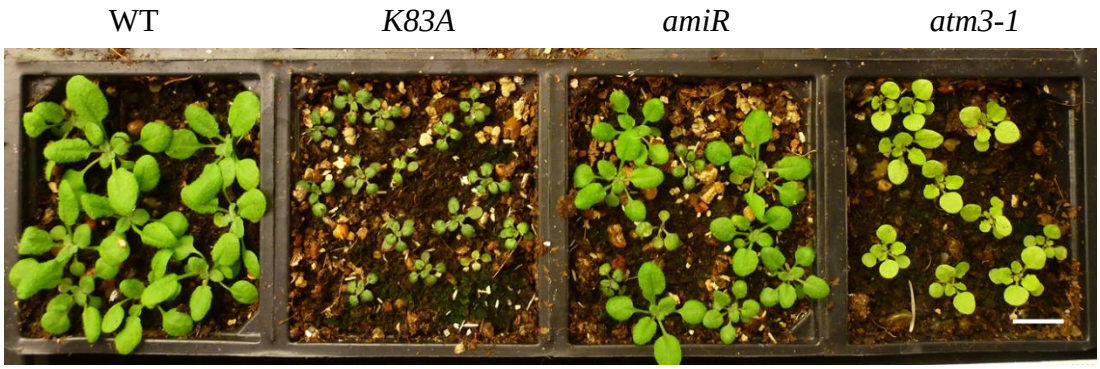

Figure 5.3 Growth of *grxS15* mutants. *grxS15-3* knock-out mutants expressing UBQ10:GRXS15K83>A (*K83A*) and an amiRNA line (*amiR*) were grown alongside the strong *atm3-1* allele and a wild type. Scale bar is 1 cm.

5.4. *grxS15* mutants have 40% mitochondrial aconitase activity but no significant decrease in aldehyde oxidase activity

The two recent publications by the groups of Harvey Millar (Stroher et al., 2016) and Andreas Meyer (Moseler et al., 2015) suggested a role of GRXS15 in mitochondrial FeS assembly. However, (Moseler et al., 2015) measured a 65% decrease in total aconitase while (Stroher et al., 2016) reported that there was no difference in aconitase activity in mitochondrial extracts. Thus I investigated further if *grxS15* mutants have a mitochondrial or cytosolic FeS enzyme defect. I visualised the mitochondrial and cytosolic aconitase activity in an in-gel assay (Figure 5.4). Results are representative for three repeats of which one was performed with Anna Moseler.

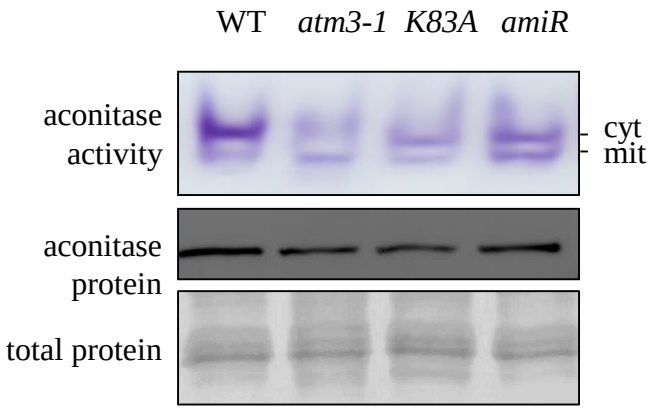

Figure 5.4 Aconitase activities in whole leaf extracts of *grxS15* mutants. Extracts were prepared from *grxS15* mutants (*K83A*, *amiR*), *atm3-1* mutants and a wild type (WT) grown for 2 weeks on plates and then transferred to soil and grown for further 3 weeks. Aconitase activity was measured in a native in-gel assay coupled to activity of isocitrate dehydrogenase activity and the formation of a purple precipitant. Aconitase protein levels were visualised by immunoblotting of an identical gel under denaturing conditions. Total protein staining served as a loading control.

In the in-gel assay, wild-type plants showed a very characteristic pattern of one strong cytosolic band and two significantly weaker mitochondrial bands (Bernard et al., 2009) which are sometimes not separated and appear as one. The *atm3-1* plants have strongly decreased cytosolic activity and can have increased mitochondrial activity (not visible in figure 1.4). Both *grxS15* mutant lines had consistently decreased cytosolic aconitase activity and the mitochondrial activities were increased.

To determine quantitatively if mitochondrial aconitase activity is affected I measured the enzyme activity spectrometrically in isolated mitochondria of wild-type, *K83A* and *amiR* plants. The mitochondria for the *grxS15* mutants were isolated in two different preparations and the activities are shown as a percentage of the wild-type which was included on each day of the mitochondrial preparation to account for variations of mitochondria-quality between preparations (Figure 5.5).

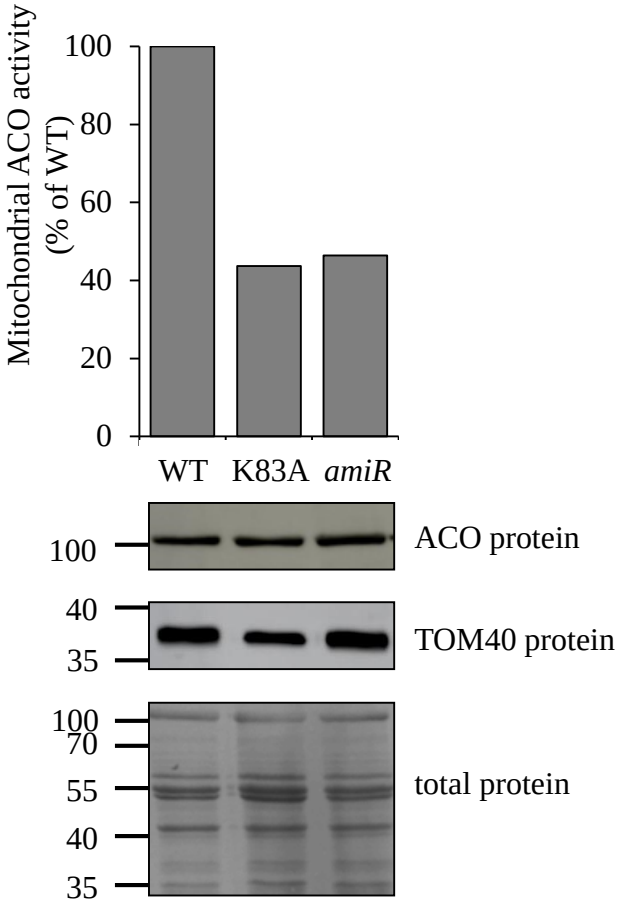

Figure 5.5 Aconitase activities in mitochondria of *grxS15* mutants. Mitochondria were extracted from *grxS15* mutants (*K83A, amiR*) and a wild type (WT). Plants were grown on soil for 29-35 days. Aconitase (ACO) activity was measured in a spectrometric assay coupled to activity of isocitrate dehydrogenase activity and the conversion of NADP to NADPH at 340 nm (two technical repeats). Activities are shown as percentage of the wild type (WT). ACO and translocase of the mitochondria 40 (TOM40) protein levels were visualised by immunoblotting of an identical gel under denaturing conditions. Total protein staining served as a loading control.

The activity of mitochondrial aconitase is decreased by about 60 % of the wild-type activity in both mutant samples. This experiment was performed on one biological replicate with two technical repeats. However, the decrease in mitochondria activity was confirmed by Anna Moseler (personal communication). Considering the strength of the mutant phenotype of the *K83A* line, this decrease in aconitase activity is not severe enough to account for the growth defect.

I also measured aldehyde oxidase activities in total leaf extracts in a native in-gel assay (Figure 5.6). Aldehyde oxidase activities were found to be wild-type like in both *grxS15* mutants while *atm3-1* had no detectable aldehyde oxidase activity.

To summarise, mitochondrial extracts of *grxS15* mutants had decreased aconitase activity. Aconitase protein levels and aldehyde oxidase activities were found to be similar to the wild type. This indicates that GRXS15 is not essential for *de-novo* FeS assembly and the observed defects could be due to secondary effects on FeS assembly or insertion.

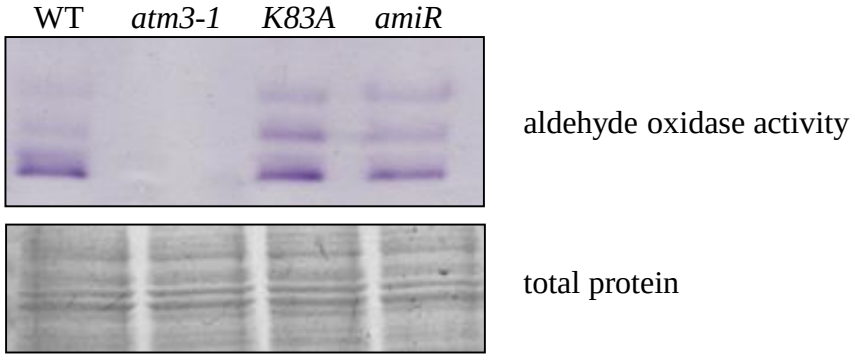

Figure 5.6 Aldehyde oxidase activities in whole seedling extracts of *grxS15* mutants. Extracts were prepared from *grxS15* mutants (*K83A*, *amiR*), *atm3-1* and a wild type (WT). Plants were grown on ½-MS agar for two weeks. Aldehyde oxidase activity was measured in a native in-gel assay coupled to the formation of a purple precipitant. Total protein was visualised in an identical gel under denaturing conditions.

5.5. *grxS15* mutant plants may have a defect in biotin and lipoate cofactor synthesis

(Stroher et al., 2016) showed that lipoate cofactor biosynthesis is affected in *grxS15* mutants for specific proteins: lipoate cofactor binding was decreased for H-proteins which are part of the glycine decarboxylase complex. Two out of three tested isoforms of E2 subunits of pyruvate dehydrogenase but not for an isoform of the E2 subunit of branched-chain acid dehydrogenase also had less lipoate. Furthermore, they found that lipoate synthase 1 (Lip1) levels were decreased in the *amiR* line. Lipoate synthase contains a Fe_4S_4 cluster which is turned over during enzyme function as two sulfur atoms from the cluster are incorporated into octanoate to form lipoate (Marquet et al., 2001).

First, I repeated the immunoblot analysis for lipoate cofactor binding and I included the *K83A* mutant which has not been tested before. Lipoate cofactor labelling was performed with Andrew Maclean (Group of Janneke Balk, John Innes Centre, Norwich) (Figure 5.7A). The H-protein immunoblot was generated by Andrew Maclean and is displayed for comparison with his permission (Figure 5.7B). Specific antibodies were used for immunodetection of the lipoate cofactor (Figure 5.7). Both *grxS15* lines showed a decrease of lipoated H-protein. A decrease in lipoated H-protein has been observed in the *amiR* line before by Stroher et al (2016) which was now observed for the K83A line as well. The levels of H-protein were not affected, indicating a lack of lipoate cofactor or a defect in incorporation into H-proteins.

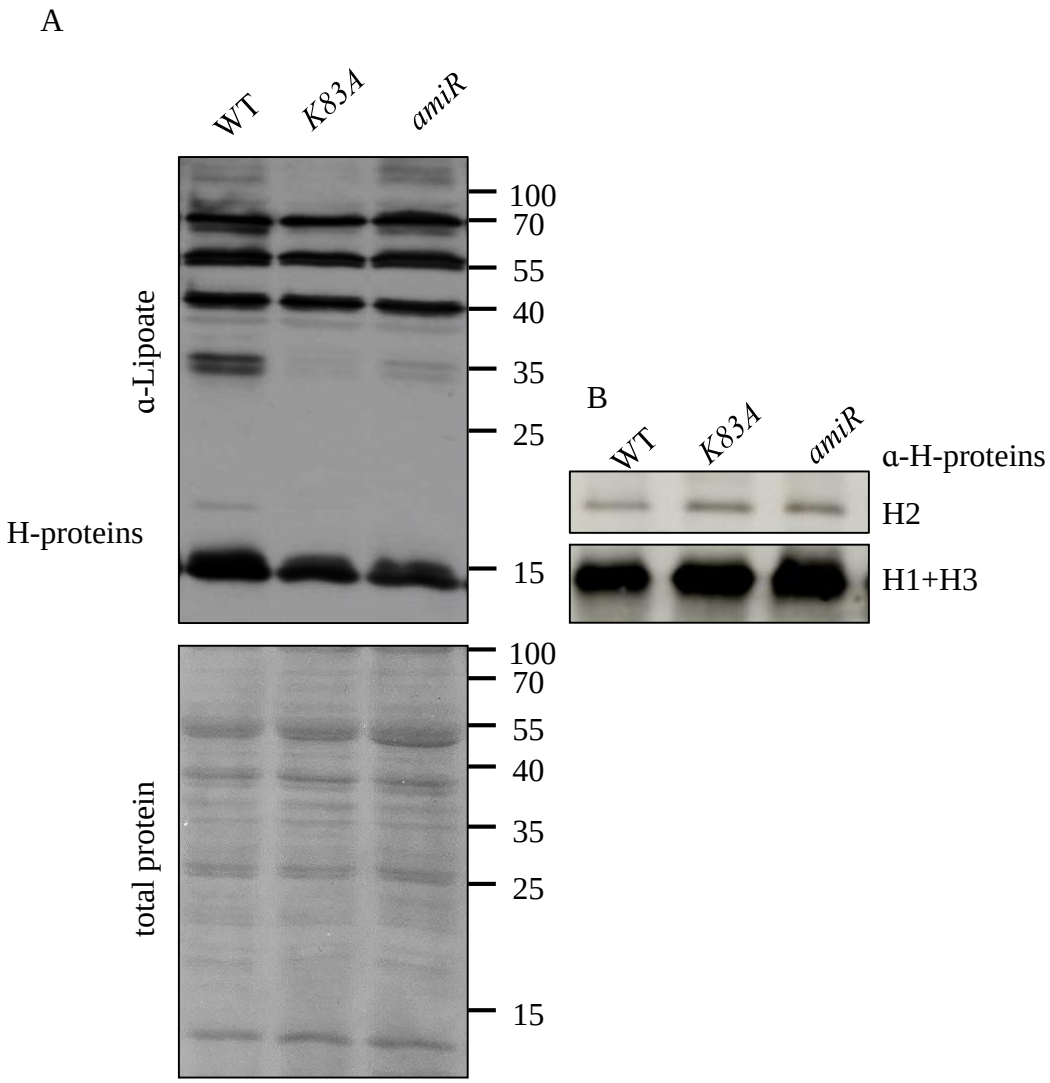

Figure 5.7 Lipoate proteins in *grxS15* mutants. A. Mitochondria were extracted from *grxS15* mutants (*K83A, amiR*) and a wild type (WT). Plants were grown on soil for 29-35 days. Lipoate proteins were labelled with a lipoate specific antibody after denaturing PAGE. Total protein served as a loading control. Mitochondria extraction and lipoate labelling was performed with Andrew Maclean (Group of Janneke Balk, John Innes Centre, Norwich). **B.** H-protein levels in an identical sample as for A. Data displayed in figure B was generated by Andrew Maclean and is displayed here for comparison with his permission.

To further investigate if GRXS15 is involved in the repair of FeS I also analysed biotin cofactor assembly. Biotin synthase contains a Fe_2S_2 cluster which is turned over during enzyme function as a sulfur from the cluster is transferred to desthiobiotin to form biotin. I visualised biotin in leaf samples separated by denaturing PAGE using a Strep-tactin® antibody conjugated to horseradish peroxidase (Figure 5.8).

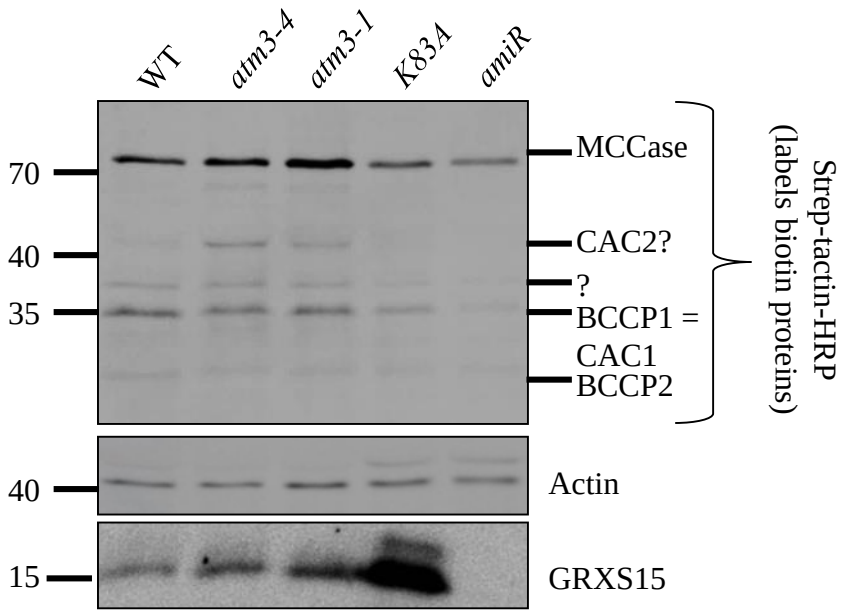

Figure 5.8 Biotin levels in whole seedling extracts of *grxS15* mutants. Extracts were prepared from *grxS15* mutants (*K83A*, *amiR*), two *atm3* alleles and a wild type (WT). Plants were grown on ½-MS agar for ten days. Biotin-containing proteins were labelled immunologically after denaturing PAGE with antibody strep-tactin antibody conjugated with horseradish peroxidase (HRP) which is specific for biotin proteins. Actin and GRXS15 protein levels served as controls.

Biotin labelling in specific bands was decreased in the *K83A* sample and the *amiR* sample. To investigate if this is due to lack of sulfur transfer to desthiobiotin by biotin-synthase, I treated plants with desthiobiotin or biotin (Figures 5.9 and 5.10) prior to immunolabelling of biotin.

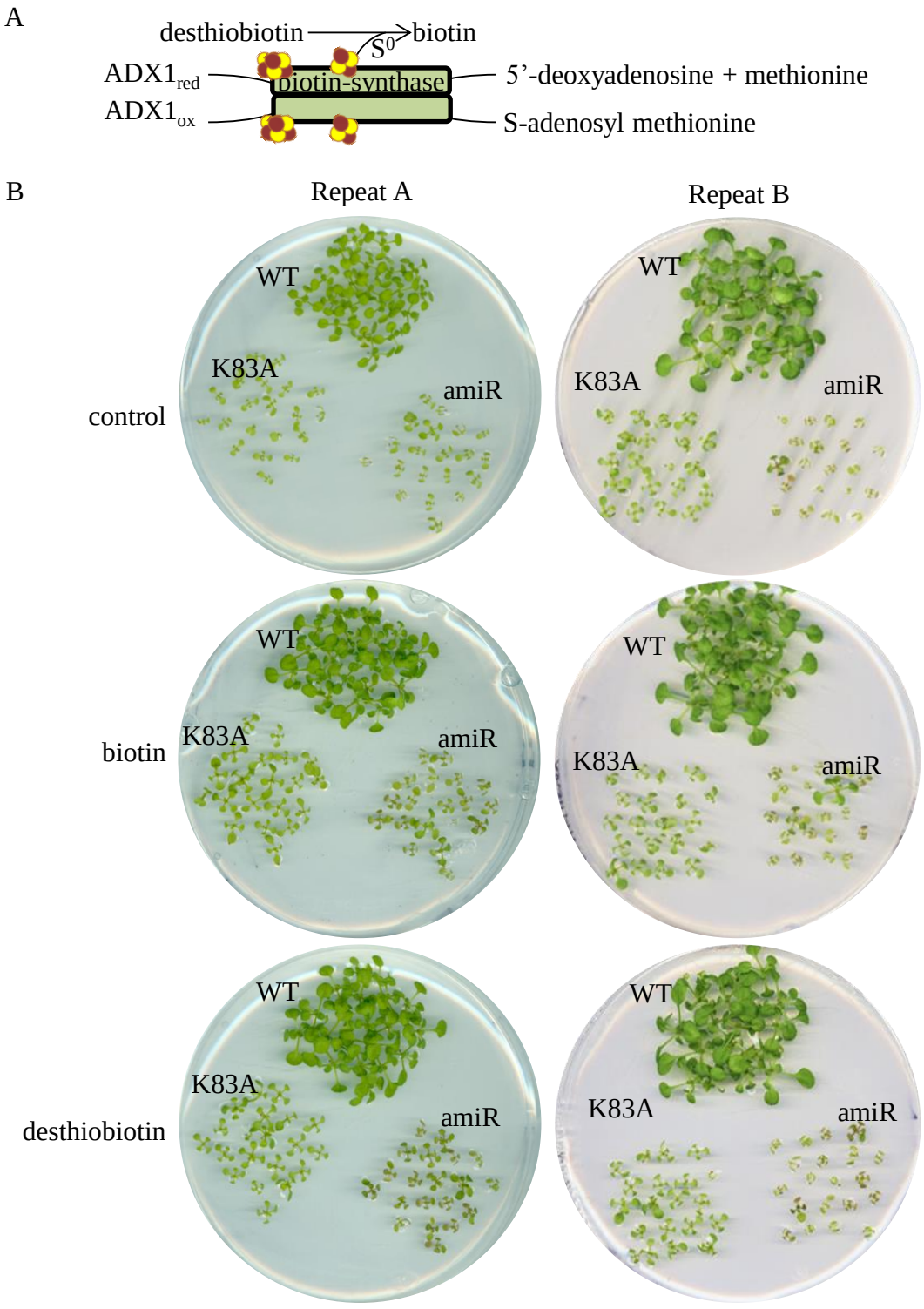

Figure 5.9 Growth phenotype of *grxS15* mutants treated with biotin or desthio-biotin. A. Biotin synthase reaction. Based on a model by (Picciocchi et al., 2003). ADX = adrenodoxin **B.** *grxS15* mutants (*K83A*, *amiR*) and a wild type (WT) were grown on ½-MS agar with 1 µM biotin,1 µM desthio-biotin or no additional treatment for ten days. For repeat A biotin was dissolved in DI H2O, for repeat B in DI H2O with a pH of 10.6 which resulted in an increase of pH from ~5.6 to ~6 in the agar.

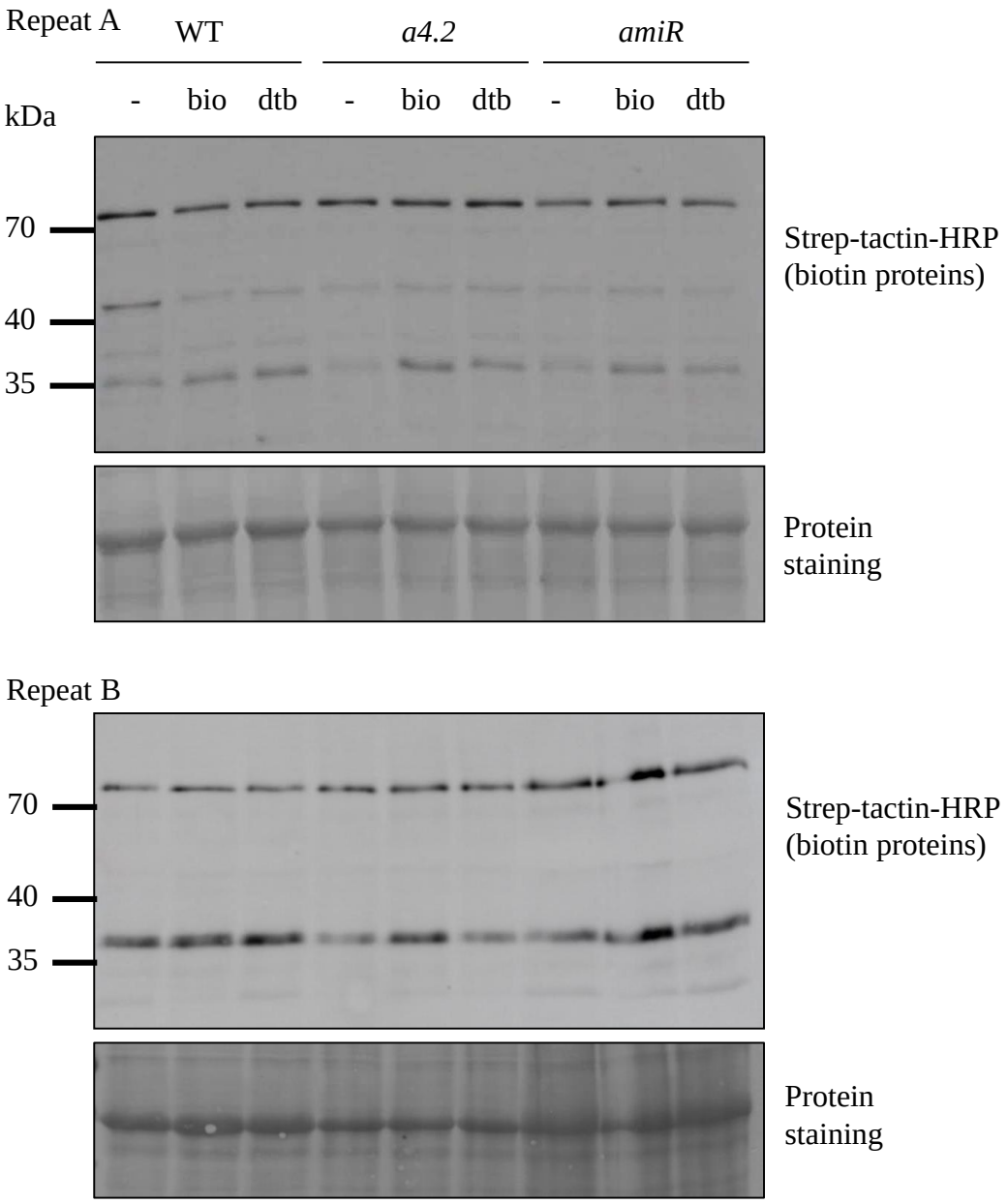

Figure 5.10 Biotin proteins in *grxS15* mutants treated with biotin or desthio-biotin. *grxS15* mutants (*K83A*, *amiR*) and a wild type (WT) were grown on ½-MS agar with 1 µM biotin,1 µM desthio-biotin or no additional treatment for ten days. For repeat A biotin was dissolved in DI H2O, for repeat B in DI H2O with a pH of 10.6 which resulted in an increase of pH from ~5.6 to ~6 in the agar. Biotin-containing proteins were labelled immunologically with a biotin-specific antibody after denaturing PAGE. Total protein served as a control.

The first experiment indicated that *grxs15* mutant plants had improved growth and biotin synthesis appeared partially rescued upon treatment with both desthiobiotin and biotin. However biotin was poorly dissolved in the first experiment, thus a repeat was performed with altered conditions to improve biotin solubility. For the second experiment the pH of the biotin stock solution was adjusted to ~10.6 for complete dissolution of biotin. The pH of the agar was consequently at 6. Results were not as distinct as for the first experiment and were contradictory. Thus it remains unclear if there is a biotin defect in *grxS15* mutants and if biotin and/or desthiobiotin treatment can rescue chemically.

In summary, only little effect was seen on FeS protein activity and FeS turnover in *grxS15* mutants which display a strong growth phenotype. The defect in lipoate cofactor biosynthesis was found by (Stroher et al., 2016) to be specific for H-proteins and two of three isoforms of a pyruvate dehydrogenase subunit while no effect was seen on the lipoate cofactor binding on the third isoform or a subunit of branched-chain acid dehydrogenase. All FeS specific defects seen could be due to secondary effects and it remains unclear what the exact function of GRXS15 is.

5.6. Discussion

Plant glutaredoxins have been proposed to be involved in *de-novo* FeS cluster assembly based on work in yeast and mammals (Couturier et al., 2013). However, investigation of the role of a cytosolic and a mitochondrial monothiol glutaredoxin in FeS assembly showed that severe mutants only had mild defects in FeS enzyme activity which could not account for the severity of the growth phenotype. This indicates that both glutaredoxins are not involved in *de-novo* FeS cluster assembly directly. GRXS17 and GRXS15 are the only monothiol glutaredoxins in the cytosol and mitochondria, respectively. Considering the involvement of glutaredoxins in FeS assembly in yeast (Rodriguez-Manzaneque et al., 2002) it is surprising that neither of the tested Arabidopsis homologues seem to have an obvious similar function. The cytosolic GRXS17 has been shown to interact with nuclear factor Y subunit C11/negative cofactor 2α (NF-YC11/NC2α) contributing to maintenance of the shoot apical meristem under long-day conditions by (Knuesting et al., 2015). Mutants of both, GRXS17 and NF-Y11 were sensitive to elevated temperatures and

elongated photoperiods (Knuesting et al., 2015). Therefore, they are proposed to function in the relay of a redox signal in response to the photoperiod to maintain meristem function. Arabidopsis flowering time is dependent on various factors including the day length with long days promoting earlier flowering (Koornneef et al., 1998). Glutathione biosynthesis is linked to bolting and flowering time (Ogawa et al., 2001; Yanagida et al., 2004). (Knuesting et al., 2015) showed that *grxS17* mutants had compromised shoot apical meristem and delayed bolting under long day conditions and suggested that GRXS17 could be involved in redox-sensing.

Combined data from (Stroher et al., 2016) and (Moseler et al., 2015) showed that GRXS15 lacks most of the common functions of glutaredoxins like deglutathionylation and antioxidant reduction activities.

(Stroher et al., 2016) discovered a defect in primary root length in mutants of GRXS15 which was aggravated by arsenite treatment and under long day conditions. Arsenite also severely decreases root tip respiration and rosette diameter. (Stroher et al., 2016) analysed protein contents in a mild *grxS15* knock-down mutant and found changes in protein levels of some FeS and lipoate containing proteins. Arsenite is known to bind to lipoate (Spuches et al., 2005) and lipoate was found to protect against oxidative stress caused by arsenicals in rats (Dixit et al., 2011; Dwivedi et al., 2014; Shila et al., 2005). A plastidial glutaredoxin from the fern *Pteris vittata* has been shown to act in arsenite tolerance (Sundaram et al., 2008) and thus it is not unlikely that GRXS15 could have a similar function in Arabidopsis.

The two recent publications regarding GRXS15 (Moseler et al., 2015; Stroher et al., 2016) show that this glutaredoxin seems to have none of the usual functions of a glutaredoxin. GRXS15 defects had most severe effects on the root meristem (Stroher et al., 2016) where it is also most highly expressed in plants (Brady et al., 2007). Interestingly, *grxS15* mutants were sensitive to long-day conditions, similar to *grxS17* mutants. As GRXS17 is involved in maintenance of the shoot apical meristem it could be possible that GRXS15 contributes to the maintenance of the root meristem. On the other hand, considering the severe effect of arsenite treatment on *grxS15* mutants, a role in arsenite detoxification is very likely and would explain the high expression of GRXS15 in root tips. The specific role of GRXS15 still has to be determined and it remains unclear if the annotated or to date unidentified glutaredoxins play a primary role in FeS assembly.

6. Identification of new proteins with a function close to ATM3

As discussed in Section1.2, the mitochondrial FeS assembly machinery is linked to the one in the cytosol but only little of this link is understood. The cysteine desulfurase NFS1 mobilises S^0 from cysteine in the mitochondria. The S^0 is used for mitochondrial FeS assembly but it is also thought to be transported into the cytosol (Lill, 2009), most likely in the form of glutathione-persulfidevia ATM3 (Schaedler et al., 2014). As discussed in previous Sections1.6 and 5, glutaredoxins are involved in *de-novo* assembly of FeS clusters in yeast but evidence found so far in Arabidopsis points to a different role of the mitochondrial and cytosolic glutaredoxins in plants. Thus it remains unknown how the S^0 is incorporated into glutathione for transport across the mitochondrial membrane, how it is delivered to and from ATM3 and if there are any other acceptor proteins.

In order to find new components involved in mitochondrial-cytosolic persulfide transport with a function close to ATM3 I characterised four mutant lines from a pool of sirtinol-resistant mutants. The genetic screen using sirtinol was originally employed to find genes involved in auxin signalling (Zhao et al., 2003). However, mutants of four components of the cytosolic part of the MoCo assembly pathway (Dai et al., 2005; Zhao et al., 2003) and also two alleles of *atm3* (Bernard et al., 2009) have been identified. The reason for detection of the MoCo and *atm3* mutants lies in the enzyme aldehyde oxidase. Aldehyde oxidase mediates the last step of the reaction that converts sirtinol into a toxic auxin analogue and the enzyme requires the cofactors MoCo, FAD and two Fe_2S_2 clusters for activity (Mendel, 2011) (Figure 6.1A). In this chapter I present the characterisation of mutants with a phenotype resembling *atm3* mutants and subsequent identification of the underlying mutation for two lines.

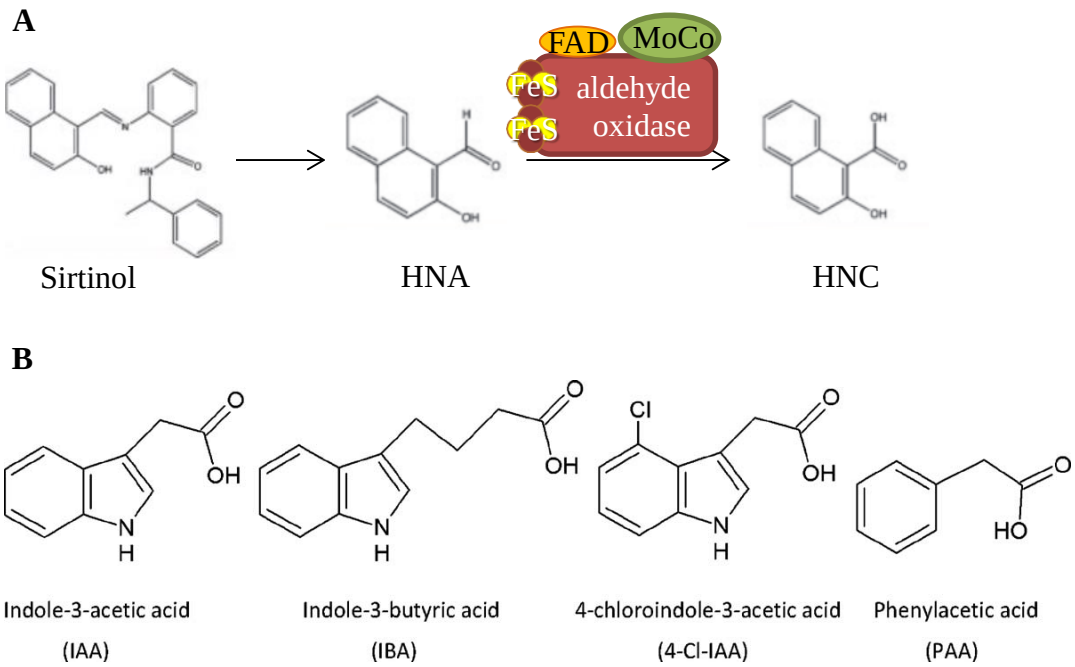

Figure 6.1 Scheme of sirtinol conversion reactions. Adapted from (Dai et al., 2005). **A.** The sirtinol screen was initially developed by (Zhao et al., 2003) to screen for auxin signalling mutants. The reaction intermediates were characterised by (Dai et al., 2005). Sirtinol is first converted by an unknown mechanism into 2-hydroxy-1-naphthaldehyde (HNA). HNA is converted into the toxic auxin analogue 2-hydroxy-1-naphthoic acid (HNC) by aldehyde oxidase. Aldehyde oxidase contains two FeS clusters, a MoCo and one flavin adenine dinucleotide (FAD. One of the aldehyde oxidase mediated reactions is the last step of auxin biosynthesis. **B.** Figure from (Simon and Petrasek, 2011), "structure of auxin species".

6.1. Selection of four *xd* mutants for further characterisation (Nina Kahlfeldt, Delphine Bernard, Andrew Maclean)

The selection process for the four mutant lines characterised in this study was carried out by Nina Kahlfeldt (Kahlfeldt, 2006), Delphine Bernard and Andrew Maclean and is summarised in figure 1.2. A large pool of EMS mutants was analysed in search of additional mutants in the MoCo assembly by Nina Kahlfeldt (Group of Ralf Mendel and Florian Bittner, Institut für Pflanzenbiologie der Technischen Universität Braunschweig). The work was carried out in the laboratory of Yunde Zhao, Section of Cell and Developmental Biology, University of California at San Diego). Nina Kahlfeldt tested about 700 lines for sirtinol resistant root growth of young seedlings on plates. 211 of these showed a strong sirtinol resistance and the seedlings were transferred to soil. Based on visual phenotype characteristics plants were sorted into three groups "ABA3-like" (small, dark green leaves, early flowering), "Auxin-like"

(abnormal leaf morphology) and "MoCo-like" (chlorosis, normal leaf morphology, no early flowering). The cytosolic cysteine desulfurase ABA deficient 3 (ABA3) mediates the sulfur transfer to sulfurated MoCo which is vital for aldehyde oxidase and xanthine dehydrogenase (Bittner et al., 2001; Leon-Kloosterziel et al., 1996; Xiong et al., 2001). Nina Kahlfeldt chose 50 representative plants (with focus on the MoCo-like group) which were tested for enzyme activities of the MoCo-containing enzymes nitrate reductase (NR), aldehyde oxidase (AldOx) and xanthine dehydrogenase (XDH). Plant lines were sorted into 5 groups based on enzyme activity levels and 25 representative lines were tested for levels of MoCo/molybdopterin (MPT) and the levels of the first MoCo intermediate cyclic pyranopterin monophosphate (cPMP, in earlier literature referred to as PrecursorZ) using HPLC. Levels of MoCo and its direct precursor MPT were measured by generating a stable derivative and MoCo and MPT could not be distinguished by this method. Nina Kahlfeldt adapted the final grouping of the lines according to MoCo enzyme activity, MoCo/MPT and cPMP levels. Seven lines grouped with M2934, which was later identified as the allele *atm3-4* (Bernard et al., 2009). These lines were *xd31*, *xd32*, *xd54*, *xd442*, *xd460*, *xd576*, *xd724*. The abbreviation was chosen for the initials of X. Dai who conducted the main work of the initial sirtinol screen (Dai et al., 2005; Zhao et al., 2003).

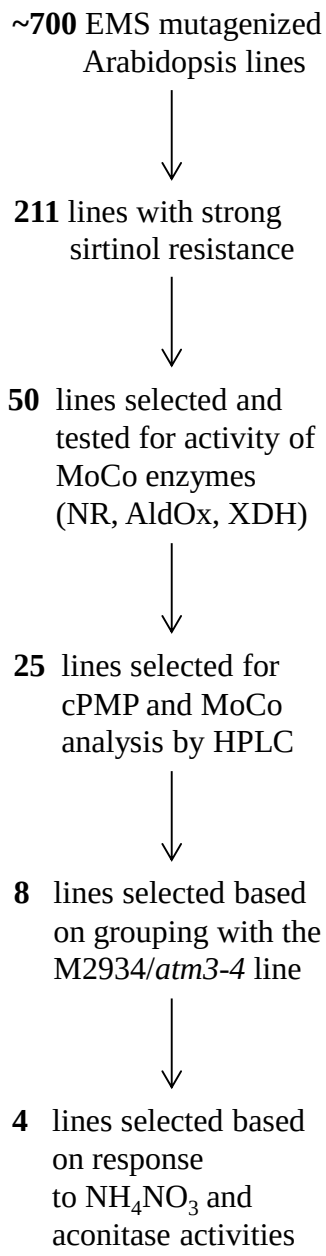

Figure 6.2 Work-flow for the selection of the four *xd* lines analysed in this study. The selection resulting in the four lines characterised in this study was performed by Nina Kahlfeldt, Delphine Bernard and Andrew Maclean. Nina Kahlfeldt performed the initial large scale screen and grouping of lines. Delphine Bernard showed that NH4NO3 treatment improves growth of the MoCo mutant *cnx5/sir1*. Andrew Maclean performed preliminary NH4NO3 treatments and aconitase activity measurements.

Analysing mutants that grouped with the *atm3-4* allele might reveal an unknown component of the CIA pathway. However, Nina Kahlfeldt's assays did not distinguish between MoCo and FeS mutants. Delphine Bernard (Group of Janneke Balk, University of Cambridge) initiated studies to separate MoCo mutants and

atm3-like mutants. She developed a treatment with NH_4NO_3 which should chemically complement a nitrate reductase (MoCo) defect allowing to distinguish between mutants of the MoCo pathway and *atm3*-like mutants (Section 1.4 and Figure 6.3A). Indeed, treatment with 50 mM NH_4NO_3 improved growth of the *cnx5* point mutant *sir1* (first characterised by (Zhao et al., 2003)) but caused a mild growth delay in *atm3* mutants. In addition to the 7 lines grouping with *atm3-4* from Nina Kahlfeldt's work, Delphine Bernard included the lines *xd22* and *xd105* because of phenotype similarities to *atm3* mutants (such as mild chlorosis and narrow leaves). The seed stock for line *xd442* was found to be not viable and thus was not analysed. Andrew Maclean performed preliminary tests on the aforementioned lines for response to NH_4NO_3 watering and for activity of cytosolic aconitase. He found that the lines *xd22*, *xd31*, *xd105* and *xd460* showed an *atm3*-like response to NH_4NO_3 watering and decreased cytosolic aconitase activity (Table 1.1) suggesting that the underlying mutations affect components of the cytosolic FeS assembly.

Table 6.1 Results of preliminary tests for 8 selected lines. Cytosolic aconitase activity is decreased in mutants in *ATM3* and cytosolic FeS assembly. Treatment with 50 mM NH_4NO_3 restores growth of a *cnx5* mutant but not of *atm3* mutants. Data from Andrew Maclean (Rotation report, 2013).

line	**Aconitase activity under standard conditions**	**Growth upon NH_4NO_3 treatment**
wild type	unaltered	unaltered
cnx5	all decreased	improved
atm3-1	cytosolic activity decreased	delayed
xd22	all strongly decreased	strongly delayed
xd31	all strongly decreased	delayed
xd32	wild-type like	improved
xd54	wild-type like	unaltered
xd105	no cytosolic activity, decreased mitochondrial activity	delayed
xd442	not viable	
xd460	cytosolic activity decreased	delayed
xd576	wild-type like	delayed
xd724	wild-type like	improved

6.2. *xd22* and *xd105* show delayed growth upon NH_4NO_3 watering

To validate that *xd22*, *xd31*, *xd105* and *xd460* were similar to atm3 in their response to NH_4NO_3 , I repeated the treatment. Plants were grown under standard conditions for two weeks before treatment. After that, plants were watered with 50 mM NH_4NO_3 as the sole source of liquid or with DI water for the mock treatment (Figure 1.3B). The mutant lines were compared to a wild type of the Landsberg ecotype (ecotype background of the *xd* mutants), two *atm3* alleles and *cnx5*. Wild-type plants were only mildly affected by NH_4NO_3 treatment and showed a darker shade of green of the leaves. Both *atm3* alleles stayed chlorotic under these conditions but also were additionally delayed in growth. The *cnx5* mutant, which was chlorotic and delayed in growth under standard conditions, shows a significant improvement in growth when treated with NH_4NO_3, as observed by Delphine Bernard. Under standard conditions (H_2O watering), the mutants *xd22* and *xd31* were similar in appearance to *atm3* and *cnx5* mutants, in that they were both chlorotic and dwarfed. While *xd31* plants were rescued in growth by the treatment, *xd22* plants did not survive a 12 day course of NH_4NO_3 watering. *xd105* plants had a resemblance to *atm3-4* under both conditions. An additional phenotype later in plant development was early bolting (Figure 6.3B) and early senescence of rosette leaves (data not shown). *xd460* plants were wild-type like with and without treatment in early plant development but this line showed a heterogeneous phenotype in late growth stages unrelated to the treatment (data not shown). Thus, *xd22* and *xd105* were chosen for further analysis.

A

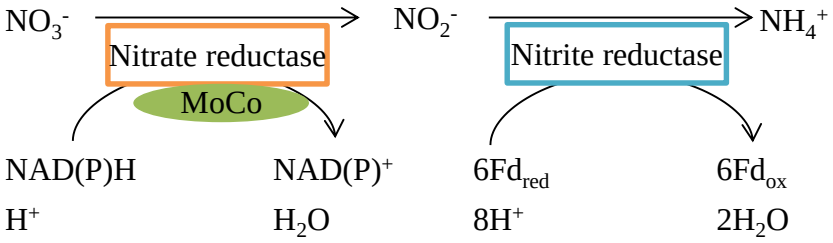

B

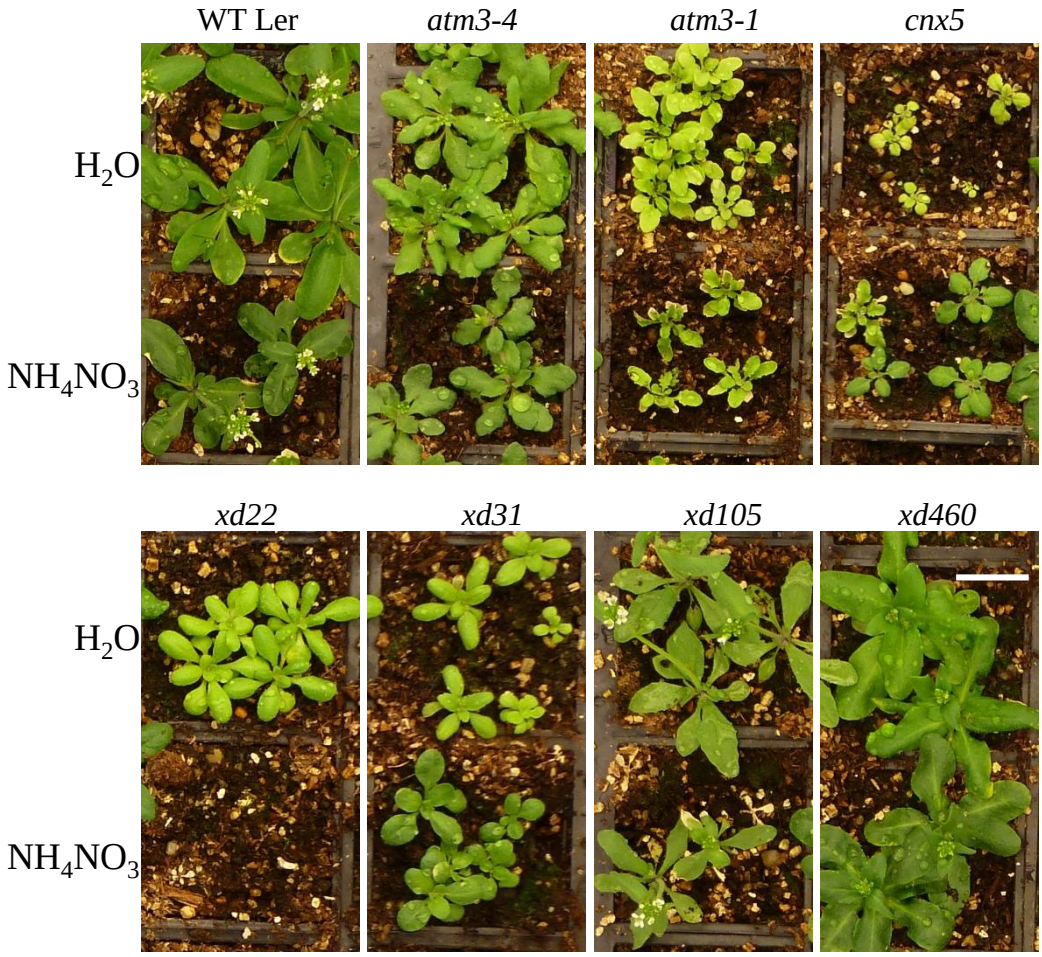

Figure 6.3 Growth of *xd22*, xd31, *xd105* and *xd460* under ammonium nitrate treatment. A. Scheme of the nitrogen assimilation reactions catalysed by nitrate reductase and nitrite reductase. **B.** Growth of *xd22*, *xd31*, *xd105* and *xd460* watered with DI water or 50 mM NH_4NO_3. A Landsberg wild type (WT Ler), two *atm3* alleles and the MoCo mutant *cnx5* served as controls. Plants were grown on soil for 2 weeks and then treated as indicated for 12 days. Scale bar is 2 cm.

6.3. Aconitase activities in *xd22* and *xd105* are impaired

To further distinguish between FeS and MoCo mutants, enzymes activities of the FeS enzyme aconitase were measured in a spectrometric coupled assay of cytosolic fractions and in an in-gel assay (mitochondrial and cytosolic isoforms) (see Figure 6.4). Aconitase mediates the conversion of citrate to cis-aconitate to isocitrate. Isocitrate can be converted to α-ketoglutarate by the NADP-dependent isocitrate-dehydrogenase, which couples the activity of aconitase to NADPH production which can be followed at 340 nm (Stehling et al., 2007). To obtain a cytosolic fraction the cell extract was filtered through Miracloth with 22-25 µm pore size and separated by centrifugation in a microcentrifuge tube. Mitochondria, chloroplasts and cell debris were pelleted while larger cell debris remained in the filter. In the *atm3-1* mutant cytosolic aconitase activity was strongly decreased to 19.5 ± 2.1% of the wild-type. In *xd22* mutants aconitase activity was decreased to 17.2 ± 1.3% and for *xd105* to 14.6 ± 6.2% (see Figure 6.4A).

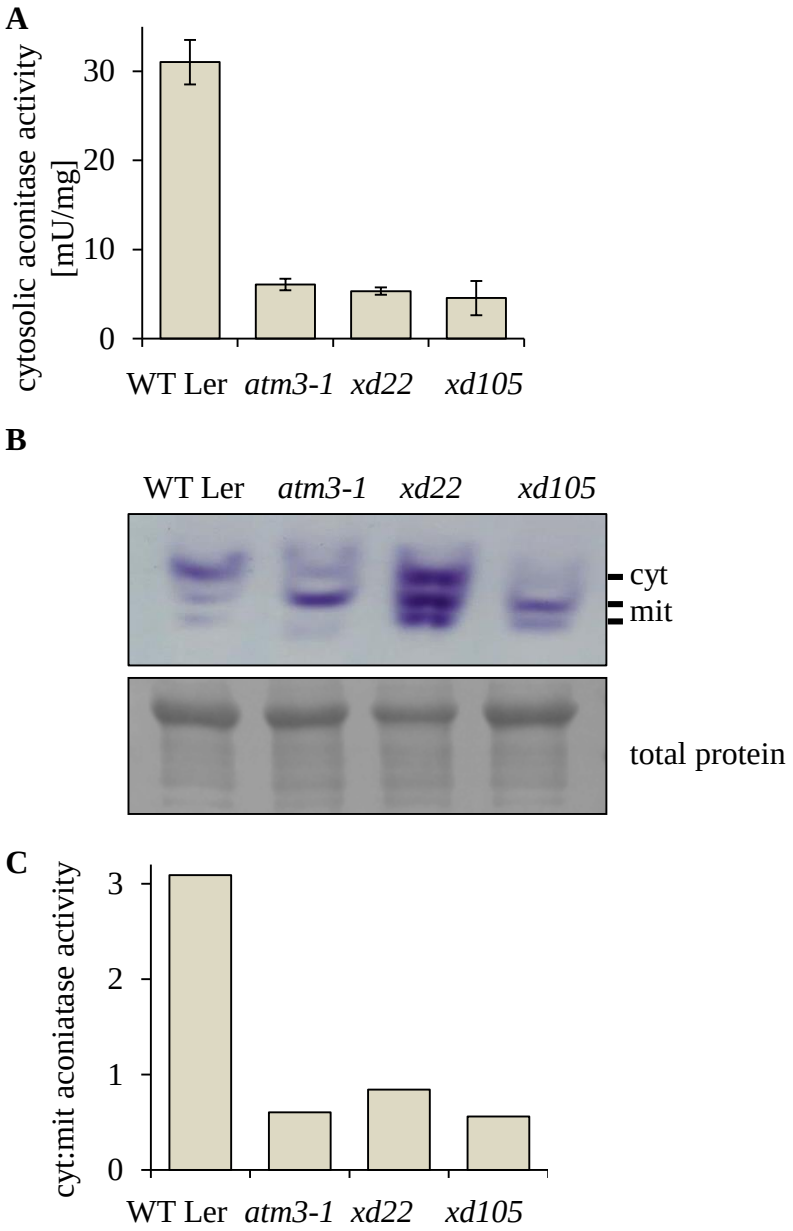

Figure 6.4 Aconitase activities in *xd22* and *xd105* mutants compared to wild type and *atm3-1*. A. Cytosolic aconitase activity measured by a photospectrometric assay in which aconitase activity is coupled to isocitrate dehydrogenase and NADPH production. Cytosolic fractions were isolated from leaf samples of 24-day-old soil-grown plants. Values are the mean ± SD (2 biological, 2 technical repeats.) **B.** Activity of aconitase isozymes separated by native starch-PAGE. Plants were grown for 2 weeks on ½-MS agar, activities were visualised in-gel coupled to isocitrate dehydrogenase activity and, formation of a purple precipitant. Results are representative for three biological repeats (independent preparations). Total protein was visualised by Ponceau S staining after SDS-PAGE and immunoblotting of a sample from the same extract. **C.** Ratio of cytosolic to mitochondrial activities quantified from bands in (B) using the ImageJ software.

In order to analyse mitochondrial as well as the cytosolic isoforms of aconitase, I performed a native in-gel assay as described by (Bernard et al., 2009). The gel shown in Figure 6.4B is representative for three biological repeats. Wild-type samples showed a pattern characteristic of rosette leaves with a stronger cytosolic activity and two weak mitochondrial bands (Bernard et al., 2009). In *atm3* mutants cytosolic aconitase activity was decreased and mitochondrial activity was increased in one or both isoforms. The *xd105* mutant line showed decreased cytosolic activity and slightly increased mitochondrial activity. Densitometric analysis was performed as it was found to be very useful for assessing the relative changes in aconitase activities (as shown in Section 5.2). While the gel does not clearly show a decrease in cytosolic activity of *xd22* samples, densitometric analysis revealed that the ratio between cytosolic and mitochondrial activity is strongly decreased in *xd22* and *xd105* samples and that the ratio is similar to *atm3-1* samples (Figure 6.4C). The ratios showed a similar trend in all experiments despite variation in the absolute intensity.

To conclude, *xd22* and *xd105* were shown to have decreased cytosolic aconitase activity and thus I proceeded to identify the mutations underlying the phenotypes.

6.4. xd105 but not *xd22* is allelic with *atm3*

Before continuing with mapping and sequencing of the *xd22* and *xd105* lines, I tested if either is allelic to *atm3*. Due to the selection process for *atm3*-like mutants and due to the previous identification of already two mutant alleles of *atm3* from the sirtinol screen it was possible that the *xd22* and *xd105* lines could be other *atm3* alleles.

For an allelism test, two homozygous mutant lines are crossed and the F1 is analysed to test if the mutations affect the same gene. Unlinked recessive mutations should have a restored phenotype while recessive mutations of the same gene maintain the defect. *xd22*, *xd105* and both *atm3* alleles are recessive (as found in various backcrosses, data not shown). *xd22* and *xd105* were crossed with both *atm3-1* and *atm3-4*. F1 seeds were collected and the growth phenotype was analysed in young seedlings grown on ½-MS agar.

The F1 generation of *xd22* crosses with *atm3* alleles was very similar to the wild type and did not show the chlorosis and dwarfed growth characteristic for all parents or the pronounced veins characteristic of *atm3* mutants.

The F1 plants from the cross between *xd105* and *atm3* alleles grew bigger than the parental lines as well as the wild types, which was surprising (Figure 6.5).

However, this could be caused by heterosis. This effect describes the increased growth vigour of heterozygous crosses over the parental lines which is exploited in crops for yield improvement. The exact mechanisms leading to the improved growth are not yet fully understood (Charlesworth and Willis, 2009; Hochholdinger and Hoecker, 2007; Lippman and Zamir, 2007; Meyer et al., 2004). In this particular case, however, *atm3* alleles are known to accumulate mutations (Luo et al., 2012). Crossing of two *atm3* lines then restores to many of the damaged loci and could lead to improved growth.

The F1 generation of *xd105* crosses was slightly chlorotic reminiscent of the parents and showed pronounced leaf veins (not visible in Figure 6.5). However, all changes were not strongly pronounced and it was difficult to distinguish between rescued growth phenotype due to non-allelic parents or due to heterosis.

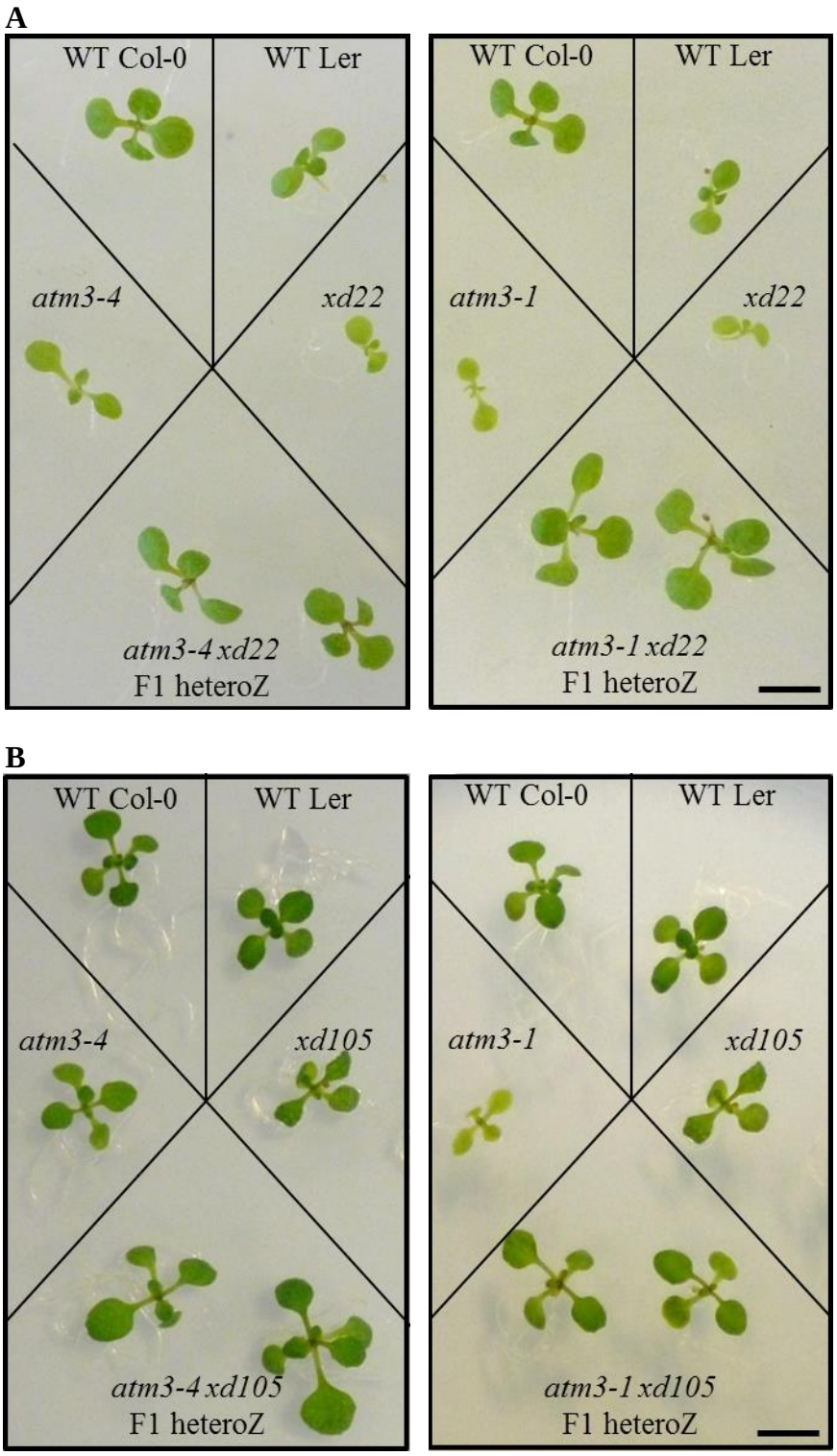

Figure 6.5 F1 plants and parental lines from crosses between *xd105* or *xd22* and two *atm3* alleles. The *xd* lines were crossed with the weak *atm3-4* or the strong *atm3-1* allele. F1 seeds were grown on ½-MS agar. A wild type of the *atm3* ecotype background (Columbia, WT Col-0) and the *xd* ecotype background (Landsberg, WT Ler) served as controls. Scale bar is 0.5 cm. **A.** 11-day-old seedlings of F1 plants and parental lines of *xd22* crosses. **B.** 15-day-old seedlings of F1 plants and parental lines of *xd105* crosses.

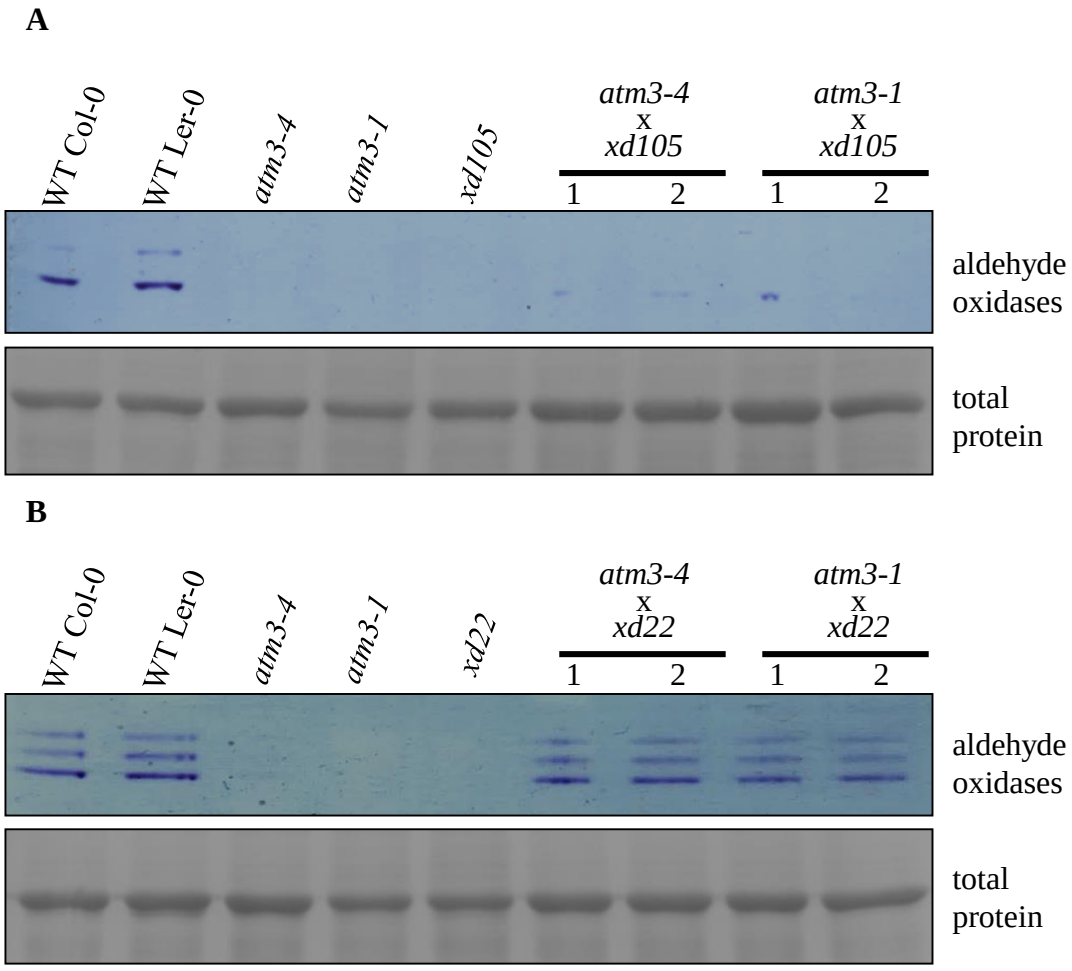

Figure 6.6 Aldehyde oxidase activities in F1 plants and parental lines from crosses between *xd105* or *xd22* and two *atm3* alleles. Plants were grown on ½-MS agar and aldehyde oxidase activities were visualised in a native in-gel assay coupled to the formation of the purple formazan. A wild type of the *atm3* ecotype background (Columbia, WT Col-0) and the *xd* ecotype background (Landsberg, WT Ler) served as controls. **A.** Aldehyde oxidase activities in 16-day-old F1 plants and parental lines of *xd22* crosses. **B.** Aldehyde oxidase activities in 20-day-old F1 plants and parental lines of *xd105* crosses. Total protein was visualised by Ponceau S staining after SDS-PAGE and immunoblotting of a sample from the same extract.

As it was not clear if the growth phenotype of F1 plants was rescued, the aldehyde oxidase levels were analysed as a biochemical marker for restoration of the mutant phenotype (see Figure 6.6). In F1 plants from *xd22* crosses with *atm3*, aldehyde oxidase activities were restored to wild-type levels. F1 plants of *xd105* crosses with *atm3* did not show recovery of the enzyme activities. Thus it can be concluded that *xd105* carries a mutation in the *ATM3* gene, while the mutation of *xd22* is in a different location.

6.5. *xd105* is an *atm3* allele with a point mutation leading to an amino acid change in the 6th transmembrane helix

To identify the mutation of *xd105*, I sequenced the *ATM3* gene and located a single point mutation (G1271>A) in the 13th exon (Figure 1.7 A). This changes codon GGA to GAA, predicted to cause an amino acid change from glycine to glutamate at position 424 (Figure 1.7B). Gly424 is located in the 6th transmembrane helix of ATM3 (Srinivasan et al., 2014) (see Figure 6.7C).

The alignment of ATM3 with homologs in mammals, fungi and bacteria (Figure 6.7C) shows that the residue occurs mainly as a glutamine or glycine (or a threonine for the bacterium *Novosphingobium aromaticivorans*). In contrast to these, glutamate contains a carboxyl group in its side chain which has a pKa of ~4. This means that the amino acid exchange caused by the *xd105* mutation introduces an additional negative charge at physiological pH.

As mentioned above, the G424E substitution is located in the 6th transmembrane region of *ATM3* and to investigate if this could alter protein folding I analysed transmembrane prediction data. Four different transmembrane prediction online tools predicted that G424>E disrupts the transmembrane region (Figure 6.8).

A

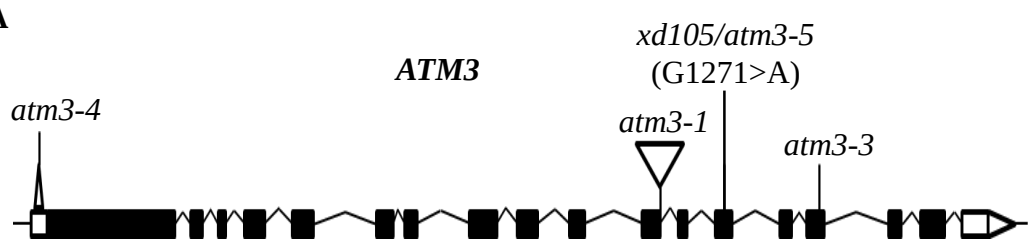

B

Ler	M	V	N	**G**	L	L	F	Q	L	S	430
	ATG	GTG	AAT	**GGA**	CTT	CTC	TTT	CAG	CTG	TCT	1290
xd105	ATG	GTG	AAT	**GAA**	CTT	CTC	TTT	CAG	CTG	TCT	1290
	M	V	N	**E**	L	L	F	Q	L	S	430

C

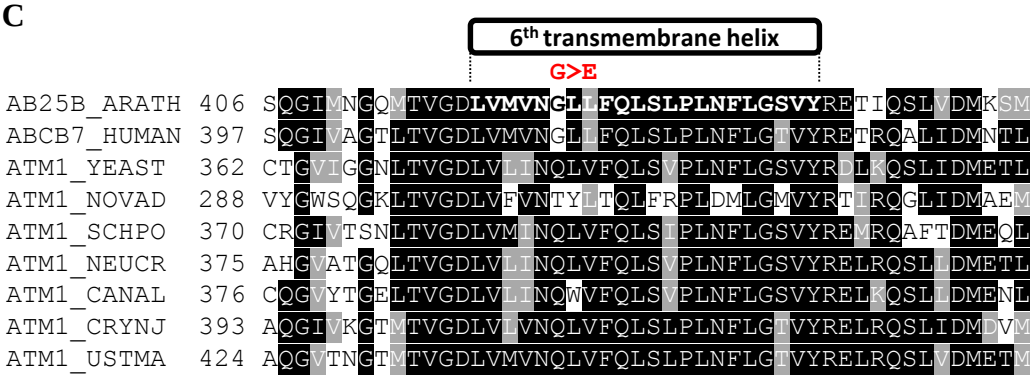

Figure 6.7 Gene model of *ATM3* and amino acid homology in the region of the *xd105* mutation. A. Gene model of *ATM3* (AT5G58270) with indicated positions of other *atm3* alleles. Exons are black boxes, introns are lines, UTRs are white boxes. **B.** Nucleotide sequence alignment of the *xd105* and the wild-type sequence with amino acid translation. The alignment was performed using the Clustal Omega server. **C.** Amino acid alignment of the 6th transmembrane region of Arabidopsis ATM3 with metazoan and bacterial homologs. Protein sequences were acquired from and aligned in the UniProt database: *Arabidopsis thaliana* (accession no. Q9LVM1) (ARATH), *Homo sapiens* (accession no. O75027) (HUMAN), *saccharomyces cerevisiae* (accession no. P40416) (YEAST), *Novosphingobium aromaticivorans* (accession no. Q2G506) (NOVAD), *Schizosaccharomyces pombe* (accession no. O14286) (SCHPO), *Neurospora crassa* (accession no. Q7RX59) (NEUCR), *Candida albicans* (accession no. Q59R09) (CANAL), *Cryptococcus neoformans var. neoformans* (accession no. P0CL92) (CRYNJ), *Ustilago maydis* (accession no. Q4PH16) (USTMA). Shading was performed using the BoxShade server. Shading indicates the level of conservation if 50% of the sequences match; black = identical amino acids, grey = similar amino acids.

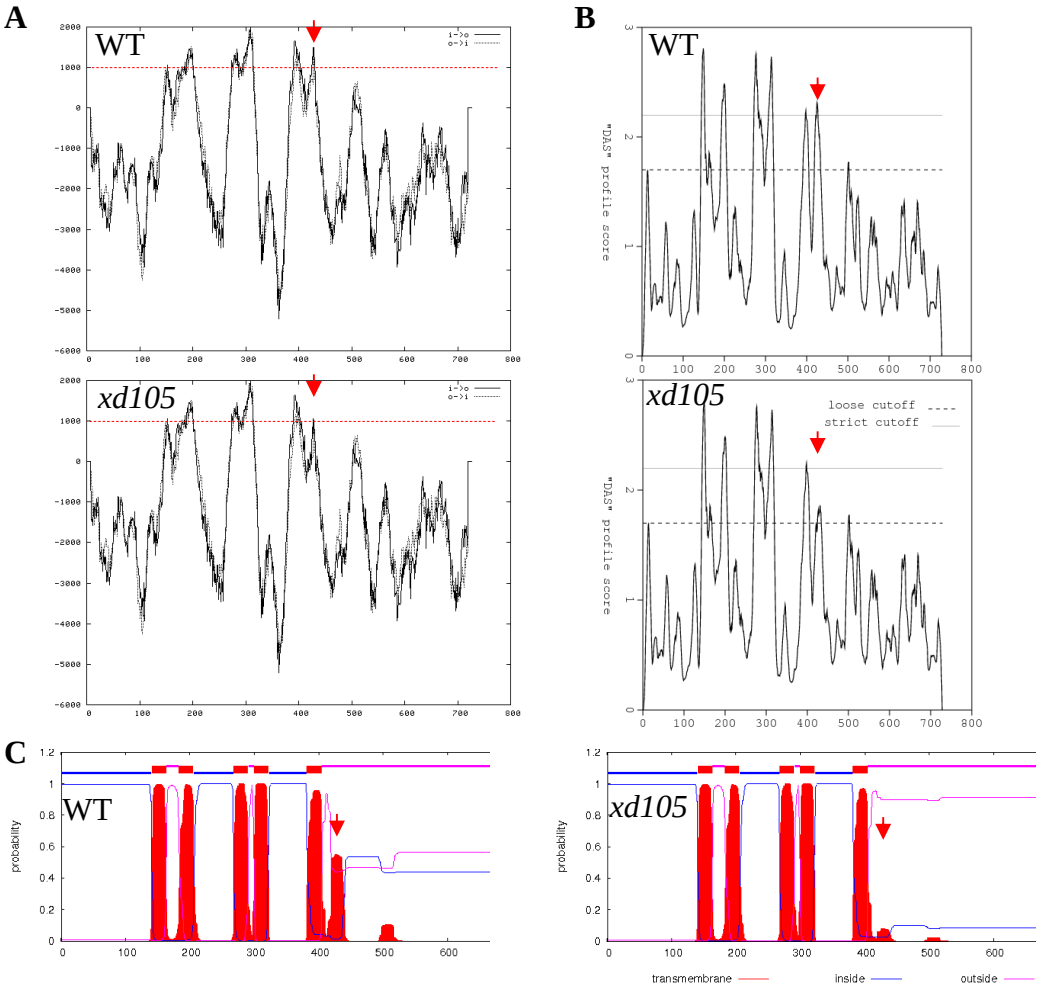

D

```
WT
seq   AMVLCSQGIV NGQMTVGDLV MVNGLLFQLS LPLNFLGSVY RETIQSLVDM    450
pred  HHHHoooooo oooooooHH HHHHHHHHHH HHHHHHHHHH iiiiiiiiii

seq   KSMFQLLEEK SDITNTSDAK PLVLKGGNIE FENVHFSYLP ERKILDGISF    500
pred  iiiiiIIIII IIIIIIIIII IIIIIIIIii iiiiiiiiii iiiHHHHHHH

seq   VVPAGKSVAI VGTSGSGKST ILRMLFRFFD TDSGNIRIDG QDIKEVRLDS    550
pred  HHHHHHHHHH HHHooooooo ooooooooOO OOOOOOOOOO OOOOOOOOOO

xd105
seq   AMVLCSQGIV NGQMTVGDLV MVNELLFQLS LPLNFLGSVY RETIQSLVDM    450
pred  HHHHoooooo oooooooooO OOOOOOOOOO OOOOOOOOOO OOOOOOOOOO

seq   KSMFQLLEEK SDITNTSDAK PLVLKGGNIE FENVHFSYLP ERKILDGISF    500
pred  OOOOOOOOOO OOOOOOOOOO OOOOOOOOOO OOOOOOOOOO OOOOOOOOOO

seq   VVPAGKSVAI VGTSGSGKST ILRMLFRFFD TDSGNIRIDG QDIKEVRLDS    550
pred  OOOOOOOOOO OOOOOOOOOO OOOOOOOOOO OOOOOOOOOO OOOOOOOOOO
```

Figure 6.8 Transmembrane helix prediction for the ATM3 protein sequence with the wild type residue or G242E substitution.
A. TMPred (http://www.ch.embnet.org/cgi-bin/TMPRED_form_parser); Arrows indicate peaks for the 6th transmembrane region.
B. DAS (http://www.sbc.su.se/~miklos/DAS/tmdas.cgi)
C. TMHMM2 (www.cbs.dtu.dk/services/TMHMM-2.0/)
D. HMMTOP (http://www.enzim.hu/hmmtop/server/hmmtop.cgi). i = inside; o = outside, h = transmembrane helix. Lower/upper case = low/high confidence.

6.6. *xd105* (*atm3-5*) lacks ATM3 protein

Misfolding of the transmembrane region can lead to protein degradation and to investigate whether the G1271>A (Gly424Glu) mutation does affect ATM3 protein levels, I isolated mitochondria and detected ATM3 levels by immunoblotting (Figure 6.9).

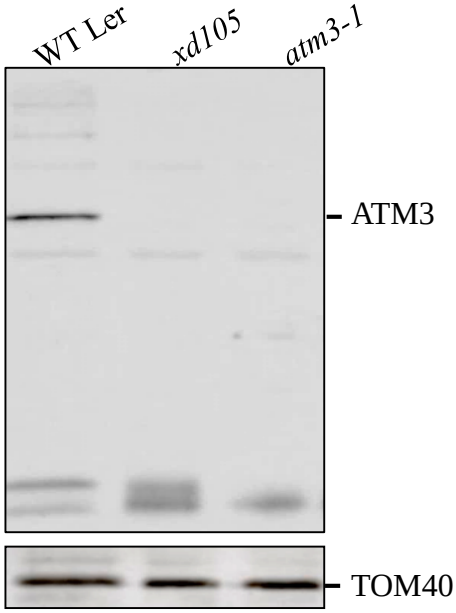

Figure 6.9 ATM3 protein levels in wild-type, *xd105* (*atm3-5*), *atm3-1*. Plants were grown for 5 weeks on soil under short day conditions. ATM3 levels were detected immunologically on isolated mitochondria. Translocase of the Outer mitochondrial Membrane 40 (TOM40) levels served as control for equal loading and mitochondrial purity. WT Ler = wild type Landsberg.

ATM3 protein levels were undetectable in mitochondria from *xd105*. These results confirm that *xd105* is another *atm3* allele and is from now on referred to as *atm3-5*. However, the absence of ATM3 protein could be due to protein degradation or due to decreased expression. To test this, I performed semi-quantitative reverse-transcriptase PCR. *ATM3* transcript levels in *atm3-5* were found to be comparable to wild-type levels (Figure 6.13) indicating that the mutation does not affect expression levels of ATM3 on a RNA level.

To summarise, the phenotype of *xd105* plants is caused by a G1271>A mutation in the *ATM3* gene which leads to a change from glycine to glutamate at the position 424. This is predicted to destabilise the 6th transmembrane helix and degradation of the ATM3 protein.

6.7. The *xd22* mutation leads to a single amino acid change in a conserved residue of CNX2

The analysis presented in the previous Sections showed that the *xd22* line was not allelic with *atm3*, growth defects were not rescued in response to NH_4NO_3 and aldehyde oxidase and aconitase levels were decreased. Thus I proceeded with the identification of the underlying mutation for the *xd22* line. I used the approach of map based cloning to approximately localise the mutation.

Map based cloning is based on the fact that Arabidopsis ecotypes have simple sequence length polymorphisms (SSLPs) throughout the genome. Primers specific for an SSLP amplify PCR products that differ in size between the two ecotypes. These SSLPs can be associated with the phenotypes caused by a mutation. A mapping population is generated by crossing one ecotype carrying the mutation (in this case Landsberg, Ler) with a different wild-type ecotype (in this case Columbia, Col-0). The heterozygous F1 generation is grown up and seeds of the F2 generation are collected, this is the mapping population. The mapping population has random recombinant events between Ler and Col-0 with an equal segregation percentage if no selection is made. Then, individual plants are selected from the mapping population which show the phenotype of the mutant line and thus must have the Ler genetic background surrounding the mutation. The segregating mapping population showed a 1:3 segregation ratio between the mutant and the wild-type phenotype which is evidence that the *xd22* mutation is recessive. For recessive mutations like the *xd22* mutation, plants showing a phenotype must be homozygous for the mutation. In the selected mutants, the probability of recombinant events is lower the closer the SSLP marker is to the mutation that was selected for. This method serves to approximately localise the mutation in the genome. The higher the number of individuals tested, the better is the resolution of the mapping but the number of PCR reactions can become unpractical. Initially I tested 40 individuals, and added 40 more when narrowing down the interval. The sequences for the initial 16 primer pairs were kindly donated by Doreen Feike and I added three more primer pairs (Table 2.8 in Section 2.8). The individual plants were tested for each of the SSLPs and percentages of recombinant events were calculated (Figure 6.10). No recombinant events were found at the genetic marker closest to *AT2G31070* and thus

the mapping interval for further sequence analysis was chosen between the two flanking markers with 1.2% (*AT2G29995*) and 11.3% (*AT2G39010*) recombination.

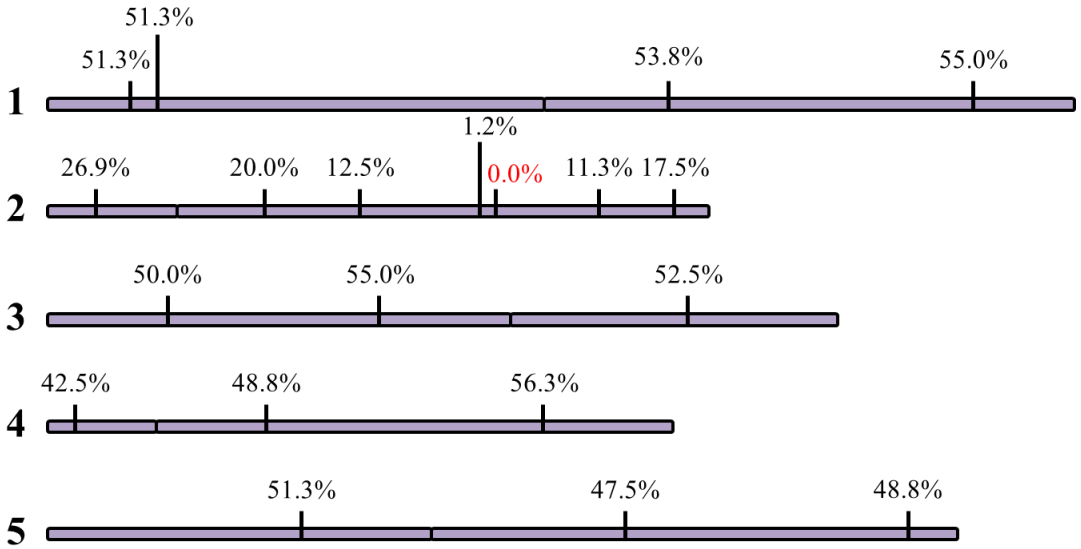

Figure 6.10 Percentages of recombination from coarse mapping of the *xd22* mutation. 40-80 plants of the *xd22* mapping population were screened for occurrence of recombinant events between Landsberg and Columbia SSLPs throughout the genome. The probability of a recombinant event to Columbia is ~50% in unlinked loci but becomes lower closer to the mutation. Numbers 1 to 5 indicate Arabidopsis chromosomes.

Nuclear DNA of about 200 individual plants was pooled and whole genome sequencing was performed by The Genome Analysis Centre (TGAC, Norwich). Sequence assembly, alignment against the Ler reference genome and initial screening for EMS mutations (G>A, C>T) was performed by Zamin Iqbal (University of Oxford) using the Cortex software and by Martin Trick (TGAC, Norwich) using Bowtie and the Integrative Genomics Viewer. I then combined the data and screened all mutations in the mapping interval for a region with decreased ecotype variation as shown in Figure 6.11. Non G>A/C>T mutations were considered as ecotype variations.

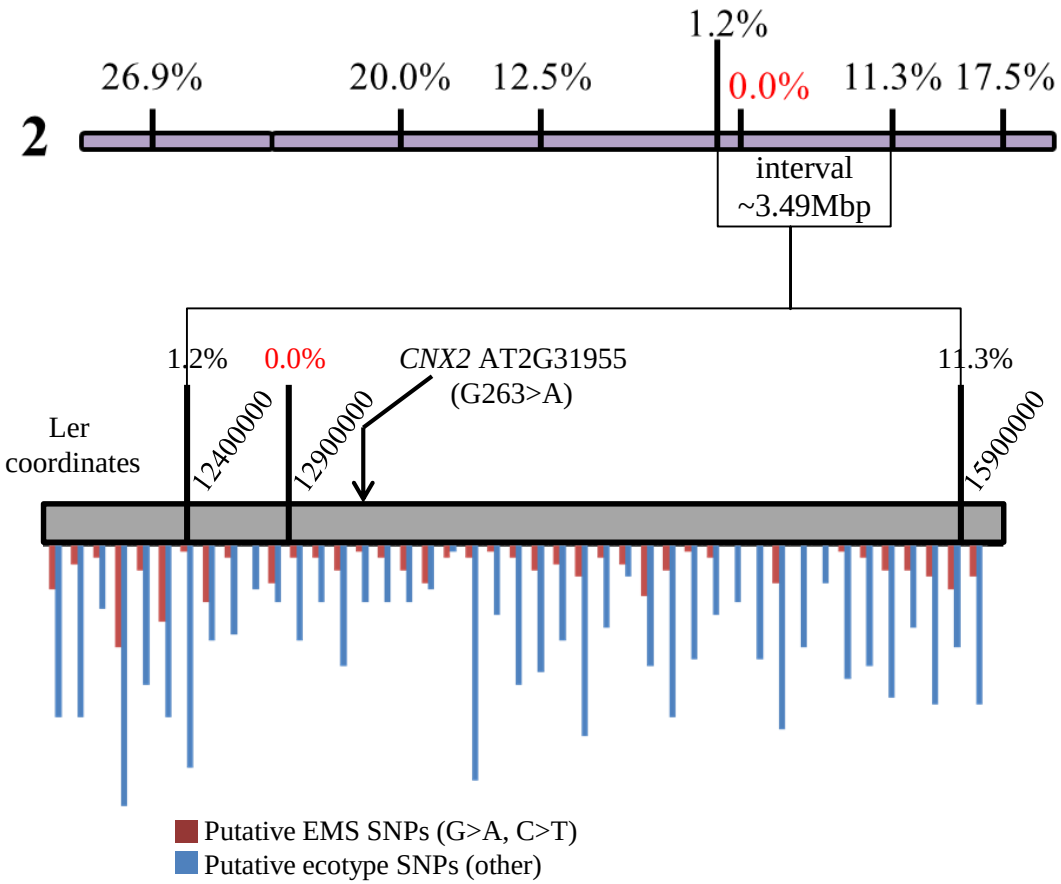

Figure 6.11 Frequency of SNPs in the mapping interval for *xd22*. Putative EMS mutations (shown in red, G>A and C>T) and putative ecotype variations (shown in blue, other nucleotide changes) in the 3.49 Mbp mapping interval on chromosome 2 of *xd22*.

The region of low ecotype variation was not very clearly pronounced but lay within the initially determined mapping interval. I decided to analyse all mutations within the initial mapping (Table 6.3) interval to identify those that cause an amino acid exchange. (Table 6.4).

Table 6.2 Single nucleotide polymorphisms (SNPs) potentially caused by EMS in the mapping interval of *xd22*. SNPs were identified by whole genome sequencing. Detection frequencies of Bowtie and Cortex are shown. (N/A): SNP detected in a stretch of multiple changes, individual frequencies do not apply. (x,y) indicates frequency of x = other nucleotides, y = indicated nucleotide.

coordinate	base change	Bowtie2	Cortex	gene	exon/intron
12572330	G>A		(0,16)	AT2G30220	Exon
12580404	G>A		(0,25)	AT2G30240	Intron - middle
12580405	C>T	(2,29)	(0,25)	At2G30240	Intron - middle
12684588	G>A	(0,28)	(0,26)	AT2G30520	exon
12813573	C>T	(2, 23)	(0,17)	AT2G30830	Intron - middle
12833768	G>A	(1,34)	not found	AT2G30910	Intron - middle
12850200	C>T	(0,16)	(0,17)	AT2G30940	Exon
12862616	C>T	(2,24)	(0,18)	AT2G30980	Intron +4
12989093	C>T	(0,12)	(0,4)	None	
13012823	G>A	(5,25)	(0,19)	None	
13025327	C>T	(2,36)	not found	AT2G31300	Intron - middle
13025535	G>A	(1,36)	not found	AT2G31300	Intron -15
13025537	G>A	(1,37)	not found	AT2G31300	Intron -13
13106900	G>A	(0,12)	not found	AT2G31540	Exon
13110318	C>T	(1,25)	not found	AT2G31550	Exon
13176602	C>T	(1,21)	(0,17)	None	
13198497	C>T	(4,31)	(0,30)	AT2G31800	Intron - middle
13262001	C>T	(0,53)	(0,39)	AT2G31955	Exon
13348745	C>T	(1,15)	not found	AT2G32180	Exon
13387295	C>T	(2,19)	(0,16)	None	
13469987	C>T	(0,28)	(0,22)	None	
13514570	G>A	(1,24)	not found	AT2G32610	Exon
13514746	C>T	(0,25)	(0,21)	AT2G32610	Exon
13527612	G>A	(0,26)	(0,21)	None	
13527823	C>T	(0,25)	not found	AT2G32650	Exon 1
13527972	C>T	(3,23)	not found	AT2G32650	Exon 1
13528608	C>T	(1,19)	not found	AT2G32645	3'UTR
13535102	G>A	(1,28)	not found	AT2G32670	Intron +10
13535134	G>A	(1,27)	not found	AT2G32670	Intron +42
13558437	C>T	(0,21)	(0,21)	AT2G32730	Intron -17
13692736	G>A	(0,27)	(0,14)	None	
13705900	G>A	(0,25)	(0,19)	AT2G33070	Exon
13710036	G>A	(0,22)	not found	AT2G33080	Exon 1
13710049	C>T	(0,19)	not found	AT2G33080	Exon 1
13984658	G>A	(1,39)	(0,14)	None	
14073597	C>T	(2,41)	(0,26)	AT2G34090	Intron -33
14085068	G>A	(7,11)	(NA)	None	
14209196	G>A	(0,12)	(NA)	None	
14220473	G>A	(9,13)	(NA)	None	
14346745	C>T	(0,18)	(0,21)	None	
14467403	C>T	(0,31)	(0,25)	AT2G35110	Intron – middle
14597511	C>T	(8,21)	(NA)	None	
14597518	G>A	(2,27)	(NA)	None	
14597521	C>T	(9,20)	(NA)	None	
14644164	C>T	(3,23)	(NA)	AT2G35635	Intron – middle
14651847	C>T	(0,9)	(NA)	AT2G35660	Intron – middle
15079862	C>T	(1,21)	not found	AT2G36780	Exon 1
15175019	C>T	(1,25)	(0,24)	None	
15272439	G>A	(0,19)	not found	AT2G37170	Intron -17
15362370	C>T	(3,31)	not found	AT2G37420	Exon
15542764	C>T	(1,27)	(0,25)	None	
15686318	C>T	(1,30)	(0,29)	None	
15856924	C>T	(0,23)	(0,20)	None	
15941764	G>A	(0,28)	(0,18)	None	

Table 6.3 Single nucleotide polymorphisms in exons of the *xd22* mapping interval.

gene affected	exon/ intron	codon change	amino acid change	surrounding sequence	conserved residue?
AT2G30220	Exon	GAC > GAT	Asp = Asp		
AT2G30520	exon	TCC > TCT	Ser = Ser		
AT2G30940	Exon	CGG > TGG	Arg > Trp	QKITRSHEV	R442: in non-conserved C-term
AT2G31540	Exon	TCC > TCT	Ser = Ser		
AT2G31550	Exon	TTG > TTA	Leu = Leu		
AT2G31955 = CNX2	Exon	CGG > CAG	Arg > Gln	RCNLRCQYC	R88: conserved in homologs, Q in related NifB's
AT2G32180	Exon	AGG > AAG	Arg > Lys	RVTCMQTE	R30: non-conserved
AT2G32610	Exon	CGA > CAA	Arg > Gln	IEAAREVGH	R435: Q in A. lyrata and in paralogs
AT2G32610	Exon	ATC > ATT	Ile = Ile		
AT2G32650	Exon 1	CCA > TCA	Pro > Ser	TTPFPGSVT	P11: in N-term, not conserved, many paralogs
AT2G32650	Exon 1	CTC > CTT	Leu = Leu		
AT2G33070	Exon	TAC to TAT	Tyr = Tyr		
AT2G33080	Exon 1	CAG to CAA	Glu = Glu		
AT2G33080	Exon 1		Asn=Asn		
AT2G36780	Exon 1	CTG > CTA	Leu = Leu		
AT2G37420	Exon	ACT > ATT	Thr > Ile	KKEKTHFTE	S, R or N in other plant species

Only six of the EMS mutations in the mapping interval caused an amino acid exchange, and only one was a conserved residue. The affected gene was *CNX2*, encoding a mitochondrial located protein which is involved in the synthesis of cPMP, the first intermediate of the MoCo assembly (Bittner, 2014; Teschner et al., 2010) (Figure 6.11).

A

```
          84   R    C    N    L    R    C    Q    Y
WT Ler   250  CGG  TGT  AAT  CTC  CGG  TGT  CAG  TAT
cnx2-2   250  CGG  TGT  AAT  CTC  CAG  TGT  CAG  TAT
          84   R    C    N    L    Q    C    Q    Y
```

B

Figure 6.12 Amino acid homology analysis of CNX2 in the region of the *xd22* mutation. A. Nucleotide sequence alignment of the *xd22* and wild-type sequence with amino acid translation. The *xd22* sequence from the whole genome sequencing was aligned against the Landsberg wild type. Alignment was performed using the Clustal Omega server. **B.** Amino acid alignment of the N-terminal sequence of Arabidopsis CNX2 and homologs. Protein sequences were acquired from and aligned in the UniProt database: *Arabidopsis thaliana* (accession no. Q39055) (ARATH), *Staphylococcus aureus* (accession no. P69848) (STAA8), *Homo sapiens* (accession no. Q9NZB8) (HUMAN) and *Escherichia coli* (accession no. P30745) (ECOLI). Shading was performed using the BoxShade server. CXXRCXXC highlights the position of the residue at the position of the *xd22* mutation in the context of the three adjacent cluster binding cysteines. Shading indicates the level of conservation if 50% of the sequences match; black = identical amino acids, grey = similar amino acids.

The point mutation (G263>A) changes the codon CGG to CAG which is predicted to cause a single amino acid change from arginine to glutamine at position 88. This amino acid is located adjacent to a cysteine involved in FeS cluster binding and is highly conserved amongst CNX2/MOCS1/MoaA from various organisms (Figure 6.12B). No antibody for CNX2 is available and thus protein levels could not be tested in *xd22* mutants. To investigate if the point mutation alters transcript levels semi-quantitative reverse transcriptase PCR was performed (Figure 6.13).

CNX2 transcript levels were not decreased but slightly elevated in *xd22* mutants. This indicates that the observed mutant phenotype is due to a defect in the protein.

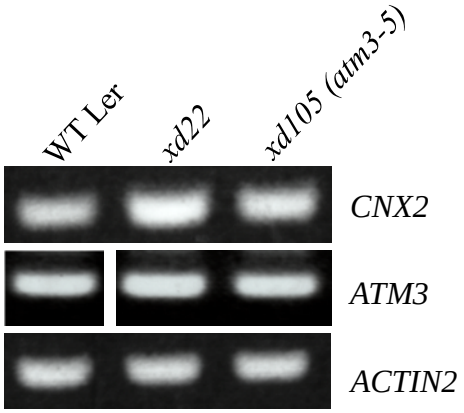

Figure 6.13 Transcript levels of *CNX2* and *ATM3* in *xd22*, *xd105* and wild type plants. Semi-quantitative reverse-transcriptase PCR was performed with specific intron-spanning primers on three week old seedlings. Arabidopsis *ACTIN2* levels served as a control for the levels of template cDNA. WT Ler = Wild type Landsberg.

6.8. The *xd22* mutation leads to a defect in MoCo enzyme activity which is complemented by reintroducing the *CNX2* sequence

For further confirmation that *xd22* plants have a defect in MoCo assembly I tested the activities of the MoCo-enzymes nitrate reductase, xanthine dehydrogenase and aldehyde oxidase in mature *xd22* plants in comparison the Landsberg wild type (Figure 6.14). Activities of the MoCo enzymes aldehyde oxidase and xanthine dehydrogenase were visualised in a native in-gel assay. Xanthine dehydrogenase specificity was assured by addition of the specific substrate hypoxanthine. Nitrate reductase activity was measured in a photospectrometric assay as the formation of nitrite. Aldehyde oxidase and xanthine dehydrogenase activities were undetectable in *cnx2-2* plants and nitrate reductase activity was decreased to ~55% +/- 5% of the wild type levels (Figure 6.14B). Activities of three MoCo enzymes were found to be significantly decreased indicating a defect in MoCo assembly in *xd22* plants.

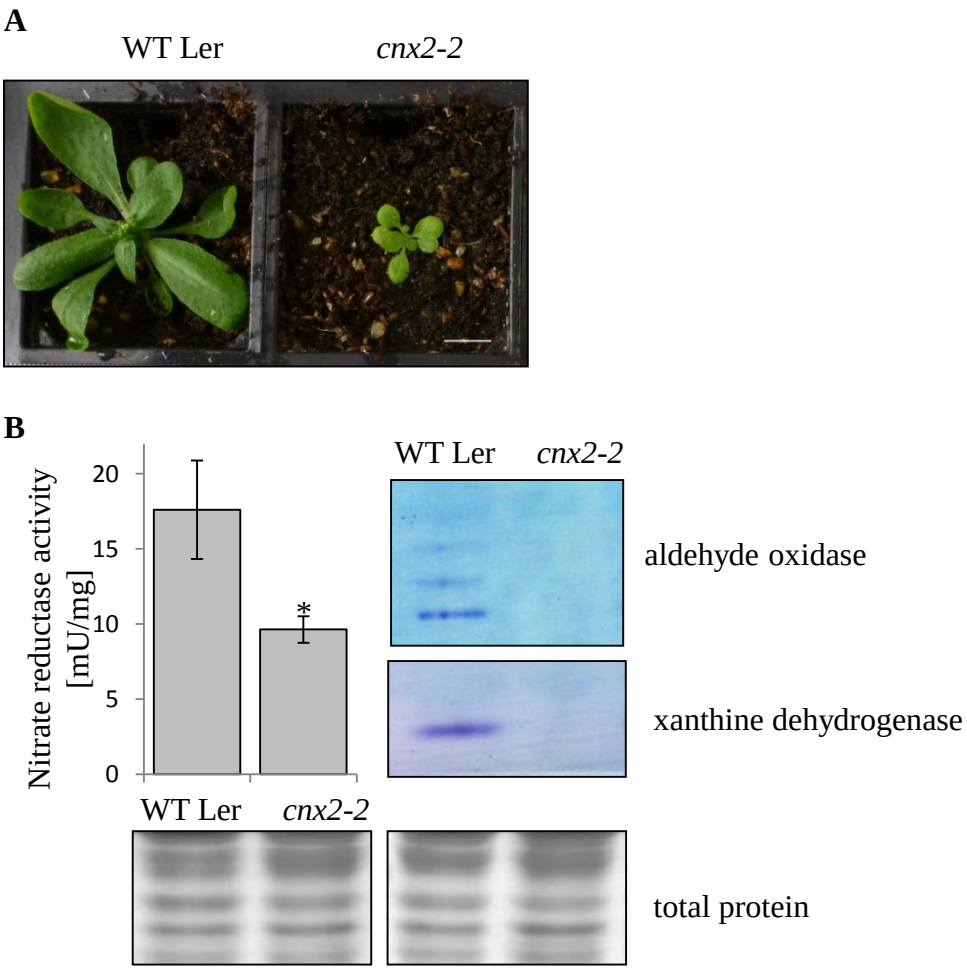

Figure 6.14 Phenotype and MoCo enzyme activities in the *xd22* point mutant.
A. Phenotype of 4-week-old *xd22* (*cnx2-2)* and wild-type plants of the Landsberg ecotype (WT Ler). Scale bar is 1cm. **B.** MoCo enzyme activities in mature *xd22 (cnx2-2)* and wild type (WT, Landsberg ecotype) plants. Total protein was visualised by instant blue™ staining after SDS-PAGE and immunoblotting of a sample from the same extract. Images are representative for three biological repeats.

To confirm that the *xd22* phenotypes are caused by the G263>A mutation in *CNX2*, the mutant was transformed with a pBINH vector carrying the wild-type *CNX2* gene including the promoter region and untranslated regions (from -1224 upstream of the start codon to +614 downstream of the stop codon). The construct also contained a hygromycin resistance gene. Plants were selected on agar plates containing hygromycin. Hygromycin resistant seedlings were transferred to soil and showed a rescue of the *xd22* growth phenotype (Figure 6.15). Genotyping confirmed that the plants carried both, the *xd22* mutation and the *CNX2* transgene.

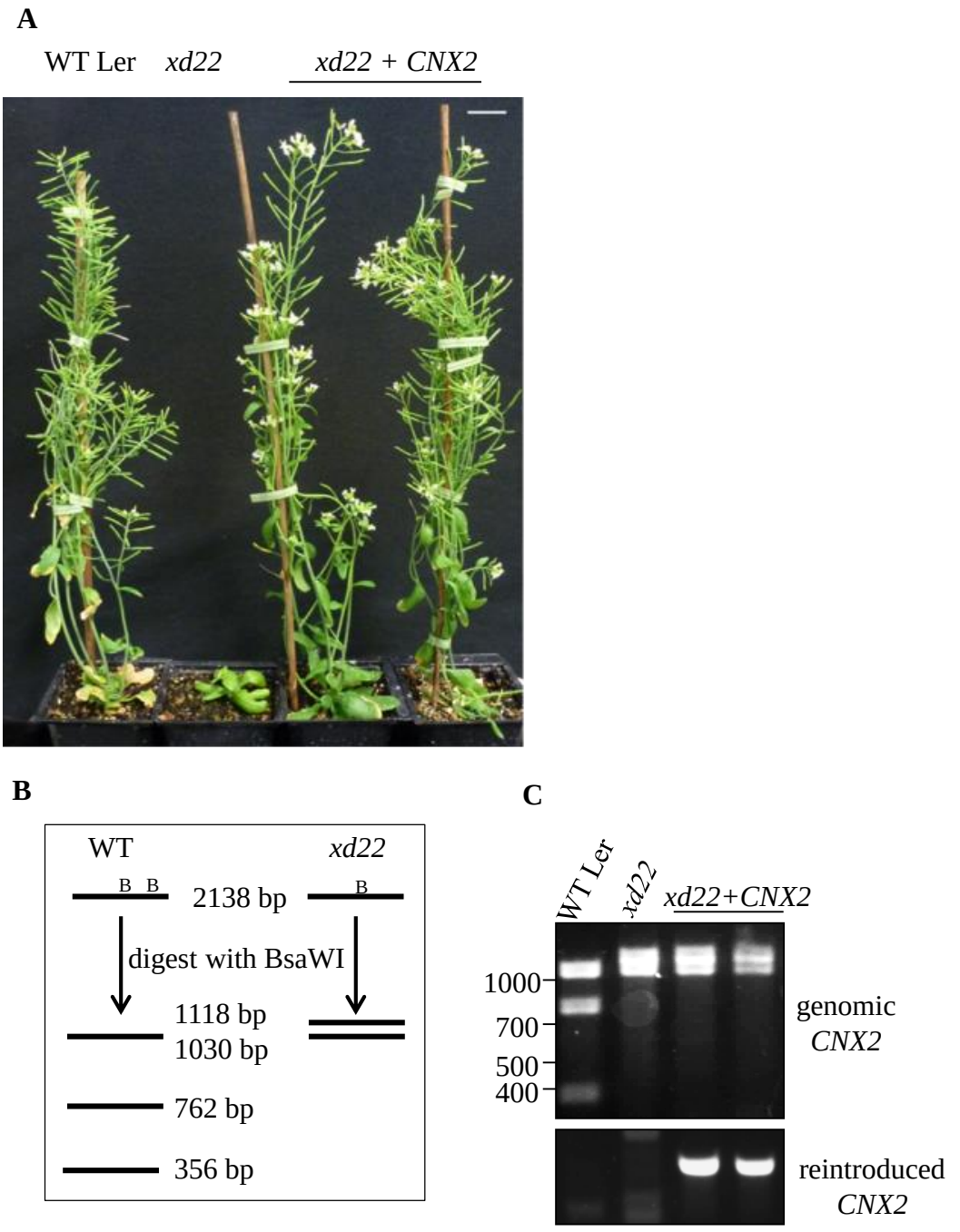

Figure 6.15 Growth phenotype of *xd22* plants expressing *CNX2* in comparison to *xd22* and a wild type. Seedlings were isolated on medium containing 25 µg/ml hygromycin and transferred to soil. WT Ler = wild type Landsberg. Plants are 3 months old. Scale bar is 2 cm. **B.** Scheme for the genotyping PCR/digest to identify plants carrying the *xd22* mutation. Two primers were designed to amplify a PCR product spanning the *xd22* mutation. BsaWI digest of this product results in three bands for the wild-type and two bands for the mutant product as one of the restriction sites is removed by the *xd22* mutation. **C.** Confirmation of the presence of the *xd22* mutation as described in A. Presence of the reintroduced *CNX2* was confirmed by PCR with the reverse primer annealing in the flanking sequence originating from the transformation vector.

To confirm the biochemical complementation of the *xd22* phenotype I analysed aldehyde oxidase activity. Enzyme activity was restored and thus it can be concluded that the observed phenotype of *xd22* plants is due to the mutation in the *CNX2* sequence (see Figure 6.16). Thus this line will be referred to as *cnx2-2*.

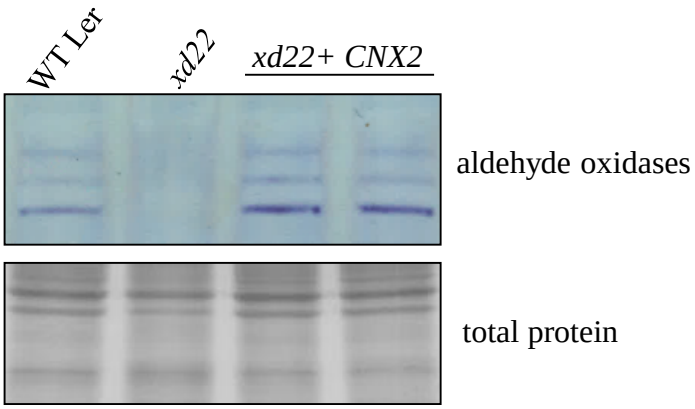

Figure 6.16 Aldehyde oxidase activities in *xd22* plants complemented with CNX2. Aldehyde oxidase activity was visualised in leaf samples from mature plants in a native in-gel assay. Total protein was visualised by instant blue^{TM} staining after SDS-PAGE and immunoblotting of a sample from the same extract.

6.9. A *cnx2* T-DNA insertion mutant is lethal in early seedling establishment

In order to gain more insight into the *cnx2* mutant phenotype another mutant allele was investigated which will be referred to as *cnx2-1* (SALK_037143). The *cnx2-1* line carries a T-DNA insertion in the second exon (see Figure 6.17). This line was mentioned before by (Dai et al., 2005) who showed sirtinol resistance in three day old seedlings but no homozygous adult plants have been reported. Therefore I genotyped 30 individuals from the progeny of a *cnx2-1/CNX2* plant. The seedlings all had a wild-type appearance and I found a 2:1 ratio of *cnx2-1/CNX2* to *CNX2* (χ^2 goodness of fit test p = 1; figure 1.18A). These results confirm that *cnx2-1* homozygous plants were not viable in the adult stage.

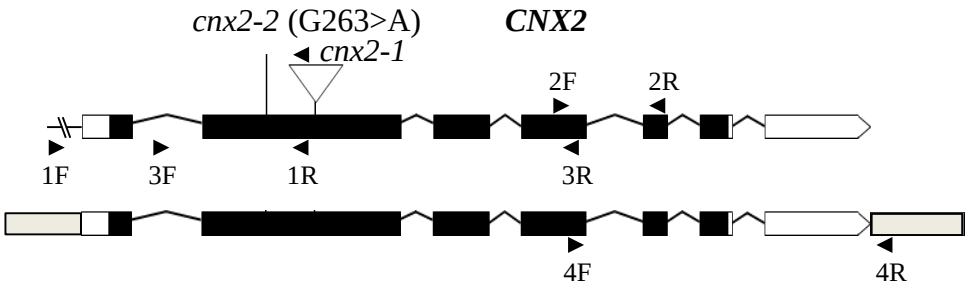

Figure 6.17 Gene model of *CNX2*. Exons (black boxes), introns (black lines) and UTRs (blank boxes) are indicated. The upper panel represents the gDNA sequence with the *cnx2-1* (triangle) and *cnx2-2* (line) mutations. Primer pair 1 was used for identification of the *xd22* mutation, primer pair 2 for reverse transcriptase PCR. The primers 3F and 3R amplify the wild-type sequence in the position of the *cnx2-1* T-DNA insertion. The left border primer of the T-DNA insertion together with the 3F primer amplifies a product if the T-DNA insertion is present. The lower panel represents the gDNA inserted in the plasmid for Arabidopsis transformation with the flanking plasmid DNA (grey box). Primer pair 4 amplifies a transgene-specific sequence.

A

n	*CNX2/CNX2* [%]	*cnx2-1/CNX2* [%]
30	33.3	66.7

B

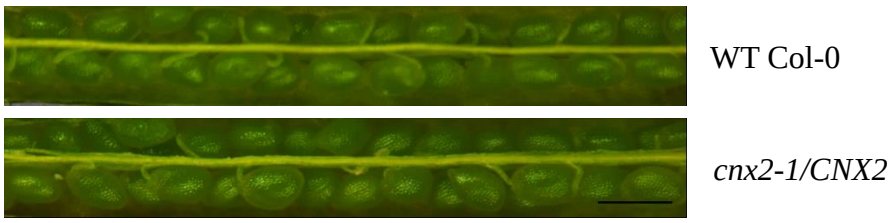

C

phenotype / line	n	healthy [%]	unfertilised [%]	aborted [%]
WT	665	98.5%	0.45%	1.05%
cnx2-1/CNX2	907	96.9%	2.4%	0.7%

Figure 6.18 Segregation analysis of the *cnx2-1* mutation from a *cnx2-1/CNX2* parent. A. Genotyping of mature plants from a *cnx2-1/CNX2* parent. **B.** Phenotype of representative siliques of plants from A. Scale bar is 0.5 cm. **C.** Seed phenotype of 3-7 fully mature siliques from *cnx2-1/CNX2* (4 plants) and wild type (2 plants) were analysed.

To investigate if the mutation is lethal in seed or early seedling development I investigated if there were any abnormalities in the phenotype of seeds and floral organs. Setting of healthy seeds in *cnx2-1/CNX2* siliques did not differ significantly from the wild type (Student's t-test p = 0.139; Figure 6.18B and C). This is evidence that the ovules carrying the *cnx2-1* gene are viable. Another explanation for the lack of *cnx2-1*/*cnx2-1* could be a defect in pollen formation. However, pollen and anthers were also found to be wild-type-like (Figure 6.19). The third possibility is that homozygous *cnx2-1* seeds develop normally, but that they fail to germinate or die during germination. To facilitate germination, seeds were planted on ½ -MS agar containing 1% sucrose.

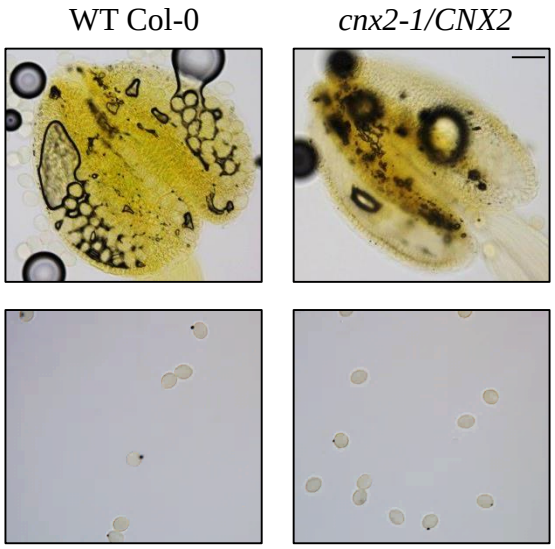

Figure 6.19 Anther and pollen development in *cnx2-1/CNX2* plants. Anthers (upper panel) and pollen (lower panel) were dissected from mature flowers and are representative for results from three (*cnx2-1/CNX2*) or two plants (wild type). Scale bar is 50 µm. WT = wild type.

These growth conditions revealed that ~21% of the seedlings showed a strong phenotype with elongated hypocotyls, chlorosis and dwarfed growth which is in accordance with the expected 1 in 4 ratio for homozygous mutants (χ^2 goodness of fit p = 0.334) (see Figure 6.20A-C). They developed necrotic tissue of the leaves and arrested in young seedling stage when the second pair of true leaves emerged.

A

phenotype / line	n	healthy [%]	mutant-like [%]	ungerminated [%]
WT Col-0	271	99.6	--	0.4
cnx2-1/CNX2	461	79.1	20.9	0.0

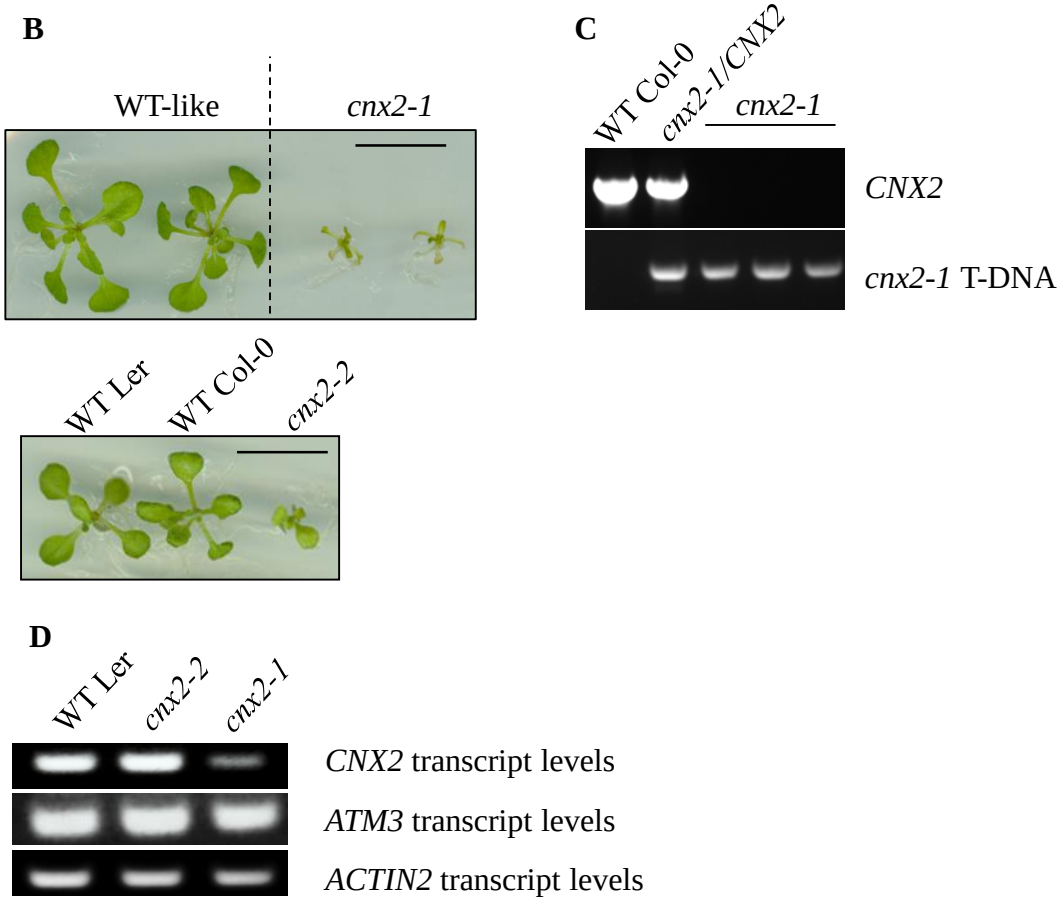

Figure 6.20 Characterisation of the *cnx2-1* T-DNA insertion mutant. A. Percentages of mutant-like plants from three different experiments with samples spread over two plates each. **B**. Growth of wild-type (WT)-like seedlings and *cnx2-1* seedlings segregating from a heterozygous parent in comparison to *cnx2-2* and wild type seedlings of both ecotypes. Scale bar is 1 cm. **C.** Genotyping of putative homozygous *cnx2-1* plants in B, upper panel. **D**. Transcript levels of *CNX2*, *ATM3* and *ACTIN2*. Specific, intron-spanning primers (downstream of the mutation) were used for all reactions. *ACTIN2* transcript levels served as a control.

The dwarfed seedlings were identified as *cnx2-1*/*cnx2-1* (Figure 6.20C). As shown in Figure 6.17, the T-DNA insertion in the *cnx2-1* mutants is located in the second exon of the gene and thus was assumed to be a knock-out mutant. However, low levels of *CNX2* transcript are still detected in the mutants, which may be due to sample contamination (Figure 6.20D). Due to the position of the T-DNA mutation, low

transcript levels and the severe phenotype of the mutant plants it is likely that no functional CNX2 protein is present in these plants.

6.10. Mild NH_4NO_3 treatment partially rescues the *cnx2-2* phenotype

As shown above, the *cnx5* mutant phenotype is partially rescued under NH_4NO_3 treatment, because of chemical complementation of a nitrate reductase defect. In contrast, plants of the *cnx2-2* line died after 12 days of NH_4NO_3 treatment. This is curious as both affected proteins function in the biosynthesis of MoCo which is a cofactor of nitrate reductase. It is possible that high concentrations of 50 mM NH_4NO_3 have a secondary effect that is lethal for plants with the *cnx2-2* mutation but not for plants with the *cnx5* mutation. Thus I repeated the NH_4NO_3 treatment with milder conditions: Two week old plants were treated on day 1, 4, 6, 9 and 12 while standard watering (tap water) was continued (see Figure 6.21).

Figure 6.21 Growth phenotype of *cnx2-2* plants under mild NH_4NO_3 treatment. Plants were grown on soil for two weeks under standard conditions. Watering was continued and plants were treated with 10 ml of 50 mM NH_4NO_3 on day 1, 4, 6, 9 and 12. Untreated plants served as a control. Scale bar is 1 cm.

After 12 days of this treatment, all plants showed improved growth. The *cnx5* mutants were not rescued to an equal extend as with the daily treatment and showed no additional greening (see Figure 6.3B). The *cnx2-2* plants remained chlorotic as well but growth was visibly improved. The *cnx2-2* phenotype was not rescued to the

same extend as the *cnx5* phenotype under daily treatment. This and the overall growth enhancing effect of the treatment indicate a general fertilising effect of NH_4NO_3 at this dosage rather than a specific rescue of the lack of nitrate reductase activity. Thus it is still unclear why the stronger treatment is lethal to *cnx2-2* but not to *cnx5* mutants.

6.11. Mutants of proteins involved in MoCo biosynthesis have decreased ATM3 protein levels

As described earlier, the selection process for mutants of proteins with a function close to ATM3 was designed to exclude MoCo mutants. It is curious that *xd22* was found to be a mutant allele of *CNX2*, which is involved in the first step of MoCo biosynthesis. To investigate if there is a link between CNX2 and ATM3, I tested if ATM3 protein levels were affected in *cnx2-2* plants (Figure 6.22). Interestingly, the *xd22* line had decreased ATM3 protein levels and what seemed to be degradation products of lower molecular weight.

However, this is not necessary linked to the *cnx2-2* mutation and could be due to another genetic variant in the plant line. Therefore I tested ATM3 protein levels in plants from the mapping population with the *xd22* phenotype, as well as in plants of the complemented *cnx2-2 + CNX2* line.

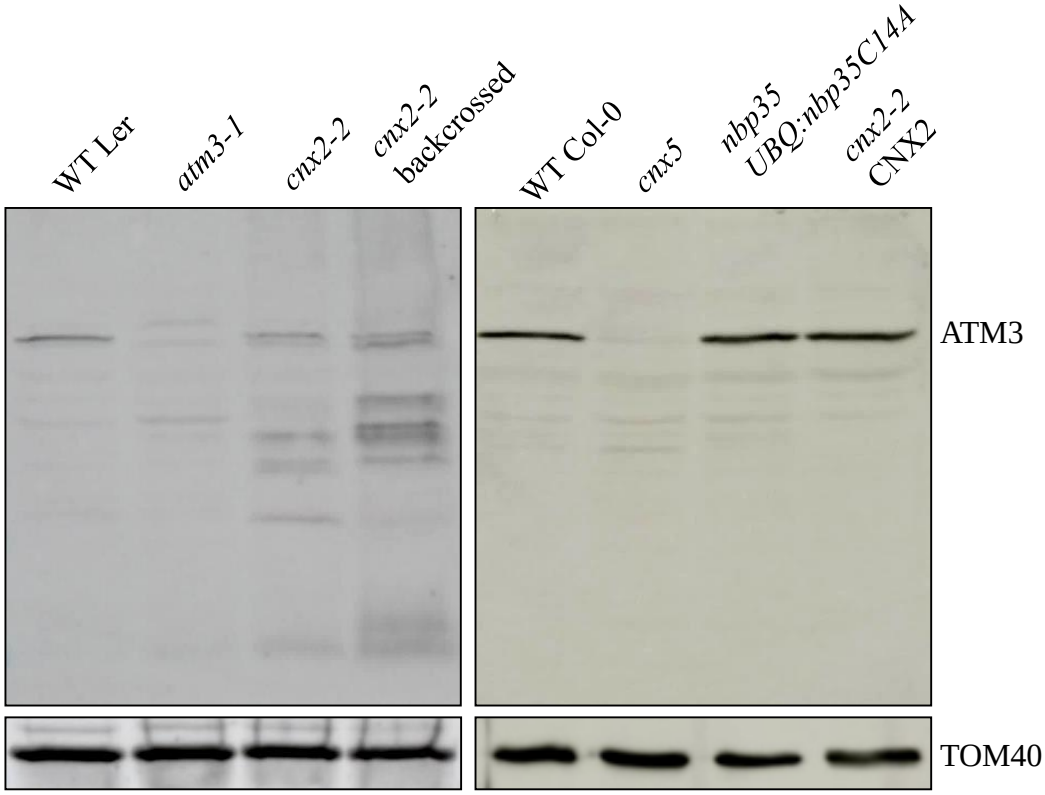

Figure 6.22 ATM3 protein levels in mutants with disrupted MoCo and cytosolic FeS assembly. Mitochondria were isolated from 4 weeks old whole plants grown on soil (left panel) or seedlings grown for 12 days in liquid cultures (right panel). A homozygous *cnx2-2* line was analysed as well as backcrossed *cnx2-2* plants isolated from a segregating line. Further lines were a *cnx5* mutant, an *atm3-1* mutant, a *nbp35* mutant kindly donated by Emma Bastow (*nbp35-1*, with reintroduced *UBQ:nbp35C14A* carrying a point mutation) and both wild-type ecotypes (Landsberg, WT Ler and Columbia, WT Col-0). The *cnx2-2* line complemented with the native CNX2 was selected from a segregating line in medium containing 10 µg/ml hygromycin. Translocase of the Outer mitochondrial Membrane 40 (TOM40) protein levels were used as a control for equal loading and mitochondrial purity.

ATM3 protein levels were decreased in the backcrossed *cnx2-2* plants and putative degradation bands were visible (Figure 6.22). However, ATM3 protein levels were restored in the complemented *cnx2-2 + CNX2* line and thus it can be concluded that the *cnx2-2* mutation affects ATM3 protein stability.

To investigate if this effect is specific to proteins involved in MoCo assembly or if ATM3 degradation also occurs in mutants of FeS assembly proteins, I tested ATM3 levels in *cnx5* and a mutant of the nucleotide binding protein 35 (*NBP35*). CNX5 is involved in the cytosolic part of MoCo assembly, downstream of CNX2. NBP35 is involved in cytosolic FeS assembly (see Section 1.2). The *nbp35-1+UBQ:nbp35C14A* (this line will be referred to as *nbp35*) is a knock-out

mutant with a reintroduced mutated version of the protein under the expression of an ubiquitin promoter (Bastow et al., accepted manuscript). While ATM3 levels were wild-type like in the *nbp35* mutant, *cnx5* mutants had no detectable ATM3 protein (Figure 6.22). However, it has to be noted that the results of ATM3 protein levels in *cnx5*, *nbp35* and the complemented *cnx2-2*+CNX2 were only from one biological replicate and this needs to be confirmed.

To conclude, the uncharacterised sirtinol resistant mutant *xd22* was identified as a mutant allele of *CNX2* (*cnx2-2*). This is the first viable mutant of a mitochondrial component of the MoCo pathway. Mutant plants show a severe growth phenotype and decreased MoCo enzyme activities which was complemented by reintroducing the native *CNX2* gene. The *cnx2-2* as well as a *cnx5* mutant showed decreased ATM3 protein levels showing that the MoCo pathway and cytosolic FeS assembly are linked. It remains unclear how the flux through the MoCo pathway affects protein levels of ATM3.

6.12. Discussion

In this Chapter I analysed mutants with a phenotype close to *atm3* in order to find unknown components of the mitochondrial-cytosolic FeS assembly. I chose two mutant lines (*xd22* and *xd105*) for identification of the underlying mutation due to their growth phenotype and biochemical properties. *xd105* was identified as a new allele of *atm3* (*atm3-5*) thus being a good internal control for the selection process. Selection of the mutants was based on a previous screen and characterisation performed by Nina Kahlfeldt. Interestingly, according to her categories *xd105*/*atm3-5* did not group with the *atm3-4* allele that was included in her analysis and none of the lines that did group with *atm3-4* showed characteristics specific for cytosolic FeS mutants (e.g. mild growth defect upon NH_4NO_3 treatment and decreased cytosolic aconitase activity). The size of an EMS mutant pool, which is usually several hundred lines for a screen for unknown mutants, renders it necessary to decrease the number of samples drastically for downstream analysis. However, the unexpected outcome of the described analysis underlines the importance of finding the balance between a thorough selection scheme and a manageable amount of mutants in order to ensure efficiency and quality of a large scale mutant screen.

The second mutant line, *xd22*, was identified as a mutant of CNX2 (*cnx2-2*) which is involved in the mitochondrial part of MoCo assembly. This outcome was puzzling as the selection process was specifically designed to exclude MoCo mutants. The NH_4NO_3 treatment was a central part of the selection between MoCo and FeS mutants. Based on the observation that *cnx5* mutants were partially rescued under the treatment it was reasonable to assume that NH_4NO_3 chemically complements for the lack of the MoCo enzyme nitrate reductase. However, the *xd22* plants were not viable under these conditions and thus were assumed to have to defect in FeS assembly. This could be due to the difference in localisation, while CNX5 is located in the cytosol, CNX2 is located in the mitochondria. However, what exactly the mechanism behind the NH_4NO_3 rescue or lethality is remains unclear. Another part of the selection was the analysis of cytosolic aconitase activity. This enzyme has no MoCo but a FeS cluster and thus depends on the cytosolic FeS assembly as well as the mitochondrial components NFS1 and ATM3. *xd22* showed a severe defect in cytosolic aconitase and this was assumed to be due to a defect in cytosolic FeS assembly. This could be explained by the link that was found between decreased functionality of CNX2 and the degradation of ATM3 protein which will be discussed in Section 7.2.

7. Discussion

7.1. The role of ATM3 in FeS and MoCo assembly and t-RNA thiomodification

As described before, ATM3 is necessary for the assembly of FeS clusters in the cytosol (Bernard et al., 2009). The substrate of ATM3 has been a matter of debate for decades and I propose that ATM3 transports oxidised glutathione carrying additional S^0 not only for cytosolic FeS assembly but also for MoCo assembly and tRNA-thiomodification in the cytosol (see Figure 7.1).

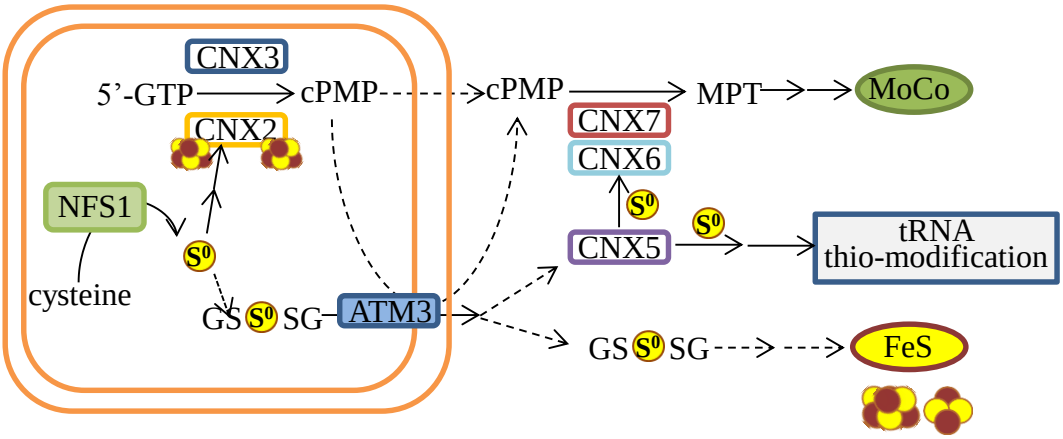

Figure 7.1 The proposed link between the mitochondrial-cytosolic sulfur transport, FeS assembly, MoCo assembly and cytosolic tRNA thiomodification. ATM3 = ABC Transporter of the Mitochondria 3; CNX = Cofactor of Nitrate reductase and Xanthine dehydrogenase; cPMP = cyclic pyranopterin monophosphate; GSH/GSSG = reduced/oxidised glutathione; GTP = guanosine triphosphate; MPT = Molybdopterin; NFS1 = Nitrogen fixation S (NIFS)-like 1. Dashed arrows indicate unknown/proposed steps.

In-vitro data presented in (Schaedler et al., 2014) showed that ATM3 in Arabidopsis and Atm1 in yeast can transport oxidised glutathione and that oxidised glutathione-persulfide can be transported by Atm1. In Chapter 3 and 4 I describe *in-vivo* evidence supporting the hypothesis that ATM3 transports oxidised glutathione with a S^0: The redox state of the glutathione pool in the mitochondria of *atm3* mutants was significantly more oxidised than in the wild type which indicates that ATM3 is involved in transport of oxidised glutathione. Furthermore I found that ATM3 interacts genetically with NFS1 and ETHE1, two enzymes directly involved in the

generation or detoxification of S^0 species, respectively. Taken together, these data indicate that ATM3 does transport an oxidised glutathione carrying a S^0.

Further to the debated role of ATM3 in cytosolic FeS assembly cPMP was proposed as a substrate in 2010 when (Teschner et al.) found that *atm3* mutants had a defect in MoCo enzyme activity and accumulated cPMP in the mitochondria. However, they also found cPMP accumulation in a *cnx5* mutant. This is unexpected, as CNX5 is a cytosolic component of the MoCo assembly machinery necessary for the sulfuration of cPMP and thus cPMP accumulation should occur in the cytosol. I found that ATM3 protein levels were decreased in plants of the same *cnx5* mutant allele. This could explain the accumulation of cPMP in *cnx5* mitochondria rather than in the cytosol and supports the hypothesis that cPMP is transported by ATM3. However cPMP deficiency in mice and humans can be treated with injections of cPMP (Schwarz et al., 2004)(Veldman et al., 2010), showing that cPMP likely can pass membranes. This indicates that either a transporter is not required or that there is a transporter for cPMP in the cell membrane. It remains unclear whether ATM3 transports cPMP as well but it is possible that the transport of a persulfide compound by ATM3 is necessary for MoCo assembly.

cPMP accepts two sulfur atoms in the cytosol which are transferred from CNX5 via CNX7 (part of the MPT-synthase complex). CNX5 does not only donate sulfur to the MoCo pathway but also to tRNA-thiomodification (Nakai et al., 2012). The source of the S^0 in plants has not yet been identified. However, in humans itoriginates from cysteine, which is generated by NFS1 in the cytosol and transferred to the MPT-synthase complex via the CNX5 homolog MOCS3 (Krepinsky and Leimkuhler, 2007; Marelja et al., 2008). There is one cytosolic cysteine desulfurases in Arabidopsis (ABA3), one plastidic (NFS2/CpNifS) and one mitochondrial (NFS1). ABA3 has been extensively studied before and it was found that the functions of aldehyde oxidase and xanthine dehydrogenase but not nitrate reductase depend on ABA3. It has been established that ABA3 catalyses the transfer of an additional sulfur to the MoCo as it is needed for aldehyde oxidase and xanthine dehydrogenase. However, nitrate reductase is not affected which means that the initial sulfuration of cPMP does not depend on ABA3 (Bittner et al., 2001; Heidenreich et al., 2005; Lehrke et al., 2012; Schwartz et al., 1997; Wollers et al., 2008). In 2013 (Bernard et al.) showed that NFS2 is not needed for aldehyde oxidase and xanthine dehydrogenase. NFS1 on the other hand is needed for the activity of the

cytosolic isoform of aconitase (FeS only) (Bernard et al., 2013) and for aldehyde oxidase (MoCo, FeS and FAD).

Taken together, this indicates that the source of S^0 for CNX5 in Arabidopsis is NFS1 in the mitochondria. This would mean that cytosolic FeS and MoCo assembly as well as tRNA-thiomodification depend on ATM3.

For future research it would be insightful to investigate whether ATM3 and its homologs can transport cPMP. ATPase activity and transport of cPMP could be tested using lactococcus inside-out vesicles expressing ATM3 or Atm1. It is also necessary to test if tRNA-thiomodification is dependent on ATM3 function and this could be achieved by testing tRNA-thiomodification in *atm3* mutants using the gel-shift assay described in (Nakai et al., 2012) or by investigating if disruption of components downstream of CNX5 can cause ATM3 breakdown.

7.2. Regulation of ATM3 protein levels

As mentioned above, I observed ATM3 protein degradation in a *cnx5* mutant. It is puzzling that *cnx2-2* mutants also showed ATM3 degradation as this would further decrease the already low cPMP export. It is unlikely that cPMP excess as well as decrease levels of cPMP both trigger ATM3 degradation as part of the same mechanism. Thus I suggest that ATM3 degradation is independent of cPMP transport and rather is a way of regulating ATM3 function. This would limit glutathione-persulfide export and contain it in the mitochondria. As described in Chapter 1.5 ETHE1 in the mitochondria accepts S^0 from glutathione. Thus it could serve as a general detoxification mechanism to prevent damage by excess S^0. The *cnx2-2* mutant plants have decreased levels of cPMP and *cnx5* mutant plants have decreased levels of S^0 transfer for MoCo assembly as well as t-RNA thiomodification thus limiting the S^0 acceptors in the cytosol. Thus the breakdown of ATM3 in both mutants could represent a mechanism to contain S^0 in the mitochondria to prevent accumulation and damage in the cytosol. However, no breakdown of ATM3 protein was observed in a mutant of the CIA scaffold *NPB35*. It is possible that the defect in cytosolic FeS assembly in *nbp35* plants does not cause an accumulation of S^0 to a similar extent as in MoCo mutants. It has to be noted that the degradation of ATM3 was incomplete in *cnx2-2* mutants while no residual

protein was detected in *cnx5*. This could be due to the double function of CNX5 which donates sulfur not only to the MoCo pathway but also to the tRNA-thiomodification pathway.

It remains unclear why ATM3 degradation occurs in *cnx2-2* mutants but not in *nbp35* mutants but it is also possible that the mutations are different in severity as the *nbp35* mutants have a mild growth phenotype in comparison to *cnx2-2* mutants. However, it has to be considered that ATM3 degradation could be due to an unknown regulatory mechanism specific for MoCo assembly and further experiments are needed. It also has to be noted that there could be a background mutation in the *cnx5* line as it originates from an EMS population and sequencing of the *ATM3* gene will be necessary As mentioned above, it will be important to test ATM3 protein levels in other components of the tRNA-thiomodification as well as the cytosolic FeS and MoCo assembly. It would also be interesting to investigate if *NFS1* overexpression causes ATM3 breakdown.

7.3. Glutathione export by ATM3 as a mechanism to control glutathione redox balance in the mitochondria.

Reduced glutathione is needed for many stress responses including the prevention of oxidative stress. Thus it is vital that the redox balance is maintained (Noctor et al., 2012). As discussed above, ATM3 can transport oxidised glutathione. Thus I want to propose that transport of oxidised glutathione by ATM3 is a mechanism to shift the redox state of the glutathione pool towards the reduced state. I found that the redox state of the glutathione pool in mitochondria of *atm3* mutants is shifted towards oxidation. Furthermore, I observed mitochondrial aggregation in *atm3-4* mutants expressing mitochondrial roGFP. This also indicates an accumulation of oxidised glutathione as oxidised glutathione can be a signal for apoptosis which causes mitochondria aggregation (Circu and Aw, 2008; Haga et al., 2003). Expression of the mitochondrial roGFP construct also means overexpression of glutaredoxin and was lethal for *atm3-1* mutants. Glutaredoxins mainly mediate reduction reactions using reduced glutathione as an electron donor thus producing oxidised glutathione. Thus overexpression of glutaredoxin could lead to cell death in combination with the accumulation of oxidised glutathione due to the *atm3-1* mutation. The wild type with

the mitochondrial roGFP construct, overexpressing GRX did not show a sign of mitochondrial aggregation. Taken together, this could indicate that ATM3 is important for the redox balance of the glutathione pool, shifting it towards the reduced state by exporting oxidised glutathione. It would be interesting to test if *ATM3* genetically interacts with proteins involved in glutathione biosynthesis and glutathione redox reactions.

7.4. Glutaredoxins in FeS assembly

For a long time there has been controversy in the discussion of glutaredoxins. The group of monothiol glutaredoxins has been thought to be involved in FeS assembly but evidence is mostly from *in-vitro* work except for yeast Grx5. I have worked on the mitochondrial GRXS15 and cytosolic GRXS17 and found evidence that they are not involved in *de-novo* cluster assembly. Instead I would like to discuss the possibility that glutaredoxins could impact the availability of substrate for ATM3. Further I propose that glutaredoxins could contribute to the reduction of thiol groups for S^0 or cluster transfer. I have found evidence that GRX overexpression in *atm3* mutants is lethal and this may also mean that reduced glutathione is needed for the synthesis of oxidised glutathione-persulfide, the substrate of ATM3. Overexpression of glutaredoxin could lead to a further decrease of glutathione-persulfide export causing a further aggravation of the *atm3-1* phenotype.

The *grxS15* mutants showed a mild decrease of mitochondrial aconitase activity, however the aconitase in-gel assay indicates that there is also a decrease in cytosolic activity. This indicates that GRXS15 promotes FeS cluster insertion in mitochondrial apoproteins. However, it could also mean that GRXS15 is important for formation of the substrate of ATM3 by reduction of thiol groups for the transfer of S^0. Thus it would also affect the cytosolic FeS assembly. On the other hand, the activity of the cytosolic FeS enzyme aldehyde oxidase was not affected in *grxS15* mutants. This would indicate that (1) cytosolic FeS assembly in general is not affected and (2) mitochondrial FeS assembly is not affected as aldehyde oxidase activity is dependent on the activity of CNX2 in the mitochondria which contains two Fe_4S_4 clusters. Furthermore, Janneke Balk found that a double mutant of the mild *grxS15-1* knockdown mutant and *atm3-4* or *atm3-1* did not show an additional phenotype

indicating that GRXS15 and ATM3 do not have a synergistic genetic interaction (personal communication with Janneke Balk). However, it is possible that the genetic interaction was not visible due to the still relatively high GRXS15 protein levels in the *grxS15-1* knockdown. This was also the case for crosses of weaker *ethe1* and *atm3* alleles for which a synergistic genetic interaction was evident from crosses of stronger alleles. All in all the evidence indicates that plant glutaredoxins are not involved in *de-novo* cluster assembly, however, it is puzzling that links keep being found. (Knuesting et al., 2015) showed that GRXS17 is involved in the maintenance of the shoot apical meristem under long day conditions. However, a recent publication shows that GRXS17 associates with most components of the cytosolic FeS assembly and also with some FeS enzymes (Inigo et al., 2016). It is interesting that they found an interaction between GRXS17 and the cytosolic thiouridylase subunits (CTU) 1 and 2 which mediate thiolation reactions for tRNA modification. (Inigo et al.) concluded that GRXS17 is not essential for FeS enzyme activity, but contributes to correct FeS enzyme function. This could also explain the minor effects on FeS enzyme activities that were observed in *grxS17* mutants.

It is possible that GRX in general could be one reducing mechanism for the reduction of thiol groups for either the transfer of a cluster throughout the FeS transfer chain and for apoproteins or more generally for transfer of S^0 but it cannot be the only mechanism as FeS cluster enzymes are not as severely affected as mutants of essential components of the assembly pathways.

References

(2011). Hoyer's Medium. Cold Spring Harb Protoc *2011*, pdb.rec12429.

Akaba, S., Seo, M., Dohmae, N., Takio, K., Sekimoto, H., Kamiya, Y., Furuya, N., Komano, T., and Koshiba, T. (1999). Production of homo- and hetero-dimeric isozymes from two aldehyde oxidase genes of *Arabidopsis thaliana*. J Biochem *126*, 395-401.

Albrecht, S.C., Sobotta, M.C., Bausewein, D., Aller, I., Hell, R., Dick, T.P., and Meyer, A.J. (2014). Redesign of Genetically Encoded Biosensors for Monitoring Mitochondrial Redox Status in a Broad Range of Model Eukaryotes. J Biomol Screen *19*, 379-386.

Allam, A.I., and Hollis, J.P. (1972). Sulfide Inhibition of Oxidases in Rice Roots. Phytopathology *62*, 634-&.

Alonso, J.M., Stepanova, A.N., Leisse, T.J., Kim, C.J., Chen, H.M., Shinn, P., Stevenson, D.K., Zimmerman, J., Barajas, P., Cheuk, R., *et al.* (2003). Genome-wide Insertional mutagenesis of *Arabidopsis thaliana*. Science *301*, 653-657.

Amunts, A., Drory, O., and Nelson, N. (2007). The structure of a plant photosystem I supercomplex at 3.4 angstrom resolution. Nature *447*, 58-63.

Arnaud, N., Ravet, K., Borlotti, A., Touraine, B., Boucherez, J., Fizames, C., Briat, J.F., Cellier, F., and Gaymard, F. (2007). The iron-responsive element (IRE)/iron-regulatory protein 1 (IRP1)-cytosolic aconitase iron-regulatory switch does not operate in plants. Biochem J *405*, 523-531.

Balk, J., and Lobreaux, S. (2005). Biogenesis of iron-sulfur proteins in plants. Trends Plant Sci *10*, 324-331.

Balk, J., and Pilon, M. (2011). Ancient and essential: the assembly of iron-sulfur clusters in plants. Trends Plant Sci *16*, 218-226.

Balk, J., and Schaedler, T.A. (2014). Iron cofactor assembly in plants. Annu Rev Plant Biol *65*, 125-153.

Bandyopadhyay, S., Gama, F., Molina-Navarro, M.M., Gualberto, J.M., Claxton, R., Naik, S.G., Huynh, B.H., Herrero, E., Jacquot, J.P., Johnson, M.K., *et al.* (2008). Chloroplast monothiol glutaredoxins as scaffold proteins for the assembly and delivery of [2Fe-2S] clusters. EMBO J *27*, 1122-1133.

Bastow, E.L., Bych, K., Crack, J.C., Le Brun, N.E., and Balk, J. (2016). NBP35 interacts with DRE2 in the maturation of cytosolic iron-sulfur proteins in *Arabidopsis thaliana*. Plant J. (accepted manuscript) DOI: 10.1111/tpj.13409.

Beinert, H. (2000a). Iron-sulfur proteins: ancient structures, still full of surprises (vol 5, pg 2, 2000). J Biol Inorg Chem *5*, 409-409.

Beinert, H. (2000b). A tribute to sulfur. Eur J Biochem *267*, 5657-5664.

Beinert, H., Holm, R.H., and Munck, E. (1997). Iron-sulfur clusters: Nature's modular, multipurpose structures. Science *277*, 653-659.

Bernard, D.G., Cheng, Y., Zhao, Y., and Balk, J. (2009). An allelic mutant series of ATM3 reveals its key role in the biogenesis of cytosolic iron-sulfur proteins in Arabidopsis. Plant Physiol *151*, 590-602.

Bernard, D.G., Netz, D.J., Lagny, T.J., Pierik, A.J., and Balk, J. (2013). Requirements of the cytosolic iron-sulfur cluster assembly pathway in Arabidopsis. Philos Trans R Soc London, Ser. B, Biological sciences *368*, 20120259.

Birke, H., Haas, F.H., De Kok, L.J., Balk, J., Wirtz, M., and Hell, R. (2012). Cysteine biosynthesis, in concert with a novel mechanism, contributes to sulfide detoxification in mitochondria of *Arabidopsis thaliana*. Biochem J *445*, 275-283.

Birke, H., Hildebrandt, T.M., Wirtz, M., and Hell, R. (2015). Sulfide detoxification in plant mitochondria. Methods Enzymol *555*, 271-286.

Bittner, F. (2014). Molybdenum metabolism in plants and crosstalk to iron. Front Plant Sci *5*, 28.

Bittner, F., Oreb, M., and Mendel, R.R. (2001). ABA3 is a molybdenum cofactor sulfurase required for activation of aldehyde oxidase and xanthine dehydrogenase in *Arabidopsis thaliana*. J Biol Chem *276*, 40381-40384.

Brady, S.M., Orlando, D.A., Lee, J.Y., Wang, J.Y., Koch, J., Dinneny, J.R., Mace, D., Ohler, U., and Benfey, P.N. (2007). A high-resolution root spatiotemporal map reveals dominant expression patterns. Science *318*, 801-806.

Bridwell-Rabb, J., Fox, N.G., Tsai, C.L., Winn, A.M. and Barondeau, D.P. (2014). Human frataxin activates Fe–S cluster biosynthesis by facilitating sulfur transfer chemistry. Biochemistry *53*, 4904-4913.

Busi, M.V., Maliandi, M.V., Valdez, H., Clemente, M., Zabaleta, E.J., Araya, A., and Gomez-Casati, D.F. (2006). Deficiency of *Arabidopsis thaliana* frataxin alters activity of mitochondrial Fe-S proteins and induces oxidative stress. Plant J *48*, 873-882.

Charlesworth, D., and Willis, J.H. (2009). The genetics of inbreeding depression. Nature Rev Genet *10*, 783-796.

Chen, W., Liu, C., Peng, B., Zhao, Y., Pacheco, A., and Xian, M. (2013). New fluorescent probes for sulfane sulfurs and the application in bioimaging. Chem Sci *4*, 2892-2896.

Cheng, N.H. (2008). AtGRX4, an Arabidopsis chloroplastic monothiol glutaredoxin, is able to suppress yeast grx5 mutant phenotypes and respond to oxidative stress. Febs Lett *582*, 848-854.

Cheng, N.H., Liu, J.Z., Liu, X., Wu, Q., Thompson, S.M., Lin, J., Chang, J., Whitham, S.A., Park, S., Cohen, J.D., *et al.* (2011). Arabidopsis monothiol glutaredoxin, AtGRXS17, is critical for temperature-dependent postembryonic

growth and development via modulating auxin response. J Biol Chem *286*, 20398-20406.

Circu, M.L., and Aw, T.Y. (2008). Glutathione and apoptosis. Free Radical Res *42*, 689-706.

Couturier, J., Przybyla-Toscano, J., Roret, T., Didierjean, C., and Rouhier, N. (2015). The roles of glutaredoxins ligating Fe-S clusters: Sensing, transfer or repair functions? BBA-Mol Cell Res *1853*, 1513-1527.

Couturier, J., Touraine, B., Briat, J.F., Gaymard, F., and Rouhier, N. (2013). The iron-sulfur cluster assembly machineries in plants: current knowledge and open questions. Front Plant Sci *4*, 259.

Dai, X., Hayashi, K., Nozaki, H., Cheng, Y., and Zhao, Y. (2005). Genetic and chemical analyses of the action mechanisms of sirtinol in Arabidopsis. Proc Natl Acad Sci U S A *102*, 3129-3134.

Desai, U. J., and Pfaffle, P. K. (1995). Single-step purification of a thermostable DNA polymerase expressed in *Escherichia coli*. Biotechniques *19*, 780-784

Dixit, S., Dhar, P., and Mehra, R.D. (2011). Protective role of exogenous alpha alpha-lipoic acid (ALA) on hippocampal antioxidant status and memory function in rat pups exposed to sodium arsenite during the early post-natal period. Toxicol Mech Method *21*, 216-224.

Dooley, C.T., Dore, T.M., Hanson, G.T., Jackson, W.C., Remington, S.J., and Tsien, R.Y. (2004). Imaging dynamic redox changes in mammalian cells with green fluorescent protein indicators. J Biol Chem *279*, 22284-22293.

Dorman, D.C., Moulin, F.J., McManus, B.E., Mahle, K.C., James, R.A., and Struve, M.F. (2002). Cytochrome oxidase inhibition induced by acute hydrogen sulfide inhalation: correlation with tissue sulfide concentrations in the rat brain, liver, lung, and nasal epithelium. Toxicol Sci *65*, 18-25.

Drennan, C.L., and Peters, J.W. (2003). Surprising cofactors in metalloenzymes. Curr Opin Struc Biol *13*, 220-226.

Dwivedi, N., Flora, G., Kushwaha, P., and Flora, S.J.S. (2014). Alpha-lipoic acid protects oxidative stress, changes in cholinergic system and tissue histopathology during co-exposure to arsenic-dichlorvos in rats. Environ Toxicol Phar *37*, 7-23.

Eilers, T., Schwarz, G., Brinkmann, H., Witt, C., Richter, T., Nieder, J., Koch, B., Hille, R., Hansch, R., and Mendel, R.R. (2001). Identification and biochemical characterization of *Arabidopsis thaliana* sulfite oxidase - A new player in plant sulfur metabolism. J Biol Chem *276*, 46989-46994.

Figueroa, P., Leon, G., Elorza, A., Holuigue, L., and Jordana, X. (2001). Three different genes encode the iron-sulfur subunit of succinate dehydrogenase in *Arabidopsis thaliana*. Plant Mol Biol *46*, 241-250.

Foyer, C.H., and Noctor, G. (2011). Ascorbate and glutathione: the heart of the redox hub. Plant Physiol *155*, 2-18.

Griesbeck, C., Schutz, M., Schodl, T., Bathe, S., Nausch, L., Mederer, N., Vielreicher, M., and Hauska, G. (2002). Mechanism of sulfide-quinone reductase investigated using site-directed mutagenesis and sulfur analysis. Biochemistry *41*, 11552-11565.

Griffith, O.W., and Meister, A. (1979). Potent and Specific-Inhibition of Glutathione Synthesis by Buthionine Sulfoximine (S-Normal-Butyl Homocysteine Sulfoximine). J Biol Chem *254*, 7558-7560.

Gruenewald, S., Wahl, B., Bittner, F., Hungeling, H., Kanzow, S., Kotthaus, J., Schwering, U., Mendel, R.R., and Clement, B. (2008). The fourth molybdenum containing enzyme mARC: cloning and involvement in the activation of N-hydroxylated prodrugs. J Med Chem *51*, 8173-8177.

Guerrero, M.G., Vega, J.M., and Losada, M. (1981). The Assimilatory Nitrate-Reducing System and Its Regulation. Annu Rev Plant Phys *32*, 169-204.

Haga, N., Fujita, N., and Tsuruo, T. (2003). Mitochondrial aggregation precedes cytochrome *c* release from mitochondria during apoptosis. Oncogene *22*, 5579-5585.

Hagerhall, C. (1997). Succinate: Quinone oxidoreductases - Variations on a conserved theme. BBA-Bioenergetics *1320*, 107-141.

Hanke, G., and Mulo, P. (2013). Plant type ferredoxins and ferredoxin-dependent metabolism. Plant Cell Environ *36*, 1071-1084.

Hanson, G.T., Aggeler, R., Oglesbee, D., Cannon, M., Capaldi, R.A., Tsien, R.Y., and Remington, S.J. (2004). Investigating mitochondrial reduction potential with redox-sensitive green fluorescent protein indicators. J Biol Chem *279*, 13044-13053.

Havemeyer, A., Bittner, F., Wollers, S., Mendel, R., Kunze, T., and Clement, B. (2006). Identification of the missing component in the mitochondrial benzamidoxime prodrug-converting system as a novel molybdenum enzyme. J Biol Chem *281*, 34796-34802.

He, Y., Chen, B., Pang, Q., Strul, J.M., and Chen, S. (2010). Functional specification of Arabidopsis isopropylmalate isomerases in glucosinolate and leucine biosynthesis. Plant Cell Physiol *51*, 1480-1487.

He, Y., Chen, L., Zhou, Y., Mawhinney, T.P., Chen, B., Kang, B.H., Hauser, B.A., and Chen, S. (2011). Functional characterization of *Arabidopsis thaliana* isopropylmalate dehydrogenases reveals their important roles in gametophyte development. New Phytol *189*, 160-175.

Heeg, C., Kruse, C., Jost, R., Gutensohn, M., Ruppert, T., Wirtz, M., and Hell, R. (2008). Analysis of the Arabidopsis O-acetylserine(thiol)lyase gene family demonstrates compartment-specific differences in the regulation of cysteine synthesis. Plant Cell *20*, 168-185.

Heidenreich, T., Wollers, S., Mendel, R.R., and Bittner, F. (2005). Characterization of the NifS-like domain of ABA3 from *Arabidopsis thaliana* provides insight into the mechanism of molybdenum cofactor sulfuration. J Biol Chem *280*, 4213-4218.

Hesberg, C., Hansch, R., Mendel, R.R., and Bittner, F. (2004). Tandem orientation of duplicated xanthine dehydrogenase genes from *Arabidopsis thaliana*: differential gene expression and enzyme activities. J Biol Chem *279*, 13547-13554.

Hochholdinger, F., and Hoecker, N. (2007). Towards the molecular basis of heterosis. Trends Plant Sci *12*, 427-432.

Hoekema, A., Hirsch, P.R., Hooykaas, P.J.J., and Schilperoort, R.A. (1983). A Binary Plant Vector Strategy Based on Separation of Vir-Region and T-Region of the Agrobacterium-Tumefaciens Ti-Plasmid. Nature *303*, 179-180.

Hoff, T., Frandsen, G.I., Rocher, A., and Mundy, J. (1998). Biochemical and genetic characterization of three molybdenum cofactor hydroxylases in *Arabidopsis thaliana*. Biochim Biophys Acta *1398*, 397-402.

Hofler, S., Lorenz, C., Busch, T., Brinkkotter, M., Tohge, T., Fernie, A.R., Braun, H.P., and Hildebrandt, T.M. (2016). Dealing with the sulfur part of cysteine: four enzymatic steps degrade l-cysteine to pyruvate and thiosulfate in Arabidopsis mitochondria. Physiol Plantarum *157*, 352-366.

Holdorf, M.M., Owen, H.A., Lieber, S.R., Yuan, L., Adams, N., Dabney-Smith, C., and Makaroff, C.A. (2012). Arabidopsis ETHE1 encodes a sulfur dioxygenase that is essential for embryo and endosperm development. Plant Physiol *160*, 226-236.

Hover, B.M., Loksztejn, A., Ribeiro, A.A., and Yokoyama, K. (2013). Identification of a cyclic nucleotide as a cryptic intermediate in molybdenum cofactor biosynthesis. J Am Chem Soc *135*, 7019-7032.

Hover, B.M., Tonthat, N.K., Schumacher, M.A., and Yokoyama, K. (2015). Mechanism of pyranopterin ring formation in molybdenum cofactor biosynthesis. Proc Natl Acad Sci U S A *112*, 6347-6352.

Hung, W.F., Chen, L.J., Boldt, R., Sun, C.W., and Li, H.M. (2004). Characterization of Arabidopsis glutamine phosphoribosyl pyrophosphate amidotransferase-deficient mutants. Plant Physiol *135*, 1314-1323.

Hunte, C., Zickermann, V., and Brandt, U. (2010). Functional Modules and Structural Basis of Conformational Coupling in Mitochondrial Complex I. Science *329*, 448-451.

Imsande, J. (1999). Iron-sulfur clusters: Formation, perturbation, and physiological functions. Plant Physiol Bioch *37*, 87-97.

Inigo, S., Nagels Durand, A., Ritter, A., Le Gall, S., Termathe, M., Klassen, R., Tohge, T., De Coninck, B., Van Leene, J., De Clercq, R., *et al.* (2016). Glutaredoxin GRXS17 Associates with the Cytosolic Iron-Sulfur Cluster Assembly Pathway. Plant Physiol.

Iqbal, Z., Caccamo, M., Turner, I., Flicek, P., and McVean, G. (2012). De novo assembly and genotyping of variants using colored de Bruijn graphs. Nature Genet *44*, 226-232.

Jacques, A.G. (1936). The Kinetics of Penetration : Xii. Hydrogen Sulfide. J Gen Physiol *19*, 397-418.

Kahlfeldt, N. (2006). Diploma Thesis.

Kang, J., Park, J., Choi, H., Burla, B., Kretzschmar, T., Lee, Y., and Martinoia, E. (2011). Plant ABC Transporters. The Arabidopsis book / ASPB *9*, e0153.

Kaufholdt, D., Baillie, C.K., Bikker, R., Burkart, V., Dudek, C.A., von Pein, L., Rothkegel, M., Mendel, R.R., and Hansch, R. (2016). The molybdenum cofactor biosynthesis complex interacts with actin filaments via molybdenum insertase Cnxl as anchor protein in *Arabidopsis thaliana*. Plant Sci *244*, 8-18.

Kim, D.Y., Bovet, L., Kushnir, S., Noh, E.W., Martinoia, E., and Lee, Y. (2006). AtATM3 is involved in heavy metal resistance in Arabidopsis. Plant Physiol *140*, 922-932.

Kim, K.D., Chung, W.H., Kim, H.J., Lee, K.C., and Roe, J.H. (2010). Monothiol glutaredoxin Grx5 interacts with Fe-S scaffold proteins Isa1 and Isa2 and supports Fe-S assembly and DNA integrity in mitochondria of fission yeast. Biochem Bioph Res Co *392*, 467-472.

Kispal, G., Csere, P., Guiard, B., and Lill, R. (1997). The ABC transporter Atm1p is required for mitochondrial iron homeostasis. Febs Lett *418*, 346-350.

Kispal, G., Csere, P., Prohl, C., and Lill, R. (1999). The mitochondrial proteins Atm1p and Nfs1p are essential for biogenesis of cytosolic Fe/S proteins. EMBO J *18*, 3981-3989.

Klein, J.M., Busch, J.D., Potting, C., Baker, M.J., Langer, T., and Schwarz, G. (2012). The mitochondrial amidoxime-reducing component (mARC1) is a novel signal-anchored protein of the outer mitochondrial membrane. J Biol Chem *287*, 42795-42803.

Knill, T., Reichelt, M., Paetz, C., Gershenzon, J., and Binder, S. (2009). *Arabidopsis thaliana* encodes a bacterial-type heterodimeric isopropylmalate isomerase involved in both Leu biosynthesis and the Met chain elongation pathway of glucosinolate formation. Plant Mol Biol *71*, 227-239.

Knuesting, J., Riondet, C., Maria, C., Kruse, I., Becuwe, N., Konig, N., Berndt, C., Tourrette, S., Guilleminot-Montoya, J., Herrero, E., *et al.* (2015). Arabidopsis glutaredoxin S17 and its partner, the nuclear factor Y subunit C11/negative cofactor 2alpha, contribute to maintenance of the shoot apical meristem under long-day photoperiod. Plant Physiol *167*, 1643-1658.

Koornneef, M., Alonso-Blanco, C., Peeters, A.J.M., and Soppe, W. (1998). Genetic control of flowering time in arabidopsis. Annu Rev Plant Phys *49*, 345-370.

Koshiba, T., Saito, E., Ono, N., Yamamoto, N., and Sato, M. (1996). Purification and Properties of Flavin- and Molybdenum-Containing Aldehyde Oxidase from Coleoptiles of Maize. Plant Physiol *110*, 781-789.

Krepinsky, K., and Leimkuhler, S. (2007). Site-directed mutagenesis of the active site loop of the rhodanese-like domain of the human molybdopterin synthase sulfurase MOCS3. Major differences in substrate specificity between eukaryotic and bacterial homologs. Febs J *274*, 2778-2787.

Krussel, L., Junemann, J., Wirtz, M., Birke, H., Thornton, J.D., Browning, L.W., Poschet, G., Hell, R., Balk, J., Braun, H.P., *et al.* (2014). The mitochondrial sulfur dioxygenase ETHYLMALONIC ENCEPHALOPATHY PROTEIN1 is required for amino acid catabolism during carbohydrate starvation and embryo development in Arabidopsis. Plant Physiol *165*, 92-104.

Kushnir, S., Babiychuk, E., Storozhenko, S., Davey, M.W., Papenbrock, J., De Rycke, R., Engler, G., Stephan, U.W., Lange, H., Kispal, G., *et al.* (2001). A mutation of the mitochondrial ABC transporter Sta1 leads to dwarfism and chlorosis in the Arabidopsis mutant starik. Plant Cell *13*, 89-100.

Laemmli, U.K. (1970). Cleavage of structural proteins during the assembly of the head of bacteriophage T4. Nature *227*, 680-685.

Langmead, B., Trapnell, C., Pop, M., and Salzberg, S.L. (2009). Ultrafast and memory-efficient alignment of short DNA sequences to the human genome. Genome Biol *10*.

Lee, C.P., Wirtz, M., and Hell, R. (2014a). Evidence for Several Cysteine Transport Mechanisms in the Mitochondrial Membranes of *Arabidopsis thaliana*. Plant Cell Physiol *55*, 64-73.

Lee, J.Y., Yang, J.G., Zhitnitsky, D., Lewinson, O., and Rees, D.C. (2014b). Structural basis for heavy metal detoxification by an Atm1-type ABC exporter. Science *343*, 1133-1136.

Lehmann, M., Schwarzlander, M., Obata, T., Sirikantaramas, S., Burow, M., Olsen, C.E., Tohge, T., Fricker, M.D., Moller, B.L., Fernie, A.R., *et al.* (2009). The metabolic response of Arabidopsis roots to oxidative stress is distinct from that of heterotrophic cells in culture and highlights a complex relationship between the levels of transcripts, metabolites, and flux. Mol Plant *2*, 390-406.

Lehrke, M., Rump, S., Heidenreich, T., Wissing, J., Mendel, R.R., and Bittner, F. (2012). Identification of persulfide-binding and disulfide-forming cysteine residues in the NifS-like domain of the molybdenum cofactor sulfurase ABA3 by cysteine-scanning mutagenesis. Biochem J *441*, 823-832.

Leon-Kloosterziel, K.M., Gil, M.A., Ruijs, G.J., Jacobsen, S.E., Olszewski, N.E., Schwartz, S.H., Zeevaart, J.A., and Koornneef, M. (1996). Isolation and characterization of abscisic acid-deficient Arabidopsis mutants at two new loci. Plant J *10*, 655-661.

Leon, G., Holuigue, L., and Jordana, X. (2007). Mitochondrial complex II is essential for gametophyte development in Arabidopsis. Plant Physiol *143*, 1534-1546.

Leschelle, X., Goubern, M., Andriamihaja, M., Blottiere, H.M., Couplan, E., Gonzalez-Barroso, M.D., Petit, C., Pagniez, A., Chaumontet, C., Mignotte, B., *et al.* (2005). Adaptative metabolic response of human colonic epithelial cells to the adverse effects of the luminal compound sulfide. Biochim Biophys Acta *1725*, 201-212.

Li, L., Rose, P., and Moore, P.K. (2011). Hydrogen sulfide and cell signaling. Annu Rev Pharmacol Toxicol *51*, 169-187.

Lill, R. (2009). Function and biogenesis of iron-sulphur proteins. Nature *460*, 831-838.

Lill, R., Dutkiewicz, R., Freibert, S.A., Heidenreich, T., Mascarenhas, J., Netz, T.J., Paul, V.D., Pierik, A.J., Richter, N., Stümpfig, M., Stehling, O. and Mühlenhoff, U. (2015). The role of mitochondria and the CIA machinery in the maturation of cytosolic and nuclear iron-sulfur proteins. Eur J Cell Biol *94*, 280-291.

Lill, R., Hoffmann, B., Molik, S., Pierik, A.J., Rietzschel, N., Stehling, O., Uzarska, M.A., Webert, H., Wilbrecht, C., and Muhlenhoff, U. (2012). The role of mitochondria in cellular iron-sulfur protein biogenesis and iron metabolism. BBA-Mol Cell Res *1823*, 1491-1508.

Lippman, Z.B., and Zamir, D. (2007). Heterosis: revisiting the magic. Trends Genet *23*, 60-66.

Luo, D., Bernard, D.G., Balk, J., Hai, H., and Cui, X. (2012). The DUF59 family gene AE7 acts in the cytosolic iron-sulfur cluster assembly pathway to maintain nuclear genome integrity in Arabidopsis. Plant Cell *24*, 4135-4148.

Marcia, M., Ermler, U., Peng, G., and Michel, H. (2010). A new structure-based classification of sulfide:quinone oxidoreductases. Proteins *78*, 1073-1083.

Marelja, Z., Stocklein, W., Nimtz, M., and Leimkuhler, S. (2008). A novel role for human Nfs1 in the cytoplasm: Nfs1 acts as a sulfur donor for MOCS3, a protein involved in molybdenum cofactor biosynthesis. J Biol Chem *283*, 25178-25185.

Marquet, A., Bui, B.T.S., and Florentin, D. (2001). Biosynthesis of biotin and lipoic acid. Vitam Horm *61*, 51-101.

Martin, M., Colman, M.J.R., Gomez-Casati, D.F., Lamattina, L., and Zabaleta, E.J. (2009). Nitric oxide accumulation is required to protect against iron-mediated oxidative stress in frataxin-deficient Arabidopsis plants. Febs Lett *583*, 542-548.

Marty, L., Siala, W., Schwarzlander, M., Fricker, M.D., Wirtz, M., Sweetlove, L.J., Meyer, Y., Meyer, A.J., Reichheld, J.P., and Hell, R. (2009). The NADPH-dependent thioredoxin system constitutes a functional backup for cytosolic glutathione reductase in Arabidopsis. Proc Natl Acad Sci U S A *106*, 9109-9114.

Mathai, J.C., Missner, A., Kugler, P., Saparov, S.M., Zeidel, M.L., Lee, J.K., and Pohl, P. (2009). No facilitator required for membrane transport of hydrogen sulfide. Proc Natl Acad Sci U S A *106*, 16633-16638.

Mendel, R.R. (2011). Cell biology of molybdenum in plants. Plant Cell Rep *30*, 1787-1797.

Mendel, R.R., and Kruse, T. (2012). Cell biology of molybdenum in plants and humans. Biochim Biophys Acta *1823*, 1568-1579.

Mendel, R.R., and Leimkuhler, S. (2015). The biosynthesis of the molybdenum cofactors. J Biol Inor Chem *20*, 337-347.

Meyer, A.J., Brach, T., Marty, L., Kreye, S., Rouhier, N., Jacquot, J.P., and Hell, R. (2007). Redox-sensitive GFP in *Arabidopsis thaliana* is a quantitative biosensor for the reduction potential of the cellular glutathione redox buffer. Plant J *52*, 973-986.

Meyer, R.C., Torjek, O., Becher, M., and Altmann, T. (2004). Heterosis of biomass production in Arabidopsis. Establishment during early development. Plant Physiol *134*, 1813-1823.

Millar, A.H., Eubel, H., Jansch, L., Kruft, V., Heazlewood, J.L., and Braun, H.P. (2004). Mitochondrial cytochrome *c* oxidase and succinate dehydrogenase complexes contain plant specific subunits. Plant Mol Biol *56*, 77-90.

Miller, J.M., and Conn, E.E. (1980). Metabolism of hydrogen cyanide by higher plants. Plant Physiol *65*, 1199-1202.

Moeder, W., Del Pozo, O., Navarre, D.A., Martin, G.B., and Klessig, D.F. (2007). Aconitase plays a role in regulating resistance to oxidative stress and cell death in Arabidopsis and *Nicotiana benthamiana*. Plant Mol Biol *63*, 273-287.

Moseler, A., Aller, I., Wagner, S., Nietzel, T., Przybyla-Toscano, J., Muhlenhoff, U., Lill, R., Berndt, C., Rouhier, N., Schwarzlander, M., *et al.* (2015). The mitochondrial monothiol glutaredoxin S15 is essential for iron-sulfur protein maturation in *Arabidopsis thaliana*. Proc Natl Acad Sci U S A *112*, 13735-13740.

Muhlenhoff, U., Gerber, J., Richhardt, N., and Lill, R. (2003). Components involved in assembly and dislocation of iron-sulfur clusters on the scaffold protein Isu1p. EMBO J *22*, 4815-4825.

Nakai, Y., Harada, A., Hashiguchi, Y., Nakai, M., and Hayashi, H. (2012). Arabidopsis molybdopterin biosynthesis protein Cnx5 collaborates with the ubiquitin-like protein Urm11 in the thio-modification of tRNA. J Biol Chem *287*, 30874-30884.

Nobel, P.S. (1991) Physicochemical & Environmental Plant Physiology. Academic press, San Diego

Noctor, G., Arisi, A.C.M., Jouanin, L., Kunert, K.J., Rennenberg, H., and Foyer, C.H. (1998). Glutathione: biosynthesis, metabolism and relationship to stress tolerance explored in transformed plants. J Exp Bot *49*, 623-647.

Noctor, G., Mhamdi, A., Chaouch, S., Han, Y., Neukermans, J., Marquez-Garcia, B., Queval, G., and Foyer, C.H. (2012). Glutathione in plants: an integrated overview. Plant Cell Environ *35*, 454-484.

Ogawa, K., Tasaka, Y., Mino, M., Tanaka, Y., and Iwabuchi, M. (2001). Association of glutathione with flowering in *Arabidopsis thaliana*. Plant Cell Physiol *42*, 524-530.

Pandey, A., Gordon, D.M., Pain, J., Stemmler, T.M., Dancis, A. and Pain, D. (2013). Frataxin directly stimulates mitochondrial cysteine desulfurase by exposing substrate-binding sites, and a mutant Fe-S cluster scaffold protein with frataxin-bypassing ability acts similarly. J Biol Chem *288*, 36773-36786.

Parent, A., Elduque, X., Cornu, D., Belot, L., Le Caer, J.P., Grandas, A., Toledano, M.B. and D'Autreaux, B. (2015). Nat Commun *6*, 5686

Pastore, A., and Puccio, H. (2013). Frataxin: a protein in search for a function. J Neurochem *126 Suppl 1*, 43-52.

Paul, V.D., and Lill, R. (2014). SnapShot: eukaryotic Fe-S protein biogenesis. Cell Metab *20*, 384-384 e381.

Picciocchi, A., Douce, R., and Alban, C. (2003). The plant biotin synthase reaction. Identification and characterization of essential mitochondrial accessory protein components. J Biol Chem *278*, 24966-24975.

Plitzko, B., Ott, G., Reichmann, D., Henderson, C.J., Wolf, C.R., Mendel, R., Bittner, F., Clement, B., and Havemeyer, A. (2013). The involvement of mitochondrial amidoxime reducing components 1 and 2 and mitochondrial cytochrome b5 in N-reductive metabolism in human cells. J Biol Chem *288*, 20228-20237.

Poor, C.B., Wegner, S.V., Li, H., Dlouhy, A.C., Schuermann, J.P., Sanishvili, R., Hinshaw, J.R., Riggs-Gelasco, P.J., Outten, C.E., and He, C. (2014). Molecular mechanism and structure of the *Saccharomyces cerevisiae* iron regulator Aft2. Proc Natl Acad Sci U S A *111*, 4043-4048.

Raichaudhuri, A. (2016). *Arabidopsis thaliana* MRP1 (AtABCC1) nucleotide binding domain contributes to arsenic stress tolerance with serine triad phosphorylation. Plant Physiol Biochem *108*, 109-120.

Raux-Deery, E., Leech, H.K., Nakrieko, K.A., McLean, K.J., Munro, A.W., Heathcote, P., Rigby, S.E.J., Smith, A.G., and Warren, M.J. (2005). Identification and characterization of the terminal enzyme of siroheme biosynthesis from *Arabidopsis thaliana* - A plastid-located sirohydrochlorin ferrochelatase containing a 2Fe-2S center. J Biol Chem *280*, 4713-4721.

Redinbaugh, M.G., and Campbell, W.H. (1983). Purification of Squash NADH:Nitrate Reductase by Zinc Chelate Affinity Chromatography. Plant Physiol *71*, 205-207.

Rees, D.C. (2002). Great metalloclusters in enzymology. Annu Rev Biochem *71*, 221-246.

Rieske, J.S. (1976). Composition, structure, and function of complex III of the respiratory chain. Biochim Biophys Acta *456*, 195-247.

Robertson, E.J., Rutherford, S.M., and Leech, R.M. (1996). Characterization of chloroplast division using the Arabidopsis mutant arc5. Plant Physiol *112*, 149-159.

Robinson, J.T., Thorvaldsdottir, H., Winckler, W., Guttman, M., Lander, E.S., Getz, G., and Mesirov, J.P. (2011). Integrative genomics viewer. Nat Biotechnol *29*, 24-26.

Rodriguez-Manzaneque, M.T., Tamarit, J., Belli, G., Ros, J., and Herrero, E. (2002). Grx5 is a mitochondrial glutaredoxin required for the activity of iron/sulfur enzymes. Mol Biol Cell *13*, 1109-1121.

Rouhier, N., Lemaire, S.D., and Jacquot, J.P. (2008). The role of glutathione in photosynthetic organisms: Emerging functions for glutaredoxins and glutathionylation. Annu Rev Plant Biol *59*, 143-166.

Saha, K., Webb, M.E., Rigby, S.E.J., Leech, H.K., Warren, M.J., and Smith, A.G. (2012). Characterization of the evolutionarily conserved iron-sulfur cluster of sirohydrochlorin ferrochelatase from *Arabidopsis thaliana*. Biochem J *444*, 227-237.

Saito, K. (2004). Sulfur assimilatory metabolism. The long and smelling road. Plant Physiol *136*, 2443-2450.

Sambrook, J., Fritsch, E.F., and Maniatis, T. (1989). Molecular cloning, Vol 2 (Cold spring harbor laboratory press New York).

Sanger, F., Nicklen, S., and Coulson, A.R. (1977). DNA Sequencing with Chain-Terminating Inhibitors. P Natl Acad Sci USA *74*, 5463-5467.

Schaedler, T.A., Faust, B., Shintre, C.A., Carpenter, E.P., Srinivasan, V., van Veen, H.W., and Balk, J. (2015). Structures and functions of mitochondrial ABC transporters. Biochem Soc T *43*, 943-951.

Schaedler, T.A., Thornton, J.D., Kruse, I., Schwarzlander, M., Meyer, A.J., van Veen, H.W., and Balk, J. (2014). A conserved mitochondrial ATP-binding cassette transporter exports glutathione polysulfide for cytosolic metal cofactor assembly. J Biol Chem *289*, 23264-23274.

Schafer, F.Q. and Buettner, G., R. (2001) Redox environment of the cell as viewed through the redox state of the glutathione disulfide/glutathione couple. Free Radic Biol Med *11*, 1191-1212

Schrader, N., Fischer, K., Theis, K., Mendel, R.R., Schwarz, G., and Kisker, C. (2003). The crystal structure of plant sulfite oxidase provides insights into sulfite oxidation in plants and animals. Structure *11*, 1251-1263.

Schwartz, S.H., Leon-Kloosterziel, K.M., Koornneef, M., and Zeevaart, J.A. (1997). Biochemical characterization of the aba2 and aba3 mutants in *Arabidopsis thaliana*. Plant Physiol *114*, 161-166.

Schwarz, G., Santamaria-Araujo, J.A., Wolf, S., Lee, H.J., Adham, I.M., Grone, H.J., Schwegler, H., Sass, J.O., Otte, T., Hanzelmann, P., *et al.* (2004). Rescue of lethal molybdenum cofactor deficiency by a biosynthetic precursor from *Escherichia coli*. Hum Mol Gen *13*, 1249-1255.

Schwarzlander, M., Fricker, M.D., Muller, C., Marty, L., Brach, T., Novak, J., Sweetlove, L.J., Hell, R., and Meyer, A.J. (2008). Confocal imaging of glutathione reduction potential in living plant cells. J Microsc *231*, 299-316.

Sekimoto, H., Seo, M., Kawakami, N., Komano, T., Desloire, S., Liotenberg, S., Marion-Poll, A., Caboche, M., Kamiya, Y., and Koshiba, T. (1998). Molecular cloning and characterization of aldehyde oxidases in *Arabidopsis thaliana*. Plant Cell Physiol *39*, 433-442.

Seo, M., Akaba, S., Oritani, T., Delarue, M., Bellini, C., Caboche, M., and Koshiba, T. (1998). Higher activity of an aldehyde oxidase in the auxin-overproducing superroot1 mutant of *Arabidopsis thaliana*. Plant Physiol *116*, 687-693.

Seo, M., Peeters, A.J., Koiwai, H., Oritani, T., Marion-Poll, A., Zeevaart, J.A., Koornneef, M., Kamiya, Y., and Koshiba, T. (2000). The Arabidopsis aldehyde oxidase 3 (AAO3) gene product catalyzes the final step in abscisic acid biosynthesis in leaves. Proc Natl Acad Sci U S A *97*, 12908-12913.Shila, S., Kokilavani, V., Subathra, A., and Panneerselvam, C. (2005). Brain regional responses in antioxidant system to alpha-lipoic acid in arsenic intoxicated rat. Toxicology *210*, 25-36.

Simon, S., and Petrasek, J. (2011). Why plants need more than one type of auxin. Plant Sci *180*, 454-460.

Sipos, K., Lange, H., Fekete, Z., Ullmann, P., Lill, R., and Kispal, G. (2002). Maturation of cytosolic iron-sulfur proteins requires glutathione. J Biol Chem *277*, 26944-26949.

Spuches, A.M., Kruszyna, H.G., Rich, A.M., and Wilcox, D.E. (2005). Thermodynamics of the As(III)-thiol interaction: Arsenite and monomethylarsenite complexes with glutathione, dihydrolipoic acid, and other thiol ligands. Inorg Chem *44*, 2964-2972.

Srinivasan, V., Pierik, A.J., and Lill, R. (2014). Crystal structures of nucleotide-free and glutathione-bound mitochondrial ABC transporter Atm1. Science *343*, 1137-1140.

Stehling, O., Smith, P.M., Biederbick, A., Balk, J., Lill, R., and Muhlenhoff, U. (2007). Investigation of iron-sulfur protein maturation in eukaryotes. Methods Mol Biol *372*, 325-342.

Stroher, E., Grassl, J., Carrie, C., Fenske, R., Whelan, J., and Millar, A.H. (2016). Glutaredoxin S15 Is Involved in Fe-S Cluster Transfer in Mitochondria Influencing

Lipoic Acid-Dependent Enzymes, Plant Growth, and Arsenic Tolerance in Arabidopsis. Plant Physiol *170*, 1284-1299.

Studier, F. W., and Moffatt, B. A. (1986). Use of bacteriophage T7 RNA polymerase to direct selective high-level expression of cloned genes. J Mol Biol *189, 113-130*

Sundaram, S., Rathinasabapathi, B., Ma, L.Q., and Rosen, B.P. (2008). An arsenate-activated glutaredoxin from the arsenic hyperaccumulator fern *Pteris vittata L.* regulates intracellular arsenite. J Biol Chem *283*, 6095-6101.

Sureshkumar, S., Todesco, M., Schneeberger, K., Harilal, R., Balasubramanian, S., and Weigel, D. (2009). A Genetic Defect Caused by a Triplet Repeat Expansion in *Arabidopsis thaliana*. Science *323*, 1060-1063.

Sweetlove, L.J., Beard, K.F., Nunes-Nesi, A., Fernie, A.R., and Ratcliffe, R.G. (2010). Not just a circle: flux modes in the plant TCA cycle. Trends Plant Sci *15*, 462-470.

Sweetlove, L.J., Taylor, N.L., and Leaver, C.J. (2007). Isolation of intact, functional mitochondria from the model plant *Arabidopsis thaliana*. Methods Mol Biol *372*, 125-136.

Szabo, C. (2007). Hydrogen sulphide and its therapeutic potential. Nat Rev Drug Discov *6*, 917-935.

Takubo, K., Morikawa, T., Nonaka, Y., Mizutani, M., Takenaka, S., Takabe, K., Takahashi, M.A., and Ohta, D. (2003). Identification and molecular characterization of mitochondrial ferredoxins and ferredoxin reductase from Arabidopsis. Plant Mol Biol *52*, 817-830.

Teschner, J., Lachmann, N., Schulze, J., Geisler, M., Selbach, K., Santamaria-Araujo, J., Balk, J., Mendel, R.R., and Bittner, F. (2010). A Novel Role for Arabidopsis Mitochondrial ABC Transporter ATM3 in Molybdenum Cofactor Biosynthesis. Plant Cell *22*, 468-480.

Thorvaldsdottir, H., Robinson, J.T., and Mesirov, J.P. (2013). Integrative Genomics Viewer (IGV): high-performance genomics data visualization and exploration. Brief Bioinform *14*, 178-192.

Tiranti, V., Viscomi, C., Hildebrandt, T., Di Meo, I., Mineri, R., Tiveron, C., Levitt, M.D., Prelle, A., Fagiolari, G., Rimoldi, M., *et al.* (2009). Loss of ETHE1, a mitochondrial dioxygenase, causes fatal sulfide toxicity in ethylmalonic encephalopathy. Nat Med *15*, 200-205.

Towbin, H., Staehelin, T., and Gordon, J. (1979). Electrophoretic Transfer of Proteins from Polyacrylamide Gels to Nitrocellulose Sheets - Procedure and Some Applications. P Natl Acad Sci USA *76*, 4350-4354.

Ueta, R., Fujiwara, N., Iwai, K., and Yamaguchi-Iwai, Y. (2012). Iron-Induced Dissociation of the Aft1p Transcriptional Regulator from Target Gene Promoters Is an Initial Event in Iron-Dependent Gene Suppression. Mol Cell Biol *32*, 4998-5008.

Vanoni, M.A., and Curti, B. (2008). Structure-function studies of glutamate synthases: A class of self-regulated iron-sulfur flavoenzymes essential for nitrogen assimilation. IUBMB Life *60*, 287-300.

Veldman, A., Santamaria-Araujo, J.A., Sollazzo, S., Pitt, J., Gianello, R., Yaplito-Lee, J., Wong, F., Ramsden, C.A., Reiss, J., Cook, I., *et al.* (2010). Successful treatment of molybdenum cofactor deficiency type A with cPMP. Pediatrics *125*, e1249-1254.

Wang, L., Ouyang, B.J., Li, Y.F., Feng, Y.G., Jacquot, J.P., Rouhier, N., and Xia, B. (2012). Glutathione regulates the transfer of iron-sulfur cluster from monothiol and dithiol glutaredoxins to apo ferredoxin. Protein Cell *3*, 714-721.

Wirtz, M., and Hell, R. (2006). Functional analysis of the cysteine synthase protein complex from plants: structural, biochemical and regulatory properties. J Plant Physiol *163*, 273-286.

Wollers, S., Heidenreich, T., Zarepour, M., Zachmann, D., Kraft, C., Zhao, Y., Mendel, R.R., and Bittner, F. (2008). Binding of sulfurated molybdenum cofactor to the C-terminal domain of ABA3 from *Arabidopsis thaliana* provides insight into the mechanism of molybdenum cofactor sulfuration. J Biol Chem *283*, 9642-9650.

Xia, H.Y., Li, B.H., Zhang, Z., Wang, Q., Qiao, T., and Li, K.Y. (2015). Human glutaredoxin 3 can bind and effectively transfer [4Fe-4S] cluster to apo-iron regulatory protein 1. Biochem Bioph Res Co *465*, 620-624.

Xiong, L.M., Ishitani, M., Lee, H., and Zhu, J.K. (2001). The Arabidopsis LOS5/ABA3 locus encodes a molybdenum cofactor sulfurase and modulates cold stress- and osmotic stress-responsive gene expression. Plant Cell *13*, 2063-2083.

Yanagida, M., Mino, M., Iwabuchi, M., and Ogawa, K. (2004). Reduced glutathione is a novel regulator of vernalization-induced bolting in the rosette plant *Eustoma grandiflorum*. Plant Cell Physiol *45*, 129-137.

Yeung, N., Gold, B., Liu, N.L., Prathapam, R., Sterling, H.J., Willams, E.R., and Butland, G. (2011). The *E. coli* Monothiol Glutaredoxin GrxD Forms Homodimeric and Heterodimeric FeS Cluster Containing Complexes. Biochemistry *50*, 8957-8969.

Zhang, B., Bandyopadhyay, S., Shakamuri, P., Naik, S.G., Huynh, B.H., Couturier, J., Rouhier, N., and Johnson, M.K. (2013). Monothiol Glutaredoxins Can Bind Linear [Fe3S4](+) and [Fe4S4](2+) Clusters in Addition to [Fe2S2](2+) Clusters: Spectroscopic Characterization and Functional Implications. J Am Chem Soc *135*, 15153-15164.

Zhao, Y., Dai, X., Blackwell, H.E., Schreiber, S.L., and Chory, J. (2003). SIR1, an upstream component in auxin signaling identified by chemical genetics. Science *301*, 1107-1110.

Appendix - Papers

Schaedler, T.A., Thornton, J.D., **Kruse, I**., Schwarzlander, M., Meyer, A.J., van Veen, H.W., and Balk, J. (2014). A conserved mitochondrial ATP-binding cassette transporter exports glutathione polysulfide for cytosolic metal cofactor assembly. J Biol Chem *289*, 23264-23274.

Knuesting, J., Riondet, C., Maria, C., **Kruse, I**., Becuwe, N., Konig, N., Berndt, C., Tourrette, S., Guilleminot-Montoya, J., Herrero, E., Gaymard, F., Balk, J., Belli, G., Scheibe, R., Reichheld, J. P., Rouhier, N. and Rey, P. (2015). Arabidopsis glutaredoxin S17 and its partner, the nuclear factor Y subunit C11/negative cofactor 2alpha, contribute to maintenance of the shoot apical meristem under long-day photoperiod. Plant Physiol *167*, 1643-1658.

THE JOURNAL OF BIOLOGICAL CHEMISTRY VOL. 289, NO. 34, pp. 23264–23274, August 22, 2014

A Conserved Mitochondrial ATP-binding Cassette Transporter Exports Glutathione Polysulfide for Cytosolic Metal Cofactor Assembly*[S]◆

Received for publication, February 4, 2014, and in revised form, July 4, 2014 Published, JBC Papers in Press, July 8, 2014, DOI 10.1074/jbc.M114.553438

Theresia A. Schaedler[‡§], Jeremy D. Thornton[‡1], Inga Kruse[‡¶2], Markus Schwarzländer[‖3], Andreas J. Meyer[‖4], Hendrik W. van Veen[5], and Janneke Balk[‡¶6]**

*From the [‡]John Innes Centre, Norwich Research Park, Norwich NR4 7UH, United Kingdom, the [§]Department of Plant Sciences, University of Cambridge, Cambridge CB2 3EA, United Kingdom, the [‖]Institute of Crop Science and Resource Conservation, University of Bonn, 53113 Bonn, Germany, the **Department of Pharmacology, University of Cambridge, Cambridge CB2 1PD, United Kingdom, and the [¶]School of Biological Sciences, University of East Anglia, Norwich NR4 7TJ, United Kingdom*

Background: ABC transporters of mitochondria (ATM) are required for formation of cytosolic iron-sulfur clusters and molybdenum cofactor.
Results: *Arabidopsis* ATM3 and yeast Atm1 transport radiolabeled glutathione disulfide (GSSG). Transport of glutathione trisulfide (GS-S-SG) was demonstrated by mass spectrometry.
Conclusion: A mitochondrial transporter exports glutathione polysulfide.
Significance: Identification of substrate(s) of ATMs defines their role in metal cofactor assembly and iron homeostasis.

An ATP-binding cassette transporter located in the inner mitochondrial membrane is involved in iron-sulfur cluster and molybdenum cofactor assembly in the cytosol, but the transported substrate is unknown. ATM3 (ABCB25) from *Arabidopsis thaliana* and its functional orthologue Atm1 from *Saccharomyces cerevisiae* were expressed in *Lactococcus lactis* and studied in inside-out membrane vesicles and in purified form. Both proteins selectively transported glutathione disulfide (GSSG) but not reduced glutathione in agreement with a 3-fold stimulation of ATPase activity by GSSG. By contrast, Fe^{2+} alone or in combination with glutathione did not stimulate ATPase activity. *Arabidopsis atm3* mutants were hypersensitive to an inhibitor of glutathione biosynthesis and accumulated GSSG in the mitochondria. The growth phenotype of *atm3-1* was strongly enhanced by depletion of the mitochondrion-localized, GSH-dependent persulfide oxygenase ETHE1, suggesting that the physiological substrate of ATM3 contains persulfide in addition to glutathione. Consistent with this idea, a transportomics approach using mass spectrometry showed that glutathione trisulfide (GS-S-SG) was transported by Atm1. We propose that mitochondria export glutathione polysulfide, containing glutathione and persulfide, for iron-sulfur cluster assembly in the cytosol.

Iron-sulfur (Fe-S)[7] proteins perform essential functions in respiration, photosynthesis, DNA metabolism, and many other processes in different compartments of the eukaryotic cell. Mitochondria and chloroplasts harbor autonomous pathways for the assembly of Fe-S clusters (1, 2). The biogenesis of Fe-S proteins in the cytosol and nucleus requires a separate set of five to six assembly proteins but also depends on mitochondria (3, 4). An ATP-binding cassette transporter of the mitochondria (ATM) has been identified in yeast, plants, and mammals, which is required for cytosolic and nuclear Fe-S cluster assembly (5–7). It is therefore likely that the mitochondria provide a compound that is exported by the ATM transporter, but this molecule has not been identified.

The assembly of Fe-S clusters starts with the extraction of sulfur from cysteine catalyzed by cysteine desulfurase. The sulfur is bound to the enzyme in the form of persulfide, also called sulfane sulfur, with an oxidation state of 0 ($RS\text{-}S^0H$). The enzyme-bound persulfide is then transferred to a scaffold protein where it is combined with iron (4). Mitochondrial localization of the cysteine desulfurase activity appears to be critical for Fe-S cluster assembly in the cytosol and nucleus in yeast and

* This work was supported in part by the Biotechnology and Biological Sciences Research Council Grant BB/H00288X/1.
◆ This article was selected as a Paper of the Week.
⌘ *Author's Choice*—Final version full access.
[S] This article contains supplemental Table S1.
[1] Supported by a Biotechnology and Biological Sciences Research Council Institute Strategic Programme grant (to the John Innes Centre).
[2] Supported by a Dean's studentship from the University of East Anglia.
[3] Supported by Deutsche Forschungsgemeinschaft through the Emmy Noether Programme Grant SCHW 1719/1-1.
[4] Supported by Deutsche Forschungsgemeinschaft Grants ME 1567/5-1 and Inst 217/651-1 FUGG.
[5] To whom correspondence may be addressed: Dept. of Pharmacology, University of Cambridge, Cambridge CB2 1PD, United Kingdom. Tel.: 44-1223-765295; Fax: 44-1223-334100; E-mail: hwv20@cam.ac.uk.
[6] Supported by a Royal Society University Research Fellowship and by a start-up grant from the University of East Anglia. To whom correspondence may be addressed: John Innes Centre, Norwich Research Park, Norwich NR4 7UH, United Kingdom. Tel.: 44-1603-450621; E-mail: janneke.balk@jic.ac.uk.

[7] The abbreviations used are: Fe-S, iron-sulfur; ABC, ATP-binding cassette; ATM, ABC transporter of the mitochondria; BSO, buthionine sulfoximine; DDM, β-D-dodecyl maltoside; GR, glutathione disulfide reductase; GRX1, glutaredoxin 1; GSH, glutathione; GSSG, glutathione disulfide; GS-S-SG, glutathione trisulfide; LMNPG, laurylmaltoside neopentylglycol; Moco, molybdenum cofactor; MTS, mitochondrial targeting sequence; NBD, nucleotide-binding domain; NTA, nitrilotriacetic acid; roGFP, redox-sensitive GFP, ANOVA, analysis of variance.

plants (3, 8), despite the occurrence of extramitochondrial cysteine desulfurases (9, 10).

The ATM proteins belong to the ABCB subfamily of ABC proteins and are half-transporters that dimerize for function. Recent crystal structures of yeast Atm1 (11) and a bacterial homologue (12) revealed their typical architecture, with two membrane domains that provide the pathway for substrate transport and two nucleotide-binding domains (NBDs) that couple the energy provided by ATP binding and hydrolysis to the translocation of substrates across the membrane. Atm1 in yeast is localized in the inner membrane of the mitochondria with the NBDs facing the matrix (13). The yeast, plant, and mammalian ATMs are functional orthologues, because *ATM3* (*ABCB25*) from the model plant *Arabidopsis* and *ABCB7* from human can complement the phenotypes of a yeast Δ*atm1* mutant (14–17).

It was initially suggested that ATMs transport an Fe-S cluster intermediate, because iron accumulates to high levels in mitochondria in yeast *atm1* mutants (18). However, recent studies have suggested that increased iron uptake is the result of disrupted iron homeostasis in the cell (19). Moreover, mitochondrial iron accumulation was not found in *Arabidopsis atm3* mutants (6) or in mouse hepatocytes depleted of ABCB7 (7). The plant *ATM3* gene has also been implicated in heavy metal resistance (20) and in molybdenum cofactor (Moco) biosynthesis (21). The assembly of Moco requires the precursor cyclic pyranopterin monophosphate synthesized in the mitochondria and two sulfur atoms of which the origin is uncertain. Therefore, ATM3 either exhibits a broad substrate specificity for different molecules or it transports a molecule shared by cytosolic Fe-S cluster assembly, Moco biosynthesis, and heavy metal detoxification.

The tripeptide glutathione has previously been implicated in the function of yeast Atm1 (22, 23). Moreover, reduced glutathione (GSH) was associated with yeast and bacterial Atm1 in the crystal structures (11, 12), whereas bacterial Atm1 also bound oxidized glutathione (glutathione disulfide, GSSG) (12). However, transport of glutathione or glutathione conjugates has not yet been shown for the mitochondrial ATM transporters.

Using our previously identified allelic series of *Arabidopsis atm3* mutants (6), we have investigated whether glutathione plays a role in the function of ATM3 in plants. In addition, various putative substrates were tested for their capacity to stimulate ATPase activity of purified *Arabidopsis* ATM3 and yeast Atm1. We found that both proteins can transport GSSG but not GSH. Further *in vitro* and genetic interaction studies provide evidence for transport of persulfide in the form of glutathione trisulfide (GS-S^0-SG) as a physiological substrate.

EXPERIMENTAL PROCEDURES

Plant Materials and Growth—Arabidopsis thaliana ecotype Columbia (Col-0) was used as wild type in all our studies. The *atm3* mutant alleles (gene identifier *AT5G58270*) and *atm1-1* (*AT4G28630*) have been described previously (6). The *oastlC* (*AT3G59760*) knock-out mutant is described in Ref. 24, and the *ethe1-1* (*AT1G53580*) knockdown mutant in Ref. 25. Plants were germinated on half-strength Murashige and Skoog medium with 0.8% (w/v) agar and transplanted to compost after 2 weeks. Buthionine sulfoximine (BSO) and glutathione were added after autoclaving the medium. BSO was either added as pure L-BSO or the racemic mix of DL-BSO (Sigma). Plants were grown in a controlled environment at 20 °C, 65% humidity in a 16-h light/8-h dark cycle with a photon flux density of 100–120 μmol m^{-2} s^{-1}.

Glutathione Levels and roGFP Analysis—Mitochondria were isolated from cell culture or hydroponic seedlings as described previously (6). Thiols were extracted with sulfosalicylic acid and quantified with dithionitrobenzoic acid (Ellman's reagent) in a cyclic assay using glutathione reductase (18). Alternatively, mitochondria were extracted with hydrochloric acid and labeled with monobromobimane for HPLC analysis of GSH (24). Quantitative *in vivo* imaging of the cytosolic GRX1-roGFP2 (26) and mitochondrial roGFP2-GRX1 sensor constructs (27) in 7–8-day-old seedlings was performed using a Zeiss LSM780 confocal microscope (Carl Zeiss MicroImaging GmbH, Goettingen, Germany). Image collection and ratiometric analysis were essentially as described previously (28, 29).

Bacterial Strains, Plasmids, and Growth Conditions—Lactococcus lactis strain NZ9000 Δ*lmrA* Δ*lmrCD* (30) was grown at 30 °C in M17 broth (Oxoid) supplemented with 0.5% (w/v) glucose and appropriate antibiotics for maintenance of plasmids. Cells were transformed with empty expression vector pNZ8048 (31), pNZ8048 encoding C-terminally His_6-tagged Atm1 or Atm1 ΔK475 (this study), empty vector pERL (32), or pERL encoding C-terminally His_{10}-tagged ATM3 or ATM3 E641Q (this study), downstream of a nisin A-inducible promoter. Medium was inoculated with a 1:50 dilution of overnight culture, and cells were grown to an OD_{660} of 0.5–0.6. Expression of ATM proteins was induced for 1.5 h at 30 °C in the presence of 0.1% (v/v) of nisin A-containing supernatant of the nisin-producing strain *L. lactis* NZ9700 (31).

Construction of ATM Mutants—The first 58 codons of the *ATM1* gene from *Saccharomyces cerevisiae* were removed, and a C-terminal His_6 tag and XbaI site were introduced by PCR using primer Sc_tr and Sc_Rev_His (for all primer sequences see supplemental Table S1). The PCR product was cloned into pJET vector (Fermentas). Site-directed mutagenesis was performed using the QuikChange lightning kit (Stratagene) to introduce the ΔK475 mutation with primers Atm1_DK_For and Atm1_DK_Rev. Wild-type and mutant *ATM1* were reamplified by PCR and cloned into pNZ8048 to generate pNZ_Atm1 and pNZ_Atm1ΔK475.

ATM3 expression constructs were generated using the backbone exchange method (32). N-terminally truncated versions of ATM3 were amplified using ATM3_FX_Rev and ATM3_FX30_For, ATM3_FX60_For, or ATM3_FX97_For and cloned into vector pREX containing a C-terminal His_{10} tag as described (32, 33). Site-directed mutagenesis was performed using primers ATM3_EQ_For and ATM3_EQ_Rev.

Preparation of Inside-out Membrane Vesicles and Protein Purification—Inside-out membrane vesicles were prepared from lactococcal cells by passage through a Basic Z 0.75-kW Benchtop Cell Disruptor (Constant Systems) at 20,000 p.s.i. as described previously (34). Protein concentration was determined using the DC assay kit (Bio-Rad), and expression of the

proteins was confirmed by protein blot analysis with antibodies against the His tag, ATM3, or Atm1.

Inside-out membrane vesicles (30 mg of total protein) were solubilized in 7.5 ml of Buffer A (50 mM HEPES-KOH buffer, pH 8.0, 100 mM NaCl, 10% (v/v) glycerol) containing 1.0% (w/v) β-D-dodecyl maltoside (DDM, Melford) or 1.0% (w/v) lauryl-maltoside neopentylglycol (LMNPG, Affymetrix). The solubilization mixture was incubated on a rotating wheel for 2 h at 4 °C. Unsolubilized particles were removed by centrifugation at 125,000 × *g* for 30 min at 4 °C, and the supernatant was transferred to 400 μl of nickel-nitrilotriacetic acid (Ni-NTA)-agarose suspension (Qiagen) pre-equilibrated with Buffer A containing 0.1% (w/v) DDM or 0.05% (w/v) LMNPG and 30 mM imidazole. The mixture was incubated for a further 2 h and subsequently transferred to a Bio-spin column (Bio-Rad). The resin was washed with 5 column volumes of equilibration buffer and with 6 volumes of Buffer B (50 mM HEPES-KOH, pH 7.0, 100 mM NaCl, 10% (v/v) glycerol, 30 mM imidazole, 0.1% (w/v) DDM, or 0.05% (w/v) LMNPG). The protein was eluted in elution buffer (Buffer B, but containing 5% (v/v) glycerol and 250 mM imidazole). Protein concentrations were determined using the Micro-BCA assay kit (Pierce).

ATPase Measurements—ATPase activity of purified ATM3 and Atm1 was determined using the malachite green colorimetric assay. Briefly, 5 μg of purified protein was added to 0.1 M HEPES-KOH, pH 7.0, supplemented with 5 mM $MgCl_2$ and 5 mM Na-ATP. The samples were incubated at 30 °C for 5 min, and subsequently 150 μl of malachite green solution was added (0.525 g of ammonium molybdate·$7H_2O$, 17 mg of malachite green, 12.5 ml of 4 N hydrochloric acid, and MilliQ water to 50 ml), which had been activated with 0.1% Triton X-100. The absorbance was measured at a wavelength of 640 nm. Background levels of P_i in the elution buffer were measured and subtracted. The NADH-coupled assay was performed as described previously (35). Where indicated, compounds were added to the assay mixture, at a final concentration of 3.3 mM unless otherwise stated, to determine their ability to stimulate ATPase activity. The GSSG polysulfide mixture was prepared as described (36). Glutathione persulfide (GSSH) was produced by mixing GSSG and Na_2S in a 1:4 ratio with subsequent incubation at 30 °C for 15 min.

Substrate Transport in Inside-out Membrane Vesicles—Inside-out membrane vesicles with expressed ATM proteins were prepared as described above. The transport reaction contained 1 mg/ml membrane vesicles, 5 mM ATP, 5 mM $MgCl_2$, and an ATP regeneration system consisting of 0.1 mg/ml creatine kinase and 5 mM phosphocreatine (both from Roche Applied Science) in 0.25 ml of 0.1 M KP_i, pH 7.0. [^{35}S]GSH (PerkinElmer Life Sciences; 944 Ci/mmol) was mixed with non-labeled GSH to obtain a final concentration of 250 μM [^{35}S]GSH (0.95 Ci/mmol). [^{35}S]GSSG was prepared from [^{35}S]GSH as described in Ref. 37. In brief, dithiothreitol was removed by solvent extraction with ethyl acetate, and GSH was oxidized to GSSG by addition of 1% (v/v) H_2O_2. The purity of [^{35}S]GSH and [^{35}S]GSSG was analyzed by thin liquid chromatography on Silica 60 F254 nm plates (Merck) in 16:3:5 isopropyl alcohol/H_2O/acetic acid. Plates were dried and exposed to Biomax MR film (Eastman Kodak) at −80 °C for 3 days.

The transport reaction was incubated for the indicated time and then filtered over nitrocellulose filters (Whatman; 0.45 μm) by rapid vacuum filtration. The filters were washed twice with 5 ml of ice-cold 0.1 M KP_i, pH 7.0, to decrease background binding of free ^{35}S-labeled compounds. Radioactivity retained on the filters was determined by liquid scintillation counting in Ultima Gold XR (PerkinElmer Life Sciences).

Transport reactions for GS-S-SG were carried out as for the radiolabeled substrate, except that the membrane vesicles were mixed with GSSG/GS-S-SG mixture containing 500 μM GSSG and 100 μM GS-S-SG as quantified by LC-MS/MS. After incubation for 30 min, samples were filtered over MultiScreen HTS+ plates (Millipore), washed with KP_i, and eluted in 70% (v/v) acetonitrile. Samples were diluted to 50% (v/v) acetonitrile, and 15 μl was applied to a Luna 3-μm NH_2 column (100 × 2 mm, Phenomenex) attached to a Thermo-Finnigan Surveyor HPLC system. GSSG and GS-S-SG were separated in Hilic mode using a 90 to 10% gradient of acetonitrile in 20 mM ammonium acetate, pH 9.45, over 15 min. Eluted peaks were resolved on a LCQ DECA XPplus MS equipped with an electrospray ionization source. This was operated in negative mode and set to trap ions of *m/z* 611.1 (GSSG) and *m/z* 643.1 (GS-S-SG) to detect characteristic fragments. Ion intensities were quantified by peak integration using XCalibur software (ThermoFisher Scientific) and normalized to standards in the same experiment.

RESULTS

Arabidopsis atm3 Mutants Are Hypersensitive to an Inhibitor of Glutathione Biosynthesis—Arabidopsis atm3-1 seedlings were previously shown to accumulate 2-fold more non-protein thiols such as glutathione, whereas transcript levels of the *GSH1* gene were elevated (20). To further investigate a possible interaction between glutathione and ATM3 function in plants, wild-type and *atm3* seedlings were germinated on medium with low concentrations of BSO, a specific inhibitor of glutamate-cysteine ligase (EC 6.3.2.2), which is encoded by *GSH1* and mediates the first step of glutathione synthesis (38). We tested three *atm3* mutant alleles as follows: the weak *atm3-3* allele that has an R612K substitution in the X-loop of the NBD; the intermediate *atm3-4* allele that has less than 10% expression of *ATM3* due to a 39-nucleotide deletion in the promoter; and the strong *atm3-1* allele that lacks the NBD (6). Concentrations of 200 or 400 μM BSO in the growth medium did not affect root growth of wild-type seedlings (Fig. 1*A*). By contrast, a significant decrease in relative root growth was seen in all three *atm3* mutant lines, with up to 60% inhibition in the stronger *atm3-1* allele exposed to 400 μM BSO. The degree of growth inhibition correlated with the severity of other phenotypic parameters in the *atm3* mutants (6) and could be reversed by addition of GSH to the growth medium. GSH alone had no major effect on root growth; however, a slight increase in root length was observed in the *atm3-3* and *atm3-4* mutant alleles (Fig. 1*B*). Thus, depletion of glutathione aggravates the slow growth phenotype of *atm3* mutants. The functional interaction between glutathione and the *Arabidopsis* ATM3 transporter echoes the findings in yeast, in which genetic depletion of both GSH and Atm1 is lethal (22).

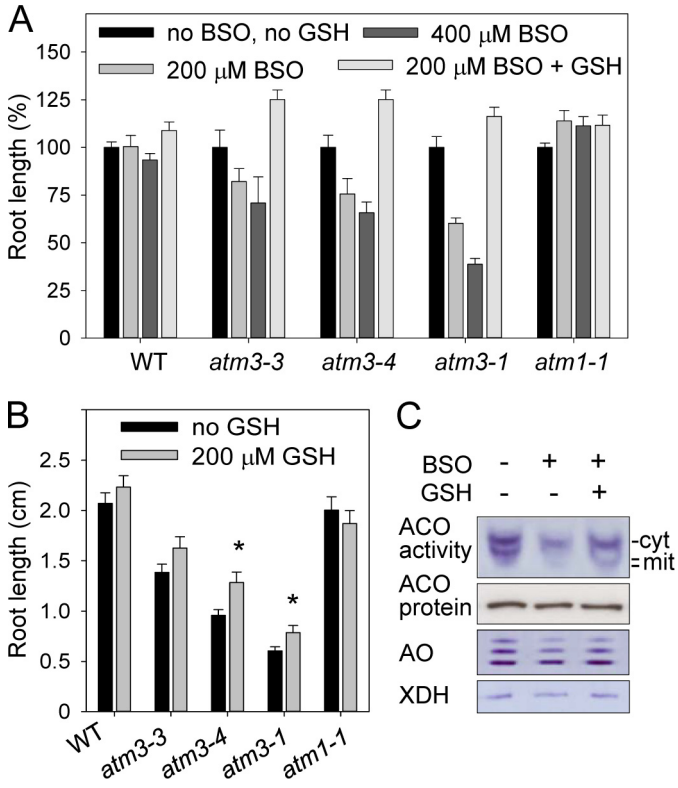

FIGURE 1. ***Arabidopsis atm3* mutants are sensitive to GSH depletion.** *A,* relative root length after 8 days in wild-type (*WT*) and *atm3* mutant seedlings without any additions or with BSO (200 and 400 μM racemic DL-buthionine-(*SR*)-sulfoximine) and GSH (reduced glutathione, 200 μM) as indicated. A knock-out allele of the paralogue *ATM1* served as a control. Values represent the mean ± S.E. ($n > 25$). *B,* absolute root length (in centimeters) in seedlings without (*black bars*) and with 200 μM GSH (*gray bars*). Values represent the mean ± S.E. for two independent experiments and $n > 25$. *, $p < 0.05$ (Student's *t* test). *C,* activities of Fe-S enzymes in wild-type seedlings treated with BSO (400 μM L-buthionine sulfoximine) and 200 μM GSH. Seedlings were grown as in *A*. Cell extracts were separated under native conditions, and stained for aconitase activities (*ACO*, 50 μg of protein per lane), aldehyde oxidases (*AO*, 50 μg of protein per lane), and xanthine dehydrogenase (*XDH*, 30 μg of protein per lane). *cyt*, cytosolic isoform; *mit*, mitochondrial isoforms. Aldehyde oxidases and xanthine dehydrogenase are cytosolic enzymes. The same samples were subsequently analyzed for aconitase protein levels by immunoblotting under denaturing conditions, in which the isoforms are not separated and the signal represents total aconitase protein.

Next, we investigated whether glutathione depletion had an effect on the activity of Fe-S enzymes as an indirect measure of Fe-S cluster assembly (5). For this purpose, wild-type seedlings were grown in the presence of 400 μM BSO. Cell extracts were separated by native gel electrophoresis, and activities of aconitases, aldehyde oxidases, and xanthine dehydrogenase were assayed by in-gel staining. Inhibition of glutathione biosynthesis by BSO resulted in strongly decreased aconitase activities for both the cytosolic and mitochondrial isoforms of wild-type seedlings, which was restored by the addition of GSH to the medium (Fig. 1*C*). However, the cytosolic aldehyde oxidase and xanthine dehydrogenase activities were hardly affected by GSH depletion. It is possible that the Fe_2S_2 clusters of the latter enzymes are more stable than the Fe_4S_4 cluster of aconitase.

Glutathione Redox State Is Shifted toward Oxidation in Mitochondria of atm3 Mutants—The greater sensitivity of *atm3* mutants to BSO could be caused by the following: (i) lower steady-state levels of glutathione; (ii) altered distribution of glutathione in the cell; or (iii) a more oxidized glutathione pool, *i.e.* an increased GSSG to GSH ratio as seen in total cell extracts of the yeast Δ*atm1* mutant (18). A previous report on the *Arabidopsis atm3-1* mutant (20) showed that non-protein thiols such as glutathione were increased 2-fold in cell extracts, so therefore we rejected point i. To analyze whether the cellular distribution of glutathione is altered when ATM3 is not functional (point ii), we measured the glutathione content in mitochondria from wild-type and *atm3* mutants. Intact and >90% pure mitochondria were isolated from cell cultures or hydroponic seedlings, extracted under acid conditions and analyzed by the cyclic dithionitrobenzoate assay for non-protein thiols (known to be mostly glutathione) or by bromobimane derivatization and HPLC. We found that the total glutathione levels (GSH + GSSG) were significantly increased by up to 2-fold in *atm3* mitochondria (Fig. 2*A*). However, compared with the overall 2-fold increase in the cell (20), we conclude that glutathione does not specifically accumulate in the mitochondria of *atm3* mutants.

To investigate the redox state of the glutathione pool on the mitochondrial and cytosolic side of the ATM3 transporter (see point iii above), we used the redox-sensitive GFP2 (roGFP2) fused to glutaredoxin1 (GRX1). This approach reflects the *in vivo* situation and is therefore superior to cell-disruptive methods, because the glutathione pool tends to become oxidized during the isolation procedure for mitochondria. The roGFP2 sensor was targeted to the mitochondrial matrix and cytosol, respectively (27, 39). Stable expression of the roGFP2 sensors in each cell compartment was confirmed by fluorescence microscopy in wild-type, *atm3-3,* and *atm3-4* mutants (data not shown). However, for the strong *atm3-1* mutant allele, we could only obtain expression of the sensor in the cytosol but not in the mitochondria. The emission ratio upon excitation of the sensor with 405 and 488 nm provides a readout of the redox potential of the surrounding GSSG/GSH buffer and ranged from ~0.2 (fully reduced) to 1–1.2 (fully oxidized). We found that the 405:488 ratio value of roGFP2 was significantly increased in images of the mitochondrial sensor in *atm3-3* and *atm3-4* mutants compared with wild type (Fig. 2, *B* and *C*). This observation was consistently made in two separate experiments and in different tissue types as follows: root tip, root elongation zone, and cotelydon epidermis. By contrast, the 405:488 ratio values for the cytosolic roGFP sensor were similar in *atm3* mutants and wild type.

The glutathione redox potential shifts toward oxidation either by a decrease in total glutathione levels or an increase in the GSSG/GSH ratio. Both lead to an increase in the roGFP ratio value (39). In mitochondria from *atm3* mutants, glutathione levels are higher than in wild type (Fig. 2*A*), and when glutathione was depleted using the inhibitor BSO, the 405:488 ratio of mitochondrial roGFP increased to a similar extent in wild-type and *atm3* mutants (data not shown). Therefore, an increased 405:488 ratio of the roGFP sensor indicates that the mitochondrial matrix of *atm3* mutants contains relatively more GSSG than in wild-type mitochondria. These data also suggest that if glutathione is a direct substrate of ATM3 it is preferentially transported in the oxidized disulfide form.

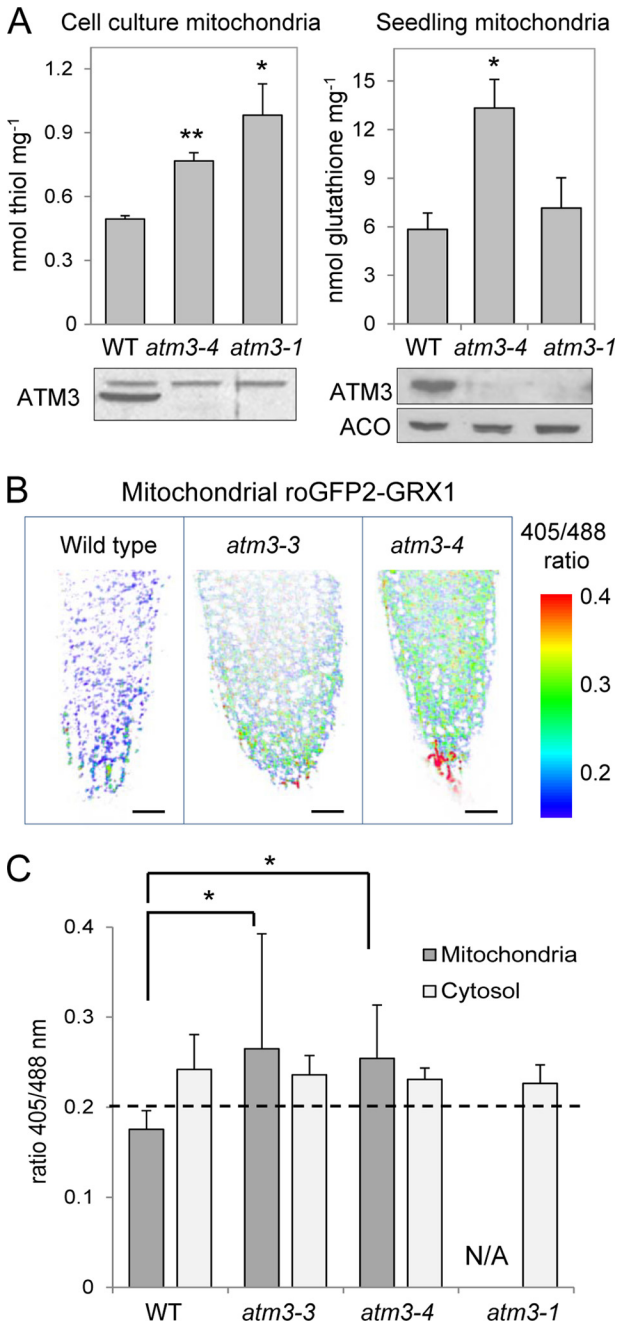

FIGURE 2. **Glutathione levels and redox status of the mitochondrial and cytosolic glutathione pools in *Arabidopsis atm3* mutants.** *A,* analysis of non-protein thiols or total glutathione levels (GSH + GSSG) in isolated mitochondria from wild-type and *atm3* mutants, from cell culture (*left panel*), or from hydroponic seedlings (*right panel*). Values are the mean ± S.E. of ≥3 mitochondrial preparations. *, $p < 0.05$; **, $p < 0.01$ (Student's *t* test). Immunoblotting confirmed the absence of ATM3 protein in mitochondria from the mutant lines. *B,* false-color images of root tips representing the readout of the ratiometric roGFP2-GRX1 sensor expressed in the mitochondria in wild-type (*WT*), *atm3-3,* and *atm3-4*. The *red* colored cells in the root cap are undergoing cell death. Note that the ratio range shown does not represent the full dynamic sensor range but has been chosen to match the ratio range of the samples. *Scale bar,* 20 μm. *C,* ratios of the emission intensities upon excitation at 405 and 488 nm in images of roGFP2-GRX1 expressed in mitochondria and cytosol in wild-type (*WT*) and *atm3* lines. The ratio provides a specific readout for the redox state of the glutathione pool and increases with oxidation, *i.e.* increased GSSG levels. The *dashed line* indicates the ratio of the fully reduced sensor (treatment with 10 mM dithiothreitol). The ratio of fully oxidized sensor was 1.27 for the cytosolic and 0.95 for the mitochondrial roGFP2 sensor construct, respectively. The values represent the mean ratio ± S.D. of 10–15 individual root tips. *, $p < 0.05$ (one-way ANOVA followed by post hoc Tukey's test; comparison of *atm3* mutants to WT). *N/A,* not available as we could not obtain *atm3-1* expressing the mitochondrial roGFP2-GRX1 construct.

Expression and Purification of Arabidopsis ATM3 and Yeast Atm1 Using L. lactis—For functional characterization of the substrate specificity of ATM3, we chose the Gram-positive bacterium *L. lactis* as an expression system (40, 41). Yeast Atm1 was also included in our study for comparison. Protein expression in lactococcal cells has several advantages such as tight regulation of expression by the nisin-inducible promotor, low proteolytic activity, and a low rate of protein misfolding. Additionally, the *L. lactis* strain used in this study, NZ9000, cannot produce glutathione (42).

To express ATM3 and Atm1, we truncated the putative N-terminal mitochondrial targeting sequence (MTS), as this sequence is known to cause instability of the protein in bacterial expression systems. For ATM3, prediction programs (MitoProt, TargetP, and SignalProt) were inconclusive as to the length of the MTS. We therefore generated three constructs in which the first 30, 60, or 97 amino acids were deleted. All three constructs were expressed, but the Δ60 construct was most active (data not shown) and is used in this study. For Atm1, a targeting sequence of 26 residues was predicted by MitoProt and TargetP, whereas alignment with bacterial AtmA homologues suggested that the first 58 residues comprise the MTS. By contrast, 93 ± 2 amino acids were cleaved off the N terminus when Atm1 was expressed in *Escherichia coli* (23). As a consensus, we decided to remove the first 58 amino acids, which yielded stable and active Atm1. A C-terminal histidine tag was introduced in both constructs to enable purification by Ni-NTA affinity chromatography.

We also generated ATM3 and Atm1 mutant proteins with an impaired ability to hydrolyze ATP (43). Deletion of the catalytic lysine in the Walker A motif, which is often used for this purpose, destabilized the ATM3 protein; therefore, we generated E641Q adjacent to the Walker B motif. For yeast Atm1, deletion of Lys-475 in the Walker A motif did not affect its stability. Equal expression of wild-type and mutant proteins in lactococcal membranes was confirmed by protein blot analysis (Fig. 3, *A* and *B*).

To assess the orientation of ATM3 and Atm1 in the lactococcal plasma membrane, we tested the accessibility of the histidine tag at the C terminus of both proteins in well defined inside-out membrane vesicles using a membrane-impermeable protease. We found that protease treatment removed the histidine tag but that the ATM protein remained intact (Fig. 3*C*). When detergent was added to solubilize the phospholipid bilayer, protease K was able to access and digest Atm1. These results suggest that the NBDs of both ATM3 and Atm1 are exposed to the exterior of the membrane vesicles and therefore that the transporter is in the physiological orientation in the plasma membrane of *L. lactis*.

Both ATM3 and Atm1 were purified to homogeneity using Ni-NTA affinity chromatography (Fig. 3*D*) and retained their ATPase activity in detergent solution (Fig. 4, *A* and *B*). The purified yeast Atm1 had a higher basal ATPase activity than *Arabidopsis* ATM3 as measured by colorimetric detection of P_i

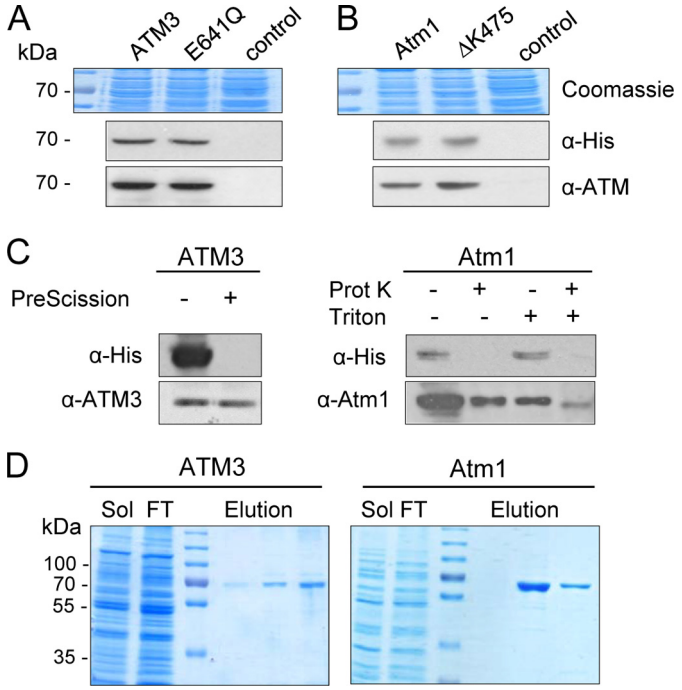

FIGURE 3. **Expression and purification of ATMs.** *Arabidopsis* ATM3 and ATM3 E641Q (*A*), and yeast Atm1 and Atm1 ΔK475 (*B*) were expressed from plasmids in *L. lactis*. Total membrane protein (24 μg) was analyzed by immunoblotting for expression of the transporter proteins using anti-His or specific antibodies. Coomassie staining confirmed equal loading. *Control*, membranes from cells carrying an empty plasmid. *C*, orientation of ATMs in inside-out membrane vesicles. Samples (24 μg of protein) were treated as indicated and then subjected to immunoblotting with anti-His or anti-ATM antibodies. ATM3 has a C-terminal His_{10} tag with a cleavage site specific for PreScission protease. Atm1 has a C-terminal His_6 tag without a cleavage site; therefore, the nonspecific protease K (*Prot K*) was used. In both cases, the His tag is accessible to the protease, indicating that the C-terminal NBD is oriented to the outside of the membrane vesicles. Addition of the detergent Triton X-100 renders Atm1 accessible to protease K. *D*, ATM3 and Atm1 were purified to homogeneity using Ni-NTA affinity chromatography. *Sol*, solubilized membranes; *FT*, flow-through.

release from ATP by malachite green. As expected, the E641Q mutation in ATM3 and the ΔK475 deletion in Atm1 led to a substantial decrease in the observed ATPase activity (Fig. 4, *A* and *B*) confirming that the measured activity was due to the expressed ATM proteins.

ATPase Activity of ATM Transporters Is Stimulated by GSSG but Not GSH—Stimulation of ATPase activity of ABC transporters by transported substrates is well documented for a wide variety of these proteins (44, 45). Therefore, ATP hydrolysis rates of ATM3 and Atm1 were measured in the presence of a range of potential substrates, such as GSH, GSSG, thiols, sulfur compounds, and glutathione conjugates. Glutathione persulfide (GSSH) was produced chemically by mixing GSSG and Na_2S. The efficiency of the reaction was analyzed by quantification of sulfane sulfur (S^0) using the cold cyanolysis method, a colorimetric assay based on the formation of a ferric thiocyanate complex (46), which showed that 33% of the GSSG was converted to GSSH, yielding a 1:1 molar ratio of GSSH and GSSG. A GSSG polysulfide mixture was generated from elemental sulfur (S_8) and GSH as described previously (36). Mass spectrometry revealed the presence of GS-S_n-SG ($n \leq 5$) and GSSG at a molar ratio of ~1:2 and no other significant reaction intermediates (data not shown).

Neither ATM3 nor Atm1 showed a significant stimulation of ATPase activity by GSH, GSSH, cysteine, acetylcysteine, Cys-Gly, dithiothreitol, or other compounds with free thiols (Fig. 4, *A* and *B*, and data not shown). There was also no stimulation by cystine (disulfide of cysteine), lactoylglutathione, sulfite, or sulfide. However, a significant enhancement of ATPase activity was measured in the presence of GSSG and GS-S-SG/GSSG, and this stimulation was concentration-dependent and similar for both substrates (compare 0.83 and 1.7 mM values for each substrate). By contrast, the GSSH/GSSG mixture did not stimulate ATPase activity, indicating that GSSH inhibits the stimulatory effect of GSSG. For both *Arabidopsis* ATM3 and yeast Atm1, the stimulation of P_i release was ~3-fold in the presence of 3.3 mM GSSG ($p < 0.01$). This is in the same range as observed for other ABC exporters (47–49).

Next, we tested whether ferrous iron was able to stimulate ATPase activity, either alone or in combination with GSH or GSSG. Because of redox chemistry between iron and malachite green, we measured the ATPase activity in an indirect enzyme assay in which the release of ADP is coupled to NADH oxidation (35). Nevertheless, $FeCl_2$ concentrations of more than 0.1 mM interfered with the reaction. We confirmed that GSSG stimulated the ATPase activity of yeast Atm1 ~2-fold (Fig. 4*C*), but neither iron alone nor iron in combination with GSH or GSSG had a stimulatory effect.

ATMs Can Mediate ATP-dependent GSSG and GS-S-SG Transport—To further assess the substrate specificity of ATM3 and Atm1, we investigated whether GSH or GSSG are transported into lactococcal inside-out membrane vesicles by rapid filtration. For this purpose, membrane vesicles containing the respective proteins were incubated with 250 μM ^{35}S-labeled GSH or GSSG (0.95 Ci/mmol). The reaction mixture contained an ATP-generating system, ATP (where indicated), and $MgCl_2$. GSSG was prepared by oxidation of GSH with hydrogen peroxide (see "Experimental Procedures"). To confirm the purity of the substrates, we analyzed 8 nCi on silica TLC plates (Fig. 5*A*). Clear separation of the two compounds under these conditions confirmed that the GSH sample did not contain detectable [^{35}S]GSSG and that the GSSG working stock solution contained less than 20% [^{35}S]GSH.

We observed ATP-dependent uptake of [^{35}S]GSSG in membrane vesicles expressing ATM3 (Fig. 5*B*) or Atm1 (Fig. 5*C*). By contrast, [^{35}S]GSH did not accumulate in the membrane vesicles. The accumulation of radiolabel was dependent on functional ATM protein as neither ATM3 E641Q nor Atm1 ΔK475 displayed significant transport activity. Kinetic analysis of Atm1-mediated [^{35}S]GSSG transport at a substrate concentration between 10 and 500 μM revealed an apparent affinity (K_m) of ~109 ± 6 μM (Fig. 5*D*), which is in a similar range as described for mammalian MRP1 (ABCC1) (50).

To investigate whether GS-S-SG can be transported, we developed a transportomics approach (51) in which the accumulated substrates in inside-out membrane vesicles were identified by LC-MS/MS. Membrane vesicles containing Atm1 were incubated with GS-S-SG/GSSG mixture. After 30 min incubation in the presence of ATP followed by rapid filtration and washes, 3.1 ± 0.6 pmol of GS-S-SG per mg of protein was detected in Atm1-containing vesicles. In contrast, GS-S-SG

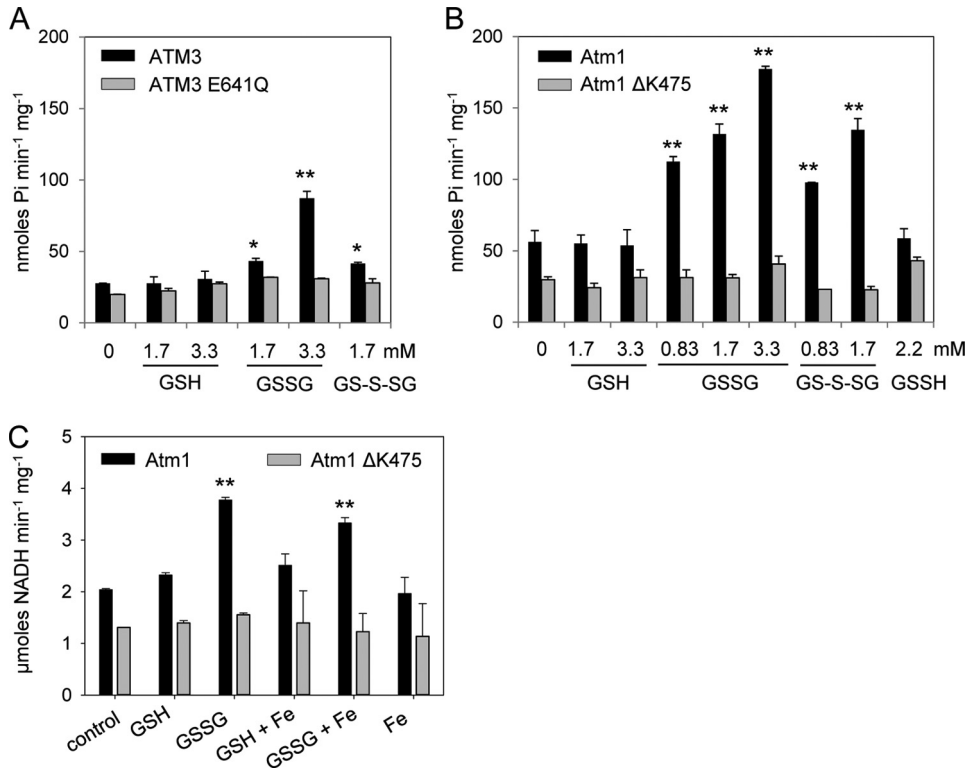

FIGURE 4. **ATPase hydrolysis measurements of ATM3 and Atm1.** *A* and *B*, ATP hydrolysis rates of purified *Arabidopsis* ATM3 (*A*) and yeast Atm1 (*B*) with GSH, GSSG, GS-S-SG (containing GS-S_n-SG and GSSG in a 1:2 molar ratio) and GSSH (containing GSSH and GSSG in a 1:1 molar ratio) at the indicated concentrations. The mutant proteins ATM3 E641Q and Atm1ΔK475, which cannot hydrolyze ATP, were used as controls. The release of phosphate (P_i) was measured by colorimetric detection using malachite green. The results are representative of two independent experiments (*A*, mean ± S.D.) or the average ± S.E. of three independent experiments (*B*). *, < 0.05; **, < 0.01 (ANOVA and post hoc Tukey's test). *C*, ATP hydrolysis rates of purified yeast Atm1 in the presence of 1.7 mM GSH or 1.7 mM GSSG and 0.1 μM $FeCl_2$ (*Fe*). The release of ADP was measured using the NADH-coupled method because iron interfered with the malachite green method. The mutant Atm1 ΔK475 was used as control. The data shown are representative of two experiments (mean ± S.D.), **, $p < 0.01$ (ANOVA and post hoc Tukey's test).

was not detected in control membrane vesicles containing the ΔK475 mutant of Atm1 (Fig. 5*E*). The Atm1 vesicles also accumulated 82.8 ± 8.4 pmol of GSSG per mg of protein.

To provide evidence for direct interactions between Atm1 and GSSG, we mutated the first arginine in a conserved (R/K)*XXX*R motif in the transmembrane domain of Atm1 (Fig. 6*A*). The R216Q change in Atm1 did not affect the stability of the protein or its basal ATPase activity (Fig. 6, *B* and *D*). Interestingly, the ATP hydrolysis rate of Atm1 R216Q could not be stimulated by GSSG (Fig. 6*C*). This correlated with the inability of the mutant protein to mediate [^{35}S]GSSG transport in inside-out membrane vesicles (Fig. 6*D*), providing further evidence that GSSG transport requires functional Atm1 in our measurements.

Overall, our experimental evidence indicates that GSSG and GS-S-SG but not GSH are transported in a micromolar range of concentrations by the ATM transporters. This correlates well with the ATP hydrolysis measurements shown above, which did not show any stimulation by GSH under these conditions.

The atm3-1 Mutant Phenotype Is Severely Enhanced by Depletion of the Mitochondrial Sulfur Dioxygenase ETHE1—Our *in vitro* data showed that ATM3 transports GSSG and, by analogy with our transportomics results for yeast Atm1, one expects ATM3 to also transport GS-S-SG. To find evidence for sulfur transport *in vivo*, we analyzed isolated mitochondria from *atm* mutants for persulfide (S^0) or sulfide (S^{2-}), but we did not find an increase in either compound. Either our analytical methods are not sensitive enough or (per)sulfide accumulating in mutant mitochondria is rapidly detoxified.

Recently, two distinct mitochondrial activities for removal of either S^{2-} or S^0 have been characterized in *Arabidopsis*. A mitochondrial isoform of *O*-acetylserine(thiol)lyase (EC 2.5.1.47) catalyzes the assimilation of S^{2-} by replacing the activated acetyl moiety in *O*-acetyl-L-serine to produce cysteine and acetate (24, 52). A knock-out mutant of mitochondrial *OAS-TL* (*oastlC*) has been characterized previously and displayed a mild growth defect (24). ETHE1 is a sulfur dioxygenase (EC 1.13.11.18) that oxidizes S^0 to sulfite using GSH as a cofactor to form the intermediary substrate GSSH (25, 53, 54). Disruption of *ETHE1* caused embryo lethality (54), but a promoter mutant with strongly decreased transcript levels and sulfur dioxygenase activity is viable and displayed only a mild growth defect under normal conditions (25).

To investigate whether depletion of either OAS-TL C or ETHE1 activity would enhance the phenotype of *atm3* mutants, the *oastlC* and the *ethe1-1* mutants were crossed with *atm3-1*. We isolated the expected frequency of *oastlC atm3-1* double mutants (17:61 from an *oastlC*$^{+/-}$ *atm3-1* parent), but we initially failed to find the double mutant of *ethe1-1* and the *atm3-1* allele. Inspection of the siliques of plants homozygous for *ethe1-1* and heterozygous for *atm3-1* revealed that about 25% of the seeds aborted (Fig. 7, *A* and *B*). Some seeds aborted early

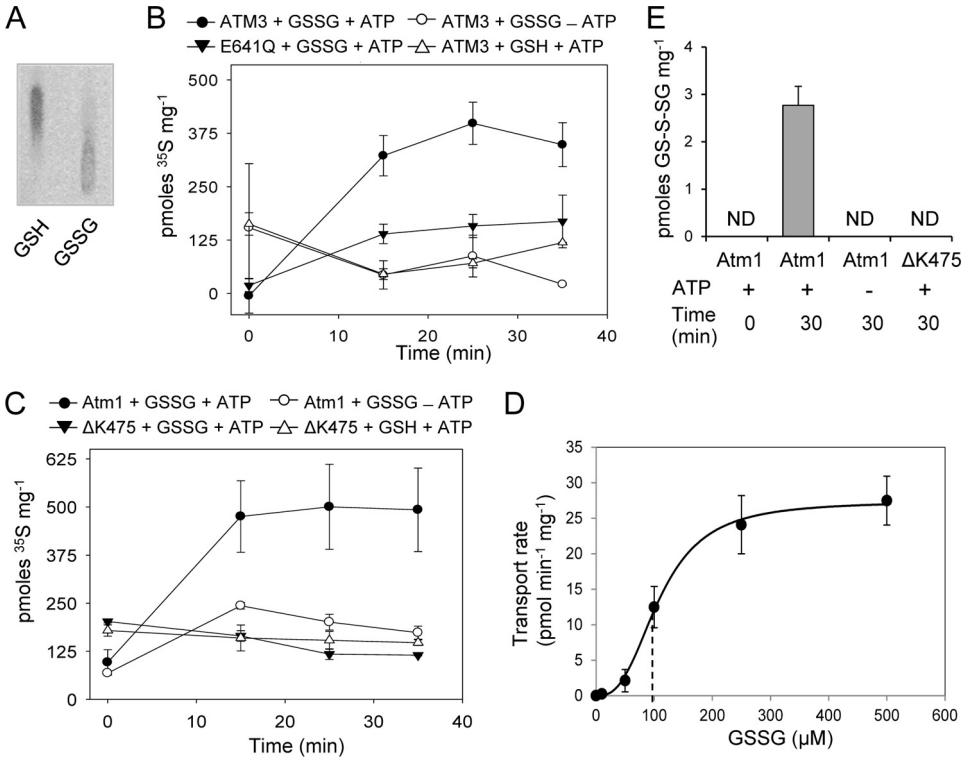

FIGURE 5. **Substrate transport measurements in inside-out membrane vesicles containing ATM3, ATM3E641Q, Atm1, or Atm1ΔK475.** *A,* separation of [^{35}S]GSH and [^{35}S]GSSG (0.95 μCi/mmol) by TLC. The samples contained 8 nCi of radioactivity. *B* and *C,* transport of 250 μM [^{35}S]GSH or GSSG in lactococcal inside-out membrane vesicles containing *Arabidopsis* ATM3 (*B*) or yeast Atm1 (*C*). The mutant proteins with amino acid changes E641Q (in ATM3) and ΔK475 (in Atm1), which cannot hydrolyze ATP, were used as controls. Alternatively, ATP was omitted from the reaction (−*ATP*). All values are background-subtracted and represent the mean ± S.E. of three independent experiments. *D,* initial rates of Atm1-mediated transport of [^{35}S]GSSG in inside-out membrane vesicles were determined at substrate concentrations between 10 and 500 μM. The data were fitted to the three-parameter Hill equation, giving an apparent average K_m of 109 ± 6 μM GSSG and V_{max} of 27.4 ± 0.8 pmol min^{-1} mg^{-1} of membrane protein, with a Hill number of 2.8 ± 0.4. *E,* transport of GS-S-SG in inside-out membrane vesicles containing Atm1, quantified by LC-MS/MS. A GSSG/GS-S-SG mixture was added as substrate in the transport assay to a final concentration of ~100 μM GS-S-SG and 500 μM GSSG. The value is the mean ± S.E. ($n = 6$). *ND,* not detectable.

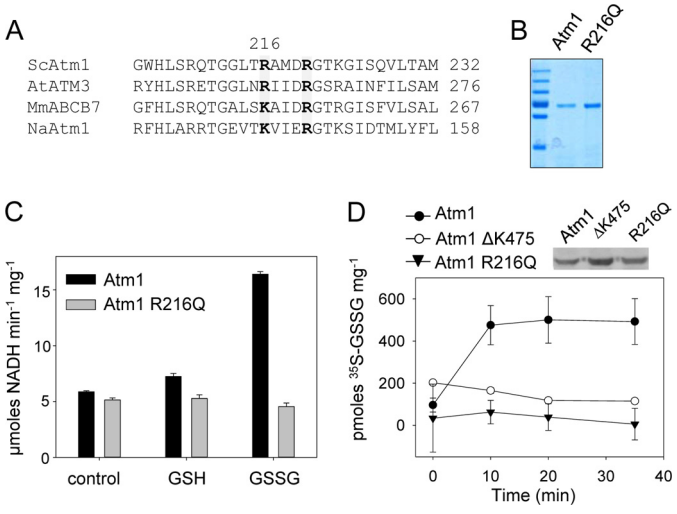

FIGURE 6. **Characterization of the arginine R216Q mutant.** *A,* alignment of Arg-216 and Arg-220 in yeast Atm1 with *Arabidopsis* ATM3, mouse ABCB7, and NaAtm1 from the α-proteobacterium *Novosphingobium aromaticivorans*. The two arginines are mostly conserved in the ATM family (marked in *gray*), although a lysine is found in ABCB7 and NaAtm1. *B,* Coomassie-stained purified proteins. *C,* stimulation of ATPase activity in purified Atm1 and the Atm1 R216Q mutant as measured using the NADH-coupled assay. Values are mean ± S.D. and representative of three independent experiments. Stimulation of Atm1 by GSSG was significant ($p < 0.01$; ANOVA and post hoc Tukey's test). *D,* ATP-dependent transport of 250 μM [^{35}S]GSSG (0.95 Ci/mmol) in inside-out membrane vesicles containing the Atm1 R216Q mutant protein was compared with the activity of wild-type Atm1 and the ΔK475 mutant. Expression of Atm1 and the mutant proteins was confirmed by protein blot analysis (*inset*). The values represent the mean ± S.E. ($n = 3$).

during development, whereas most died shortly before maturity. More careful scrutiny of the germinated seedlings revealed a very low percentage (1.9%) of small, pale seedlings that survived after transfer to soil (Fig. 7*C*). PCR analysis confirmed these were *ethe1-1 atm3-1* double mutants (Fig. 7*D*). The *ethe1-1 atm3-1* plants were infertile (Fig. 7*A*). In contrast, *oastlC atm3-1* mutants were similar in appearance to the *atm3-1* parental line. These data suggest that toxic persulfide, but not sulfide, accumulates in mitochondria when ATM3 is nonfunctional.

DISCUSSION

Only a small number of ABC transporters are found in the inner mitochondrial membrane, where members of the mitochondrial carrier family are far more abundant. ATMs have been maintained during the evolution of the eukaryotic cell, apart from a few exceptions in unicellular parasitic eukaryotes, suggesting that they transport compounds essential for conserved biochemical pathways. In the light of the proposed role of ATMs in Fe-S protein biogenesis in the cytosol, and previous implication of glutathione (18, 20, 22), we focused on glutathione conjugates as possible substrates of ATMs. We found that ATP hydrolysis activity of plant ATM3 and yeast Atm1 is stimulated by GSSG but not by GSH, and that both proteins preferentially transport GSSG (Figs. 4 and 5). This substrate specificity is not unprecedented for ABC transporters and has also been

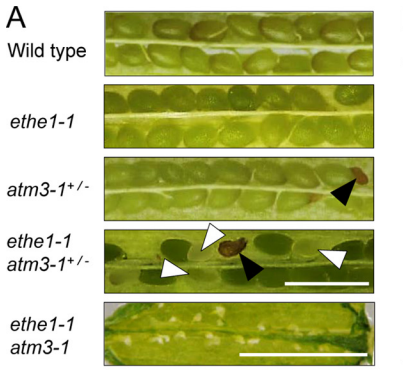

B

Parental genotype	Seed phenotypes (%) n	normal	aborted	gaps
Wild type	847	97.2	1.4	1.4
ethe1-1	1266	97.7	1.9	0.4
atm3-1	619	83.4	5.7	11.0
atm3-1+/-	1209	94.6	4.7	0.7
ethe1-1 atm3-1+/-	1212	74.1	25.2	0.7
ethe1-1 atm3-1		No seed		
oastlC atm3-1	577	80.9	1.9	17.6

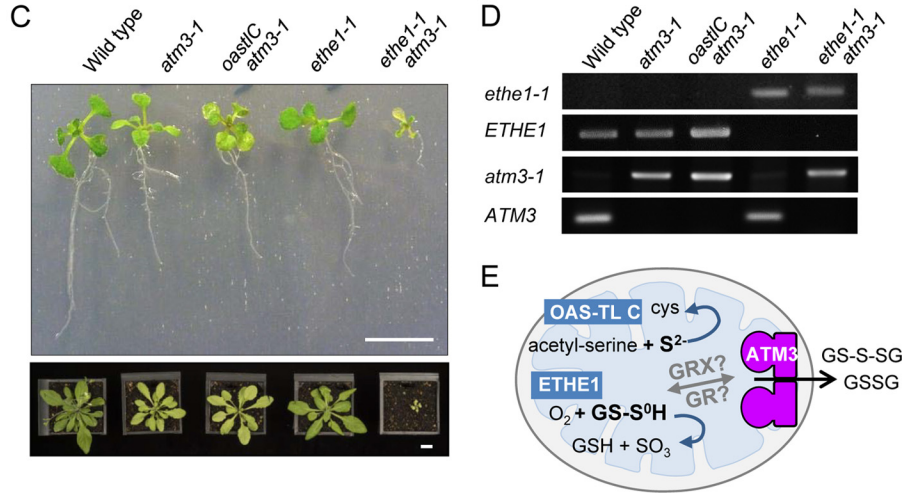

FIGURE 7. **ATM3 interacts genetically with *ETHE1* but not with *OASTL C*.** The *atm3-1* mutant was crossed with the *oastlC* knock-out mutant lacking the mitochondrial *O*-acetylserine(thiol)lyase or with the *ethe1-1* mutant, which has strongly depleted levels of the mitochondrial sulfur dioxygenase specific for GSH-persulfide as substrate. *A,* detail of opened seed pods from wild type and the indicated mutant plants. *Black arrowheads* indicate seeds aborted early in development which have turned brown; *white arrowheads* point to seeds delayed in development that will not mature. *Scale bar,* 1 mm. *B,* numbers of healthy seed, aborted seed, or nonfertilized ovules (gaps) in seed pods of the indicated lines. For each parental genotype, two separate plants were analyzed, or five plants in the case of *ethe1-1 atm3*+/−. *C,* 16-day-old seedlings with the indicated genotypes grown on agar plates (*top*) were transferred to soil and grown for another 2 weeks (*bottom panel*). *Scale bar,* 1 cm. *D,* PCR analysis to confirm the genotypes of the plants shown in *C*. *E,* schematic to illustrate the relation of ATM3 and the reactions catalyzed by OAS-TL C and ETHE1 in the mitochondrial matrix.

reported for a bacterial Atm1-type transporter (12) and for MRP1/ABCC1 (50). In contrast, a previous study by Kunhke and co-workers (23) found that yeast Atm1, which was expressed in *E. coli* and reconstituted into liposomes, was stimulated by a range of molecules with a free thiol group, including GSH. Interestingly, their study showed that GSSG also stimulated ATPase activity but not other disulfides. The discrepancy with our study may be due to the choice of bacterial expression system. The *Lactococcus* NZ9000 strain used here does not produce glutathione; therefore, all effects seen are due to exogenously added GSH or GSSG to the *in vitro* assays.

Expression of roGFP2-GRX1 sensors showed that plant *atm3* mutants accumulate relatively more GSSG in the mitochondrial matrix (Fig. 2, *B* and *C*), providing *in vivo* support for this substrate. It should be pointed out that although the change in the mitochondrial glutathione redox state is significant, the overall effect is modest. This is not surprising considering that plant mitochondria contain an active GSH regeneration system consisting of GSSG reductase (GR2). GR2 is dual localized to the mitochondria and plastids (55). Depletion of GR2 from the mitochondria, in a *gr2* mutant expressing only plastid GR2, led to a highly oxidized mitochondrial glutathione pool.[8] Oxidation of the mitochondrial glutathione pool can happen in the presence of GR2, for instance under stress conditions (39), although reasons for this phenomenon are not yet known. We did not observe a redox change in the cytosolic glutathione pool in *atm3* mutants. Decreased export of GSSG resulting in over-reduction of the cytosol is unlikely to be detectable using the roGFP2 reporter, which is already close to its fully reduced state under control conditions (39). In addition, the high activity and low K_m value of cytosolic GR (GR1) for GSSG will efficiently buffer any variation in organellar export of oxidized glutathione.

The relatively small changes in the cellular glutathione redox state in *atm3* mutants suggest that the primary role of ATM3 is not to mediate export of GSSG from the mitochondria. Instead, we propose that GSSG serves as a vehicle to transport persulfide (sulfane sulfur with oxidation state 0), which is required for both Fe-S cluster assembly and Moco biosynthesis. The activated state of persulfide is important for the formation of Fe-S

[8] A. J. Meyer, unpublished data.

clusters, and sulfide (S^{2-}) cannot be used for this purpose (4, 56). For reasons that are not yet understood, the cysteine desulfurase that generates persulfide for Fe-S cluster assembly resides in the mitochondrial matrix of plants and yeast. Export of persulfide in the form of RS-S^0H across the inner mitochondrial membrane would be a challenge because of its reactivity. However, persulfide in the form of GS-S-SG is relatively more stable. We found that GSSH could not stimulate the ATPase activity of ATM3 and Atm1, and in fact it inhibited the stimulatory effect of GSSG. In contrast, GS-S-SG did not have an inhibitory effect on stimulation by GSSG (Fig. 4, *A* and *B*), and accumulated in inside-out membrane vesicles containing Atm1 in a reproducible manner (Fig. 5*E*). Recent advances in the synthesis and quantitative analysis of glutathione polysulfides by Ida *et al.* (57) will enable a more detailed kinetic analysis of GS-S-SG transport by ATMs in the near future.

The severely compromised growth of the *ethe1-1 atm3-1* double mutant compared with either parent suggests that an excess of glutathione persulfide accumulates in *atm3-1* mutants but is rapidly detoxified by the sulfur dioxygenase ETHE1 localized in the mitochondrial matrix (Fig. 7*E*). GS-S-SG would need to be chemically or enzymatically converted to GSSH to be a substrate of ETHE1, and GR2 or glutaredoxins are likely to catalyze this conversion (57). It should be noted that ETHE1 itself does not play a role in Fe-S cluster assembly (25), and the gene is absent from yeast. The physiological role of ETHE1 appears to be restricted to detoxification of persulfide bound to GSH rather than protein (53) and, in plants, to the catabolism of cysteine in cells undergoing high protein turnover (25).

In conclusion, we have identified two substrates of the mitochondrial ABC transporters, GSSG and GS-S-SG. Further biochemical studies are needed to establish how GS-S-SG is formed and delivered to the transporter and how the persulfide is transferred across the mitochondrial intermembrane space and delivered to cofactor assembly proteins in the cytosol.

Acknowledgments—We thank the following: Delphine G. Bernard for the generation of the oastlC atm3-1 double mutant; Jonathan M. Foster and Luke W. Browning for technical assistance; Lionel Hill for mass spectrometry; Markus Wirtz and Rüdiger Hell for analysis of thiols and for the oastlC mutant; Florian Bittner for antibodies raised against the NBD of Arabidopsis ATM3; Roland Lill for antibodies against yeast Atm1; Bert Poolman for the pERL plasmid; and Eric Geertsma for pREX plasmids.

REFERENCES

1. Balk, J., and Schaedler, T. A. (2014) Iron cofactor assembly in plants. *Annu. Rev. Plant Biol.* **65,** 125–153
2. Couturier, J., Touraine, B., Briat, J. F., Gaymard, F., and Rouhier, N. (2013) The iron-sulfur cluster assembly machineries in plants: current knowledge and open questions. *Front. Plant Sci.* **4,** 259
3. Bernard, D. G., Netz, D. J., Lagny, T. J., Pierik, A. J., and Balk, J. (2013) Requirements of the cytosolic iron-sulfur cluster assembly pathway in Arabidopsis. *Philos. Trans. R. Soc. Lond. B Biol. Sci.* **368,** 20120259
4. Lill, R. (2009) Function and biogenesis of iron-sulphur proteins. *Nature* **460,** 831–838
5. Kispal, G., Csere, P., Prohl, C., and Lill, R. (1999) The mitochondrial proteins Atm1p and Nfs1p are essential for biogenesis of cytosolic Fe/S proteins. *EMBO J.* **18,** 3981–3989
6. Bernard, D. G., Cheng, Y., Zhao, Y., and Balk, J. (2009) An allelic mutant series of ATM3 reveals its key role in the biogenesis of cytosolic iron-sulfur proteins in *Arabidopsis*. *Plant Physiol.* **151,** 590–602
7. Pondarré, C., Antiochos, B. B., Campagna, D. R., Clarke, S. L., Greer, E. L., Deck, K. M., McDonald, A., Han, A. P., Medlock, A., Kutok, J. L., Anderson, S. A., Eisenstein, R. S., and Fleming, M. D. (2006) The mitochondrial ATP-binding cassette transporter Abcb7 is essential in mice and participates in cytosolic iron-sulfur cluster biogenesis. *Hum. Mol. Genet.* **15,** 953–964
8. Mühlenhoff, U., Balk, J., Richhardt, N., Kaiser, J. T., Sipos, K., Kispal, G., and Lill, R. (2004) Functional characterization of the eukaryotic cysteine desulfurase Nfs1p from *Saccharomyces cerevisiae*. *J. Biol. Chem.* **279,** 36906–36915
9. Nakai, Y., Nakai, M., Hayashi, H., and Kagamiyama, H. (2001) Nuclear localization of yeast Nfs1p is required for cell survival. *J. Biol. Chem.* **276,** 8314–8320
10. Bittner, F., Oreb, M., and Mendel, R. R. (2001) ABA3 is a molybdenum cofactor sulfurase required for activation of aldehyde oxidase and xanthine dehydrogenase in *Arabidopsis thaliana*. *J. Biol. Chem.* **276,** 40381–40384
11. Srinivasan, V., Pierik, A. J., and Lill, R. (2014) Crystal structures of nucleotide-free and glutathione-bound mitochondrial ABC transporter Atm1. *Science* **343,** 1137–1140
12. Lee, J. Y., Yang, J. G., Zhitnitsky, D., Lewinson, O., and Rees, D. C. (2014) Structural basis for heavy metal detoxification by an Atm1-type ABC transporter. *Science* **343,** 1133–1136
13. Leighton, J., and Schatz, G. (1995) An ABC transporter in the mitochondrial inner membrane is required for normal growth of yeast. *EMBO J.* **14,** 188–195
14. Kushnir, S., Babiychuk, E., Storozhenko, S., Davey, M. W., Papenbrock, J., De Rycke, R., Engler, G., Stephan, U. W., Lange, H., Kispal, G., Lill, R., and Van Montagu, M. (2001) A mutation of the mitochondrial ABC transporter Sta1 leads to dwarfism and chlorosis in the *Arabidopsis* mutant *starik*. *Plant Cell* **13,** 89–100
15. Chen, S., Sánchez-Fernández, R., Lyver, E. R., Dancis, A., and Rea, P. A. (2007) Functional characterization of AtATM1, AtATM2, and AtATM3, a subfamily of *Arabidopsis* half-molecule ATP-binding cassette transporters implicated in iron homeostasis. *J. Biol. Chem.* **282,** 21561–21571
16. Csere, P., Lill, R., and Kispal, G. (1998) Identification of a human mitochondrial ABC transporter, the functional orthologue of yeast Atm1p. *FEBS Lett.* **441,** 266–270
17. Allikmets, R., Raskind, W. H., Hutchinson, A., Schueck, N. D., Dean, M., and Koeller, D. M. (1999) Mutation of a putative mitochondrial iron transporter gene (ABC7) in X-linked sideroblastic anemia and ataxia (XLSA/A). *Hum. Mol. Genet.* **8,** 743–749
18. Kispal, G., Csere, P., Guiard, B., and Lill, R. (1997) The ABC transporter Atm1p is required for mitochondrial iron homeostasis. *FEBS Lett.* **418,** 346–350
19. Outten, C. E., and Albetel, A. N. (2013) Iron sensing and regulation in *Saccharomyces cerevisiae*: Ironing out the mechanistic details. *Curr. Opin. Microbiol.* **16,** 662–668
20. Kim, D. Y., Bovet, L., Kushnir, S., Noh, E. W., Martinoia, E., and Lee, Y. (2006) AtATM3 is involved in heavy metal resistance in *Arabidopsis*. *Plant Physiol.* **140,** 922–932
21. Teschner, J., Lachmann, N., Schulze, J., Geisler, M., Selbach, K., Santamaria-Araujo, J., Balk, J., Mendel, R. R., and Bittner, F. (2010) A novel role for *Arabidopsis* mitochondrial ABC transporter ATM3 in molybdenum cofactor biosynthesis. *Plant Cell* **22,** 468–480
22. Sipos, K., Lange, H., Fekete, Z., Ullmann, P., Lill, R., and Kispal, G. (2002) Maturation of cytosolic iron-sulfur proteins requires glutathione. *J. Biol. Chem.* **277,** 26944–26949
23. Kuhnke, G., Neumann, K., Mühlenhoff, U., and Lill, R. (2006) Stimulation of the ATPase activity of the yeast mitochondrial ABC transporter Atm1p by thiol compounds. *Mol. Membr. Biol.* **23,** 173–184
24. Heeg, C., Kruse, C., Jost, R., Gutensohn, M., Ruppert, T., Wirtz, M., and Hell, R. (2008) Analysis of the *Arabidopsis* *O*-acetylserine(thiol)lyase gene family demonstrates compartment-specific differences in the regulation

of cysteine synthesis. *Plant Cell* **20,** 168–185
25. Krüssel, L., Junemann, J., Wirtz, M., Birke, H., Thornton, J. D., Browning, L. W., Poschet, G., Hell, R., Balk, J., Braun, H. P., and Hildebrandt, T. M. (2014) The mitochondrial sulfur dioxygenase ETHE1 is required for amino acid catabolism during carbohydrate starvation and seed development in *Arabidopsis thaliana*. *Plant Physiol.* **165,** 92–104
26. Marty, L., Siala, W., Schwarzländer, M., Fricker, M. D., Wirtz, M., Sweetlove, L. J., Meyer, Y., Meyer, A. J., Reichheld, J. P., and Hell, R. (2009) The NADPH-dependent thioredoxin system constitutes a functional backup for cytosolic glutathione reductase in *Arabidopsis*. *Proc. Natl. Acad. Sci. U.S.A.* **106,** 9109–9114
27. Albrecht, S. C., Sobotta, M. C., Bausewein, D., Aller, I., Hell, R., Dick, T. P., and Meyer, A. J. (2014) Redesign of genetically encoded biosensors for monitoring mitochondrial redox status in a broad range of model eukaryotes. *J. Biomol. Screen.* **19,** 379–386
28. Schwarzländer, M., Fricker, M. D., Müller, C., Marty, L., Brach, T., Novak, J., Sweetlove, L. J., Hell, R., and Meyer, A. J. (2008) Confocal imaging of glutathione redox potential in living plant cells. *J. Microsc.* **231,** 299–316
29. Lehmann, M., Schwarzländer, M., Obata, T., Sirikantaramas, S., Burow, M., Olsen, C. E., Tohge, T., Fricker, M. D., Møller, B. L., Fernie, A. R., Sweetlove, L. J., and Laxa, M. (2009) The metabolic response of *Arabidopsis* roots to oxidative stress is distinct from that of heterotrophic cells in culture and highlights a complex relationship between the levels of transcripts, metabolites, and flux. *Mol. Plant* **2,** 390–406
30. Venter, H., Velamakanni, S., Balakrishnan, L., and van Veen, H. W. (2008) On the energy-dependence of Hoechst 33342 transport by the ABC transporter LmrA. *Biochem. Pharmacol.* **75,** 866–874
31. de Ruyter, P. G., Kuipers, O. P., and de Vos, W. M. (1996) Controlled gene expression systems for *Lactococcus lactis* with the food-grade inducer nisin. *Appl. Environ. Microbiol.* **62,** 3662–3667
32. Geertsma, E. R., and Poolman, B. (2007) High-throughput cloning and expression in recalcitrant bacteria. *Nat. Methods* **4,** 705–707
33. Geertsma, E. R., and Dutzler, R. (2011) A versatile and efficient high-throughput cloning tool for structural biology. *Biochemistry* **50,** 3272–3278
34. Schaedler, T. A., Tong, Z., and van Veen, H. W. (2012) The multidrug transporter LmrP protein mediates selective calcium efflux. *J. Biol. Chem.* **287,** 27682–27690
35. Ravaud, S., Do Cao, M. A., Jidenko, M., Ebel, C., Le Maire, M., Jault, J. M., Di Pietro, A., Haser, R., and Aghajari, N. (2006) The ABC transporter BmrA from *Bacillus subtilis* is a functional dimer when in a detergent-solubilized state. *Biochem. J.* **395,** 345–353
36. Rohwerder, T., and Sand, W. (2003) The sulfane sulfur of persulfides is the actual substrate of the sulfur-oxidizing enzymes from *Acidithiobacillus* and *Acidiphilium* spp. *Microbiology* **149,** 1699–1710
37. Leier, I., Jedlitschky, G., Buchholz, U., Center, M., Cole, S. P., Deeley, R. G., and Keppler, D. (1996) ATP-dependent glutathione disulphide transport mediated by the MRP gene-encoded conjugate export pump. *Biochem. J.* **314,** 433–437
38. Griffith, O. W., and Meister, A. (1979) Potent and specific inhibition of glutathione synthesis by buthionine sulfoximine (*S-n*-butyl homocysteine sulfoximine). *J. Biol. Chem.* **254,** 7558–7560
39. Meyer, A. J., Brach, T., Marty, L., Kreye, S., Rouhier, N., Jacquot, J.-P., and Hell, R. (2007) Redox-sensitive GFP in *Arabidopsis thaliana* is a quantitative biosensor for the redox potential of the cellular glutathione redox buffer. *Plant J.* **52,** 973–986
40. de Ruyter, P. G., Kuipers, O. P., Beerthuyzen, M. M., van Alen-Boerrigter, I., and de Vos, W. M. (1996) Functional analysis of promoters in the nisin gene cluster of *Lactococcus lactis*. *J. Bacteriol.* **178,** 3434–3439
41. Mierau, I., and Kleerebezem, M. (2005) 10 years of the nisin-controlled gene expression system (NICE) in *Lactococcus lactis*. *Appl. Microbiol. Biotechnol.* **68,** 705–717
42. Li, Y., Hugenholtz, J., Abee, T., and Molenaar, D. (2003) Glutathione protects *Lactococcus lactis* against oxidative stress. *Appl. Environ. Microbiol.* **69,** 5739–5745
43. Seeger, M. A., and van Veen, H. W. (2009) Molecular basis of multidrug transport by ABC transporters. *Biochim. Biophys. Acta* **1794,** 725–737
44. Janvilisri, T., Venter, H., Shahi, S., Reuter, G., Balakrishnan, L., and van Veen, H. W. (2003) Sterol transport by the human breast cancer resistance protein (ABCG2) expressed in *Lactococcus lactis*. *J. Biol. Chem.* **278,** 20645–20651
45. Scarborough, G. A. (1995) Drug-stimulated ATPase activity of the human P-glycoprotein. *J. Bioenerg. Biomembr.* **27,** 37–41
46. Wood, J. L. (1987) Sulfane sulfur. *Methods Enzymol.* **143,** 25–29
47. Mao, Q., Leslie, E. M., Deeley, R. G., and Cole, S. P. (1999) ATPase activity of purified and reconstituted multidrug resistance protein MRP1 from drug-selected H69AR cells. *Biochim. Biophys. Acta* **1461,** 69–82
48. Senior, A. E., al-Shawi, M. K., and Urbatsch, I. L. (1995) The catalytic cycle of P-glycoprotein. *FEBS Lett.* **377,** 285–289
49. Bodo, A., Bakos, E., Szeri, F., Varadi, A., and Sarkadi, B. (2003) Differential modulation of the human liver conjugate transporters MRP2 and MRP3 by bile acids and organic anions. *J. Biol. Chem.* **278,** 23529–23537
50. Cole, S. P., and Deeley, R. G. (2006) Transport of glutathione and glutathione conjugates by MRP1. *Trends Pharmacol. Sci.* **27,** 438–446
51. Krumpochova, P., Sapthu, S., Brouwers, J. F., de Haas, M., de Vos, R., Borst, P., and van de Wetering, K. (2012) Transportomics: screening for substrates of ABC transporters in body fluids using vesicular transport assays. *FASEB J.* **26,** 738–747
52. Birke, H., Haas, F. H., De Kok, L. J., Balk, J., Wirtz, M., and Hell, R. (2012) Cysteine biosynthesis, in concert with a novel mechanism, contributes to sulfide detoxification in mitochondria of *Arabidopsis thaliana*. *Biochem. J.* **445,** 275–283
53. Tiranti, V., Viscomi, C., Hildebrandt, T., Di Meo, I., Mineri, R., Tiveron, C., Levitt, M. D., Prelle, A., Fagiolari, G., Rimoldi, M., and Zeviani, M. (2009) Loss of ETHE1, a mitochondrial dioxygenase, causes fatal sulfide toxicity in ethylmalonic encephalopathy. *Nat. Med.* **15,** 200–205
54. Holdorf, M. M., Owen, H. A., Lieber, S. R., Yuan, L., and Adams, N. (2012) Arabidopsis *ETHE1* encodes a sulfur dioxygenase that is essential for embryo and endosperm development. *Plant Physiol.* **160,** 226–236
55. Chew, O., Whelan, J., and Millar, A. H. (2003) Molecular definition of the ascorbate-glutathione cycle in *Arabidopsis* mitochondria reveals dual targeting of antioxidant defenses in plants. *J. Biol. Chem.* **278,** 46869–46877
56. Kessler, D. (2006) Enzymatic activation of sulfur for incorporation into biomolecules in prokaryotes. *FEMS Microbiol. Rev.* **30,** 825–840
57. Ida, T., Sawa, T., Ihara, H., Tsuchiya, Y., Watanabe, Y., Kumagai, Y., Suematsu, M., Motohashi, H., Fujii, S., Matsunaga, T., Yamamoto, M., Ono, K., Devarie-Baez, N. O., Xian, M., Fukuto, J. M., and Akaike, T. (2014) Reactive cysteine persulfides and *S*-polythiolation regulate oxidative stress and redox signaling. *Proc. Natl. Acad. Sci. U.S.A.* **111,** 7606–7611

Supplemental Table S1. List of all primers used.

NAME OF PRIMER	APPLICATION	SEQUENCE (5'-3')
SC_tr	Generation of Atm1 construct into pJET plasmid	ACG CAC AAA AAA TCC GTC GAG C
SC_REV_HIS	Generation of Atm1 construct into pJET plasmid	CTA AAA GAC CAG CAA GAA CTA CAC CAC CAC CAC CAC CAC TGA TCT AGA TTG G
ATM3_FX30_FOR	Generation of ATM3 construct for cloning into pREX plasmid	GCG TAT GCT CTT CTA GTT ACA GTC TTC GCT CTG
ATM3_FX60_FOR	Generation of ATM3 construct for cloning into pREX plasmid	GCG GAT GCT CTT CTA GTT TCC TCT CAG ATA ACT CAC
ATM3_FX97_FOR	Generation of ATM3 construct for cloning into pREX plasmid	GCA TAT GCT CTT CTA GT G ACC AAA CCA CCA CCA AGA C
ATM3_FX_REV	Generation of ATM3 construct for cloning into pREX plasmid	GCA TAT GCT CTT CTA GTG ACC AAA CCA CCA CCA AGA C
ATM1_DK_FOR	Site directed mutagenesis	CTA GCG GGA GCG GCT CAA CAA TTC TTA G
ATM1_DK_REV	Site directed mutagenesis	CTA AGA ATT GTT GAG CCG CTC CCG CTA G
ATM3_EQ_FOR	Site directed mutagenesis	GAT TCT GTT GTG TGA TCA GGC AAC GAG TGC GC
ATM3_EQ_REV	Site directed mutagenesis	GCG CAC TCG TTG CCT GAT CAC ACA ACA GAA TC
ETHE1_LP	Genotyping	ACAATTATC TCATGATTCGTGG
ETHE1_RP	Genotyping	CAGTCTTGTCCACCGGATCAAT
LBa1	Genotyping	TGGTTCACGTAGTGGGCCATCG
ATM3-F3	Genotyping	GACATCACAAATACAAGTGACGC
ATM3-R6	Genotyping	TTAGATGCTTAAACAGAAGAGG
NPTII-R2	Genotyping	CATAGCCGAATAGCC TCTCC

A Conserved Mitochondrial ATP-binding Cassette Transporter Exports Glutathione Polysulfide for Cytosolic Metal Cofactor Assembly

Theresia A. Schaedler, Jeremy D. Thornton, Inga Kruse, Markus Schwarzländer, Andreas J. Meyer, Hendrik W. van Veen and Janneke Balk

J. Biol. Chem. 2014, 289:23264-23274.
doi: 10.1074/jbc.M114.553438 originally published online July 8, 2014

Arabidopsis Glutaredoxin S17 and Its Partner, the Nuclear Factor Y Subunit C11/Negative Cofactor 2α, Contribute to Maintenance of the Shoot Apical Meristem under Long-Day Photoperiod[1]

Johannes Knuesting[2], Christophe Riondet[2], Carlos Maria, Inga Kruse, Noëlle Bécuwe, Nicolas König, Carsten Berndt, Sébastien Tourrette, Jocelyne Guilleminot-Montoya, Enrique Herrero, Frédéric Gaymard, Janneke Balk, Gemma Belli, Renate Scheibe, Jean-Philippe Reichheld, Nicolas Rouhier, and Pascal Rey*

Department of Plant Physiology, FB5, University of Osnabrück, D–49069 Osnabrueck, Germany (J.K., N.K., R.S.); Laboratoire Génome et Développement des Plantes, Université Perpignan Via Domitia, F–66860 Perpignan, France (C.R., J.G.-M., J.-P.R.); Laboratoire Génome et Développement des Plantes, Centre National de la Recherche Scientifique, F–66860 Perpignan, France (C.R., J.G.-M., J.-P.R.); Departament de Ciències Mèdiques Bàsiques, IRB Lleida, Universitat de Lleida, 25008 Lleida, Spain (C.M., E.H., G.B.); Department of Biological Chemistry, John Innes Centre, Norwich NR4 7UH, United Kingdom (I.K., J.B.); Commissariat à l'Energie Atomique et aux Energies Alternatives, DSV, IBEB, Laboratoire d'Ecophysiologie Moléculaire des Plantes, F–13108 Saint-Paul-lez-Durance, France (N.B., S.T., P.R.); Centre National de la Recherche Scientifique, Unité Mixte de Recherche 7265 Biologie Végétale and Microbiologie Environnementale, F–13108 Saint-Paul-lez-Durance, France (N.B., S.T., P.R.); Aix-Marseille Université, Service de Biologie Végétale et de Microbiologie Environnementales Unité Mixte de Recherche 7265, F–13284 Marseille, France (N.B., S.T., P.R.); Division for Biochemistry, Department for Medical Biochemistry and Biophysics, Karolinska Institutet, 17177 Stockholm, Sweden (C.B.); Department of Neurology, Medical Faculty, Heinrich-Heine-University, 40225 Duesseldorf, Germany (C.B.); Biochimie et Physiologie Moléculaire des Plantes, Centre National de la Recherche Scientifique, Institut National de la Recherche Agronomique, Université Montpellier, Montpellier cedex 1, France (F.G.); Université de Lorraine, Interactions Arbres-Microorganismes, Unité Mixte de Recherche 1136, F–54500 Vandoeuvre-lès-Nancy, France (N.R.); and Institut National de la Recherche Agronomique, Interactions Arbres-Microorganismes, Unité Mixte de Recherche 1136, F–54280 Champenoux, France (N.R.)

ORCID IDs: 0000-0002-6640-1240 (C.M.); 0000-0002-6140-6181 (R.S.).

Glutaredoxins (GRXs) catalyze the reduction of protein disulfide bonds using glutathione as a reductant. Certain GRXs are able to transfer iron-sulfur clusters to other proteins. To investigate the function of Arabidopsis (*Arabidopsis thaliana*) GRXS17, we applied a strategy combining biochemical, genetic, and physiological approaches. GRXS17 was localized in the nucleus and cytosol, and its expression was elevated in the shoot meristems and reproductive tissues. Recombinant GRXS17 bound Fe_2S_2 clusters, a property likely contributing to its ability to complement the defects of a Baker's yeast (*Saccharomyces cerevisiae*) strain lacking the mitochondrial GRX5. However, a *grxs17* knockout Arabidopsis mutant exhibited only a minor decrease in the activities of iron-sulfur enzymes, suggesting that its primary function is as a disulfide oxidoreductase. The *grxS17* plants were sensitive to high temperatures and long-day photoperiods, resulting in elongated leaves, compromised shoot apical meristem, and delayed bolting. Both environmental conditions applied simultaneously led to a growth arrest. Using affinity chromatography and split-Yellow Fluorescent Protein methods, a nuclear transcriptional regulator, the Nuclear Factor Y Subunit C11/Negative Cofactor 2α (NF-YC11/NC2α), was identified as a GRXS17 interacting partner. A mutant deficient in NF-YC11/NC2α exhibited similar phenotypes to *grxs17* in response to photoperiod. Therefore, we propose that GRXS17 interacts with NF-YC11/NC2α to relay a redox signal generated by the photoperiod to maintain meristem function.

[1] This work was supported by the Agence Nationale de la Recherche (grant nos. 2010 BLAN–1616 to C.R., N.B., S.T., J.G.-M., F.G., J.-P. R., N.R., and P.R.; BLAN 12–BSV6–0011 to C.R. and J.-P.R.; and JC07–204825 to N.R. and P.R.) and the German Research Foundation (grant nos. SPP 1710 BE3259/5–1 to C.B. and SCHE217/16–1 to R.S.).

[2] These authors contributed equally to the article.

* Address correspondence to pascal.rey@cea.fr.

The author responsible for distribution of materials integral to the findings presented in this article in accordance with the policy described in the Instructions for Authors (www.plantphysiol.org) is: Pascal Rey (pascal.rey@cea.fr).

www.plantphysiol.org/cgi/doi/10.1104/pp.15.00049

Glutaredoxins (GRXs) are small oxidoreductases structurally related to thioredoxins (TRXs) and present in most organisms (Rouhier et al., 2008; Meyer et al., 2009). Their capacity to reduce disulfide bonds is usually dependent on glutathione (GSH) and relies on a four-residue active-site motif comprising at least one redox-active Cys (Rouhier et al., 2006). In higher plants, GRXs are encoded by multigene families and subdivided into four classes (Couturier et al., 2009). GRXs from classes I and II are present in all photosynthetic organisms and possess, in most cases, the

motifs CPXC and CGFS as active sites, respectively. GRXs from class III are restricted to terrestrial plants and display a CCXX motif. Class IV GRXs are present in both green algae and terrestrial plants and composed of three domains: one N-terminal GRX module carrying a CXXC/S motif followed by two domains of unknown function.

Through their biochemical function as disulfide reductases, GRXs are thought to alter the activity of metabolic enzymes and transcriptional factors (Michelet et al., 2005; Murmu et al., 2010; Couturier et al., 2014). They also participate in the regeneration of thiol-dependent antioxidant enzymes (Rouhier et al., 2001; Gama et al., 2007; Tarrago et al., 2009; Couturier et al., 2011). Also, other functions have been proposed for classes I and II GRXs owing to their capacity to bind iron-sulfur clusters (Rouhier et al., 2007, 2010; Bandyopadhyay et al., 2008). For instance, oxidized GSH promotes iron-sulfur cluster disassembly from human GRX2 and restores disulfide reductase activity; therefore, class I GRXs may constitute redox sensors (Lillig et al., 2005). GRXs belonging to class II, also named monothiol GRXs, seem intimately linked to iron metabolism. Those present in mitochondria participate in iron-sulfur cluster assembly, most likely as iron-sulfur transfer proteins from scaffold proteins to acceptor proteins (Rodríguez-Manzaneque et al., 2002; Mühlenhoff et al., 2003; Bandyopadhyay et al., 2008). In addition, nucleocytosolic monothiol GRXs participate in iron sensing and trafficking in Baker's yeast (*Saccharomyces cerevisiae*) and animals (Ojeda et al., 2006; Pujol-Carrion et al., 2006; Kumánovics et al., 2008; Mühlenhoff et al., 2010; Haunhorst et al., 2013). However, it is not known if GRXs play a role in iron-sulfur cluster assembly or iron sensing in plants.

Recently, essential roles of plant GRXs have been unveiled in developmental processes and stress responses. Several Arabidopsis (*Arabidopsis thaliana*) GRXs from class III participate in the tolerance to photooxidative stress (Laporte et al., 2012) and defense against pathogens (Ndamukong et al., 2007; La Camera et al., 2011). Others are required for proper reproductive development through interaction with basic Leu zipper-type TGA transcription factors (Xing and Zachgo, 2008; Murmu et al., 2010). Concerning class I GRXs, an Arabidopsis mutant deficient in both GRXC1 and C2 has a lethal phenotype because of impaired embryo development (Riondet et al., 2012). Among the four class II GRXs (S14, S15, S16, and S17), the plastidial S14 isoform participates in arsenic tolerance in a hyperaccumulating fern (*Pteris vittata*; Sundaram et al., 2008) and is induced in response to high temperature in Arabidopsis (Sundaram and Rathinasabapathi, 2010). Tomato (*Solanum lycopersicum*) plants silenced for the expression of *GRXS16* encoding another plastid-localized GRX display increased sensitivity to osmotic stress (Guo et al., 2010). GRXS14 and GRXS15 are presumed to participate in responses to oxidative stress (Cheng et al., 2006; Cheng, 2008). Concerning GRXS17, Arabidopsis knockout plants growing at 28°C exhibited impaired primary root growth, impaired flowering, and altered sensitivity to auxin (Cheng et al., 2011). Consistently, ectopic expression of Arabidopsis GRXS17 in tomato plants resulted in enhanced thermotolerance (Wu et al., 2012).

In this work, we examined the physiological role of Arabidopsis GRXS17, which belongs to class II and has three CGFS active sites, in relation to its biochemical functions. Recombinant GRXS17 incorporated Fe_2S_2 clusters and complemented the Baker's yeast *grx5* mutant. However, in plants, GRXS17 had a minor role in iron-sulfur cluster metabolism, because the activities of cytosolic iron-sulfur-dependent enzymes were not substantially altered in *grxs17* mutant plants. In fact, *grxS17* plants exhibited severe developmental defects as a consequence of a perturbed shoot meristem, specifically at elevated temperatures and in long-day conditions. We show that GRXS17 interacts with the Nuclear Factor Y Subunit C11/Negative Cofactor 2α (NF-YC11/NC2α), which is also involved in the control of plant development as a function of photoperiod duration. Our data indicate that GRXS17 plays an important role in meristem maintenance and suggest that this role is fulfilled through the relay of a redox-dependent signal to NF-YC11/NC2α.

RESULTS

Expression of *GRXS17* in Arabidopsis Plant Organs and Subcellular Localization

To investigate the function of *GRXS17* in planta, we first analyzed its expression pattern. Previously published quantitative reverse transcription (RT)-PCR and promoter-GUS fusion data showed high *GRXS17* expression in growing leaves and anthers of Arabidopsis (Cheng et al., 2011). To gain more detail, the GRXS17 protein abundance in various organs was determined using a serum raised against the whole recombinant protein. The serum specifically recognized a protein at approximately 50 kD as shown by western-blot analysis of flower protein extracts from the wild type, and the signal was absent in homozygous *grxS17* plants (Fig. 1A; Supplemental Fig. S1). GRXS17 was substantially more abundant in stems, young leaves, and flowers. Note that the electrophoretic mobility of GRXS17 varies in leaf samples because of the proximity of Rubisco, which appears as a light-gray background band in *grxS17* extracts (Fig. 1, A and B). In situ hybridization was performed on shoot apical meristem (SAM) and flowers of Arabidopsis wild-type plants. A strong digoxigenin staining was found in all meristematic cells, particularly stem cells (Fig. 1, C and D), pollen, and ovules (Fig. 1, E and F). These data reveal that *GRXS17* is expressed in very different cell types localized in meristematic areas or reproductive and vascular organs.

To determine the subcellular localization of GRXS17, transient expression in protoplasts and stable expression of *P35S:GRXS17:GFP* fusion were undertaken. The results indicated that the protein is targeted to both cytosol

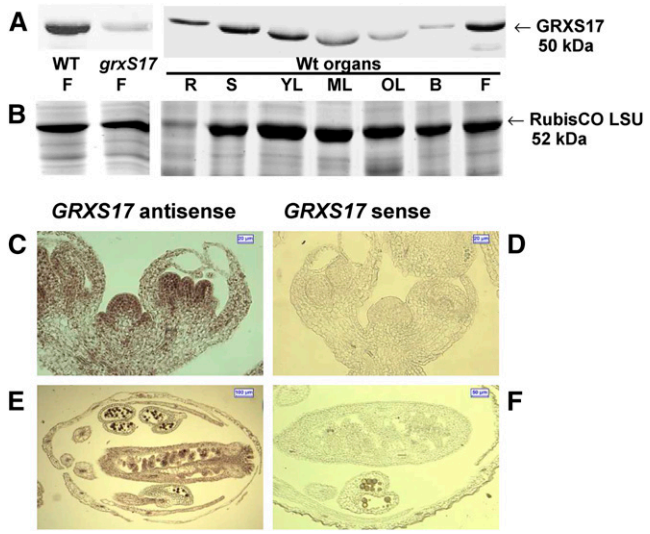

Figure 1. Expression of *GRXS17* in Arabidopsis plants. A and B, Western analysis of GRXS17 abundance. A, Western-blot analysis in flowers from wild-type and *grxS17* plants and organs of wild-type plants grown under standard conditions (20 μg per lane). The Rubisco Large Subunit (LSU) appears as a light-gray background band in the *grxS17* lane. B, Floral bud; F, flower; ML, mature leaf; OL, old leaf; R, root from adult plant; S, stem from bolting plant; WT, wild type; YL, young leaf. B, Loading controls: Coomassie Blue-stained gels (50-kD region). C to F, RNA in situ hybridization. Longitudinal sections of wild-type meristem inflorescences (C and D) and flower buds (E and F). Hybridizations were performed with antisense (C and E) or sense (D and F) GRXS17 cDNA probes.

and nucleus (Fig. 2, A and B). The nuclear localization is surprising considering the absence of a recognizable nuclear localization signal in GRXS17 sequence and the size of the fusion protein, which should be too big to freely diffuse through nuclear pores. Therefore, we prepared nuclear and cytosolic fractions from Arabidopsis inflorescences. Their relative purity was verified using sera against cytosolic and nuclear markers TRXh5 (Marchal et al., 2014) and Nucleolin1 (NUC1; Pontvianne et al., 2010), respectively. GRXS17 was detected in both fractions in agreement with GRXS17-GFP localization (Fig. 2C). No signal for GRXS17 was detected in mitochondrial or chloroplastic extracts (Supplemental Fig. S2).

Using bimolecular fluorescence complementation (BiFC; i.e. transient expression of two GRXS17 constructs fused to one-half Yellow Fluorescent Proteins (YFPs) in Arabidopsis protoplasts), we observed YFP signal confirming the nucleocytosolic localization and indicating that GRXS17 forms dimers in both compartments (Fig. 2D; Supplemental Fig. S3). The ability of GRXS17 to dimerize in vivo was further investigated in crude leaf extracts incubated with the cross-linker dimethyl pimelimidate/2 HCl (DMP). Upon nonreducing SDS-PAGE and western-blot analysis, a single band at 50 kD was apparent in untreated wild-type samples, and an additional 100-kD band, corresponding to a GRXS17 dimer, was specifically observed in the cross-linked extract (Fig. 2E). These data indicate that the GRX dimer is not formed by disulfide bridging.

Development of the *grxS17* Mutant in Response to Photoperiod

To analyze the physiological function of AtGRXS17, we isolated homozygous *grxS17* knockout plants from the Arabidopsis SALK_021301 line (Supplemental Fig. S1) and transformed this line with the *GRXS17* complementary DNA (cDNA) under the control of the *Cauliflower mosaic virus*-35S promoter. Two independent *grxS17* complemented lines, termed 3.3 and 17.8, were generated, and transgene expression was confirmed at the protein level (Supplemental Fig. S1). The phenotype

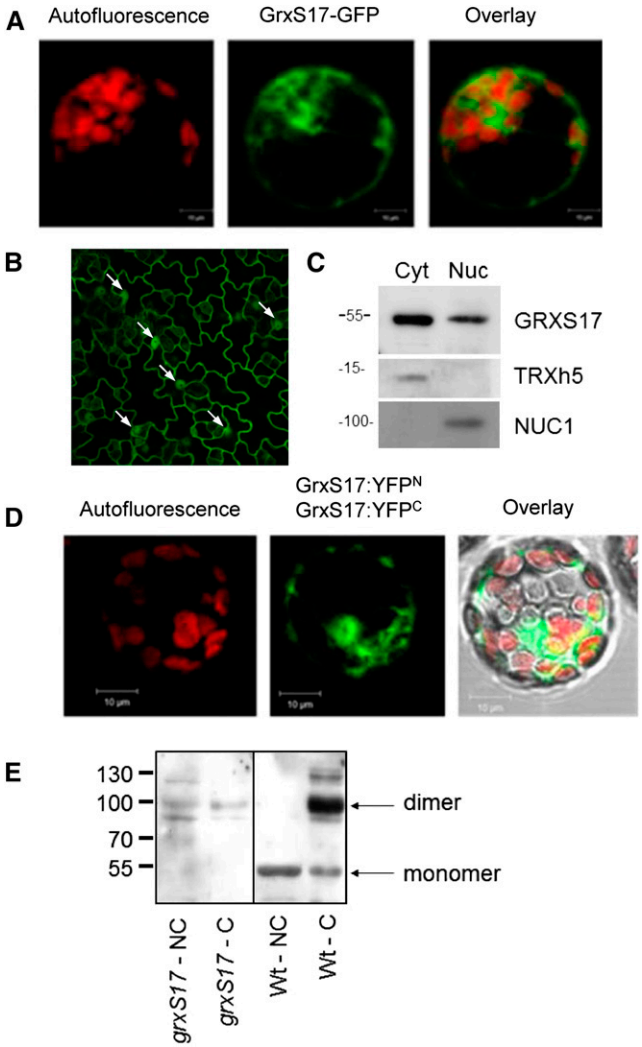

Figure 2. Subcellular localization and dimerization of GRXS17. A, Transient expression of a GRXS17:GFP fusion in Arabidopsis mesophyll protoplasts. Autofluorescence of chlorophyll indicates chloroplasts. B, Stable expression of a GRXS17:GFP fusion in Arabidopsis leaves. White arrows indicate nuclei. C, Immunodetection of GRXS17, TRXh5, and nucleolin NUC1 in cytosolic (Cyt) and nuclear (Nuc) extracts of Arabidopsis flower buds. D, BiFC assay of GRXS17. Vectors encoding C- and N-terminal split-YFP fusions with GRXS17 were cotransformed into Arabidopsis mesophyll protoplasts. E, Immunodetection of GRXS17 in *grxS17* and wild-type extracts cross-linked (C) or not (NC) with DMP. WT, Wild type.

characteristics of *grxS17* mutant and complemented lines were investigated under various light and temperature conditions. When cultivated under standard conditions (22°C/18°C day-night regime, 8-h photoperiod, and 200 μmol photons m^{-2} s^{-1}), all lines showed a similar development (Fig. 3A). Transfer of 2.5-week-old seedlings to 28°C and standard light for 2.5 weeks strongly impaired development of all genotypes, which displayed thin and elongated leaves. In addition, the *grxS17* mutant failed to form new leaves, which was partially or entirely complemented in lines 3.3 and 17.8, respectively (Fig. 3B). These data indicate that GRXS17 is required for maintenance of the SAM at high temperature, consistent with the previously reported thermosensitivity of the *grxS17* line (Cheng et al., 2011).

When plants were grown at 22°C and moderate light but under long-day photoperiod (16-h-day/8-h-night cycle), we observed that 4-week-old *grxS17* plants displayed elongated and thickened lamina (Fig. 3C). The development of the main floral spike (raceme) was delayed, which entirely failed to form when plants were shifted to continuous light (Fig. 3D). To analyze whether the phenotype appearance is caused by day length or related to the total light inception, plants grown for 2 weeks under standard conditions were transferred to high-light (500 μmol photons m^{-2} s^{-1}), 22°C, and short-day conditions. After 3 weeks, there was no change in *grxS17* development in this light regime (Supplemental Fig. S4A), indicating that photoperiod duration is the primary determinant for the observed phenotype. When plants were grown under the same high-light intensity under long days, *grxS17* exhibited strongly impaired development (Supplemental Figs. S4B and S5G). It is worth mentioning that the temperature measured at the plant level is elevated by 2°C (24°C) in high-light conditions, thus possibly explaining the more severe phenotype in long days at high light compared with moderate light. Under this light regime, there was no visual evidence of photooxidative damage in *grxS17* leaves (Supplemental Fig. S4B). This was confirmed by autoluminescence imaging (Supplemental Fig. S6), which allows recording of the photon emission associated with lipid peroxidation (Havaux et al., 2006). When combining high temperature and long day, we observed that *grxS17* growth stopped after a few days (Fig. 3E). Interestingly, the growth and the reproductive development of *grxS17* plants cultivated for 4 weeks in long-day conditions at 15°C were not modified (Fig. 3F). Similarly, when young

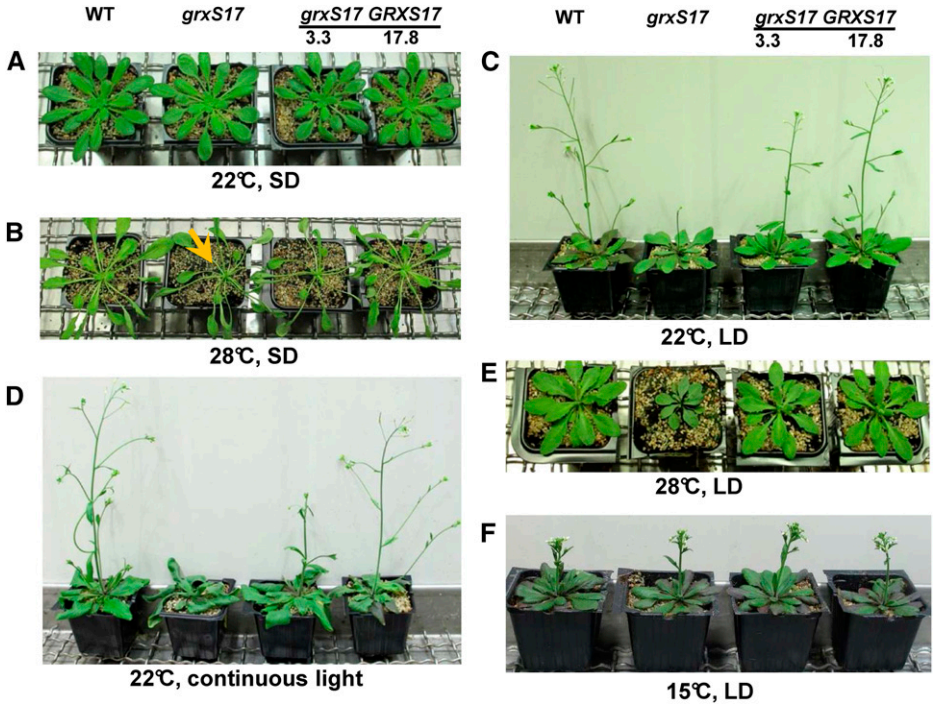

Figure 3. Growth and development of plants modified in *GRXS17* expression as a function of photoperiod and temperature. A, Five-week-old plants grown in standard conditions (8-h photoperiod and 200 μmol photons m^{-2} s^{-1}) at 22°C. B, Plants grown for 2.5 weeks in standard conditions and transferred to 28°C (8-h photoperiod and 200 μmol photons m^{-2} s^{-1}) for 2.5 weeks. The arrow indicates the absence of young leaves. C, Plants grown in long-day photoperiod conditions (16 h and 200 μmol photons m^{-2} s^{-1}) at 22°C. D, Plants grown for 2 weeks in standard conditions and transferred to continuous light (200 μmol photons m^{-2} s^{-1} and 22°C) for 3 weeks. E, Plants grown for 2 weeks in standard conditions and transferred to 28°C and long-day photoperiod (16 h and 200 μmol photons m^{-2} s^{-1}) for 2.5 weeks. F, Plants grown for 3 weeks in standard conditions and transferred to 15°C and long-day photoperiod (16 h and 200 μmol photons m^{-2} s^{-1}) for 4 weeks. *grxS17*, Homozygous SALK_021301 plants; *grxS17* 3.3 and 17.8, two independent *grxS17* lines expressing *GRXS17*; LD, long (16-h) day; SD, short (8-h) day; WT, wild type.

plants were transferred to long-day conditions at 15°C and high light (500 μmol photons m^{-2} s^{-1}), no alteration was noticed in *grxS17* (Supplemental Fig. S4C). Altogether, these data reveal that plants deficient in GRXS17 display sensitivity to a long-day regime in a temperature-dependent manner.

When *grxS17* plants were grown under long-day and high-light conditions, a significant delay of bolting was observed. These plants only formed secondary floral spikes after some time (Supplemental Fig. S5, B, D, F, and G). In short-day conditions, floral development was even accelerated (Supplemental Fig. S5, A, C, and E), whereas *grxS17* vegetative growth was not affected. Complemented lines exhibited contrasting phenotypes under short day: one line (3.3) flowering like the mutant and the other (17.8) flowering like the wild type. The difference could originate from the much higher GRXS17 amount in the latter (Supplemental Fig. S1). Collectively, these data point to the central role of GRXS17 in conveying environmental variations, such as temperature and day length, to coordinate the flowering response in plants.

The SAM Is Compromised in the *grxS17* Mutant

Because floral induction depends on the transition of the SAM from vegetative to reproductive fate (Levy and Dean, 1998), we performed histological analysis of SAM in *grxS17* mutants. The SAM overall structure was not altered in the mutant grown in short-day conditions (Supplemental Fig. S7). On the contrary, when grown under long days, the meristem area was smaller in *grxS17* compared with the wild type (Fig. 4A). The cell numbers in L1, L2, and L3 layers were 45% lower in *grxS17* than in the wild type, revealing impairment in the division of stem cells (Fig. 4C). Moreover, the size of meristematic cells was noticeably increased in the mutant (Fig. 4A), suggesting that the lower cell division rates are associated with increased cell expansion. These changes in meristematic cell size and numbers are consistent with the high *GRXS17* expression level observed in the meristem (Fig. 1C) and likely lead to the impaired development of *grxS17* plants observed under conditions of long-day photoperiod and/or high temperature (Fig. 3; Supplemental Fig. S5). Histological analysis of mesophyll cells in plants grown under long-day and high-light conditions revealed a reduced cell density in mutant plants (652 ± 79 cells mm^{-2}) compared with the wild type (1,148 ± 68 cells mm^{-2}) and a much larger cell size (Fig. 4, B and D). These data indicate that GRXS17 is required for cell division under long-day conditions.

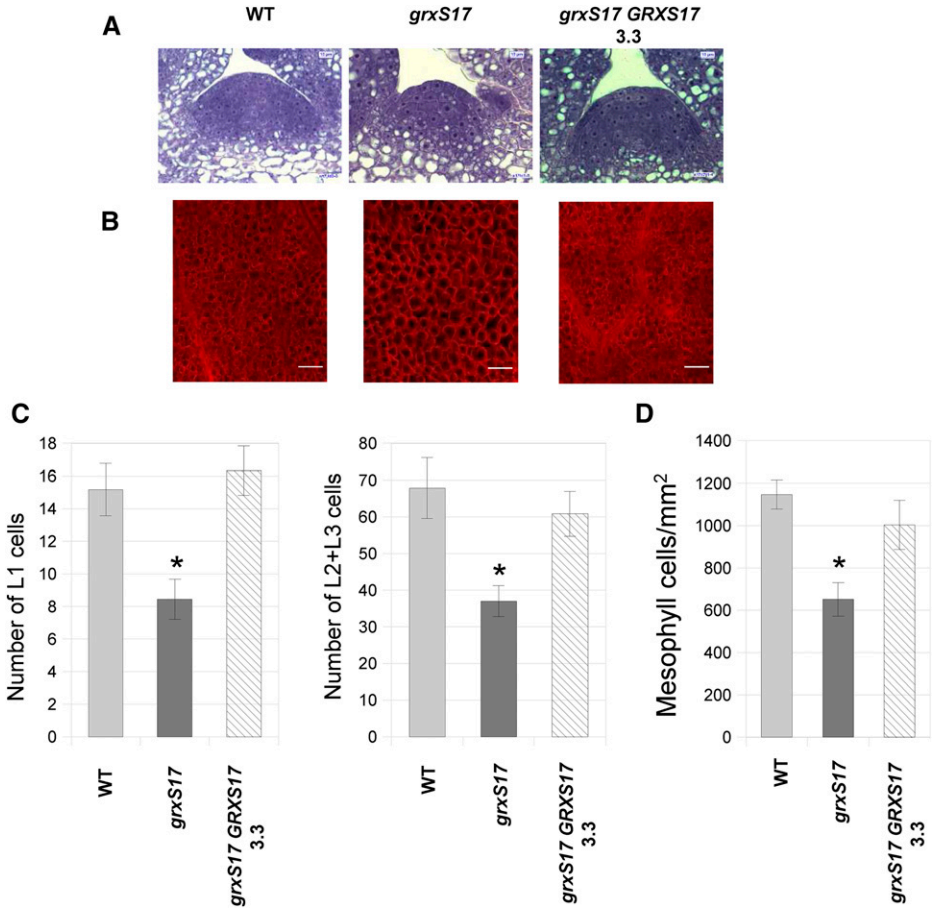

Figure 4. Structure of SAM and leaves in *grxS17* plants. A, Histological structure of the SAM stained by toluidine blue in 7-d-old wild-type, *grxS17*, and g*rxS17 GRXS17* (line 3.3) plants grown in long-day conditions (16 h) and high light (500 μmol photons m^{-2} s^{-1}). B, Observation of mesophyll cells in leaves of 3-week-old plants grown under long-day/high-light conditions. C, Number of L1, L2, and L3 layer stem cells in the SAM cross sections shown in A. Ten sections per genotype were analyzed. D, Density of mesophyll cells in the sections shown in B (n = 12). WT, Wild type. *, Value significantly different from wild-type value with $P < 0.05$ (Student's t test).

AtGRXS17 Architecture and Capacity to Bind Iron-Sulfur Clusters

To investigate the biochemical function of AtGRXS17 and how this could affect meristem development, we first analyzed the capacity of the protein to bind iron-sulfur clusters. Arabidopsis GRXS17 possesses an N-terminal TRX-like domain with a WCDAS motif in place of the canonical WCGPC active site followed by three GRX domains containing CGFS motifs (Fig. 5A). This architecture is unique to land plants, because mammalian, fungal, and algal homologs consist of one TRX and maximally, two GRX domains (Couturier et al., 2009a, 2009b). The GRX modules of GRXS17 share 62% to 65% identity and are subsequently referred to as M2, M3, and M4. From secondary structure prediction and three-dimensional structure modeling, the four AtGRXS17 domains all adopt a classical TRX fold and are connected by long linker sequences (Supplemental Fig. S8). The capacity of recombinant AtGRXS17 to incorporate iron-sulfur clusters, like other Arabidopsis CGFS GRXs (Bandyopadhyay et al., 2008), was analyzed after anaerobic in vitro reconstitution mediated by the Cys desulfurase *Isc*S in the presence of GSH. Indeed, upon purification of GRXS17, the oxygen-sensitive iron-sulfur clusters are lost; therefore, reconstitution of the clusters guarantees a sufficient amount of holo-GRXS17 for spectroscopy analysis. The UV-visible spectrum of the reconstituted GRXS17 showed absorbance peaks at 320 nm and around 420 nm, similar to other iron-sulfur cluster-coordinating GRXs and typical for Fe_2S_2 clusters (Fig. 5B). Estimation of the iron content in a freshly reconstituted wild-type protein indicated the presence of 2.48 $\pm$ 0.58 iron atoms per monomer. To investigate the contribution of each domain to cluster binding, the active-site cysteines were replaced by Ser either individually or in all three GRX domains. Whereas the triple-Cys mutant (C179/309/416S) did not incorporate any iron-sulfur cluster upon in vitro reconstitution, variants carrying one single substitution all incorporated between 40% and 60% of clusters as assessed by relative absorbance measurements at 420 nm (Fig. 5C). Because each of the active-site cysteines of the GRX subunits contributed to Fe_2S_2 incorporation, these data—together with the quantification of iron—indicate that AtGRXS17 dimers incorporate three Fe_2S_2 clusters in vitro, involving each GRX domain. Furthermore, the stoichiometry indicates that the GSH included in the reconstitution assay acts as an iron-sulfur cluster ligand as described for all other CGFS GRXs.

Arabidopsis GRXS17 Rescues Most Baker's Yeast *grx5* Mutant Phenotypes

To further investigate a possible role of GRXS17 as an iron-sulfur cluster transfer protein, its capacity to rescue the defects of a Baker's yeast *grx* mutant was examined. The entire protein or the three individual GRX domains were fused to the Grx5 mitochondrial targeting sequence and a C-terminal hemaglutinin (HA) tag. The constructs were expressed in Baker's yeast, and the localization of the Arabidopsis proteins in the mitochondrial matrix was confirmed by western-blot analysis (Supplemental Fig. S9). Phenotype studies indicated that only the entire protein (the wild type) and the M3 module, to a lesser extent, rescued the sensitivity to two externally added oxidants, for which Baker's yeast *grx5* mutant cells are hypersensitive (Rodríguez-Manzaneque et al., 2002): *tert*-butyl hydroperoxide (causing general oxidative damage on cellular macromolecules) and diamide (specific oxidant of thiol groups; Fig. 6A). When grown under

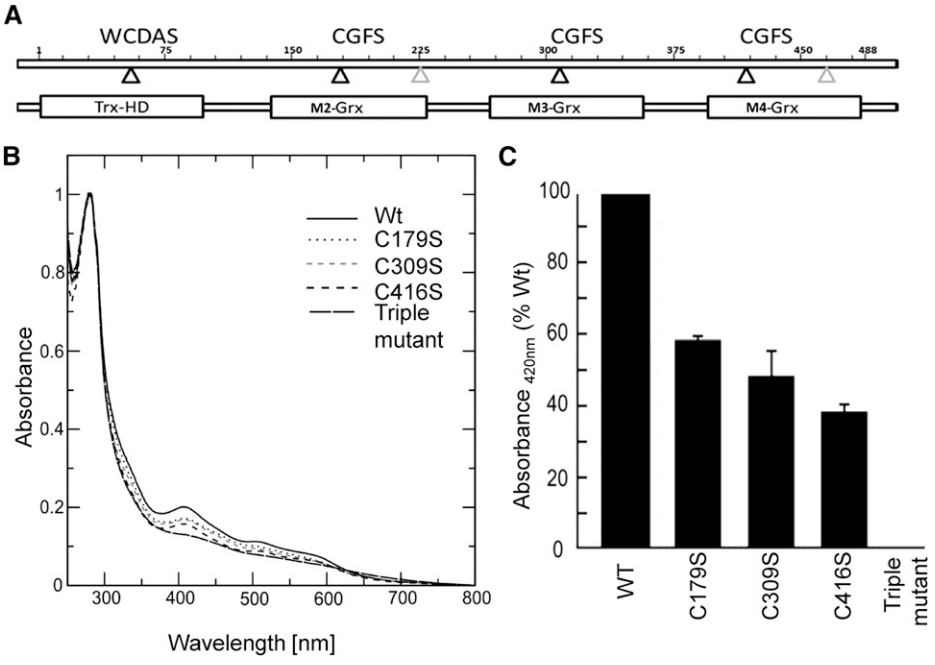

Figure 5. Incorporation of iron-sulfur clusters into recombinant wild-type and mutated AtGRXS17. A, Domain structure of GRXS17. Positions of active-site cysteines are indicated by black triangles, and positions of other Cys are indicated by gray triangles. M2-GRX, M3-GRX, and M4-GRX are three monothiol-GRX domains. TRX-HD, TRX-like homology domain; WCDAS. B, Absorption spectra of GRXS17 and Cys mutants. UV-visible absorption spectra were recorded immediately after in vitro reconstitution in anaerobic conditions. The active-site cysteines of each GRX domain were individually or together substituted by Ser (M2:C179S, M3:C309S, M4:C416S, and C179/309/416S). C, Relative absorption at 420 nm of GRXS17 mutants. WT, Wild type.

obligate respiratory conditions (glycerol as the carbon source), both the M3 and M4 modules in addition to the entire GRXS17 molecule totally or partially rescued the Baker's yeast *grx5*-defective phenotype (Fig. 6B). The M3 module also fully rescued, like GRXS17, the ability to express active aconitase holoenzyme (Fig. 6C) and mostly restored isopropylmalate isomerase (Leu-1) activity (Fig. 6D). These two iron-sulfur-containing enzymes are located in mitochondria and cytosol, respectively, and both are dependent on the mitochondrial iron-sulfur cluster assembly pathway. We then checked the expression of iron uptake genes by determining the transcript levels of two reporter genes of the Activation of ferrous transport1 regulon, *FTR1* (for *Fe Transporter1*) and *FIT3* (for *Facilitator of Iron Transport3*). Of the three modules, only M3 restored repression of both genes in *grx5* cells, whereas the entire GRXS17 molecule was unable to repress *FTR1* and *FIT3* expression (Fig. 6E), indicating that one component participating in iron status signaling is still deficient and that this could be caused by some steric incompatibility linked to the modular architecture of GRXS17. Accordingly, the M3 domain suppressed iron accumulation in *grx5*. Of note, expression of the entire GRXS17 protein also prevented iron accumulation (Fig. 6F). To summarize, the entire AtGRXS17 rescued most *grx5* phenotypes, notably the activities of iron-sulfur-containing enzymes.

GRXS17 Plays a Minor Role in Maintaining the Activity of Cytosolic Iron-Sulfur Enzymes

Next, we investigated whether GRXS17 fulfils a role in iron-sulfur cluster assembly in Arabidopsis. Therefore, activities and/or abundance of iron-sulfur enzymes were analyzed, including aconitases (one Fe_4S_4), aldehyde oxidases (two Fe_2S_2, FAD, and molybdenum cofactors), and PSI (three Fe_4S_4). All measurements were performed using 2-week-old seedlings grown under conditions where mild phenotypic changes are visible (22°C and 16 h of light) or conditions leading to severely impaired growth in *grxS17* (plants shifted to 28°C and 16 h of light; Supplemental Fig. S10A). Two mutant alleles of *ABC TRANSPORTER OF THE MITOCHONDRIA3/ABCB25* (*ATM3*) encoding a transporter that provides persulfide for cytosolic iron-sulfur cluster assembly (Schaedler et al., 2014) were used for comparison. The *atm3-1* and *atm3-4* mutants are strong and weak mutant alleles, respectively, that have significantly decreased activities of aldehyde oxidases and cytosolic aconitase (Bernard et al., 2009). Protein

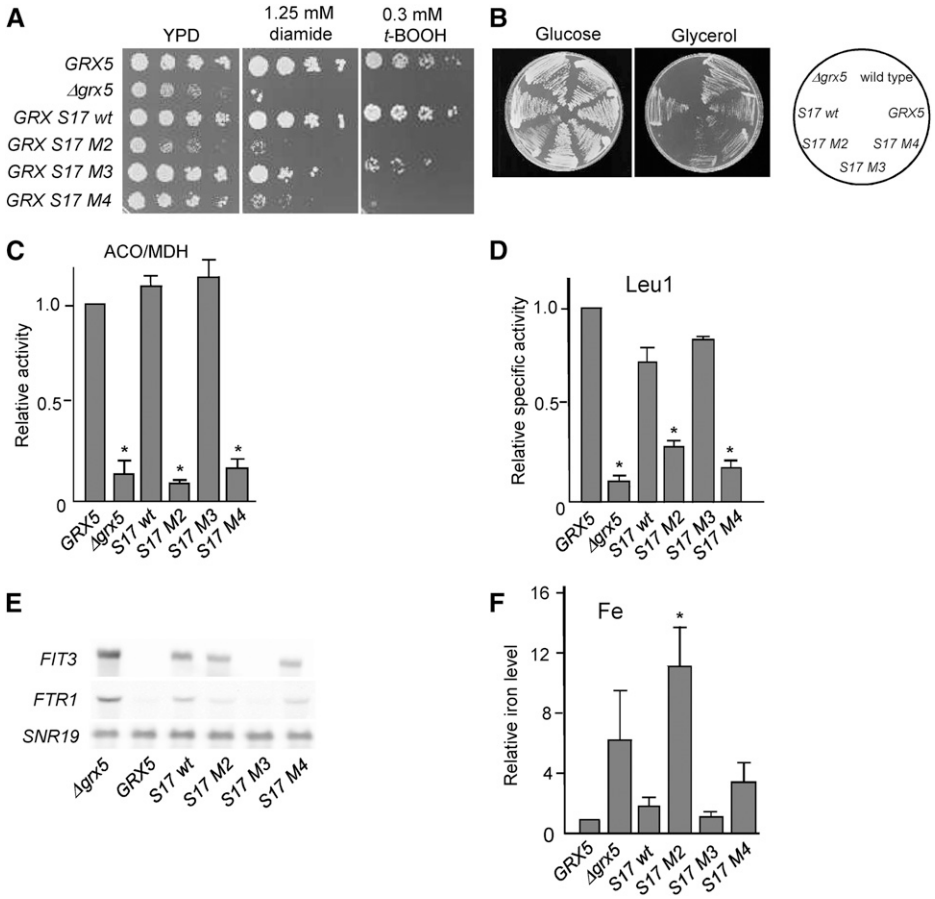

Figure 6. Rescue of the Baker's yeast *grx5* mutant defects by AtGRXS17. A, Sensitivity to *tert*-butyl hydroperoxide (*t*-BOOH) or diamide. The indicated Baker's yeast strains were spotted on YPD plates at 10× serial dilutions and grown for 3 d at 30°C on YPD plates. B, Growth on Glc (YPD plates) or glycerol (YPGly plates) after 3 d at 30°C. C, Relative ratio between aconitase and malate dehydrogenase (MDH) activities normalized with respect to the ratio in the wild-type strain in exponential cultures at 30°C in yeast extract-peptone-Gal medium. D, Relative specific Leu-1 activity. E, Northern-blot analysis of *FIT3* and *FTR1* mRNA levels from exponential cultures at 30°C. Loading control: *SNR19* (for *Small Nuclear RNA*). F, Relative iron content from exponential cultures at 30°C in YPD medium. Mean ± SD ($n = 3$). ACO, Aconitase; WT, wild type. *, Statistically significant differences (Student's *t* test, $P < 0.05$) compared with wild-type (*GRX5*) cultures.

extracts from leaf samples were separated by native gel electrophoresis followed by in-gel activity staining. Part of the same protein extract was subjected to denaturing SDS-PAGE and western blotting to estimate protein levels of aconitase and PSI. As expected for a cytosolic protein, GRXS17 is not required for the maturation of mitochondrial (aconitases) and plastidial (PSI) iron-sulfur proteins (Fig. 7A). In *grxS17* plants grown at 22°C, the amount of total aconitase protein was approximately 40% of the wild type, corresponding to a similar decrease in activity of the cytosolic isoform (Fig. 7). Aldehyde oxidase activity was decreased to approximately 50% in *grxS17* at this temperature compared with less than 5% in *atm3-4* (Fig. 7A, left; Supplemental Fig. S10B). In the complemented 3.3 line, the activities at 22°C of cytosolic aconitase and aldehyde oxidase were partially restored, and they were fully restored in the 17.8 line. In *grxS17* plants grown at 28°C, the activities of the mitochondrial aconitase isoforms were increased, and total aconitase protein levels were close to wild-type levels (Fig. 7, right). Furthermore, there was no difference in aldehyde oxidase activity at this temperature (Supplemental Fig. S10B, right). Compared with the *atm3* alleles, neither of which is a knockout, the *grxS17* knockout mutant displayed a relatively moderate decrease in cytosolic iron-sulfur enzymes in environmental conditions that leads to strongly impaired development. Taken together, these data suggest that GRXS17, despite its capacity to bind iron-sulfur clusters in vitro and rescue the Baker's yeast *grx5* mutant, does not play a critical function in de novo synthesis of iron-sulfur clusters in planta.

Identification of a Nuclear Factor Interacting with GRXS17

To explore other possibilities for how GRXS17 functions in meristem development, we performed affinity chromatography using a nickel matrix loaded with His-tagged GRXS17 to identify interacting proteins. After applying a crude leaf extract, the bound proteins were eluted with dithiothreitol (DTT) and identified by mass spectrometry. A number of proteins were repeatedly isolated in 15 independent affinity experiments (Table I). Interestingly, the predicted or experimentally determined localization of most proteins (e.g. cytosol or nucleus) is comparable with that of GRXS17. In accordance with a role of GRXS17 in redox signaling pathways and the known interaction of GRX3/protein kinase C-interacting cousin of thioredoxin with protein kinase C in animal cells, one transcription factor and one kinase were identified. The At3g12480 gene product NF-YC11/NC2α isolated in 7 of 15 experiments displayed high peptide sequence coverage. This partner was selected for deeper investigations, because proteins of the NF-Y family are known nuclear factors regulating developmental processes (Kumimoto et al., 2010). Transient expression of NF-YC11/NC2α-GFP in Arabidopsis protoplasts indicated that the protein is localized in both cytosol and nucleus (Fig. 8A), like GRXS17. The interaction between both proteins was further confirmed using BiFC exclusively in the nucleus (Fig. 8B; Supplemental Fig. S3).

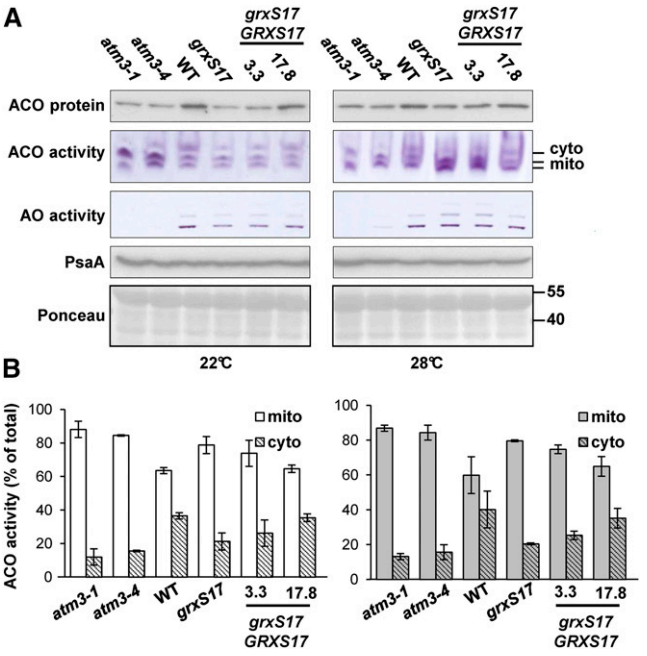

Figure 7. Activities and levels of iron-sulfur enzymes in plants modified in *GRXS17* expression. The wild type, a *grxS17* knockout mutant, and two complemented lines (3.3 and 17.8) were grown for 14 d under standard conditions (22°C) or transferred to 28°C after 7 d (Supplemental Fig. S10). Mutant alleles in the *atm3-1* and *atm3-4* were used for comparison. A, Activities of aconitase (ACO) and aldehyde oxidase (AO) isozymes visualized as a formazan precipitate in a native gel assay. Cytosolic (cyto) and mitochondrial (mito) isoforms of ACO are indicated. Equal protein amounts (160 μg for ACO and 60 μg for AO) were loaded per lane. Immunoblotting of ACO and *Psa*A (a subunit of PSI) in Arabidopsis seedlings (10 μg of protein per lane) and loading control (Ponceau). B, Relative activities of cyto and mito ACO isoforms from A quantified using ImageJ software. The values are given as percentages of the sum of the band intensities per lane (mean ± SD). The data are representative of three independent experiments. WT, Wild type.

Development of *nf-yc11/nc2α* Plants as a Function of Photoperiod

We isolated knockout plants for *NF-YC11/NC2α* expression from the German Plant Genomics Research Program-Kat 042E02 line (Kleinboelting et al., 2012), and only 4% as opposed to the expected 25% homozygous *nf-yc11/nc2α* plants were recovered in the T2 progeny (Fig. 9, A and B). When grown under short-day conditions and moderate light, *nf-yc11/nc2α* plants showed slow and altered development, with a compact rosette, small leaves, and a disorganized floral spike (Fig. 9D; Supplemental Fig. S11C). We transferred 33-d-old *nf-yc11/nc2α* plants grown in short- to long-day conditions and observed a strongly reduced development of the main spike and many secondary inflorescences compared with the wild type (Fig. 3C; Supplemental Fig. S11C). We then compared the development of wild-type, *nf-yc11/nc2α*, and *grxS17* seedlings under short- and long-day conditions (Fig. 9C). We did not observe any difference in germination and cotyledon development for the three genotypes in both photoperiod conditions. Whereas in

Table I. *Putative interaction partners of AtGRXS17*

The list includes the proteins identified at least four times in 15 independent affinity chromatography experiments with His-tagged AtGRXS17. CY, Cytosol; ER, endoplasmic reticulum; ES, extracellular space; MI, mitochondria; NU, nucleus; PL, plastid; PM, plasma membrane; PX, peroxisome.

Accession No.	Protein Name	Function	Subcellular Localization[a]	Sequence Length	Protein Identification[b]	Sequence Coverage[c]
				Amino acids	*Times*	*%*
At4g04950	GRXS17	Cell redox homeostasis	CY, NU, PL	488	15	90
At1g50570	Calcium-dependent lipid-binding family protein	Unknown	NU	388	13	68
At3g12480	NF-YC11/NC2α	Transcription factor	CY, MI, NU, PL	293	7	59
At4g25860	Oxysterol-binding protein-related protein 4A	Sterol transport	CY	386	11	56
At3g13460	Calcineurin B-Like-Interacting Protein Kinase1 interacting protein Evolutionarily Conserved C-terminal Region2	Unknown	CY, NU, PL	667	6	52
At2g39960	Microsomal signal peptidase	Peptidase activity	CY, ER, MI, PM	192	5	45
At1g13440	GapC2	Glycolysis	CY, MI, NU, PL, PX	338	9	41
At5g46570	Brassinosteroid-signaling kinase2	Protein phosphorylation	CY, PM	492	5	41
At4g31180	Asp-tRNA ligase-like protein	Aspartyl-tRNA synthetase activity	CY, PL	270	4	31
At5g11870	Alkaline phytoceramidase	Hydrolase activity	ES, MI, PL, PM	270	8	28
At5g54050	Cys/His-rich C1 domain-containing protein	Protein-disulfide reductase activity	ES, NU	580	8	21
At5g20830	Suc synthase1	UDP-glycosyltransferase activity	CY, MI	808	4	19
At1g24510	T-complex protein1 subunit-ε	Chaperone activity	CY, MI, PM	535	6	18
At4g22030	Probable F-box protein	Unknown	CY, MI, PL	626	5	12

[a]Subcellular localization predicted by the BAR Cell eFP Browser. [b]Proteins were identified because of the presence of their peptides in the indicated number of experiments. [c]Identified peptides with a MOWSE score higher than 15 were used to calculate the total sequence coverage.

the short-day photoperiod, the first two leaves appeared at the same time in the three lines, the development of these two leaves was substantially delayed in *nf-yc11/nc2α* and *grxS17* plants in long-day conditions (Fig. 9C). We analyzed the phenotype of *nf-yc11/nc2α* plants after sowing in long-day photoperiod and high-light conditions. We observed that growth and development of these plants were more perturbed than in control conditions (Fig. 9D). Particularly, *nf-yc11/nc2α* plants remained much smaller than wild-type and *grxS17* plants. They exhibited elongated and distorted leaves, a trait characteristic shared by the *grxS17* mutant. In these long-day conditions, no main floral spike was observed, and only secondary small spikes developed (Supplemental Fig. S11C). Taken together, these observations indicate that NF-YC11/NC2α participates in plant developmental processes in relation to the photoperiod duration and reveal that *nf-yc11/nc2α* and *grxS17* plants share similar developmental characteristics in long-day conditions.

DISCUSSION

Physiological Function of GRXS17 in Relation to Its Biochemical Properties

In this work, we showed that GRXS17 is a central element for plant development in relation to environmental factors, such as photoperiod and temperature, and we investigated whether a major function in iron-sulfur protein biogenesis may underpin its physiological role. Previous studies indicated that multidomain GRX orthologs from Baker's yeast and vertebrates bind iron-sulfur clusters and modify the activity of iron-responsive transcriptional regulators (Ojeda et al., 2006; Pujol-Carrion et al., 2006; Kumánovics et al., 2008; Mercier and Labbé, 2009; Jbel et al., 2011), affecting the intracellular iron distribution

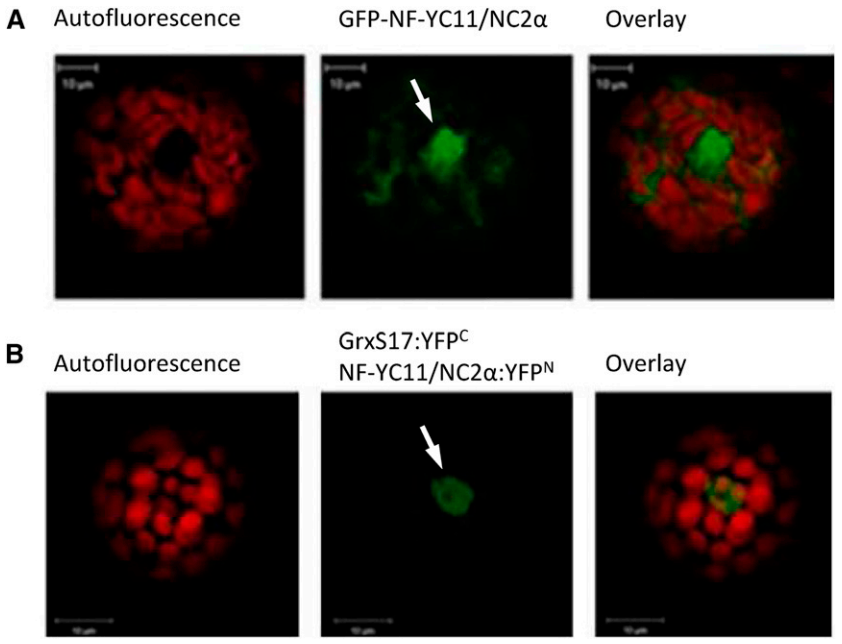

Figure 8. Localization of NF-YC11/NC2α and interaction with GRXS17. Isolated Arabidopsis mesophyll protoplasts were transiently transformed with an NF-YC11/NC2α:GFP fusion (A) or split-YFP constructs containing GRXS17 or NF-YC11/NC2α (B). White arrows indicate nuclei.

through the maturation of most iron-containing proteins (Mühlenhoff et al., 2010; Haunhorst et al., 2013). Accordingly, we showed that AtGRXS17 is able to bind Fe_2S_2 clusters by in vitro reconstitution experiments and complement the defects in iron-sulfur cluster maturation of the Baker's yeast *grx5* strain (Figs. 5 and 6). However, we found that GRXS17 in Arabidopsis does not play a major role in iron-sulfur protein biogenesis. Although *grxS17* seedlings do have decreased activities of cytosolic aconitase and aldehyde oxidases in control conditions (Fig. 7), the effect is far less severe than that observed in the *atm3* mutant lines (Bernard et al., 2009). Moreover, the aldehyde oxidase activity, which depends on two Fe_2S_2 clusters, is not decreased in *grxS17* plants at 28°C, a temperature condition leading to a severe phenotype. Therefore, our data indicate that GRXS17 is not involved in de novo biosynthesis of cytosolic Fe_2S_2 clusters, which is in agreement with the viability of the knockout mutant. Indeed, because many cytosolic and nuclear iron-sulfur proteins are essential, mutants in iron-sulfur cluster assembly are generally embryo lethal (Balk and Schaedler, 2014). An alternative explanation is that the function of GRXS17 is redundant or compensated for by another component of the iron-sulfur cluster assembly pathway. However, because GRXS17 is the only class II GRX present in cytosol and nucleus, it is unlikely that such a function is fulfilled by another GRX. Taking into consideration the in vitro capacity of GRXS17 to bind iron-sulfur clusters and the variations observed in aconitase activity in *grxS17* plants, we can speculate that it protects iron-sulfur proteins from oxidative stress and destruction of clusters. Such a hypothesis will need further investigation.

We assumed a function of GRXS17 in connection with its redox properties and hypothesized that it participates in signaling pathways related to the changes in the cellular redox status occurring in response to environmental variations. Of note, AtGRXS17 has been recently reported as prone to hydrogen peroxide-induced Cys sulfenation (Waszczak et al., 2014). Redox changes might affect the subcellular localization of AtGRXS17 or the set of interacting partners through posttranslational redox modifications. Concerning the first point, our experiments (GFP fusion and cellular fractionation) show that GRXS17 is localized in both nucleus and cytosol (Fig. 2), and a former study indicated that high temperature induces GRXS17 translocation from cytosol to nucleus (Wu et al., 2012). Thus, in response to environmental signals or a specific physiological state, the GRXS17 function might be associated with nucleocytosolic shuttling. With regard to 14 putative GRXS17 interaction partners identified by affinity chromatography, their localization is consistent with an interaction in vivo. Note that BOLA2, a possible transcriptional regulator interacting with GRXS17 in binary yeast two-hybrid and BiFC experiments (Couturier et al., 2014), was not isolated. This could originate from a low abundance or the type of plant material used in this work. Nevertheless, the data gained from affinity experiments clearly show the ability of GRXS17 to interact with different types of partners and thus, possibly modify their conformation or regulate their activity through posttranslational redox modification.

GRXS17: A Hub Integrating Hormonal and Redox Signals?

Consistent with the pleiotropic phenotype of *grxS17* plants, western data revealed the presence of the GRXS17 protein in all organs, particularly those containing actively dividing or elongating cells. In addition, in situ hybridization showed a high transcript level in apical meristem, and histological analyses of plants grown in long-day

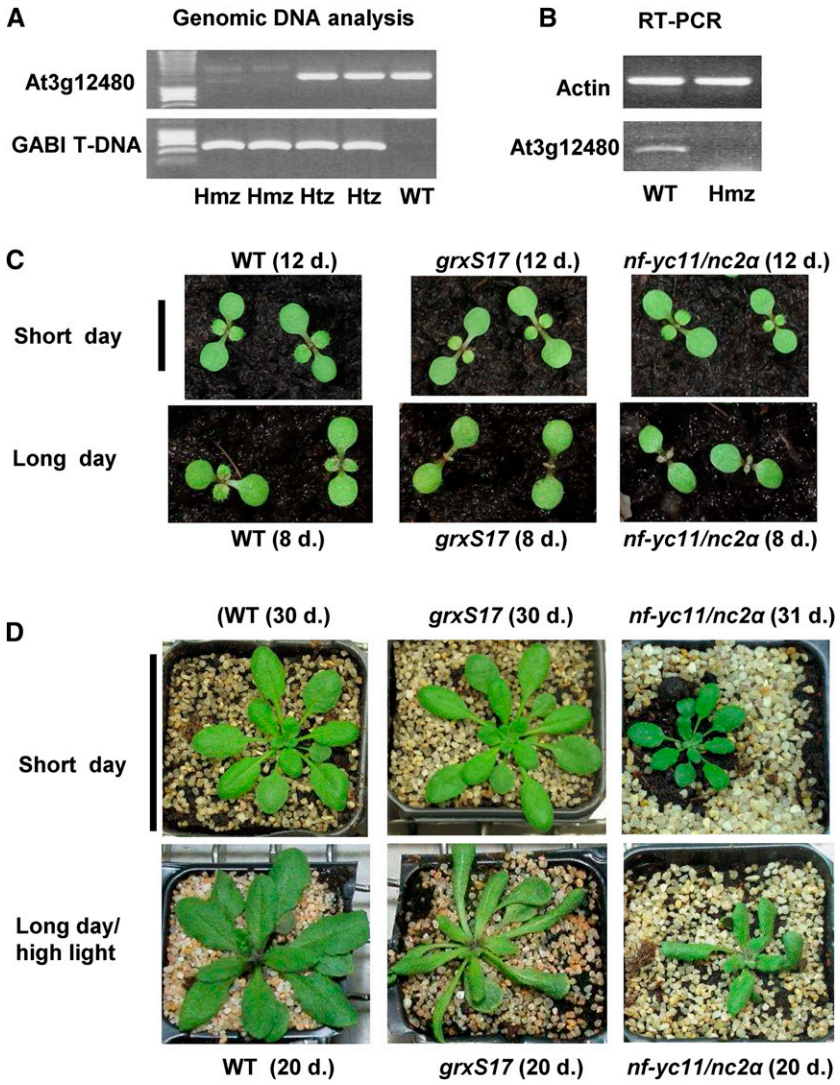

Figure 9. Characterization of an *nf-yc11/nc2α* mutant and comparison of the growth of *grxS17* and *nf-yc11/nc2α* plants as a function of photoperiod duration. A, PCR analysis of genomic DNA of At3g12480 and transfer DNA in wild-type, heterozygous, and homozygous plants of the German Plant Genomics Research Program-042E02 mutant line. B, RT-PCR analysis of wild-type and homozygous plants. C, Seedling development in short- and long-day conditions (8 and 16 h, respectively) at moderate light (200 μmol photons m^{-2} s^{-1}) and 22°C. The seedlings were grown simultaneously in the same conditions, and the original photographs are shown in Supplemental Figure S10. D, Vegetative growth of plants in standard light conditions (short day, 8-h photoperiod and moderate light at 200 μmol photons m^{-2} s^{-1}) and long-day and high-light conditions (16-h photoperiod and 500 μmol photons m^{-2} s^{-1}) at 22°C. The plant age is indicated for each genotype and culture condition. Hmz, Homozygous; Htx, heterozygous; WT, wild type. Bar in C = 1 cm. Bar in D = 6 cm.

conditions specifically revealed a larger cell size in both meristems and leaves of *grxS17* plants. All of these data suggest a crucial role of GRXS17 in meristem activity and cell division. Several studies provided evidence for a tight relationship between intracellular redox status, disulfide reductases, and development (Considine and Foyer, 2014). For instance, the development of root meristems is influenced by changes in the overall redox status and auxin content/distribution (Vernoux et al., 2000; Jiang et al., 2003; Yu et al., 2013). Another example is the Arabidopsis *NADPH-dependent thioredoxin reductase A* (*ntra*), *NADPH-dependent thioredoxin reductase B* (*ntrb*), and *cadmium-sensitive2* (*cad2*), *ntra ntrb cad2* triple mutant, which is defective in TRX reduction and GSH synthesis and exhibits strongly impaired reproductive development in relation to altered auxin metabolism (Bashandy et al., 2010). The plastidial TRXm3 is essential for meristem maintenance in Arabidopsis through a role in symplastic permeability (Benitez-Alfonso et al., 2009), and the nucleoredoxin1 participates in the establishment of pollen fertility (Qin et al., 2009; Marchal et al., 2014). With regard to GRXs, the fate of germ cells in maize (*Zea mays*) anthers is determined by the redox status by a GRX, termed MALE STERILE CONVERTED ANTHER1, presumed to play a role in gene transcription (Kelliher and Walbot, 2012). The nuclear class III GRXs, ROXY1 and ROXY2, are required for proper development of floral organs in Arabidopsis, likely through interaction with TGA transcription factors (Xing and Zachgo, 2008; Hong et al., 2012). Altogether, these reports support the view that disulfide reductases finely control plant development.

Arabidopsis *grxS17* plants display hypersensitivity to high temperature and altered auxin-mediated signaling pathways in roots (Cheng et al., 2011). This work unveils another function for GRXS17 in integrating photoperiod signals for proper development. Temperature is, however, an important determinant, because the phenotype is evident in long-day conditions at 22°C and 28°C but not at 15°C. In this study, we mainly investigated the phenotype of aerial parts of plants grown on soil and observed an altered shape of the leaves, which turned thick and elongated and displayed a reduced number of

large cells. Looking for mutants with a similar phenotype (Bensmihen et al., 2008), we noticed that *drl1* and *elo* mutants exhibit elongated leaves and a strongly reduced number of larger palisade cells compared with the wild type (Nelissen et al., 2003, 2005). DEFORMED ROOTS AND LEAVES1 (DRL1) regulates RNA polymerase II-mediated transcription through the elongator complex, which is composed of several ELONGATED (ELO) proteins and displays histone acetyltransferase activity preferentially in regions of auxin-related genes (Nelissen et al., 2010). Importantly, the floral development of *drl1* plants is delayed, and the root development of both *elo* and *drl1* mutants is substantially reduced (Nelissen et al., 2003). Interestingly, by investigating the genes coexpressed with *GRXS17* using Genevestigator (Hruz et al., 2008), a high correlation was found with *ELO2* (At5g13680). It is, thus, tempting to hypothesize that the *grxS17* phenotype is linked to defects in ELO- and/or DRL1-dependent transcription mechanisms.

Possible Roles of GRXS17 in Interaction with the NF-YC11/NC2α Nuclear Factor

Among the GRXS17 partners identified using affinity chromatography, we focused on the nuclear factor NF-YC11/NC2α. Because the interaction between this factor and the GRX was confirmed by BiFC experiments in Arabidopsis protoplasts, a physiologically relevant interaction can be assumed. The Arabidopsis NF-Y family comprises three main types (A–C). Initially named CCAAT-box-binding factor or Heme Activator Protein (HAP), they usually form trimeric complexes of A, B, and C subunits binding to CCAAT-promoter sequences and transcriptionally regulating genes participating in plant development and stress responses (Dolfini et al., 2012; Laloum et al., 2013). In animal cells, they are central to cell-cycle progression (Benatti et al., 2011), and in fungi, the corresponding trimeric complex formed by HAP2, HAP3, and HAP5 includes a fourth HAP4 subunit. Interestingly, in *Schizosaccharomyces pombe*, the function and subcellular localization of HAP4, which participates in iron homeostasis, are under the control of the multidomain GRX4 (Mercier and Labbé, 2009). In relation to the *grxS17* phenotype, it is worth mentioning that AtNF-YC11 specifically interacts with the Arabidopsis nuclear factor Y subunit B3 (AtNF-YB3), an isoform controlling flowering time (Kumimoto et al., 2008). To date, the only evidence for redox control was obtained for a mammalian NF-YB, which has an association to NF-YC that is dependent on the reduction of an intermolecular disulfide bond (Nakshatri et al., 1996). Interestingly, all plant NF-YC11 orthologs exhibit a unique N-terminal sequence clearly distinguishing them from other NF-YCs. On this basis, they have been reclassified as homologs to NC2α factors (Petroni et al., 2012). NC2α together with another factor called NC2β form a tight heterodimer able to associate with the TATA-binding complex and act as a transcription repressor as shown in Baker's yeast and rice (*Oryza sativa*; Kim et al., 1997; Song et al., 2002). Two Cys residues are present in the NF-YC11/NC2α N-terminal extension (Supplemental Fig. S12). Of note, one is strictly conserved in plant orthologs and also, human NC2α protein, whereas the position of the second varies in Dicotyledons and Monocotyledons. Unfortunately, all attempts to produce recombinant NF-YC11/NC2α failed, which precluded investigations on a possible redox-mediated interaction with GRXS17. The data gained from the characterization of the Arabidopsis *nf-yc11/nc2α* mutant line (Fig. 9; Supplemental Fig. S11) revealed that the nuclear factor is a central element for proper plant development. In short-day conditions, *nf-yc11/nc2α* plants display developmental defects (slow growth and altered floral spikes). Most interestingly, comparing the phenotypes of *grxS17* and *nf-yc11/nc2α* plants, we noticed that both mutants share common photoperiod-dependent characteristics, such as delayed appearance of the first two leaves, abnormal leaf shapes, and impaired flowering (Fig. 9; Supplemental Fig. S11). This phenotype resemblance, which is revealed in long- but not short-day conditions, gives further credence to a concerted action of GRXS17 and NF-YC11/NC2α in the control of plant development in relation to environmental conditions. We might, thus, speculate that GRXS17 modulates the NF-YC11/NC2α function by controlling its redox state, and we propose a working model illustrating such a role for GRXS17 (Fig. 10). Based on the resemblance of *grxS17* and *nf-yc11/nc2α* mutants, it is conceivable that GRXS17-mediated redox changes modify the capacity of AtNF-YC11/NC2α to bind to an NC2β subunit (AtNF-YB11-13), ultimately resulting in the

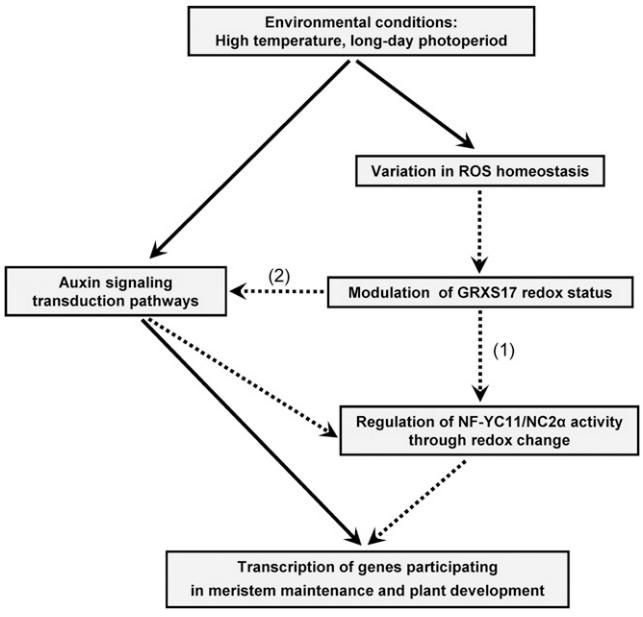

Figure 10. Suggested role of GRXS17 during plant development in connection with environmental conditions and auxin-related mechanisms. Dotted lines indicate the proposed steps in signal transduction involving GRXS17. The model is based on the data presented in this work (1) and those reported in Cheng et al., 2011 (2). ROS, Reactive oxygen species.

modification of the transcription level of genes involved in meristem maintenance and plant developmental programs, such as those related to auxin action (Fig. 10). Taken collectively, these data lead us to propose that Arabidopsis GRXS17 relays environmental signals, possibly through subtle changes in the cellular/nuclear redox state, and then, enters this information into the control of gene transcription to initiate essential developmental steps. The use of mutant lines expressing mutated GRXS17 and NF-YC11/NC2α forms will help to determine the precise mechanisms underlying the functions of these two key actors in plant development in relation to the presence and the redox status of their cysteines.

MATERIALS AND METHODS

Plant Material and Growth Conditions

Arabidopsis (*Arabidopsis thaliana*) Columbia-0 plants were grown in standard conditions under an 8-h photoperiod and a photon flux density of 200 μmol photons m^{-2} s^{-1} at 22°C. Other conditions of light (500 μmol photons m^{-2} s^{-1}), temperature (15°C or 28°C), and photoperiod (16 h or continuous light) were applied in controlled growth chambers either from sowing or on 2- to 3-week-old plants grown under standard conditions.

Transformation of Arabidopsis Plants

The full-length GRXS17 cDNA (At4g04950) was cloned into the pB2GW7 vector (GATEWAY; Invitrogen). After transformation using *Agrobacterium tumefaciens* C58 strain (Clough and Bent, 1998), homozygous lines (T2) were obtained from resistance segregation assays. Leaf genomic DNA was extracted using the DNeasy Plant Mini Kit (Qiagen) to perform PCR using appropriate primers (Supplemental Table S1), Taq DNA Polymerase (Life Technologies), and the GeneAmp PCRSystem 2700 (Applied Biosystems). RT-PCR was performed using Sensiscript III (Life Technologies) after leaf RNA extraction (NucleoSpin; Macherey-Nagel).

Expression of the Recombinant Wild Type and Cys-Mutant GRXS17

AtGRXS17 cDNA was cloned into the pET-16b vector (Novagen; Merck Biosciences) for expression in *Escherichia coli* BL21(DE3)-pLysS. The protein was purified by nickel-chelate chromatography (GE Healthcare). Site-directed mutagenesis was performed using the QuikChange II protocol (Stratagene) and appropriate primers (Supplemental Table S3).

In Vitro Reconstitution Assay of Iron-Sulfur Clusters and Analytical Measurements

GRXS17 (50 μM) was reconstituted in vitro by incubation with $Fe(NH_4)_2(SO_4)_2$: Cys:GSH:pyridoxal phosphate:*E. coli* IscS in the molar ratio of 1 GRX:6:9:10:0.04:0.02 in 50 mM sodium phosphate buffer, pH 8.0, 300 mM NaCl, and 5 mM DTT under argon atmosphere for 2 h. After centrifugation (4 min at 4°C at 13,000 rpm), UV-visible spectra were recorded with a Shimadzu UV-2100 Spectrophotometer. Iron content was determined after reconstitution of 100 μM GRXS17 according to Fish (1988).

Cytology and in Situ Hybridization

Meristem cross sections were prepared using a microtome (Leica RM2255) from tissues fixed with formaldehyde/glutaraldehyde, embedded in hydroxyethyl methacrylate (Technovit 7100; Heraeus Kulzer), and counterstained with toluidine blue. Measurements of mesophyll cells were performed after propidium iodide staining (5 ng mL^{-1}). Confocal microscopic observations were carried out using the Axio Observer Z1 Microscope with the LSM 700 Scanning Module, the ZEN 2010 software (Zeiss), and the propidium iodide (566–1,000 bp) filters. In situ hybridization was performed as in Bashandy et al. (2010). After fixation, dehydration, and embedding in paraffin wax, sample sections (7 mm thick) were attached to precoated glass slides (DAKO). Probes were synthesized using digoxigenin-UTP (Boehringer Mannheim). Immunodetection was performed using an antidigoxigenin antibody coupled to alkaline phosphatase.

Transient Transformation of Protoplasts with GFP and Split-YFP Constructs

Protoplasts were isolated from leaves of 6-week-old Arabidopsis plants for transient expression of fusion proteins (Wojtera-Kwiczor et al., 2012). cDNAs encoding GRXS17 and NF-YC11/NC2α were cloned in the sense direction into the pGFP2-vector for C-terminal GFP fusion. The GRXS17 and NF-YC11/NC2α cDNAs were inserted in frame with YFP N- and C-terminal parts in pSPYNE and pSPYCE vectors obtained from Jörg Kudla (University of Muenster). Combinations of empty vectors and fusion constructs were used as controls. GFP and chlorophyll autofluorescence were visualized with excitation at 488 nm and emission at 500 to 530 and 650 to 710 nm, respectively, using the cLSM 510 META (Carl Zeiss). YFP was visualized with excitation at 514 nm and emission at 535 to 590 nm.

Affinity Chromatography and Electrospray Ionization Mass Spectrometry

His-tagged GRXS17 was bound to a nickel-nitrilotriacetic acid column and used as affinity matrix. Leaves of 5-week-old plants grown under short-day conditions were homogenized in 20 mL of 50 mM Bicine, pH 7.8, 100 mM Suc, and 50 mM NaCl. After filtration through Miracloth and centrifugation (10 min at 6,000*g* at 4°C and 50 min at 4°C at 100,000*g*), the clarified supernatant (30 mg of protein) was applied to the matrix and incubated for 2 h at 4°C. Nonbound material was removed by washing the column four times with 10 mL of 20 mM Bicine, pH 7.8. Elution was achieved with 4 mL of the same buffer containing 150 mM DTT. After tryptic digestion (50 μg of proteins per analysis), the fragments were separated by reverse-phase HPLC and analyzed by electrospray ionization-mass spectrometry (Holtgrefe et al., 2008). Results were analyzed using the Brucker Daltronics software.

Biochemical Methods

Soluble proteins were prepared from plant material, separated by SDS-PAGE, and electrotransferred onto a nitrocellulose membrane (Pall Corporation; Rey et al., 2005). Protein cross-linking was achieved using DMP (Thermo Fisher Scientific; Riondet et al., 2012). Polyclonal antibodies were raised in rabbit against His-tagged AtGRXS17 (Genecust). Immunodetection of AtGRXS17 was carried out using primary antibodies diluted 1:1,000 and the goat anti-rabbit Alexa Fluor 680 IgG at 1:10,000 (Invitrogen). Bound antibodies were revealed at 680 nm using the Odyssey Infrared Imager (LiCor). For immunodetection of aconitase (Bernard et al., 2009) and *Psa*A (Agrisera), horseradish peroxidase-conjugated secondary antibodies and chemiluminescence were used. Autoluminescence imaging of lipid peroxidation was performed as in Collin et al. (2008).

Baker's Yeast Plasmids, Strains, and Growth Conditions

The GRXS17 entire sequence and each GRX module, M2 ($S17_{167–252}$), M3 ($S17_{297–383}$), and M4 ($S17_{404–488}$), were cloned in frame in the Baker's yeast (*Saccharomyces cerevisiae*) plasmid pMM221. pMM221 contains the Baker's yeast GRX5 mitochondrial targeting sequence plus a C-terminal 3HA/His-6 tag under the control of the doxycycline-regulatory tetO2 promoter (Supplemental Tables S1 and S2; Molina et al., 2004). pMM54 contains a Baker's yeast *GRX5-3HA* construction under its endogenous promoter (Rodríguez-Manzaneque et al., 2002). Strains are described in Supplemental Table S3. Plasmids were linearized by *Cla*I previous to chromosomal integration. Samples were taken from cultures grown exponentially (Molina et al., 2004) for at least 10 generations at 30°C. Sensitivity to oxidants was determined on yeast extract-peptone-dextrose plates by spotting 1:5 serial dilutions of exponential cultures and recording growth after 2 d at 30°C. Subfractionation of mitochondria was performed as in Bandyopadhyay et al. (2008). Northern-blot analyses using Baker's yeast RNA were performed with digoxigenin (Bellí et al., 1998). Gene probes were generated by PCR from genomic DNA using appropriate oligonucleotides (Supplemental Table S3).

Enzyme Activity Determinations

Aconitase and malate dehydrogenase were assayed in extracts from Baker's yeast growing exponentially in yeast extract-peptone-Gal medium (Robinson

et al., 1987). Isopropylmalate isomerase activity was determined in extracts prepared from cells growing exponentially in synthetic complete medium supplemented with the specific auxotrophy requirement (Pierik et al., 2009). In the case of Leu, only one-third of the standard concentration was added into the medium to allow growth. In-gel activity assays for aldehyde oxidase and aconitase were as previously described (Bernard et al., 2009).

Supplemental Data

The following supplemental materials are available.

Supplemental Figure S1. Molecular characterization of Arabidopsis plants modified in *GRXS17* expression and GRXS17 protein abundance.

Supplemental Figure S2. Subcellular localization of GRXS17.

Supplemental Figure S3. Controls of the bimolecular fluorescence complementation assay of GRXS17 and NF-YC11/NC2α.

Supplemental Figure S4. Growth of Arabidopsis plants modified in *GRXS17* expression as a function of light and temperature.

Supplemental Figure S5. Floral development of Arabidopsis plants modified in *GRXS17* expression as a function of photoperiod and light intensity.

Supplemental Figure S6. Autoluminescence in Arabidopsis plants modified in *GRXS17* expression.

Supplemental Figure S7. Structure of the shoot apical meristem in the *grxS17* mutant.

Supplemental Figure S8. Hypothetical structure of GRXS17.

Supplemental Figure S9. Analysis of the GRXS17 forms expressed in yeast.

Supplemental Figure S10. Growth phenotypes and quantification of aldehyde oxidase enzyme activity.

Supplemental Figure S11. Development of *nf-yc11/nc2*α plants as a function of light environment.

Supplemental Figure S12. Sequence alignment of plant, human, and yeast proteins containing an NC2α domain.

Supplemental Table S1. List of primers used in the study.

Supplemental Table S2. Plasmids used for experiments on Baker's yeast.

Supplemental Table S3. Baker's yeast strains.

ACKNOWLEDGMENTS

We thank the Groupe de Recherche Appliquée en Phytotechnologie (Commissariat à l'Energie Atomique, Institut de Biologie Environnementale et Biotechnologie, and Service de Biologie Végétale et Microbiologie Environnementales) for technical assistance with controlled growth chambers; Patricia Henri (Commissariat á l'Energie Atomique, Institut de Biologie Environnementale et Biotechnologie, and Service de Biologie Végétale et Microbiologie Environnementales) for valuable technical assistance; Delphine Cerveau, Brigitte Ksas, and Dr. Michel Havaux (Commissariat á l'Energie Atomique, Institut de Biologie Environnementale et Biotechnologie, and Service de Biologie Végétale et Microbiologie Environnementales) for helpful assistance in phenotype characterization and imaging experiments; and Drs. Mohammed Bendahmane and Michiel Vandenbussche (Laboratoire de Reproduction et Développement des Plantes-Unité Mixte de Recherche 5667 Ecole Normale Supérieure-Centre National de la Recherche Scientifique-Institut National de la Recherche Agronomique-Université de Lyon) for fruitful discussion about NF-Y transcription factors.

Received January 14, 2015; accepted February 10, 2015; published February 19, 2015.

LITERATURE CITED

Balk J, Schaedler TA (2014) Iron cofactor assembly in plants. Annu Rev Plant Biol **65:** 125–153

Bandyopadhyay S, Gama F, Molina-Navarro MM, Gualberto JM, Claxton R, Naik SG, Huynh BH, Herrero E, Jacquot JP, Johnson MK, et al (2008) Chloroplast monothiol glutaredoxins as scaffold proteins for the assembly and delivery of [2Fe-2S] clusters. EMBO J **27:** 1122–1133

Bashandy T, Guilleminot J, Vernoux T, Caparros-Ruiz D, Ljung K, Meyer Y, Reichheld JP (2010) Interplay between the NADP-linked thioredoxin and glutathione systems in *Arabidopsis* auxin signaling. Plant Cell **22:** 376–391

Bellí G, Garí E, Piedrafita L, Aldea M, Herrero E (1998) An activator/repressor dual system allows tight tetracycline-regulated gene expression in budding yeast. Nucleic Acids Res **26:** 942–947

Benatti P, Dolfini D, Viganò A, Ravo M, Weisz A, Imbriano C (2011) Specific inhibition of NF-Y subunits triggers different cell proliferation defects. Nucleic Acids Res **39:** 5356–5368

Benitez-Alfonso Y, Cilia M, San Roman A, Thomas C, Maule A, Hearn S, Jackson D (2009) Control of Arabidopsis meristem development by thioredoxin-dependent regulation of intercellular transport. Proc Natl Acad Sci USA **106:** 3615–3620

Bensmihen S, Hanna AI, Langlade NB, Micol JL, Bangham A, Coen ES (2008) Mutational spaces for leaf shape and size. HFSP J **2:** 110–120

Bernard DG, Cheng Y, Zhao Y, Balk J (2009) An allelic mutant series of *ATM3* reveals its key role in the biogenesis of cytosolic iron-sulfur proteins in Arabidopsis. Plant Physiol **151:** 590–602

Cheng NH (2008) AtGRX4, an Arabidopsis chloroplastic monothiol glutaredoxin, is able to suppress yeast *grx5* mutant phenotypes and respond to oxidative stress. FEBS Lett **582:** 848–854

Cheng NH, Liu JZ, Brock A, Nelson RS, Hirschi KD (2006) AtGRXcp, an Arabidopsis chloroplastic glutaredoxin, is critical for protection against protein oxidative damage. J Biol Chem **281:** 26280–26288

Cheng NH, Liu JZ, Liu X, Wu Q, Thompson SM, Lin J, Chang J, Whitham SA, Park S, Cohen JD, et al (2011) Arabidopsis monothiol glutaredoxin, AtGRXS17, is critical for temperature-dependent postembryonic growth and development via modulating auxin response. J Biol Chem **286:** 20398–20406

Clough SJ, Bent AF (1998) Floral dip: a simplified method for Agrobacterium-mediated transformation of *Arabidopsis thaliana*. Plant J **16:** 735–743

Collin VC, Eymery F, Genty B, Rey P, Havaux M (2008) Vitamin E is essential for the tolerance of *Arabidopsis thaliana* to metal-induced oxidative stress. Plant Cell Environ **31:** 244–257

Considine MJ, Foyer CH (2014) Redox regulation of plant development. Antioxid Redox Signal **21:** 1305–1326

Couturier J, Jacquot JP, Rouhier N (2009) Evolution and diversity of glutaredoxins in photosynthetic organisms. Cell Mol Life Sci **66:** 2539–2557

Couturier J, Ströher E, Albetel AN, Roret T, Muthuramalingam M, Tarrago L, Seidel T, Tsan P, Jacquot JP, Johnson MK, et al (2011) Arabidopsis chloroplastic glutaredoxin C5 as a model to explore molecular determinants for iron-sulfur cluster binding into glutaredoxins. J Biol Chem **286:** 27515–27527

Couturier J, Wu HC, Dhalleine T, Pégeot H, Sudre D, Gualberto JM, Jacquot JP, Gaymard F, Vignols F, Rouhier N (2014) Monothiol glutaredoxin-BolA interactions: redox control of *Arabidopsis thaliana* BolA2 and SufE1. Mol Plant **7:** 187–205

Dolfini D, Gatta R, Mantovani R (2012) NF-Y and the transcriptional activation of CCAAT promoters. Crit Rev Biochem Mol Biol **47:** 29–49

Fish WW (1988) Rapid colorimetric micromethod for the quantitation of complexed iron in biological samples. Methods Enzymol **158:** 357–364

Gama F, Keech O, Eymery F, Finkemeier I, Gelhaye E, Gardestrom P, Dietz KJ, Rey P, Jacquot JP, Rouhier N (2007) The mitochondrial type II peroxiredoxin from poplar. Physiol Plant **129:** 196–206

Guo Y, Huang C, Xie Y, Song F, Zhou X (2010) A tomato glutaredoxin gene SlGRX1 regulates plant responses to oxidative, drought and salt stresses. Planta **232:** 1499–1509

Haunhorst P, Hanschmann EM, Bräutigam L, Stehling O, Hoffmann B, Mühlenhoff U, Lill R, Berndt C, Lillig CH (2013) Crucial function of vertebrate glutaredoxin 3 (PICOT) in iron homeostasis and hemoglobin maturation. Mol Biol Cell **24:** 1895–1903

Havaux M, Triantaphylidès C, Genty B (2006) Autoluminescence imaging: a non-invasive tool for mapping oxidative stress. Trends Plant Sci **11:** 480–484

Holtgrefe S, Gohlke J, Starmann J, Druce S, Klocke S, Altmann B, Wojtera J, Lindermayr C, Scheibe R (2008) Regulation of plant cytosolic glyceraldehyde 3-phosphate dehydrogenase isoforms by thiol modifications. Physiol Plant **133:** 211–228

Hong L, Tang D, Zhu K, Wang K, Li M, Cheng Z (2012) Somatic and reproductive cell development in rice anther is regulated by a putative glutaredoxin. Plant Cell **24:** 577–588

Hruz T, Laule O, Szabo G, Wessendorp F, Bleuler S, Oertle L, Widmayer P, Gruissem W, Zimmermann P (2008) Genevestigator v3: a reference

expression database for the meta-analysis of transcriptomes. Adv Bioinforma **2008:** 420747

Jbel M, Mercier A, Labbé S (2011) Grx4 monothiol glutaredoxin is required for iron limitation-dependent inhibition of Fep1. Eukaryot Cell **10:** 629–645

Jiang K, Meng YL, Feldman LJ (2003) Quiescent center formation in maize roots is associated with an auxin-regulated oxidizing environment. Development **130:** 1429–1438

Kelliher T, Walbot V (2012) Hypoxia triggers meiotic fate acquisition in maize. Science **337:** 345–348

Kim S, Na JG, Hampsey M, Reinberg D (1997) The Dr1/DRAP1 heterodimer is a global repressor of transcription *in vivo*. Proc Natl Acad Sci USA **94:** 820–825

Kleinboelting N, Huep G, Kloetgen A, Viehoever P, Weisshaar B (2012) GABI-Kat SimpleSearch: new features of the *Arabidopsis thaliana* T-DNA mutant database. Nucleic Acids Res **40:** D1211–D1215

Kumánovics A, Chen OS, Li L, Bagley D, Adkins EM, Lin H, Dingra NN, Outten CE, Keller G, Winge D, et al (2008) Identification of FRA1 and FRA2 as genes involved in regulating the yeast iron regulon in response to decreased mitochondrial iron-sulfur cluster synthesis. J Biol Chem **283:** 10276–10286

Kumimoto RW, Adam L, Hymus GJ, Repetti PP, Reuber TL, Marion CM, Hempel FD, Ratcliffe OJ (2008) The Nuclear Factor Y subunits NF-YB2 and NF-YB3 play additive roles in the promotion of flowering by inductive long-day photoperiods in Arabidopsis. Planta **228:** 709–723

Kumimoto RW, Zhang Y, Siefers N, Holt BF III (2010) NF-YC3, NF-YC4 and NF-YC9 are required for CONSTANS-mediated, photoperiod-dependent flowering in *Arabidopsis thaliana*. Plant J **63:** 379–391

La Camera S, L'haridon F, Astier J, Zander M, Abou-Mansour E, Page G, Thurow C, Wendehenne D, Gatz C, Métraux JP, et al (2011) The glutaredoxin ATGRXS13 is required to facilitate *Botrytis cinerea* infection of *Arabidopsis thaliana* plants. Plant J **68:** 507–519

Laloum T, De Mita S, Gamas P, Baudin M, Niebel A (2013) CCAAT-box binding transcription factors in plants: Y so many? Trends Plant Sci **18:** 157–166

Laporte D, Olate E, Salinas P, Salazar M, Jordana X, Holuigue L (2012) Glutaredoxin GRXS13 plays a key role in protection against photooxidative stress in Arabidopsis. J Exp Bot **63:** 503–515

Levy YY, Dean C (1998) The transition to flowering. Plant Cell **10:** 1973–1990

Lillig CH, Berndt C, Vergnolle O, Lönn ME, Hudemann C, Bill E, Holmgren A (2005) Characterization of human glutaredoxin 2 as iron-sulfur protein: a possible role as redox sensor. Proc Natl Acad Sci USA **102:** 8168–8173

Marchal C, Delorme-Hinoux V, Bariat L, Siala W, Belin C, Saez-Vasquez J, Riondet C, Reichheld JP (2014) NTR/NRX define a new thioredoxin system in the nucleus of *Arabidopsis thaliana* cells. Mol Plant **7:** 30–44

Mercier A, Labbé S (2009) Both Php4 function and subcellular localization are regulated by iron via a multistep mechanism involving the glutaredoxin Grx4 and the exportin Crm1. J Biol Chem **284:** 20249–20262

Meyer Y, Buchanan BB, Vignols F, Reichheld JP (2009) Thioredoxins and glutaredoxins: unifying elements in redox biology. Annu Rev Genet **43:** 335–367

Michelet L, Zaffagnini M, Marchand C, Collin V, Decottignies P, Tsan P, Lancelin JM, Trost P, Miginiac-Maslow M, Noctor G, et al (2005) Glutathionylation of chloroplast thioredoxin f is a redox signaling mechanism in plants. Proc Natl Acad Sci USA **102:** 16478–16483

Molina MM, Bellí G, de la Torre MA, Rodríguez-Manzaneque MT, Herrero E (2004) Nuclear monothiol glutaredoxins of *Saccharomyces cerevisiae* can function as mitochondrial glutaredoxins. J Biol Chem **279:** 51923–51930

Mühlenhoff U, Gerber J, Richhardt N, Lill R (2003) Components involved in assembly and dislocation of iron-sulfur clusters on the scaffold protein Isu1p. EMBO J **22:** 4815–4825

Mühlenhoff U, Molik S, Godoy JR, Uzarska MA, Richter N, Seubert A, Zhang Y, Stubbe J, Pierrel F, Herrero E, et al (2010) Cytosolic monothiol glutaredoxins function in intracellular iron sensing and trafficking via their bound iron-sulfur cluster. Cell Metab **12:** 373–385

Murmu J, Bush MJ, DeLong C, Li S, Xu M, Khan M, Malcolmson C, Fobert PR, Zachgo S, Hepworth SR (2010) Arabidopsis basic leucine-zipper transcription factors TGA9 and TGA10 interact with floral glutaredoxins ROXY1 and ROXY2 and are redundantly required for anther development. Plant Physiol **154:** 1492–1504

Nakshatri H, Bhat-Nakshatri P, Currie RA (1996) Subunit association and DNA binding activity of the heterotrimeric transcription factor NF-Y is regulated by cellular redox. J Biol Chem **271:** 28784–28791

Ndamukong I, Abdallat AA, Thurow C, Fode B, Zander M, Weigel R, Gatz C (2007) SA-inducible Arabidopsis glutaredoxin interacts with TGA factors and suppresses JA-responsive PDF1.2 transcription. Plant J **50:** 128–139

Nelissen H, Clarke JH, De Block M, De Block S, Vanderhaeghen R, Zielinski RE, Dyer T, Lust S, Inzé D, Van Lijsebettens M (2003) DRL1, a homolog of the yeast TOT4/KTI12 protein, has a function in meristem activity and organ growth in plants. Plant Cell **15:** 639–654

Nelissen H, De Groeve S, Fleury D, Neyt P, Bruno L, Bitonti MB, Vandenbussche F, Van der Straeten D, Yamaguchi T, Tsukaya H, et al (2010) Plant Elongator regulates auxin-related genes during RNA polymerase II transcription elongation. Proc Natl Acad Sci USA **107:** 1678–1683

Nelissen H, Fleury D, Bruno L, Robles P, De Veylder L, Traas J, Micol JL, Van Montagu M, Inzé D, Van Lijsebettens M (2005) The *elongata* mutants identify a functional Elongator complex in plants with a role in cell proliferation during organ growth. Proc Natl Acad Sci USA **102:** 7754–7759

Ojeda L, Keller G, Mühlenhoff U, Rutherford JC, Lill R, Winge DR (2006) Role of glutaredoxin-3 and glutaredoxin-4 in the iron regulation of the Aft1 transcriptional activator in *Saccharomyces cerevisiae*. J Biol Chem **281:** 17661–17669

Petroni K, Kumimoto RW, Gnesutta N, Calvenzani V, Fornari M, Tonelli C, Holt BF III, Mantovani R (2012) The promiscuous life of plant NUCLEAR FACTOR Y transcription factors. Plant Cell **24:** 4777–4792

Pierik AJ, Netz DJ, Lill R (2009) Analysis of iron-sulfur protein maturation in eukaryotes. Nat Protoc **4:** 753–766

Pontvianne F, Abou-Ellail M, Douet J, Comella P, Matia I, Chandrasekhara C, Debures A, Blevins T, Cooke R, Medina FJ, et al (2010) Nucleolin is required for DNA methylation state and the expression of rRNA gene variants in *Arabidopsis thaliana*. PLoS Genet **6:** e1001225

Pujol-Carrion N, Belli G, Herrero E, Nogues A, de la Torre-Ruiz MA (2006) Glutaredoxins Grx3 and Grx4 regulate nuclear localisation of Aft1 and the oxidative stress response in *Saccharomyces cerevisiae*. J Cell Sci **119:** 4554–4564

Qin Y, Leydon AR, Manziello A, Pandey R, Mount D, Denic S, Vasic B, Johnson MA, Palanivelu R (2009) Penetration of the stigma and style elicits a novel transcriptome in pollen tubes, pointing to genes critical for growth in a pistil. PLoS Genet **5:** e1000621

Rey P, Cuiné S, Eymery F, Garin J, Court M, Jacquot JP, Rouhier N, Broin M (2005) Analysis of the proteins targeted by CDSP32, a plastidic thioredoxin participating in oxidative stress responses. Plant J **41:** 31–42

Riondet C, Desouris JP, Montoya JG, Chartier Y, Meyer Y, Reichheld JP (2012) A dicotyledon-specific glutaredoxin GRXC1 family with dimer-dependent redox regulation is functionally redundant with GRXC2. Plant Cell Environ **35:** 360–373

Robinson JB Jr, Inman L, Sumegi B, Srere PA (1987) Further characterization of the Krebs tricarboxylic acid cycle metabolon. J Biol Chem **262:** 1786–1790

Rodríguez-Manzaneque MT, Tamarit J, Bellí G, Ros J, Herrero E (2002) Grx5 is a mitochondrial glutaredoxin required for the activity of iron/sulfur enzymes. Mol Biol Cell **13:** 1109–1121

Rouhier N, Couturier J, Jacquot JP (2006) Genome-wide analysis of plant glutaredoxin systems. J Exp Bot **57:** 1685–1696

Rouhier N, Couturier J, Johnson MK, Jacquot JP (2010) Glutaredoxins: roles in iron homeostasis. Trends Biochem Sci **35:** 43–52

Rouhier N, Gelhaye E, Sautiere PE, Brun A, Laurent P, Tagu D, Gerard J, de Faÿ E, Meyer Y, Jacquot JP (2001) Isolation and characterization of a new peroxiredoxin from poplar sieve tubes that uses either glutaredoxin or thioredoxin as a proton donor. Plant Physiol **127:** 1299–1309

Rouhier N, Lemaire SD, Jacquot JP (2008) The role of glutathione in photosynthetic organisms: emerging functions for glutaredoxins and glutathionylation. Annu Rev Plant Biol **59:** 143–166

Rouhier N, Unno H, Bandyopadhyay S, Masip L, Kim SK, Hirasawa M, Gualberto JM, Lattard V, Kusunoki M, Knaff DB, et al (2007) Functional, structural, and spectroscopic characterization of a glutathione-ligated [2Fe-2S] cluster in poplar glutaredoxin C1. Proc Natl Acad Sci USA **104:** 7379–7384

Schaedler TA, Thornton JD, Kruse I, Schwarzländer M, Meyer AJ, van Veen HW, Balk J (2014) A conserved mitochondrial ATP-binding

cassette transporter exports glutathione polysulfide for cytosolic metal cofactor assembly. J Biol Chem **289:** 23264–23274

Song W, Solimeo H, Rupert RA, Yadav NS, Zhu Q (2002) Functional dissection of a Rice Dr1/DrAp1 transcriptional repression complex. Plant Cell **14:** 181–195

Sundaram S, Rathinasabapathi B (2010) Transgenic expression of fern *Pteris vittata* glutaredoxin PvGrx5 in *Arabidopsis thaliana* increases plant tolerance to high temperature stress and reduces oxidative damage to proteins. Planta **231:** 361–369

Sundaram S, Rathinasabapathi B, Ma LQ, Rosen BP (2008) An arsenate-activated glutaredoxin from the arsenic hyperaccumulator fern *Pteris vittata* L. regulates intracellular arsenite. J Biol Chem **283:** 6095–6101

Tarrago L, Laugier E, Zaffagnini M, Marchand C, Le Maréchal P, Rouhier N, Lemaire SD, Rey P (2009) Regeneration mechanisms of *Arabidopsis thaliana* methionine sulfoxide reductases B by glutaredoxins and thioredoxins. J Biol Chem **284:** 18963–18971

Vernoux T, Wilson RC, Seeley KA, Reichheld JP, Muroy S, Brown S, Maughan SC, Cobbett CS, Van Montagu M, Inzé D, et al (2000) The *ROOT MERISTEMLESS1/CADMIUM SENSITIVE2* gene defines a glutathione-dependent pathway involved in initiation and maintenance of cell division during postembryonic root development. Plant Cell **12:** 97–110

Waszczak C, Akter S, Eeckhout D, Persiau G, Wahni K, Bodra N, Van Molle I, De Smet B, Vertommen D, Gevaert K, et al (2014) Sulfenome mining in *Arabidopsis thaliana*. Proc Natl Acad Sci USA **111:** 11545–11550

Wojtera-Kwiczor J, Groß F, Leffers HM, Kang M, Schneider M, Scheibe R (2012) Transfer of a redox-signal through the cytosol by redox-dependent microcompartmentation of glycolytic enzymes at mitochondria and actin cytoskeleton. Front Plant Sci **3:** 284

Wu Q, Lin J, Liu JZ, Wang X, Lim W, Oh M, Park J, Rajashekar CB, Whitham SA, Cheng NH, et al (2012) Ectopic expression of Arabidopsis glutaredoxin AtGRXS17 enhances thermotolerance in tomato. Plant Biotechnol J **10:** 945–955

Xing S, Zachgo S (2008) ROXY1 and ROXY2, two Arabidopsis glutaredoxin genes, are required for anther development. Plant J **53:** 790–801

Yu X, Pasternak T, Eiblmeier M, Ditengou F, Kochersperger P, Sun J, Wang H, Rennenberg H, Teale W, Paponov I, et al (2013) Plastid-localized glutathione reductase2-regulated glutathione redox status is essential for *Arabidopsis* root apical meristem maintenance. Plant Cell **25:** 4451–4468